Title
Assessment of the Effect of Different Isolation Systems on Seismic Response of a Nuclear Power Plant

Author
Wong, Jenna

Publication Date
2014

Peer reviewed|Thesis/dissertation

Assessment of the Effect of Different Isolation Systems on Seismic Response of a Nuclear Power Plant

By

Jenna Barbie Wong

A dissertation submitted in partial satisfaction of the

requirements for the degree of

Doctor of Philosophy

in

Engineering – Civil and Environmental Engineering

in the

Graduate Division

of the

University of California, Berkeley

Committee in Charge:

Professor Stephen Mahin, Chair
Professor James Kelly
Professor Ming Gu

Fall 2014

Assessment of the Effect of Different Isolation Systems on Seismic Response of a Nuclear Power Plant

ABSTRACT

Assessment of the Effect of Different Isolation Systems on Seismic Performance

by

Jenna Barbie Wong

Doctor of Philosophy in Engineering - Civil and Environmental Engineering

University of California, Berkeley

Professor Stephen Mahin, Chair

Seismic isolation is utilized in both traditional and industrial structures for its ability to reduce structural responses while effectively protecting sensitive building contents. Although this mature technology has been studied extensively, there is limited research on its application to Nuclear Power Plants (NPPs). Studies have yet to address topics such as sensitivity of equipment and the effects of seismic isolation on floor response spectra (FRS) caused by high frequencies and the inclusion of vertical motion. This paper's studies investigate the relationship between structural response and isolator mechanics, ground motion sensitivity, and the effectiveness of various isolator types, especially nonlinear isolators. Overall trends are identified that provide insight into the interaction between the isolation system and the response at various levels of the NPP. By understanding these relationships and connections, a set of valid recommendations for the selection and design of isolation systems is provided. This work is pursued through analyzing the performance of an APR1400 plant considering regulatory guidelines and utilizing a variety of ground motions, isolator types, and isolator models.

DEDICATION

To my mom and dad, without whom none of this would have been possible.

ACKNOWLEDGMENTS

This report summarizes information developed as part of the overall research project entitled "Seismic Isolation of Nuclear Power Plants (Phase 2)." This work was supported by contract KCN04-12-96 from KEPCO Engineering and Construction Company, Inc. to the Pacific Earthquake Engineering Research Center (PEER). I am grateful for this financial support. In addition, I am appreciative of the advice and technical support provided by the engineering staff of the KEPCO Engineering and Construction Company, Inc., especially Mr. Chul Soon Choi, Dr. Sang-Hoon Lee, Dr. Seung-Ryong Han, and Dr. C.G. Seo.

I am also appreciative of the advice and support of the members of my thesis committee. This committee includes Dr. Stephen Mahin, Dr. James Kelly, and Dr. Ming Gu. I am grateful for the assistance of various researchers participating in this project from the University of California Berkeley including Dr. Vasileios Drosos, Dr. Andreas Schellenberg, Dr. Matt Schoettler, Dr. Vesna Terzic (now at CSU Long Beach), and Dr. Zhi-Guang Zhou (now at Tongji University, Shanghai, China).

Any opinions, findings, and conclusions or recommendations expressed in this report are those of the author and do not necessarily reflect those of KEPCO Engineering and Construction, the Pacific Earthquake Engineering Research Center, or the Regents of the University of California.

TABLE OF CONTENTS

LIST OF FIGURES

LIST OF TABLES

1 Introduction

The events in Japan after the Great East Japan Earthquake and Tsunami of 2011 have raised significant questions about seismic safety and emergency management of nuclear power plants (NPPs). Because nuclear power remains a viable means of supplying economical electrical energy with a limited carbon footprint considerable effort is being made worldwide to assess the safety of NPPs under abnormal conditions, such as those created by severe earthquakes, and to develop and assess new technologies for increasing the seismic safety of new and existing NPPs. In the case of new plants to be constructed in regions of moderate to high seismic hazard, greater consideration is being given to the use of seismic isolation and related technologies to achieve with high confidence the necessary high levels of seismic performance.

1.1 STUDY REVIEW

While protection against collapse is a major focus of structural performance, for sensitive facilities such as NPPs, performance is extended to include the integrity of equipment and machinery. Based on recent earthquakes, studies such as Konstantinidis and Nikfar (2014) have begun analyzing the sliding of contents in isolated structures. They noted that 80 to 90% of a building's value consists of its contents and not the structure itself. From another study, the Building Research Institute (2011) observed that the majority of structures did not suffer structural damage such as story collapse but did have non-structural damage. Thus, nonstructural damage presents a major challenge to the performance of structures especially critical facilities with major machinery.

Loss of nonstructural components in a traditional facility may impact the resilience of the business and community. However, in the case of NPPs, reduced operation can lead to a more wide spread impact due to the health and safety effects associated with malfunctions or loss of operation at these plants.

Based on the Great Eastern Japan Earthquake of 2011, the operation of the Fukushima-Daiichi plant has questioned the use of nuclear power internationally and has devastated the local area for decades to come due to the health hazard. In the case of this accident, the exact failure of equipment is still debatable, however, the results present a strong case for the necessity of continued operation not only of the structure but its nonstructural components. With the loss of operation for a single reactor building, a major problem not just for the immediate community but a larger portion of the population was created.

As of 2010, nuclear power was being presented as a viable energy source with a potential renaissance (Russell, 2010). However, after 2011 earthquake, countries worldwide began to re-evaluate their use of nuclear power and the standards controlling their design. Many required new testing and review of existing plants for any corrections needed. Although, the Fukushima-Daiichi plant's reactor was severely damaged in the seismic event, the recently seismically isolated operations building withstood the event with no major damage. As a result, seismic isolation is being considered for future plant designs.

Seismic isolation is a relatively mature field. It is the subject of several books that describe the fundamentals of its application to various types of structures (e.g., Naeim and Kelly, 1999; Higashino and Okamoto, 2006). Research on seismic isolation is extensive with studies focusing on various aspects of the technology including materials, mechanics, and performance. The most relevant studies focus on the structural response with the presence of strong vertical ground motions. The impact on sensitive machinery and equipment is a major concern for facilities such as NPPs. Several recent studies have begun to look more closely at these nonstructural components.

In a study on seismic protection of equipment in essential buildings (Marin-Artieda, 2014), amplification of accelerations in the upper floors of fixed base buildings strongly depends on the modal characteristics of the building and are independent of the type of ground motion. Their study also concluded that there is a possible tuning effect of the equipment in the upper stories of structures around the fundamental period. As a result, this suggested that response can be modified by lengthening the fundamental period of the equipment. The results of the Marin-Artieda study do agree with some expectations from this report's research. However, the root of the increase acceleration response may not necessary be only connected to the fundamental period of the equipment. Several studies in this report investigate the influence of isolator properties on the response. As a result, this report will suggest that the equipment may not need individual adjustments with the overall isolation system being designed such that it can accommodate for a range of equipment frequencies.

In a study analyzing the ability to use isolation to achieve seismic performance objectives, Morgan and Mahin (2011), noted the possible introduction of high frequency content due to the hysteretic behavior of isolation. This study takes this a step further to examine this behavior for bilinear isolators with respect to FRS.

In terms of vertical motion, in 2012, Motosaka and Mitsuji noted vertical motion observed at the roof level was a result of horizontal input motion from the 2011 Tohoku earthquake. Due to this vertical motion, they concluded the ceilings in a series of structures studied lacked the strength in the vertical direction leading to collapse. Although their study focused primarily on the non-structural ceiling components, the results show that there is an interaction between the vertical and horizontal components of motion supporting 3D analysis.

The application of seismic isolation to nuclear power related facilities is not extensive. Several preliminary studies have been carried out recently to identify any special issues related to dynamic response that might need to be considered in the design and analysis of seismically isolated NPPs. For example, Blandford et al. (2009), Huang et al. (2008), Huang et al. (2009), Wong et al. (2013a, 2013c), and Zhou et al. (2013a, 2013b and 2013c) are among a few of these studies.

A relatively comprehensive overview report (Wong et al, 2013b) is also available that describes: the underlying isolation technology as applied to NPPs; the general types of isolation and supplemental damping devices available commercially; situations where isolation has been

applied to nuclear power plants and other nuclear facilities as well as to other critical infrastructure elements; performance of seismically isolated nuclear related facilities and other critical infrastructure systems during actual earthquakes; special maintenance and operations issues raised by the use of seismic isolation in NPPs; experimental and numerical research that has been carried out related to seismically isolated nuclear facilities; available regulations, codes, standards and guidelines; some preliminary numerical results to identify the effect of isolator and ground motion properties on response of the bearings, the supported structure, and contents; and special issues introduced in the planning, design, construction, maintenance and operations and decommissioning of seismically isolated NPPs. This report also provides recommendations regarding the overall benefits and detriments of applying seismic isolation to nuclear facilities, and also regarding high priority research and development needs.

In addition to such studies, a number of regulatory guides and codes are being developed to help steer the application of seismic isolation to nuclear facilities and NPPs. Such guidelines have existed in many countries for several decades for buildings (e.g., ASCE, 2005) and bridges (e.g., AASHTO 2010). A summary of requirements worldwide for building structures is available (Higashino and Okamoto, 2006). Recently, several countries have developed guidelines or are in the process of updating guidelines to address the design of seismically isolated nuclear facilities (e.g., Kammerer et al., 2011; ASCE, 1998; ASCE 2005; JEA, 2000; JEAG, 2000).

While these guidelines, technical documents and general studies are very informative and useful; few examples of their trial application to an actual NPP have been undertaken and published. As such, more focused investigations of specific issues that arise in the design and analysis of a realistic model of an existing standard NPP would be beneficial. Such plant specific studies would help quantify the specific advantages and pitfalls of applying seismic isolation, and help identify technical challenges and issues that should be the addressed through more intensive research and development efforts.

2 Study Overview

2.1 PROBLEM STATEMENT

In this context, a simplified, but realistic numerical model of an Advanced Power Reactor 1400 (APR1400) is used in the studies presented in this report. The APR1400 is a standardized fixed base NPP developed by the Korea Electric Power Corporation (KEPCO). The plant in its fixed based condition is intended for use at sites having a nominal peak ground acceleration of up to 0.3g. The goal of applying seismic isolation in the APR1400 would be to extend its use to situations where nominal peak ground accelerations on the order of 0.5g would be expected. Based on preliminary designs developed by the KEPCO Engineering and Construction Division (KEPCO E&C), two basic types of seismic isolation systems are considered. In one case, elastomeric bearings are used, and in the other case, friction-based isolators are used.

A series of nonlinear time history analyses have been undertaken and presented in this report to help understand the effects of different isolator and ground motion characteristics on response and seismic performance. For these studies, simplified models of two different types of isolation systems are used. To assess the dependency of findings on the characteristics of ground motions, various sets of ground motions are used in the parametric studies. Special attention is placed on engineering demand parameters related to displacements and forces in the isolation systems, forces and drifts in the supported structure, and floor spectra at key locations throughout the structure.

To limit the scope of the current study, consistent with the preliminary nature of these investigations, a number of simplifying assumptions will be imposed:

1. A “stick” lumped mass model will be used to simulate the 3D dynamic response of the structure;
2. The foundation supporting the isolation system is assumed fixed. That is, no soil structure interaction is considered in this report. However, additional information on the effects of soil-structure interaction on the seismic performance of the APR1400 NPP can be found in Drosos et al., 2014.
3. While different ground motion characteristics are considered, emphasis is placed on excitations consistent with design basis events and where hard stops due to impact with moat walls or other restraining elements are not encountered.
4. Relatively conventional models of bearings are considered, and potentially important characteristics such as geometric nonlinearities, dependency of bearing properties on changes in temperature due to energy dissipation, and so on are not considered in these studies.

2.2 OBJECTIVES

The overall goal of this research is to identify the dependency of the seismic performance of a seismically isolated NPP (i.e., the APR1400) to characteristics of the isolation system, structural system and ground motion, and to compare the performance of the isolated plant to comparable ones that are fixed base. The specific research objectives considered in this report are the following:

1. Investigate the effects of ground motion excitations, including the shape of target spectrum used to characterize the seismic hazard; the intensity of shaking; number of components included in analysis, and the use of dispersion appropriate and spectrum compatible motions
2. Investigate the effects of isolator hysteretic behavior on seismic performance;
3. Identify from results the specific influences of the vertical component of ground motion excitation on seismic performance; and
4. Identify from the results obtained the specific factors controlling the seismic gap size;

2.3 APPROACH

Studies are conducted using a simplified lumped mass numerical model of the APR1400 plant designed by KEPCO E&C. This section discusses the details of the numerical model and nonlinear analysis methods used in this report. The overall configuration of the structure and isolation plane is discussed below. The specific sets of ground motions used are also described.

2.3.1 Method of Analysis

All analysis was conducted using OpenSees, the Open System for Earthquake Engineering Simulation (McKenna and Fenves, 2000). Result post-processing was completed using MATLAB (MATLAB, 2013). Additional information on numerical procedures used in the research program, including OpenSees, can be found in a report by Schellenberg et al., 2014.

2.3.2 Model

The APR1400 lumped-mass stick model used in this study was adapted from a model (Revision B) provided by KEPCO E&C. It contains the auxiliary (AUX) building and reactor containment building (RCB), as shown in Figure 2.1 below. More details about the OpenSees model developed for this project are available in Schellenberg et al., 2014.

Modal characteristics were computed for a fixed based (non-isolated) model. Table 2.1 provides the modal information for the horizontal, vertical, and rotation directions for various components of this model.

For the isolated model of the APR1400, 454 isolators were installed between the upper and lower mats of the foundation as shown in Figure 2.2. The isolators were set atop pedestals having a height of about 6 ft. (1.8 m).

In total, the isolated NPP weighs 1,231,825 kips (5,479,404 kN). Of this, 1,027,785 kips (4,571,793 kN) is supported on the isolator system. Variations to this model were introduced for several analyses.

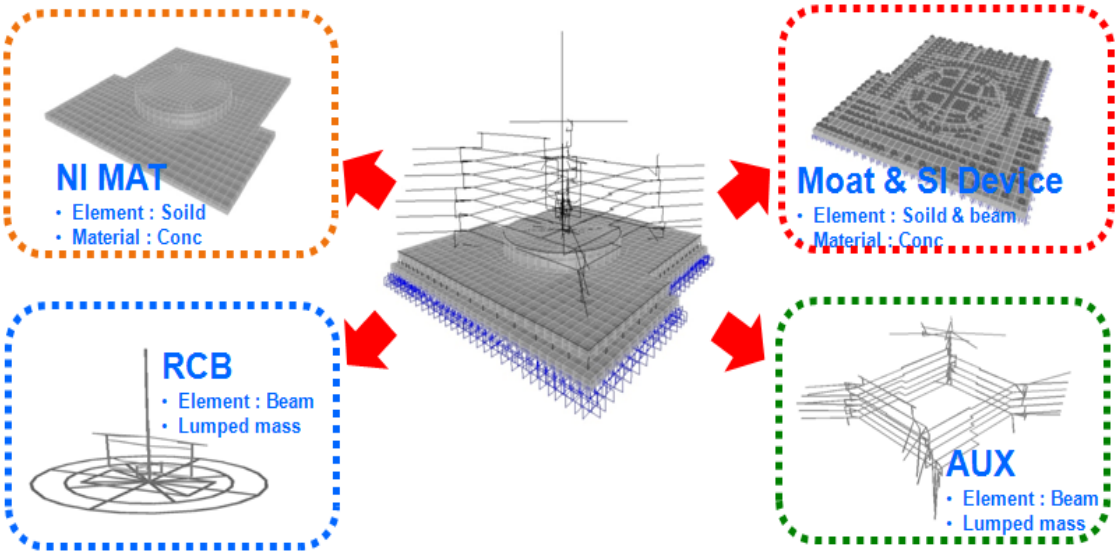

Figure 2.1 Full APR1400 Model (Lee, 2013).

Table 2.1 Modal Information for APR1400 Components

Mode	Period (Sec.)	Frequency (Hz)	Building	Direction
1	0.260	3.850	RCB	H2 translation
2	0.260	3.852	RCB	H1 translation
3	0.169	5.926	AUXB	H2 translation
4	0.159	6.282	AUXB	H1 translation
5	0.136	7.373	AUXB	V rotation
6	0.119	8.382	RCB	V rotation
9	0.091	11.020	RCB	V translation
11	0.086	11.610	RCB	H2 translation
12	0.086	11.617	RCB	H1 translation

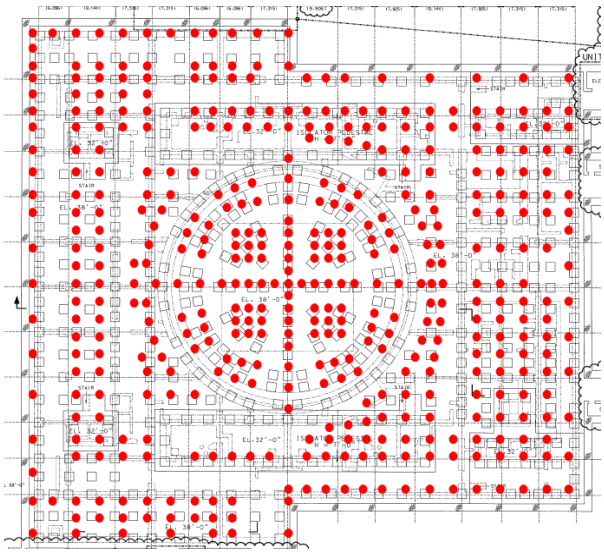

Figure 2.2 Plan View of Isolator Layout for APR1400 (Lee, 2013).

There are a substantial number of nodes in the APR1400 model. However, to illustrate responses observed, only a select number of locations in the NPP are shown in the plots provided in this report. These locations are in the reactor building's primary shield wall, which contains the majority of the essential equipment. The locations selected are shown in Figure 1.3. The reactor containment building consists of three concentric structures. The locations being monitored and reported in this report are shown in relation to these substructures in Figure 2.4.

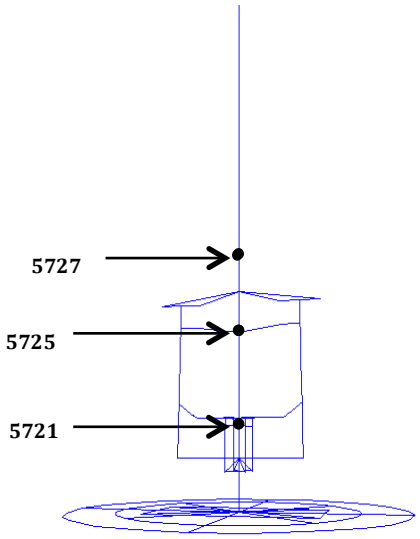

Figure 2.3 Key Locations of Interest for the Reactor Building; Identified by Node Number and Location in the OpenSees Model.

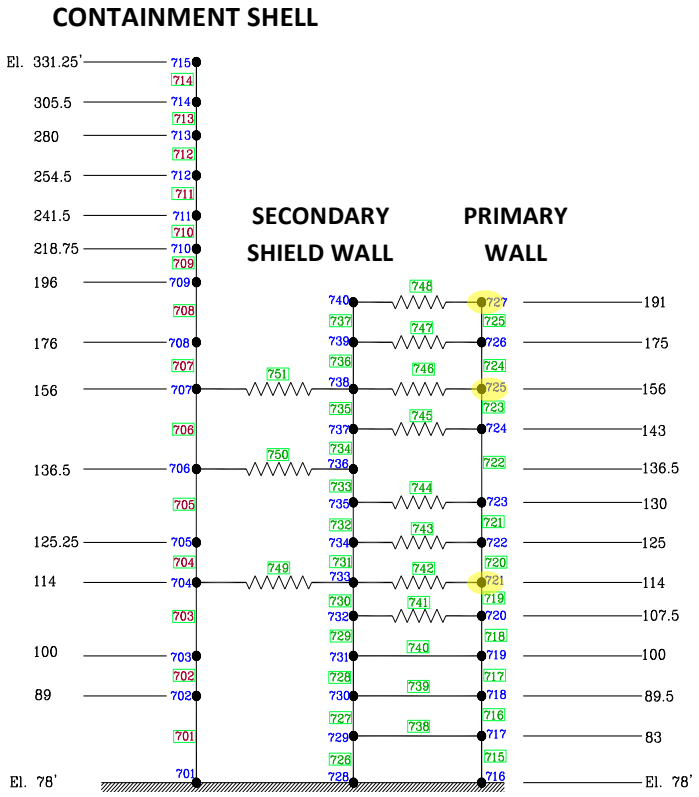

Figure 2.4 Reactor Building Sub-Structures with Key Locations of Interest Highlighted in Yellow; Node Numbers and Elevations in OpenSees Model Shown. (Elevations in feet (1 ft. = 0.3048 m))

As discussed by Schellenberg et al. 2014, viscous damping in the OpenSees model was characterized as being stiffness proportional, with 5% of critical damping assumed around the fundamental mode of the RCB. Isolator elements were assumed not to contribute to viscous damping, since hysteretic damping in the isolators was included in the nonlinear model. The effective viscous damping in the system is anchored at 4Hz with 5% equivalent viscous damping. At the effective frequency of the target isolation system (0.5 Hz), stiffness proportional damping results in about 0.6% effective viscous damping.

For the linear elastomeric, the isolator properties were defined differently from the nonlinear isolators. The linear elastomeric is modeled in OpenSees using a TwoNodeLink element with six uncoupled degrees of freedom (DOF). For each DOF, a material was defined describing the force-displacement behavior. In the two horizontal orthogonal directions an elastic uniaxial material was used which provides linear-elastic and linear-viscous damping. Thus, the linear elastomeric is modeled such that it behaves as linear viscous dampers in the two horizontal directions.

2.3.3 Isolator Models

These studies considered the use of lead plug rubber bearings (LPRB) and EradiQuake™ System (EQS) friction bearing.[1] The isolators have an effective period of 2.2s based on a maximum displacement of 5.9 in (150 mm) under the design basis earthquake. These parameters were chosen by KEPCO E&C based on the design requirements.

To study the differences in response among different types of bearings, three basic types of isolator models are used: simple linear elastic model (representative of natural rubber or other elastomeric bearing with supplemental damping provided to achieve the 20% effective linear viscous damping cited above), bilinear hysteretic models (representative of LPRB and EQS and certain other types of friction bearings); and Bouc-Wen hysteretic models (representative of a broader range of elastomeric bearings with or without supplemental damping properties). These models are available in the current version of OpenSees.

The bilinear plasticity and Bouc-Wen models are implemented using generalized plasticity theory to capture the force-displacement behavior of a bearing in two horizontal directions. The basic bilinear model's force displacement curve for a single bearing is shown in Figure 2.5. The model idealizes the isolator's nonlinear behavior where a single point defines the transition from the elastic to inelastic range. The model is characterized by three parameters: K_e, the initial elastic stiffness, K_d, the post yield displacement hardening tangent stiffness, and F_y, the shear force in the bearing at the transition from elastic to yield behavior. The models parameters can be adjusted to approximate the behavior of the baseline LPRB being considered for the APR1400 (Figure 1.6a) or the simple friction bearing (Figure 1.6b). When the model was used to represent friction bearings, only constant friction cases were considered.

The Bouc-Wen model can be used to represent more complex behavior exhibited by elastomeric bearings, especially a more gradual transition from elastic to yield response, and a progressive deformation hardening characteristic at large deformations. Some of the behavior that can be reproduced using a Bouc-Wen model is shown in Figure 2.7. This model provides hysteresis loops with rounded transitions to better resemble the actual hysteretic behavior of elastomeric isolators. The roundness of the yielding region is controlled by a number of input parameters.[2]

The bilinear hysteretic and Bouc-Wen models are used to explore the effects of the shape of the bearing hysteretic loop on structural response, and floor spectra. Tables 2.2 to 2.5 summarize input parameters used for the different isolations considered in the studies. In these tables the values given correspond to the unidirectional stiffness and strength of the entire isolation plane (the average value for each bearing times the total number of bearings).

Various parametric variations of isolator input parameters will be undertaken in the report to assess the effect of different bearing properties on response.

---

[1] Recent publications have presented the general background of these and other isolator types [Wong and Mahin 2012; Wong, Zhou, and Mahin 2013].

[2] Several papers further discuss the Bouc-Wen model [Bouc 1967; Bouc 1971; Wen 1976].

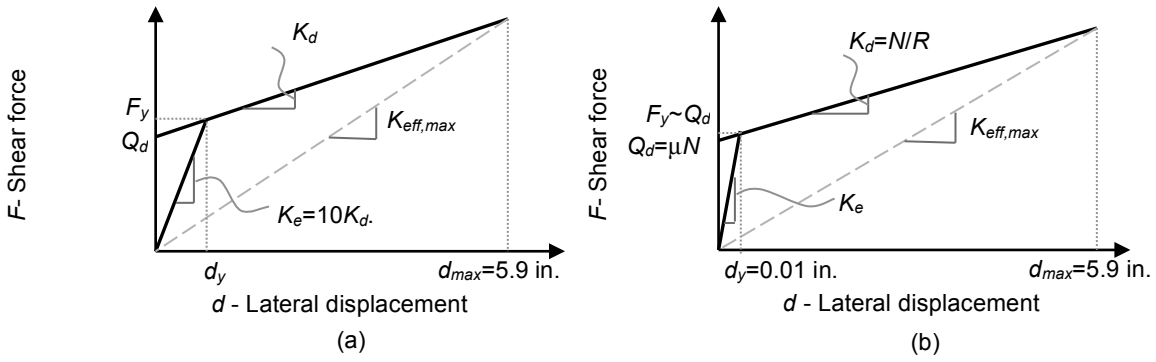

Figure 2.5 Idealized Bilinear Force-Displacement Curves for (a) the Baseline LPRB Model and (b) the Simple Friction Model Note: Plots are for a single bearing. The curves are not drawn to scale.

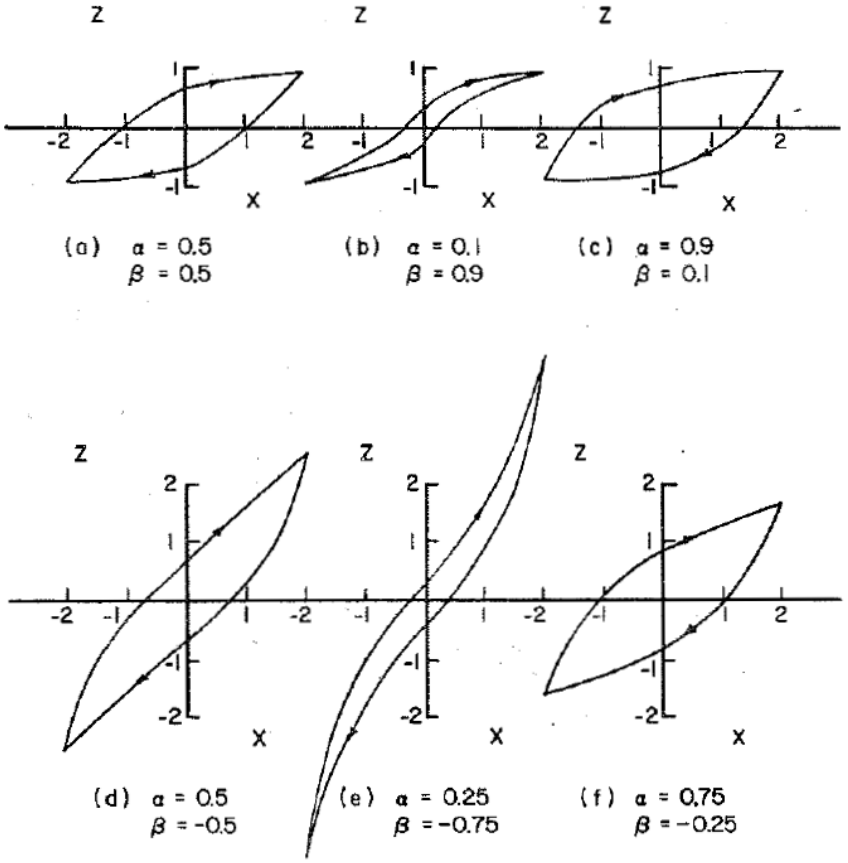

Figure 2.7 Bouc-Wen Hysteresis Shapes for Different Input Parameters (Wen, 1976).

Table 2.2 Linear Elastomeric Isolator Properties

Isolator Period	2.0 s
Initial Stiffness	3,147,326 k/ft. (45,932,076 kN/m)

Table 2.3 Bilinear Plasticity Elastomeric Isolator Properties

Isolator Period	2.0 s
Initial Stiffness	3,147,326 k/ft. (45,932,076 kN/m)
Yield Strength	42,730 k (190,072 kN)
Hardening Ratio (α)	0.1

Table 2.4 Bilinear Bouc-Wen Elastomeric Isolator Properties

Isolator Period	2.0 s
Initial Stiffness	3,147,326 k/ft. (45,932,076 kN/m)
Yield Strength	42,730 k (190,072 kN)
Linear Hardening Ratio (α_1)	0.1
Nonlinear Harding Ratio (α_2)	0
Nonlinear Hardening Exponent (μ)	3
Yielding Exponent (η)	1
Hysteretic Shape Parameter (β)	0.5

Table 2.5 Simple Friction Isolator Properties

Friction Coefficient	0.07
Initial Shear Stiffness	86,501,300 k/ft. (1262,399,972 kN/m)
Effective Radius of Sliding Surface	3 ft. (0.9 m)

Throughout this report the isolators will be referenced by a number of abbreviations for tables and figures. Table 2.6 summarizes the abbreviations used.

Table 2.6 Abbreviations for Isolator Types and Models

Isolator Type and Model	Abbreviation
Linear Elastomeric	Linear
Bilinear Elastomeric – Plasticity Model	BL-P
Bilinear Elastomeric – Bouc-Wen Model	BL-BW
Simple Friction – Constant Friction	SF-C

2.3.4 Ground Motions

A variety of ground motions were used for this research.

For the APR1400, the fixed based plant is currently designed for a PGA of 0.3g. For the seismically isolated version of the APR1400, designers intend to utilize this plant in areas with a PGA of about 0.5g. Thus, the design basis earthquake (DBE) is taken for the isolated plant as having a nominal PGA of 0.5g. Since a particular site for locating the plant has not been established, standard design response spectrum stipulated in US NRC RG 1.60 (NRC, 1973) and in the "European Utility Requirements (EUR) for LWR Nuclear Power" will be used in selecting ground motion records. The development of these motions is described in Schellenberg et al., 2014b.

In addition, the NRC Draft NUREG document for seismically isolated NPPs suggests (Kammerer et al., 2011) that an extended design basis (EDB) be considered. The minimum beyond design basis earthquake must be taken at least 1.67 times the spectrum for the DBE (Kammerer et al., 2011). Thus, for certain studies, the DBE ground motions were also scaled by 1.67 to represent the EDB event.

For some of the investigations, ground motion records provided by KEPCO E&C were used. For other analyses, a larger set of motions generated within the project were used. Details of these motions are described by Schellenberg et al. 2014.

For the time ground motion time histories provided by KEPCO, two 3-component records were available. Each three-dimensional (3D) record consisted of three components (2 horizontal, 1 vertical). One of the records was developed to be spectrally matched to the response spectrum stipulated by the European Utility Requirements and the other was spectrally matched based on the US NRC RG 1.60 design response spectrum. In each case, 5% damping and a peak ground acceleration of 0.5g was considered. Each time history is 20.48 seconds long.

Figure 2.6 compares the EUR and NRC spectra. There are significant differences, especially in the low and moderate frequency ranges, and in the vertical direction. These differences will likely have significant effects on the response.

A more extensive set of ground motions was developed as part of this project. In this case, it was desired to have relatively large sets of ground motions to be able to characterize the dispersion as well as median values of response. To this end, twenty sets of 3-component records were developed for the NRC and EUR DBE spectra. Three types of processing were done on these records. In the first case, they were amplitude scaled so that the median spectral values in the horizontal direction for all twenty motions were close to the target spectrum in question and the dispersion of the spectrum for individual records was appropriate considering the dispersion expected all records having desired properties. In addition to these dispersion appropriate sets of motions, two spectrum compatible sets of motion were developed. In one case, the records were modified so each record closely matched the target spectrum based on 5% viscous damping. For the second case, the records were modified so that the modified records matched as closely as possible the response spectra computed at five different damping values.

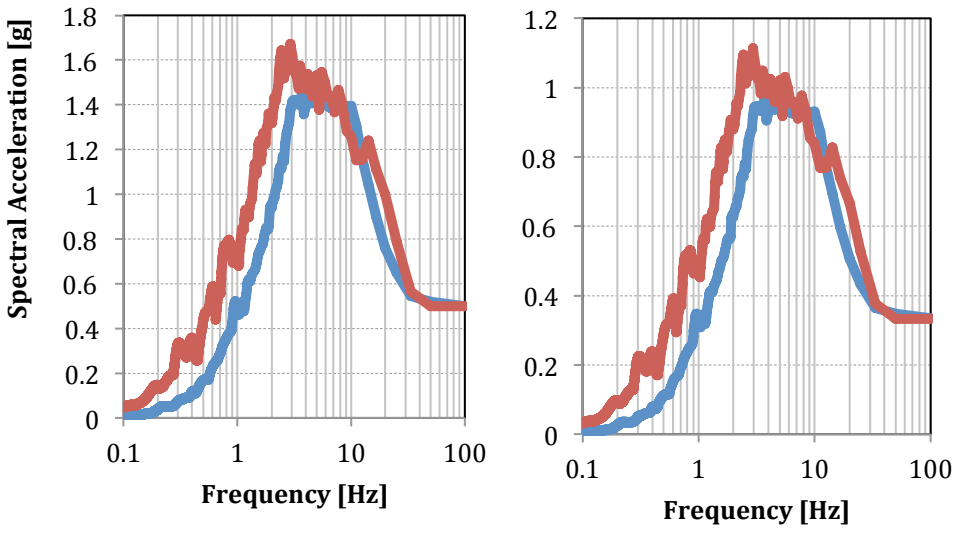

(a) (b)

Figure 2.6 Comparison of the EUR (blue) and US NRC RG 1.60 Spectra (red): (a) Horizontal and (b) Vertical.

2.4 SCOPE OF THIS REPORT

This report is divided into two basic parts. In the first, results of numerical analysis are presented and in the second discussions are made based on these results.

The analytical studies are contained in Chapters 2 through 9. Chapter 2 examines the basic response of the isolated and fixed based APR1400 models considering one and then two components of excitation. Chapters 3 and 4 relate to the effect the hysteretic characteristics of the isolator on performance. Chapter 5 through 7 investigates the effect of the vertical component of motion on bearing and system behavior. Lastly, Chapters 8 and 9 respectively analyze factors controlling the minimum size of the seismic gap and ground motion subsets.

A brief summary, conclusions and recommendations are provided in Chapter 11.

3 Identify General Relations Between Characteristics of Isolators and Performance

The relationship between isolator, structural system and ground motion characteristics and seismic performance is complex. For a single isolation system, a number of isolator parameters must be considered including strength, initial and post-yield stiffness, and hysteretic properties. The dependency of these parameters during the seismic response on the instantaneous temperature, axial load, and rate of loading further complicates response prediction. Earthquake response is also dependent on the dynamic and mechanical characteristics of the supported structure, its symmetry, and where its instantaneous centers of mass, stiffness, and resistance are located relative to the instantaneous centers of stiffness and resistance of the overall isolation system. The dynamic and other characteristics of ground motions experienced can also significantly affect response. Moreover the isolators may act to couple the vertical excitation of the ground with the horizontal response of the supported structure. As such, vertical ground motion characteristics, vertical stiffness, and hysteretic characteristics of bearings can introduce many new variables into a study of performance. Lastly, it is reasonable that trends in performance may vary depending on the location in the structure for which response is being characterized. All of these parameters that may affect performance make it difficult to understand the relative importance of different parameters, or the variables that should be changed to improve response. Thus, it is desirable to conduct a systematic parameter study examining the dependence of different performance variables on specific characteristics of bearings, ground motions, and locations where response is being predicted.

Given the complexity of both the APR1400 and the isolation system, the performance of the overall system is examined in this chapter in a systematic manner. In this report, one bearing or ground motion's parameter of interest is changed at a time to identify and understand observed trends in performance outcomes. The studies begin with simplified models examining various isolator parameters and points of interest in the APR1400 primary shield wall to develop a basic understanding of this interaction. These initial studies consider response to 1- and 2-dimensional (1D, 2D) horizontal ground motion excitations. Studies then begin to examine how more complicated 3D analysis results compare with these simple studies. By identifying the most influential isolator properties on structural performance, recommendations for isolation system design are developed.

Specifically, this and the following chapters uses models of varying levels of complexity to examine:

1. The effect relative to that observed in a comparable fixed base plant of having more than one horizontal component of excitation at the DBE level on floor spectrum at different locations in the plant and considering different baseline isolator models compared to.
2. The effect of the isolator type and modeling assumptions on peak isolator force and displacement demands at the DBE level of horizontal excitation.
3. The effect of the isolator modeling assumptions on floor spectra for a plant subjected to horizontal excitation.
4. The effect of the isolator stiffness and strength characteristics on floor spectra at different locations in the plant subjected to horizontal components of excitation.
5. The effect of vertical (only) and vertical plus horizontal components of motion on vertical and horizontal floor spectra for different baseline bearing types and locations in the plant.
6. The effects on floor response spectra of modifying the key horizontal and vertical stiffness properties, and lateral strength properties of the isolated plant under three-dimensional excitations.
7. How floor spectra compare for an isolated NPP to a fixed base plant, considering different isolator and ground motion characteristics.
8. What seismic gap sizes would be needed to insure different confidences levels of not contacting a hard stop for different isolator types and ground motion characteristics?

4 Study 1: Effects of Multiple Components of Ground Motions (1D and 2D Horizontal Motion)

4.1 INTRODUCTION

This study examines the effectiveness of isolation in comparison to the fixed base case. Secondly, it investigates the influence of using 1D versus 2D horizontal motion for analysis.

Using a further simplified isolated APR1400 model described previously, the effect of the isolation is examined in terms of the floor response spectra (FRS) computed at various locations. The influence on floor level acceleration response of the isolator type, isolator model, and numbers of components of horizontal excitation input is emphasized in this section.

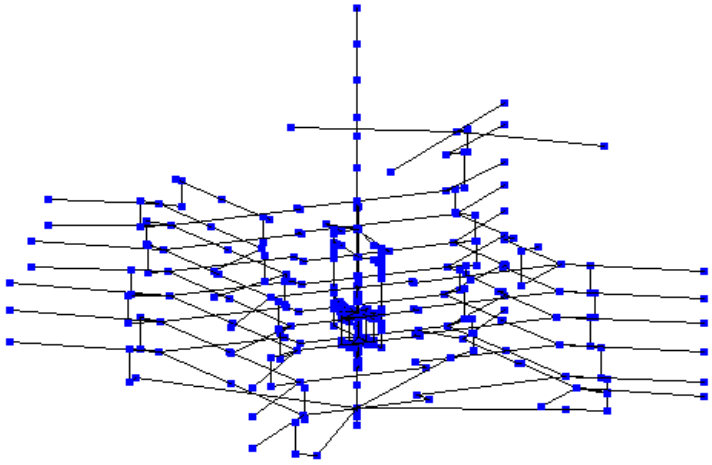

Figure 4.1 Simplified APR1400 Lumped-Mass Stick Model with a Single Isolator at its Base (Rocking and Torsion at the Base are Fully Restrained).

4.2 SIMPLIFIED APR1400 MODELING

The isolated APR1400 model from the previous chapter is simplified using a rigid mat foundation that prevents rocking and torsion (Figure 4.1). Underneath this mat foundation, a single isolator is used with effective properties of all of the bearings under the plant consistent with a 2.2 second effective period and a maximum displacement of 5.9 in. The resulting bearing results in properties shown in previous chapters.

4.3 RESULTS

OpenSees was used to perform the analysis. The H1 (M1) and H2 (M2) horizontal components of the dispersion appropriate time histories were used and applied in the global x and y direction of the model, respectively.

High frequency content is detrimental to nonstructural components, equipment and contents. Large localized peak acceleration responses and associated large high frequency pseudo-acceleration values in floor spectra create a challenge to the designer. Instead of focusing on a single parameter like the peak acceleration response in this section, focus will be on floor spectra, which provide information on the peak floor accelerations as well as the spectral accelerations for components that need to be attached to the structure. Here, we will assume primary attention will be placed on components having fundamental frequencies above 2 Hz. Observations presented address the means of shifting or reducing acceleration response in this frequency range. In comparing seismic response, this section evaluates FRS at several key locations in the plant's primary shield wall with results presented for the EUR time histories. Responses to the NRC time histories show similar results with the plots available in Appendix A.

4.3.1 Influence of Isolation

First, floor spectra are shown at an elevation of 156 ft in the primary shield wall (mid-height of structure) in Figure 4.2. These plots show the difference in response identified between the floor spectra for the fixed base structure and the isolated structures, supported by different types of isolation bearings. In this plot, and others in this sub-section, only one component of horizontal excitation is applied at a time, and rotations about a horizontal or vertical axis are not permitted in the analyses.

The floor spectra for the fixed base case in either horizontal direction show a significant amplification of the input motion for higher frequencies. This is especially true at about 10 Hz, which corresponds to the natural frequency of the primary shield wall in the RCB (Table 2.1). Peak floor pseudo-accelerations range from nearly 4g to 5.5g at this frequency for the fixed base case.

With the introduction of the isolation layer, these accelerations are reduced by nearly a factor of 10 in either direction, except for the SF-C model. The simple friction bearing shows higher horizontal floor accelerations than might be expected from the other isolated responses. Nonetheless, the peak spectral pseudo-accelerations are still reduced by factors ranging from 4 to 5 relative to the fixed base case.

It should be noted that in the low frequency range (< 1 Hz), there is a slight amplification of the horizontal FRS for the isolated systems compared to the fixed base system, especially for the bilinear models. The greatest amplification occurs around a frequency of 1 Hz. However, this increase occurs outside the frequency region of typical concern for typical components (< 2 Hz).

To better differentiate between the FRS for different isolation systems, Figure 4.3 shows the same FRS but only for the isolated systems. A peak is seen in all FRS around the horizontal period of the supported structure, approximately 10 Hz (see Table 2.1). The peak floor accelerations, and the pseudo-acceleration values near 10 Hz, are greatest by a considerable margin for the SF-C bearing, followed by the BL-BW and BL-P bearing models, and are the least for the linear bearing model (having 20% linear viscous damping). As such, isolation does

not eliminate the amplification near the natural frequencies of the supported structure, but the degree of amplification depends on the characteristics of the bearing beyond the effective period and damping of the bearings (here these were all the same). However, in the low frequency range, the trends are substantially altered. For example, around 0.5 Hz, the simple friction bearing has the lowest FRS values and the BL-BW model having the highest, with the bilinear plasticity model and linear model in between. These results are explored further in the next chapter.

Overall, these results show that any of the baseline isolation systems considered are likely to be able to protect equipment during a 0.5g DBE that is qualified for a fixed base plant based on the horizontal components of the EUR DBE spectra anchored to 0.3g. It is noted that the linear bearings with 20% supplemental viscous damping are able to achieve the lowest FRS except for low frequencies below 0.5 Hz. The nonlinear isolators produce higher floor accelerations and introduce high frequency components in FRS around the natural period of the supported structure. The nature of this amplification is sensitive to the type of bearing used, and will be examined in more detail below.

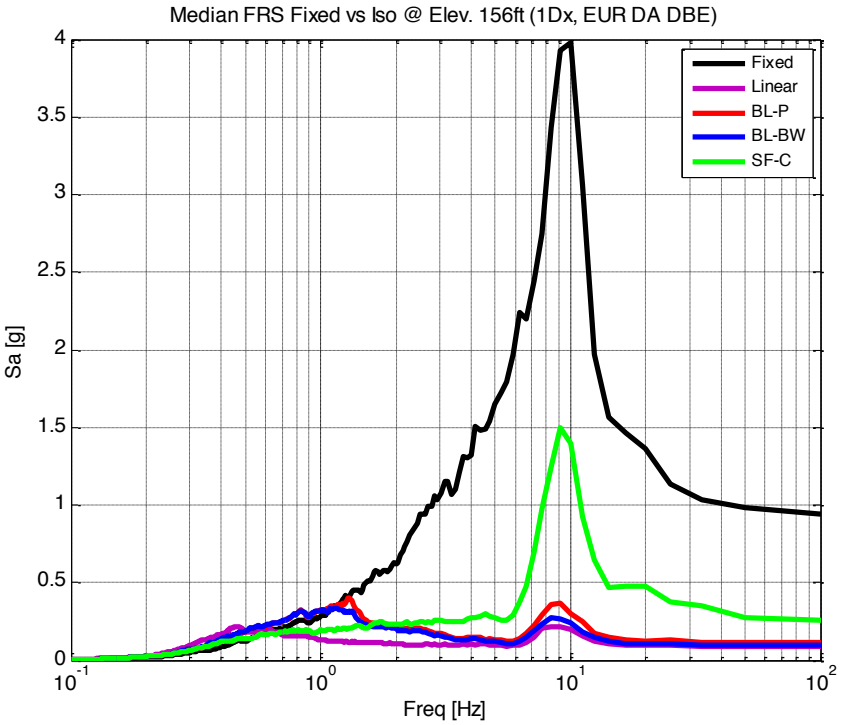

(a)

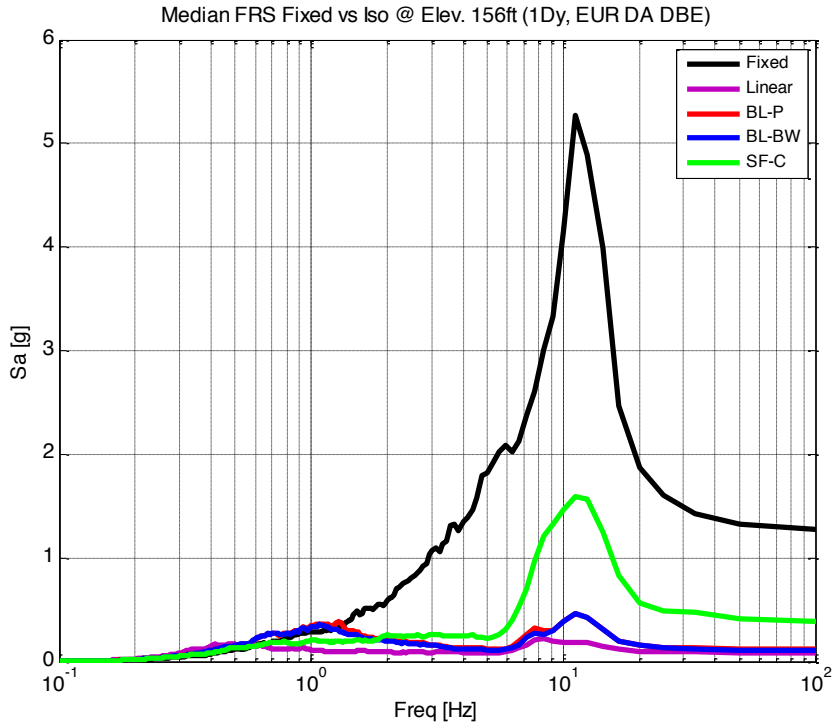

(b)

Figure 4.2 Median FRS for Isolated and Fixed Base Cases (Elev. 156', DBE) using (a) H1 Component and (b) H2 Component.

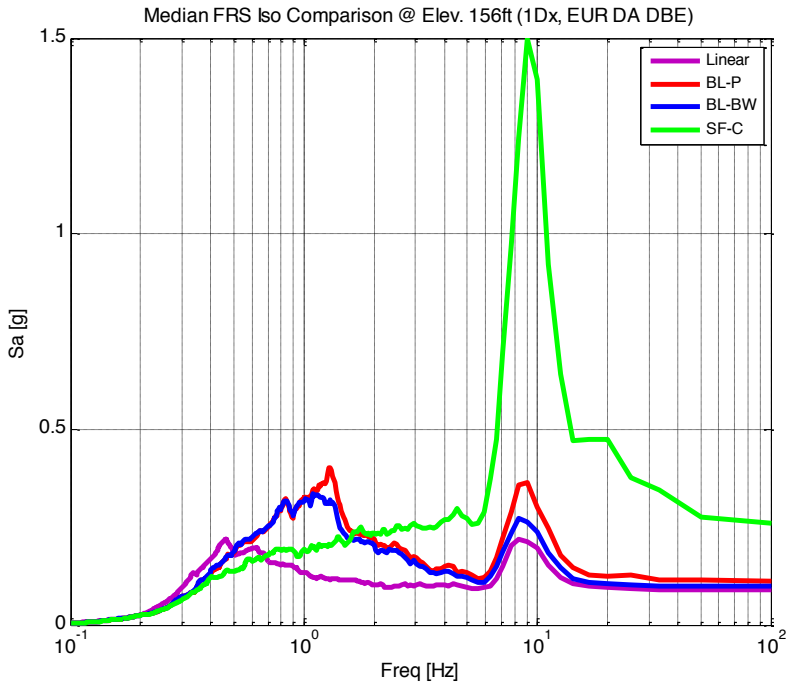

(a)

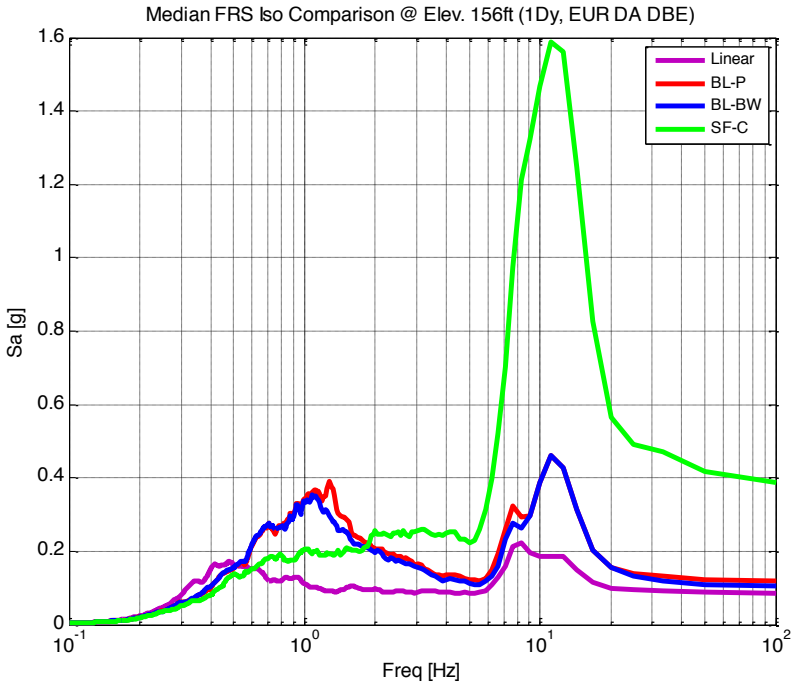

(b)

Figure 4.3 Median Isolated FRS (Elev. 156', DBE) using (a) H1 Component and (b) H2 Component.

4.3.2 1D vs. 2D Analysis

Before investigating the sensitivity of response to changes in isolator characteristics, this subsection examines how the trends in the 1D analyses described above differ when two horizontal components of motion are imposed. Figures 4.4 and 4.5 allow the floor response spectra computed for a single component of input motion at the key location to be compared to the spectrum computed when two horizontal components of motion are imposed. In these figures, the FRS for the 1Dx and 1Dy cases are the FRS in the x or y directions computed for the case where only the H1 or the H2 records are imposed in the analysis. The FRS for the 2D case is based on the SRSS combination of the FRS in the x and y directions when both the H1 and H2 records are imposed.

For the linear elastomeric bearing (Figure 4.4(a)), the maximum horizontal floor spectral pseudo-accelerations increase slightly over the entire frequency range when two horizontal components of ground acceleration are imposed. However, for the bilinear plasticity elastomeric bearing (Figure 4.4(b)) and the simple friction bearing (Figure 4.5), this trend is not as consistent. At some frequencies, the bidirectional input excitation results in higher floor response spectral ordinates, while at other frequencies the response is less. The nonlinearity of these isolators in relation to bidirectional response creates a more complex situation. For the high frequency range of behavior, there appears to be a slight reduction in peak floor spectral ordinates for the nonlinear bearing models when 2D horizontal input motions are considered.

These results show structural response cannot be entirely characterized by 1D analysis, or by simple vector addition of the spectral ordinates obtained by applying 1D motions in orthogonal directions.

Up to this point, the results presented have focused on one location in the primary shield wall. The following results show how FRS change over the height of the structure. In fixed base structures, there is a tendency for an increase in floor acceleration response with an increase in elevation. However, with isolation, the response is expected to remain constant throughout the structure's height if the structure was rigid and the base of the structure did not pitch. This response is desirable as it reduces the acceleration demands on components located in the upper elevations of the structural system and reduces contributions of higher modes in the structural response

The following figures present the FRS at three elevations along the primary shield wall with isolation using the linear and bilinear plasticity models for one component of motion. Fixed base response spectra are shown in Figures 4.6, 4.8 and 4.10 for comparison. Firstly, the similarity of the FRS at all three levels of the isolated structures reinforces the expected reduction in horizontal accelerations compared to the fixed base case. The amplitude of the FRS for the fixed base case increases substantially with elevation, especially above 5 Hz. Secondly, it is clear that isolation reduces the variation in response between elevations compared to a fixed base structure. Between an elevation of 156 ft and 191 ft, there is approximately a change in 5g of the peak floor acceleration without isolation. With isolation, the difference in accelerations reduces to about 0.1g. It is important to notice that the change in floor spectra with elevation is most predominant for frequencies at and above the natural frequency of the supported structure being considered. It is noted that even the bearing with linear stiffness and linear viscous damping amplifies the FRS in this range.

From these results, the importance of 2D analysis is re-emphasized. However, the basic trends observed for the 1D cases are seen for the cases when two horizontal components of motion are applied.

Based on the substantially lower value of FRS for the isolated structure in comparison to the fixed base structure at frequencies above 1 Hz, and the relatively small variation of FRS throughout the height of an isolated structure, design of acceleration-sensitive components is likely greatly simplified in isolated NPPs. It is anticipated on the basis of this limited analysis that a standard plant might well be able to withstand substantially greater horizontal ground accelerations when isolated than for the fixed base case.

More results from this study can be found in Appendix A.

4.4 CONCLUSIONS FOR STUDY 1

Seismic isolation is advantageous because it effectively reduces the floor accelerations consistently in a structure.

Results reinforce the ability of seismic isolation to decrease horizontal FRS for the APR1400 compared to a fixed base structure (except at frequencies near and lower than the fundamental frequency of the isolation system). However, the FRS are dependent on a number of factors. Firstly, results are sensitive to the number of horizontal components considered. Two-dimensional analysis is necessary to ensure the most accurate results, since the nonlinear mechanical properties of the bearings are sensitive to bidirectional movement. Considering only unidirectional motion may over- or under-estimate responses.

The fixed base FRS exhibits a single large peak near the natural frequency of the supported structure. With isolation, especially nonlinear isolators, while the amplitude of the FRS is decreased significantly in the high frequency range, localized high frequency content still occurs near the natural frequencies of the supported components. Thus, it is necessary to understand the sensitivity of these peaks to various properties of the structure, bearings and ground motion, and to develop effective methods of reducing or shifting these peaks in isolated structures.

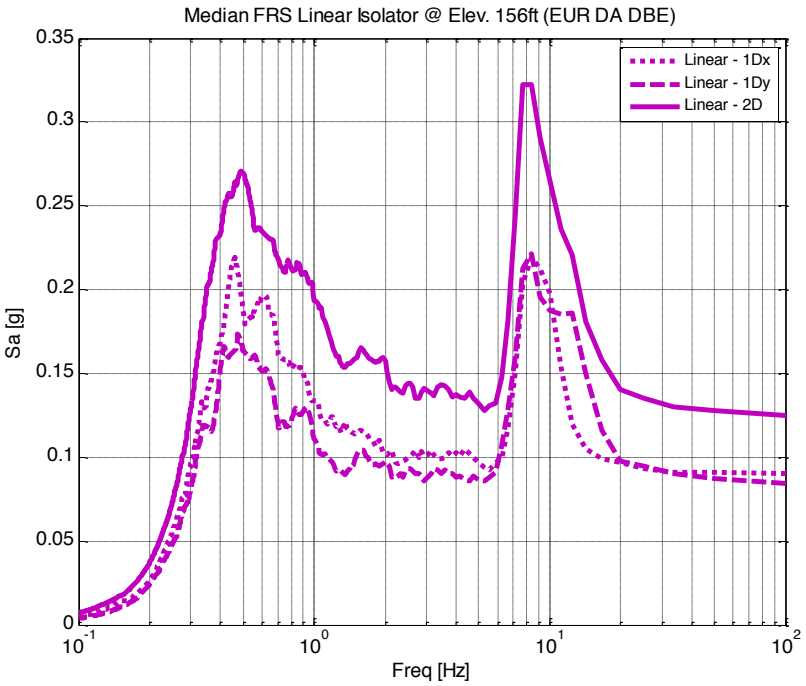

(a)

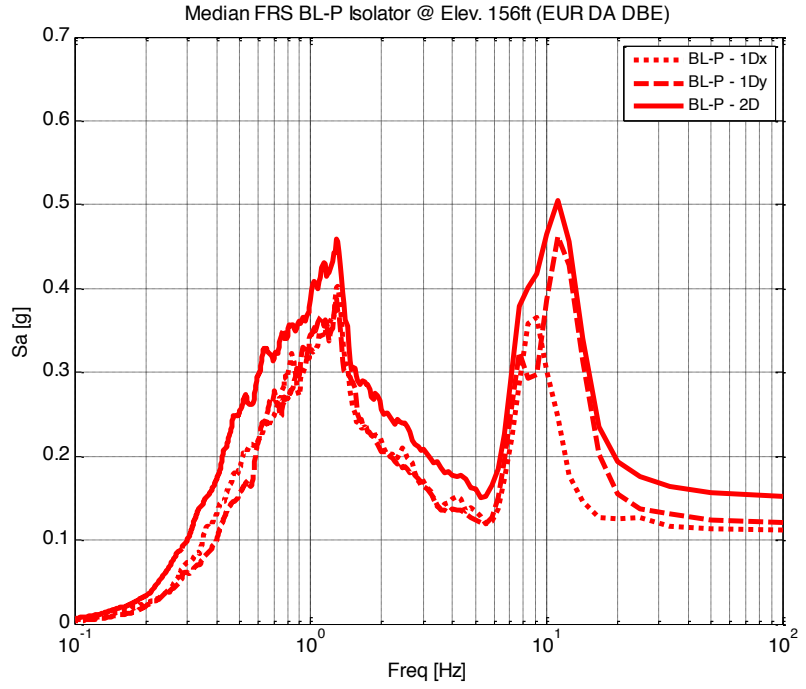

(b)

Figure 4.4 Median Isolated FRS for Various Input Motion Scenarios (Elev. 156', DBE) using (a) Linear Elastomeric and (b) Bilinear Plasticity Elastomeric.

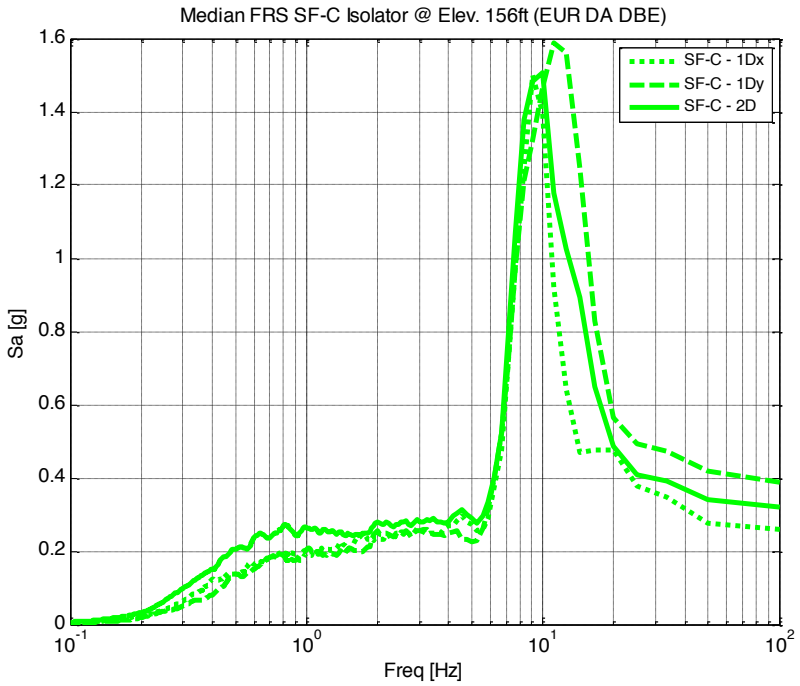

Figure 4.5 Median Isolated FRS for Various Input Motion Scenarios (Elev. 156', DBE) using Simple Friction Bearing.

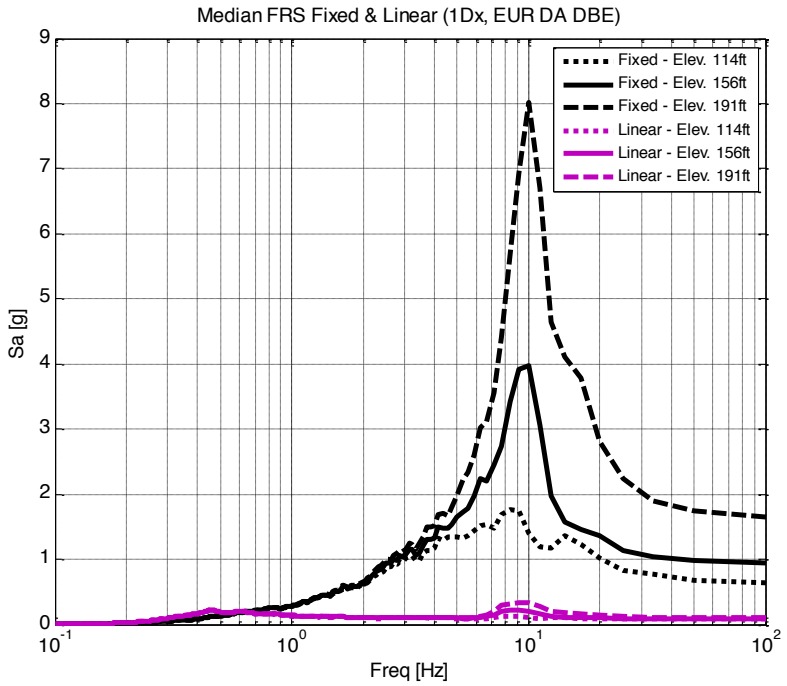

(a)

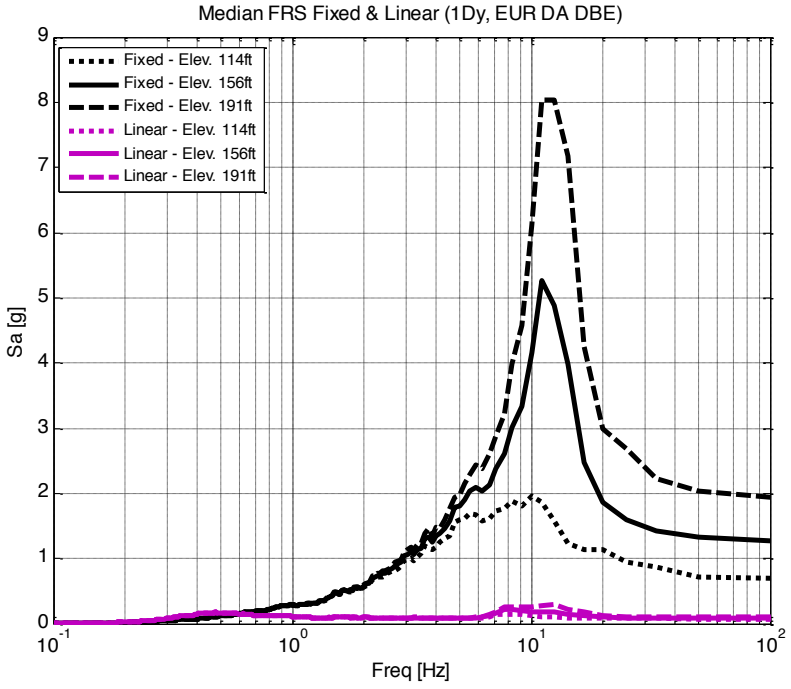

(b)

Figure 4.6 Median FRS for Primary Shield Wall with Fixed base and Linear Elastomeric for DBE for (a) H1 Component and (b) H2 Component.

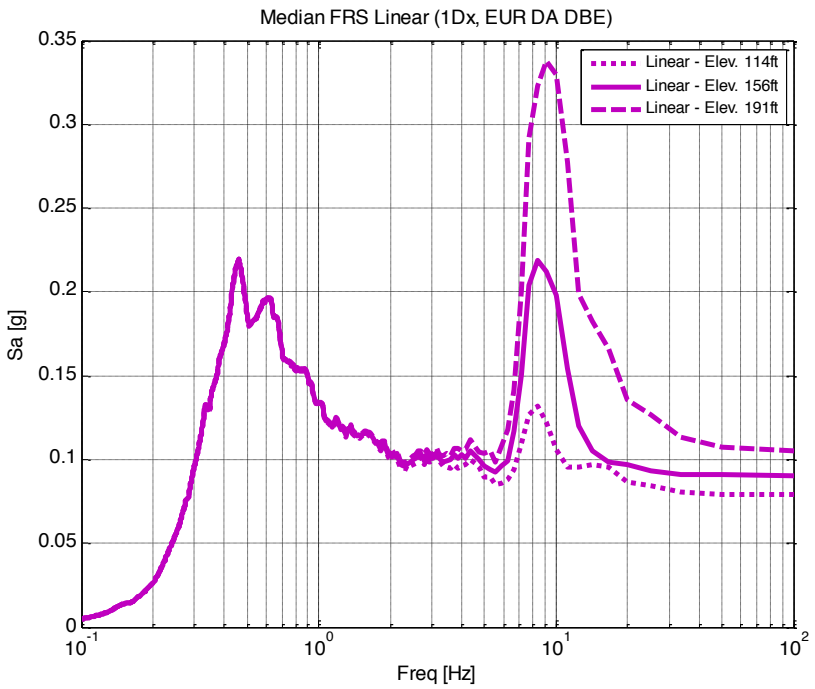

(a)

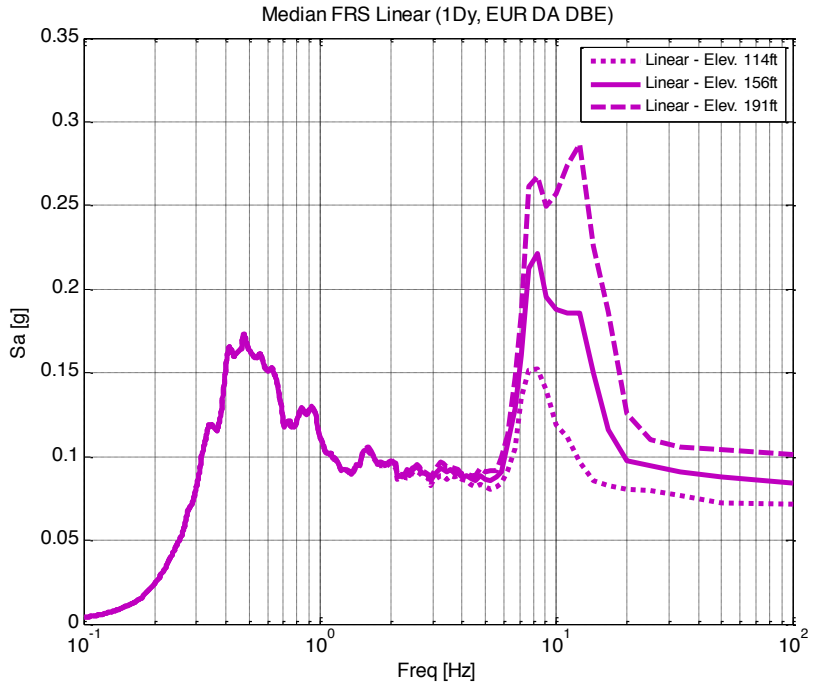

(b)

Figure 4.7 Median FRS for Primary Shield Wall with Linear Elastomeric for DBE for (a) H1 Component and (b) H2 Component.

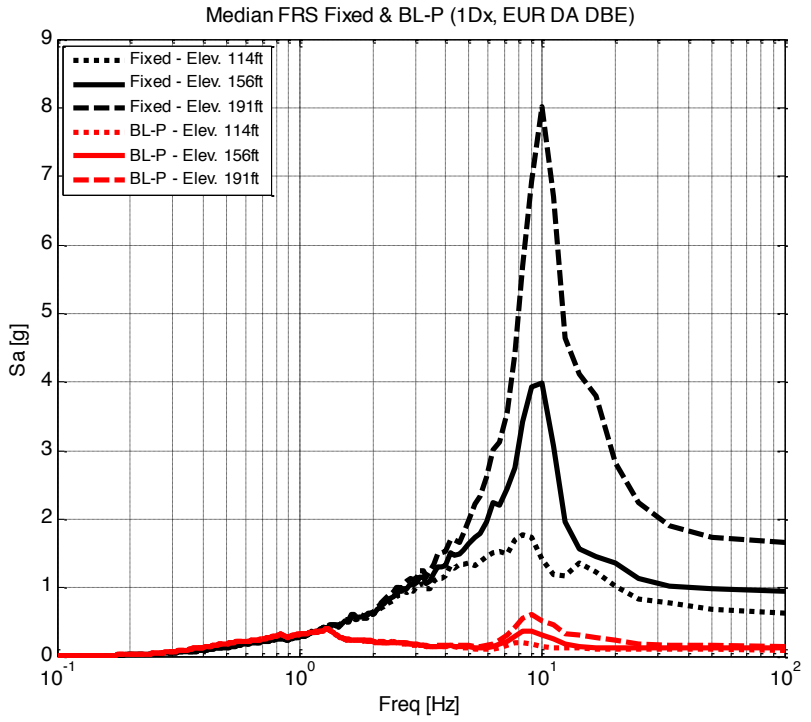

(a)

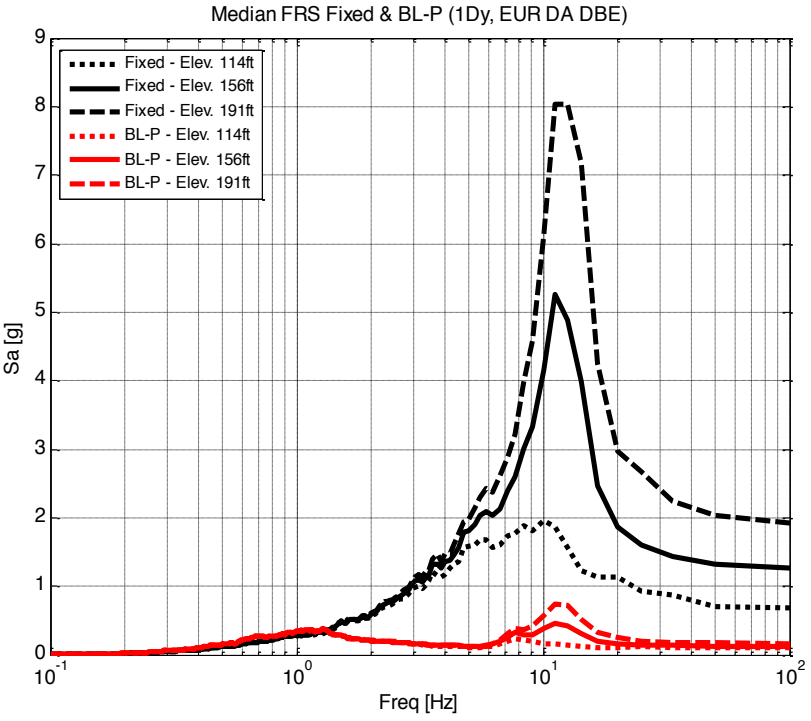

(b)

Figure 4.8 Median FRS for Primary Shield Wall with Fixed base and Bilinear Plasticity Elastomeric for DBE for (a) H1 Component and (b) H2 Component.

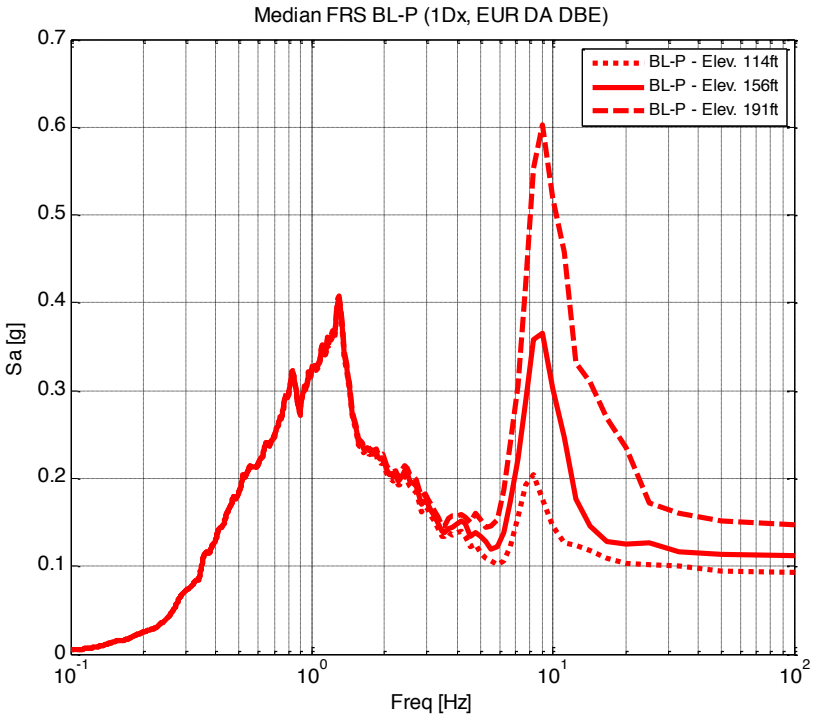

(a)

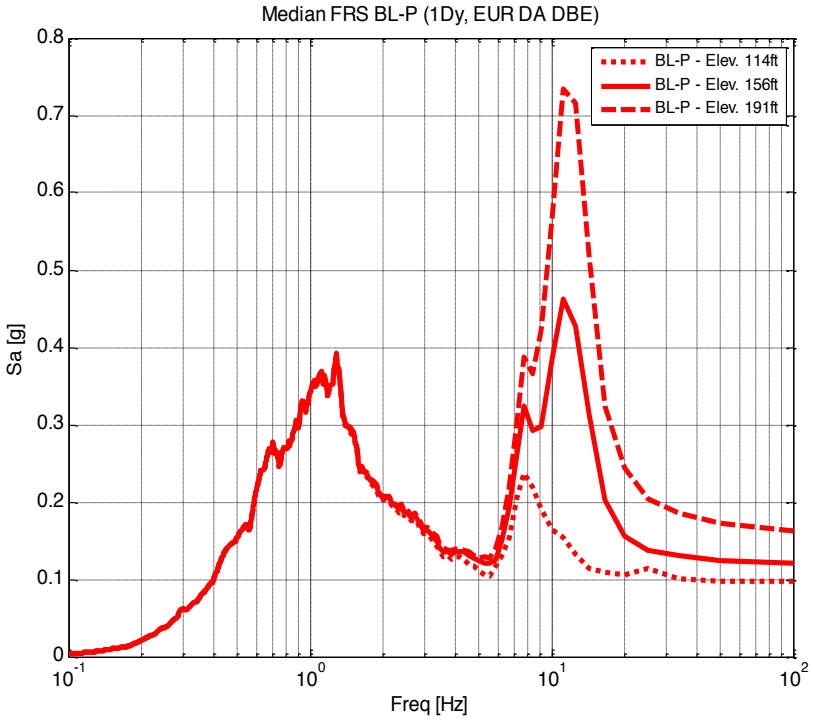

(b)

Figure 4.9 Median FRS for Primary Shield Wall with Bilinear Plasticity Elastomeric for DBE for (a) H1 Component and (b) H2 Component.

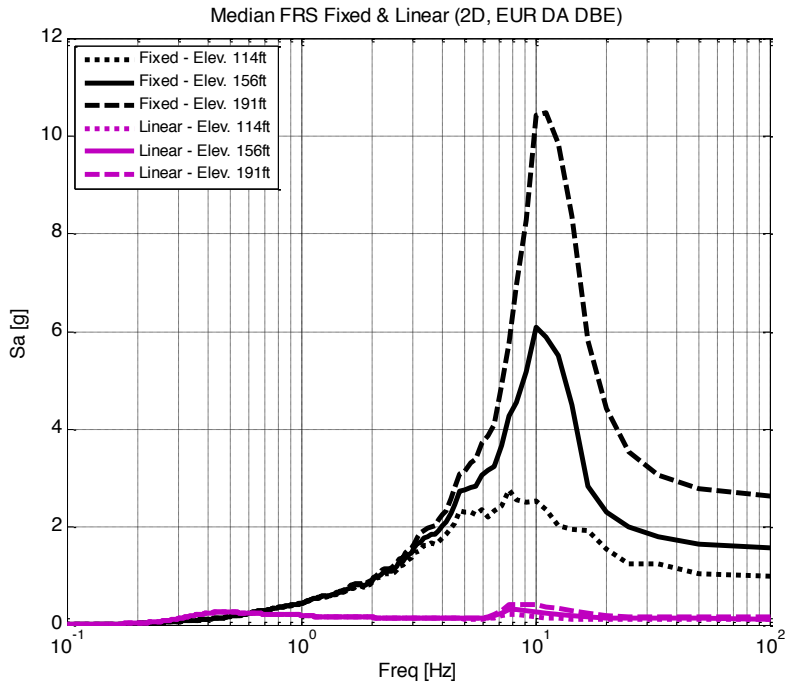

(a)

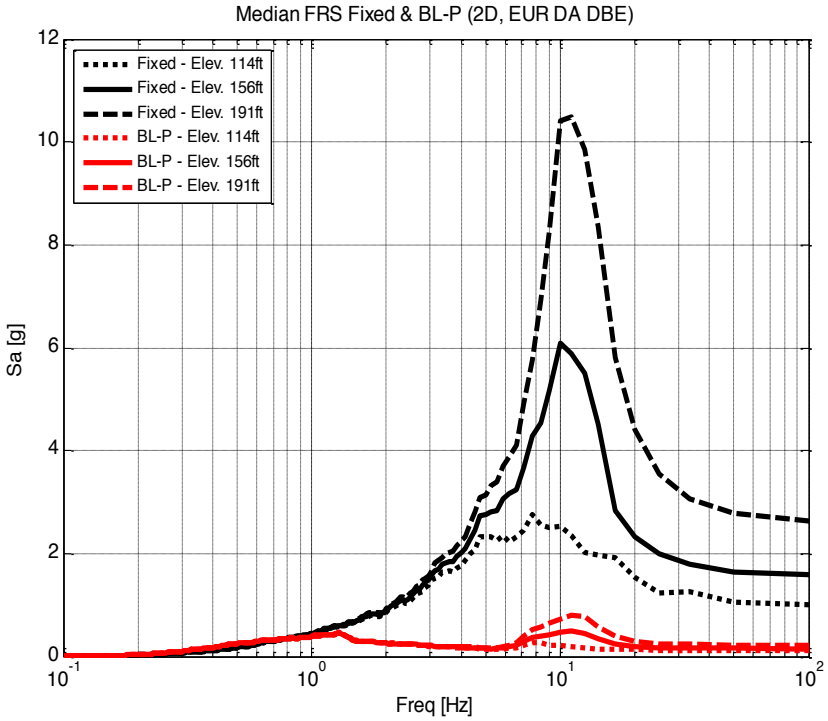

(b)

Figure 4.10 Median FRS of Primary Shield Wall for Fixed base and Isolated Cases for DBE H1 and H2 Components using (a) Linear Elastomeric and (b) Bilinear Plasticity Elastomeric.

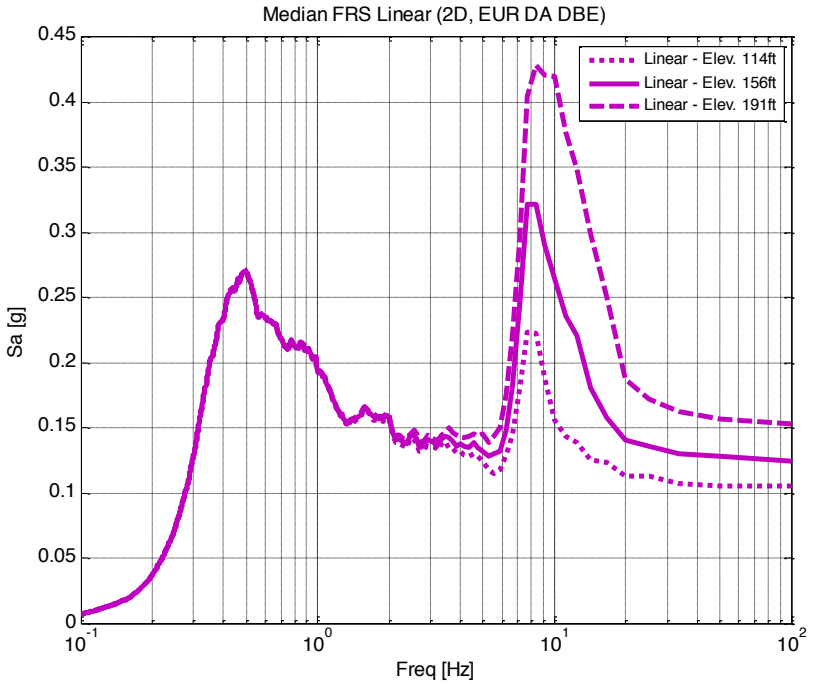

(a)

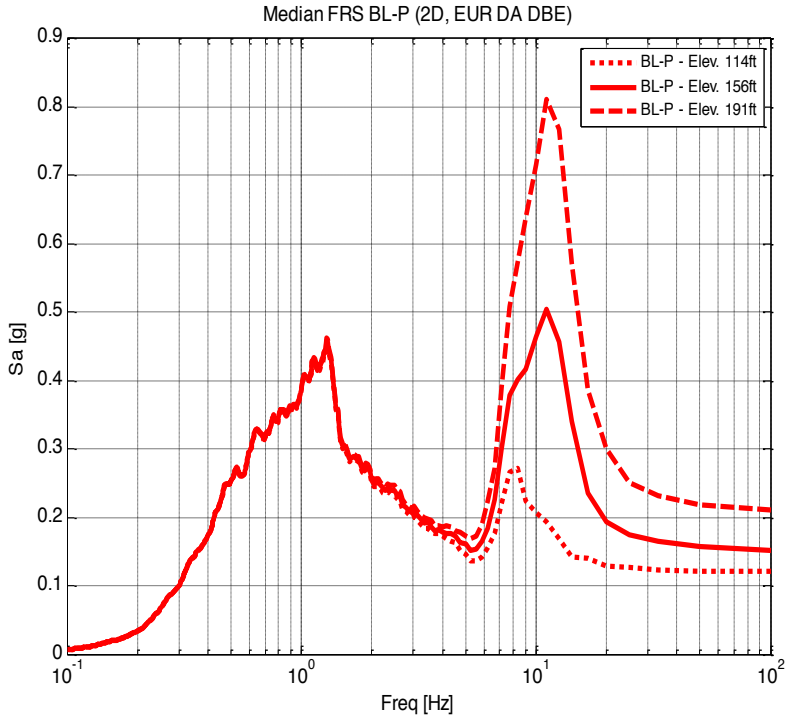

(b)

Figure 4.11 Median Isolated FRS of Primary Shield Wall for DBE H1 and H2 Components using (a) Linear Elastomeric and (b) Bilinear Plasticity Elastomeric.

5 Study 2: Understanding Effect of Isolator Hysteretic Characteristics on Performance

5.1 INTRODUCTION

This study investigates the effect of different isolator models on response by examining isolator hysteresis and changes in response due to variations in model parameters.

5.2 RESULTS

5.2.1 Hysteresis and Displacements

Isolator displacements are another major response parameter to consider because they influence design of the isolator and the seismic gap size. Here, we consider two horizontal components of motion. As before, rotations of the structure at the isolation plane about vertical and horizontal axes are not permitted. As seen in Table 5.1 the isolator's maximum displacement is approximately 3 in. and 4.5 in. for the DBE and EDB, respectively. The design had targeted a DBE displacement of 5.9 inches.

About the same displacement demand is computed for all of the isolation systems. The linear elastomeric bearing undergoes the highest displacement for the DBE; however, it undergoes the least displacement for the EDB. The ratio of the bearing displacement at the EDB and DBE levels is 1.08 for the linear bearing and 2.25 for the nonlinear bearings. The increase in the displacement of the linear bearing is less than the ratio used to increase the amplitude of the ground shaking. However, the displacement of the nonlinear bearing in this case is disproportionately larger than the increase in ground acceleration.

Table 5.2 lists the maximum isolator forces at the two excitation levels. The envelope curves for each bearing type differ so that at the same displacement, each develops a different lateral force. For instance, at the DBE level, the linear bearing has a displacement that is 8% more than the others but its maximum force is 25% less. At this excitation level, the Bouc-Wen and bilinear plasticity models predict the same displacement as predicted for the simple friction model, but the simple friction model develops about 10% more force. This behavior is due to differences in the actual strength and stiffness properties of the bearings even though they have the essentially the same effective period and damping. As the excitations increase 67% in going from the DBE to the EDB excitation level, the displacements increase by a factor of 1.08 to 2.25, but the forces increase by smaller factors (1 to 1.56).

The various figures below show representative hysteresis loops for the linear (with supplemental damping) and bilinear plasticity bearing models at the DBE level of excitation under unidirectional excitation.

Additional results are presented in Appendix B.

Table 5.1 Median Isolator Displacements for DBE and EDB Level Excitation considering two horizontal components of the EUR motions (1 inch = 2.54cm)

Isolator	H1 & H2 (DBE) [in.]	H1 & H2 (EDB) [in.]	Ratio of EDB to DBE Disp.
Linear	3.90	6.51	0.60
Bilinear Plasticity	3.43	6.83	0.50
Bilinear Bouc-Wen	3.42	6.93	0.49
Simple Friction	3.03	6.81	0.45

Table 5.2 Median Isolator Forces for DBE and EDB Level Excitation considering two horizontal components of the EUR motions (1 k = 4.448 kN)

Isolator	H1 & H2 (DBE) [k]	H1 & H2 (EDB) [k]	Ratio of EDB to DBE Disp.
Linear	9.45e4	1.58e5	0.60
Bilinear Plasticity	1.04e5	1.62e5	0.64
Bilinear Bouc-Wen	1.04e5	1.63e5	0.64
Simple Friction	9.78e4	1.60e5	0.61

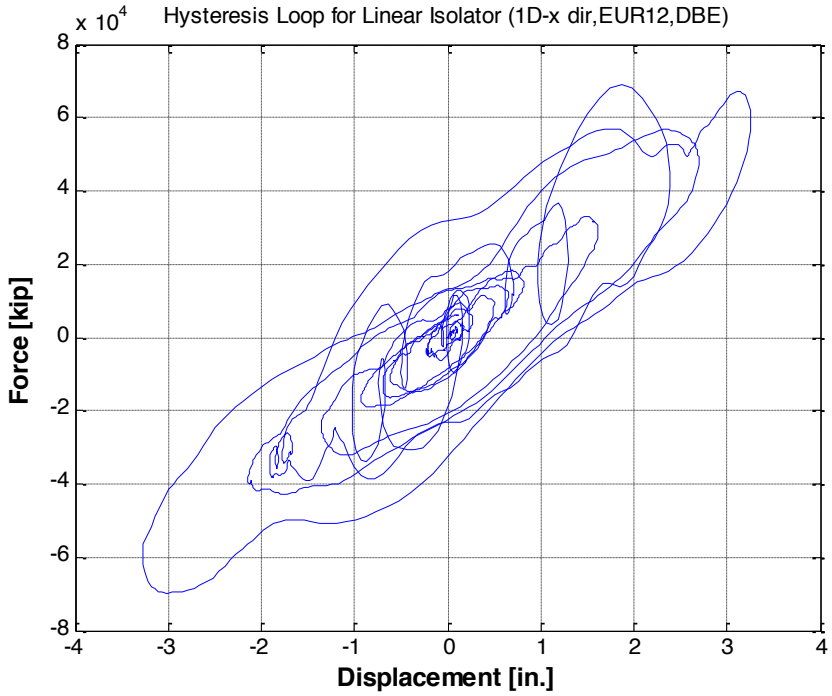

Figure 5.1 Linear Elastomeric Hysteresis for DBE for x and y Directions (H1 Component of EUR Ground Motion 12).

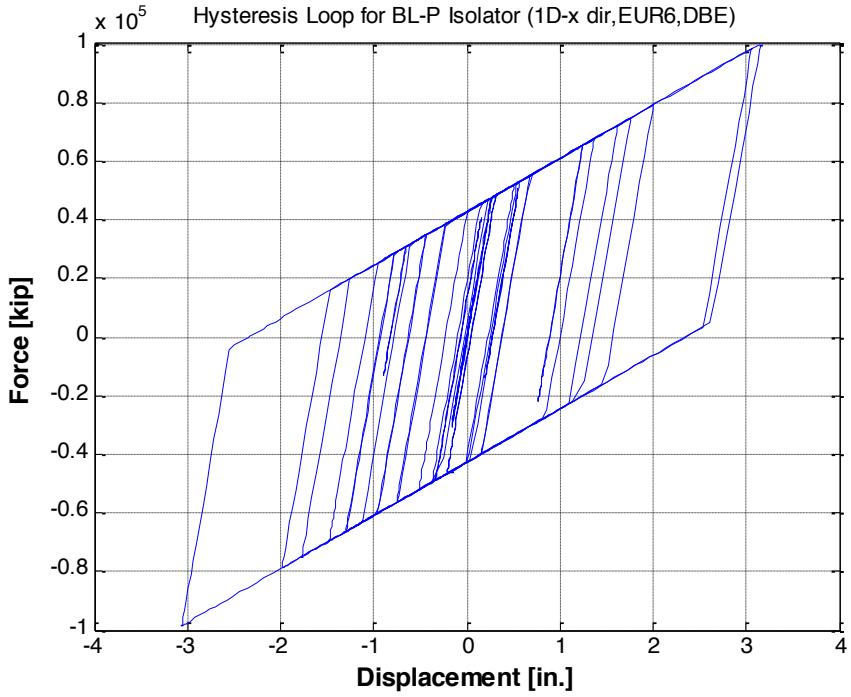

Figure 5.2 Bilinear Elastomeric Hysteresis for DBE for x and y Directions (H1 Component of EUR Ground Motion 12).

5.2.2 Bilinear Elastomeric Models

Results from Study 1 suggest the isolation model influences response in terms of amplitude of response and high frequency content. This section explores the influence of specific isolator parameters on performance.

For the case of FRS for the NPP supported on the bilinear models, two models are considered: plasticity and Bouc-Wen. From Study 1, the FRS were relatively similar for these two models except the bilinear model was higher at a couple locations along the frequency range. To examine the behavior in more detail, a single cycle of hysteresis is plotted during the 5 to 7 second range of the time history of response to the H1 motions in the x direction. The selected ground motion generated the closest values to the median displacement and force of the set. The hysteretic loops are for the bearing horizontal shear and displacement in the x direction. These segments, shown in Figure 5.7 to Figure 5.9, have color-coded nodes to allow matching between the hysteresis and the time history.

Based on this set of ground motions, the variation between the two responses is not as easily visible. The current parameters of the isolation along with the frequency content of the ground motion do not amplify the differentiation between the responses.

To better observe the difference in performance of these isolators, another ground motion was investigated. This motion was provided by KEPCO E&C. For this time history, two 3-component records were available. Each three-dimensional (3D) record consisted of three components (2 horizontal, 1 vertical). One of the records was developed to be spectrally matched to the response spectrum stipulated by the EUR and the other was spectrally matched based on the US NRC RG 1.60 design response spectrum. In each case, 5% damping and a peak ground acceleration of 0.5g was considered. Each time history is 20.48 seconds long.

In Figure 5.6, the time histories of the two ground motions are shown. The KEPCO motion has a higher level of high frequency content throughout the entire time span. This ground motion will present a more amplified response in the isolation, which will enhance the ability to observe the changes in performance between the specific isolators. This is done while maintaining the current isolator design parameters.

The hysteretic loops are for the bearing horizontal shear and displacement in the x direction. These segments, shown in Figure 5.7 to Figure 5.9, have color-coded nodes to allow matching between the hysteresis and the time history.

Observing the displacement time histories, there is negligible difference between responses with the two models. The two models result in the essentially the same isolator displacement histories. While the isolator displacement histories are rather smooth with a long period characteristic frequency (about 1 Hz in this window), the acceleration time history follows the same general trend but a high frequency oscillation is superimposed. These high frequency oscillations can be tracked to the time when the bearing transitions between elastic and post-yield behavior, and vice versa. At the yielding point for the bilinear plasticity model, there is an initial spike in the acceleration to approximately 0.02g. The amplitude of the subsequent cycles of oscillation in the acceleration history decrease rapidly with time (due to damping in the bearings). The amplitude of the oscillation is more severe for the bilinear model than for the Bouc-Wen model. The presence of these oscillations in responses of isolated systems with significant damping has been noted previously and the causes of the oscillations have been postulated (e.g., Morgan and Mahin, 2011).

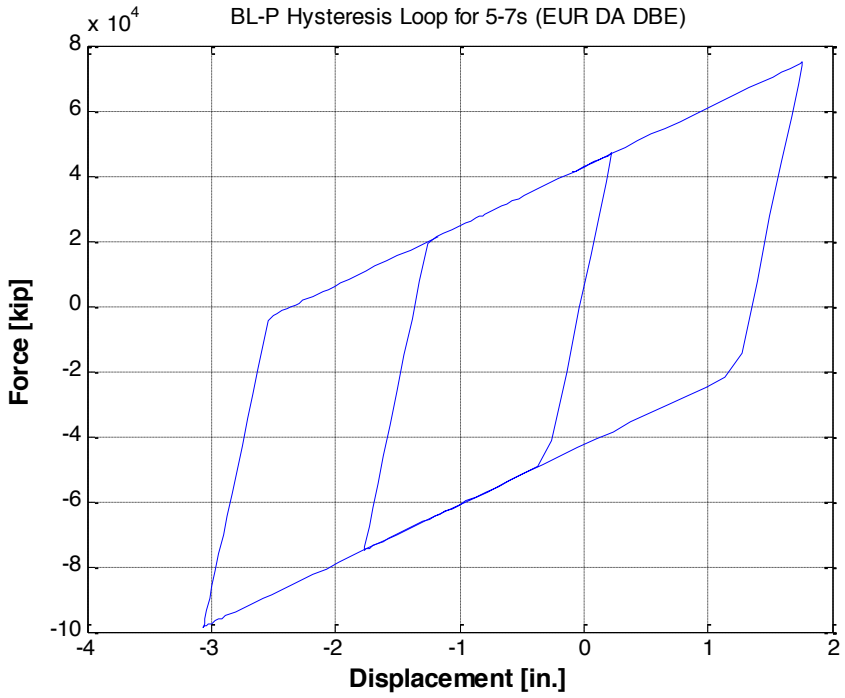

(a)

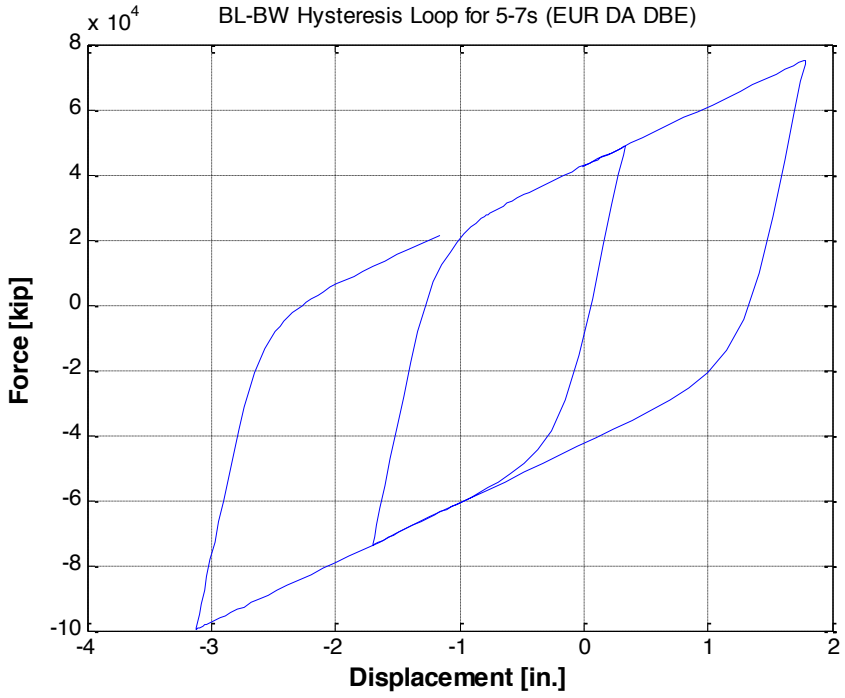

(b)

Figure 5.3 Hysteresis in x Direction for (a) Plasticity Model and (b) Bouc-Wen Model for 5-7s Time Range (H1 and H2 Ground Motion Components).

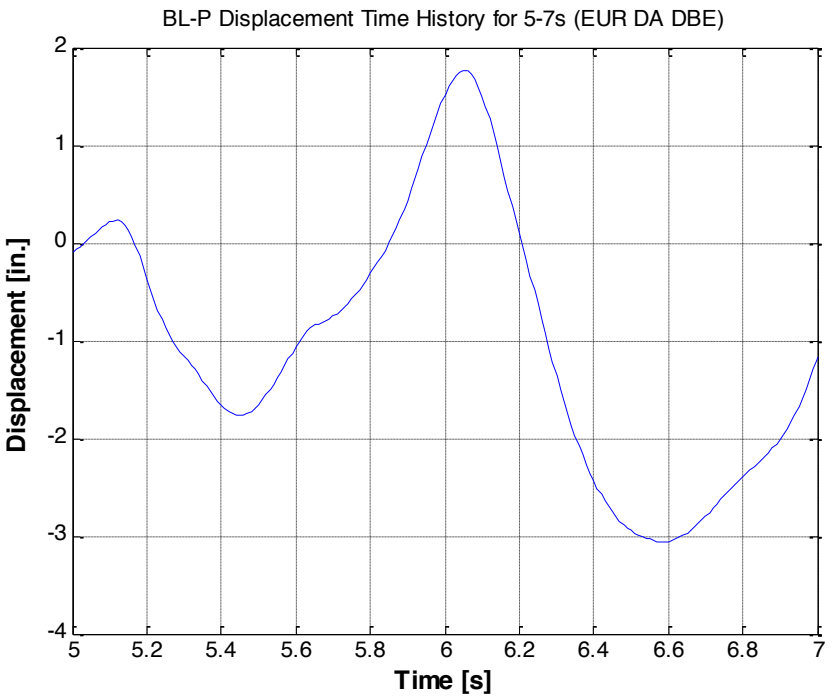

(a)

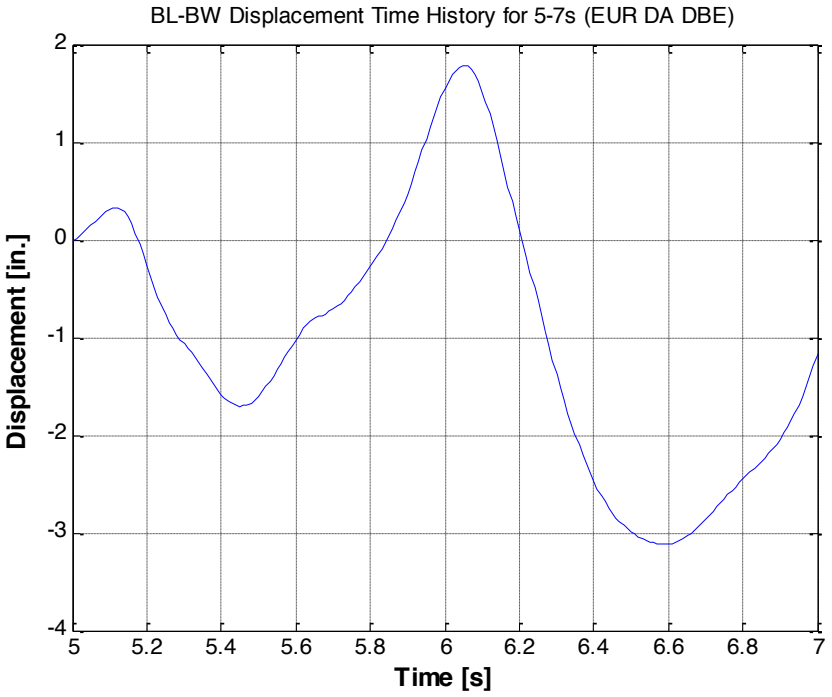

(b)

Figure 5.4 Isolator Displacement Time Histories in x Direction during 5 to 7s for (a) Plasticity and (b) Bouc-Wen Models (H1 and H2 Ground Motion Components).

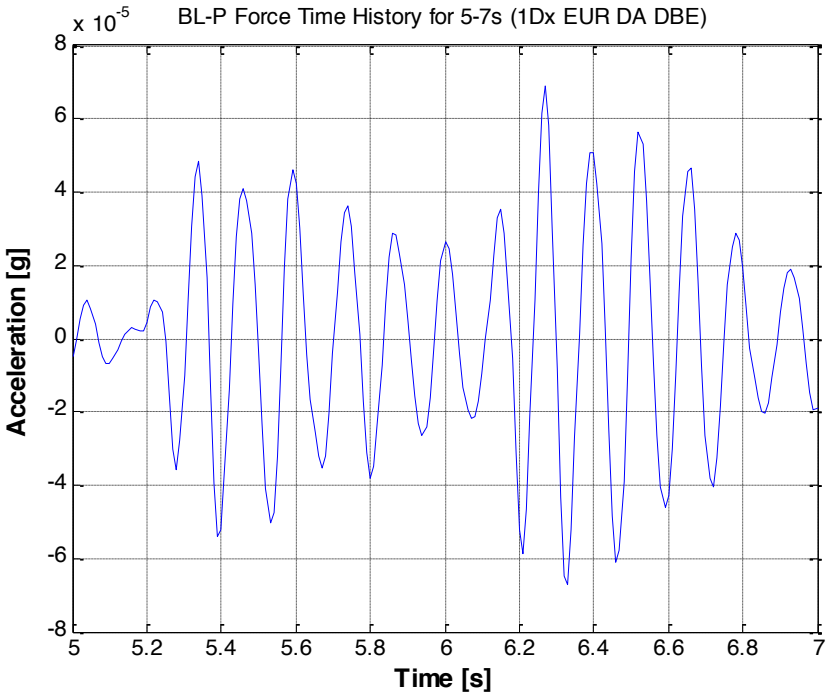

(a)

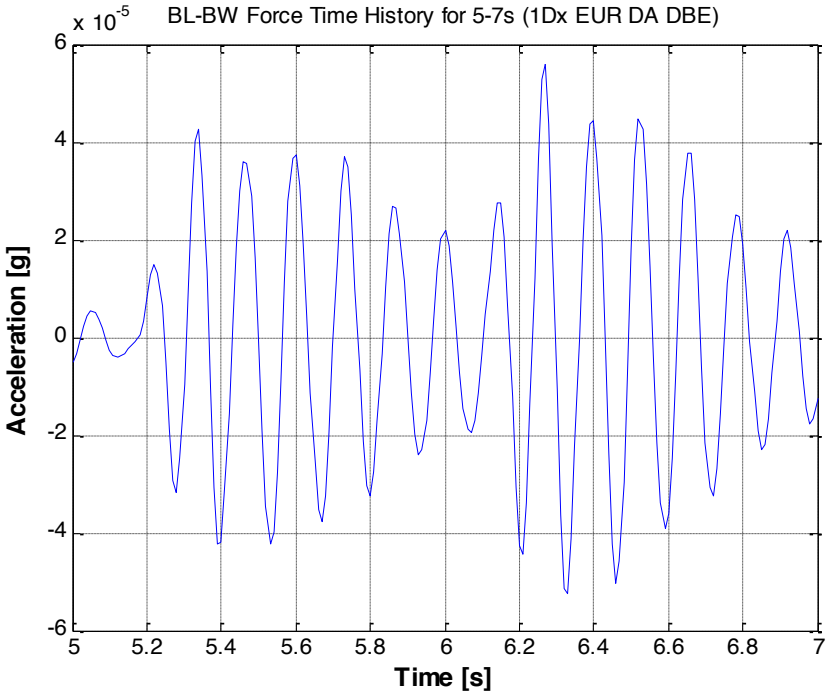

(b)

Figure 5.5 Acceleration Time Histories in x Direction during 5 to 7s for (a) Plasticity and (b) Bouc-Wen Models under (H1 and H2 Ground Motion Components).

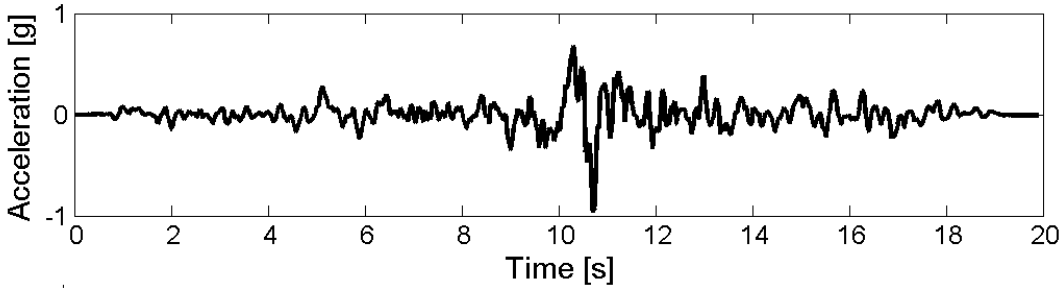

(a)

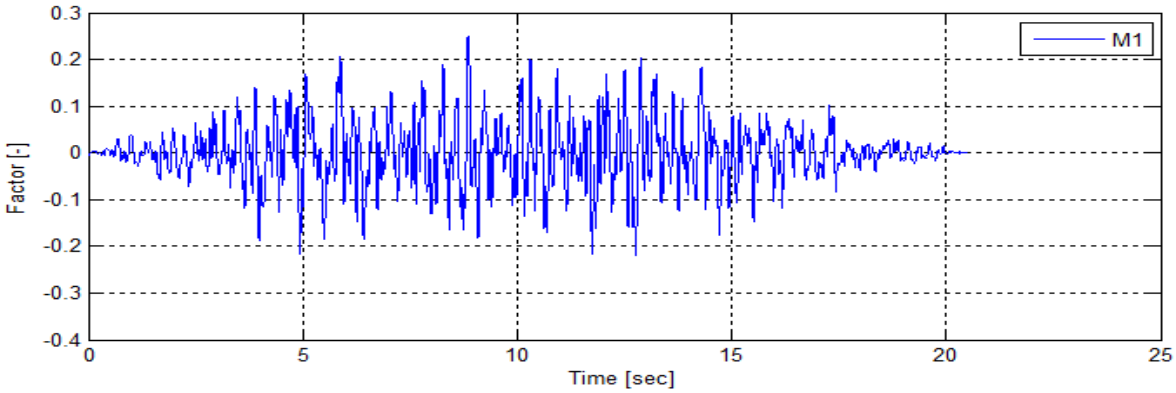

(b)

Figure 5.6 Time History in the X direction for (a) Baker Motion (GM6) and (b) EUR KEPCO Motion.

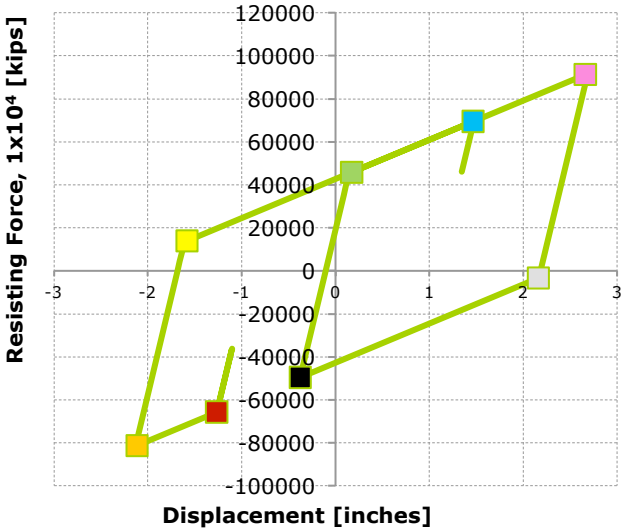

(a)

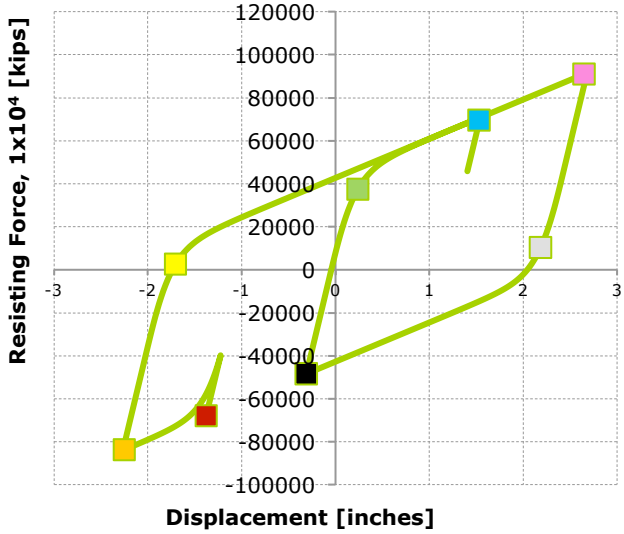

(b)

Figure 5.7 Hysteresis in x Direction for (a) Plasticity Model and (b) Bouc-Wen Model for 5-7s Time Range (H1 and H2 Ground Motion Components).

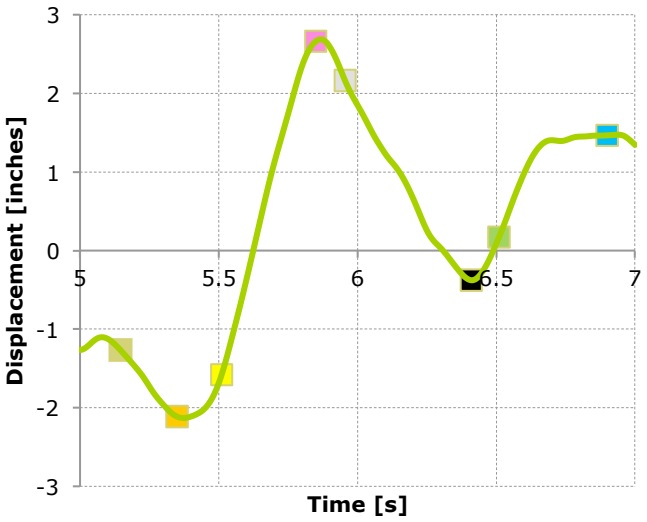

(a)

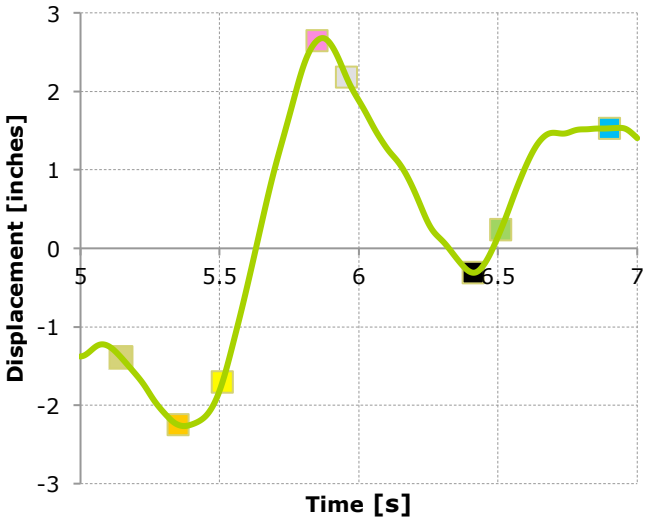

(b)

Figure 5.8 Isolator Displacement Time Histories in x Direction during 5 to 7s for (a) Plasticity and (b) Bouc-Wen Models (H1 and H2 Ground Motion Components).

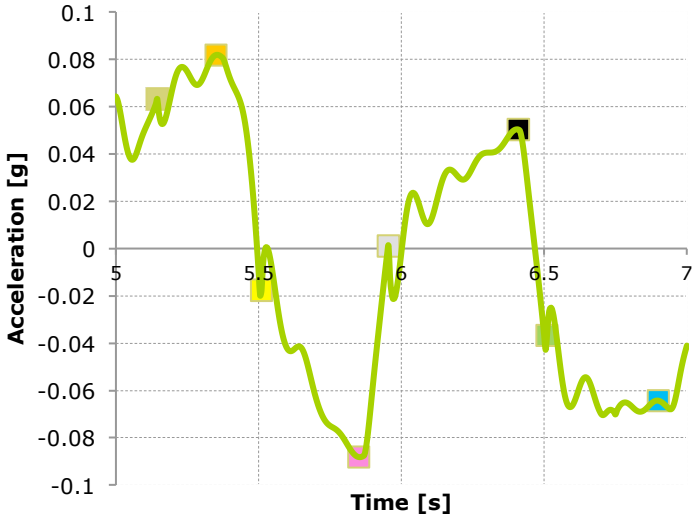

(a)

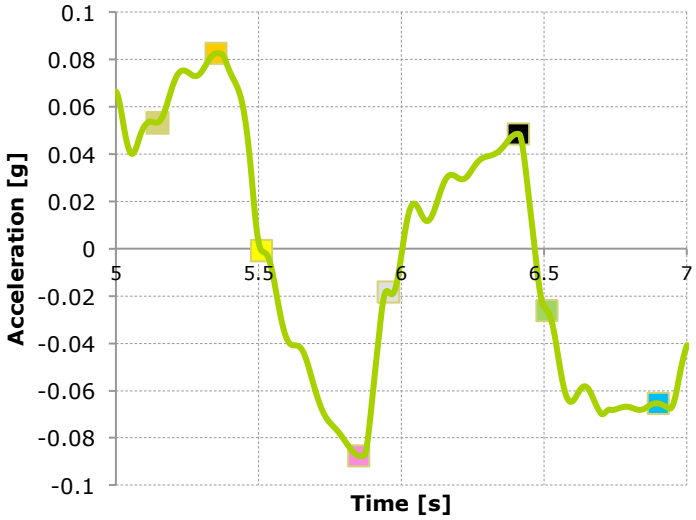

(b)

Figure 5.9 Acceleration Time Histories in x Direction during 5 to 7s for (a) Plasticity and (b) Bouc-Wen Models under (H1 and H2 Ground Motion Components).

These results confirm a difference in response between the bilinear and Bouc-Wen models, but the differences in the acceleration time histories at the top of the isolation plane may not be significant enough to justify the observed difference in the FRS for these systems.

5.2.3 Bouc-Wen Study

The next step in this study investigates how changes in the Bouc-Wen model parameters alter response. This section explores variations in the η value, which controls the roundness of the Bouc-Wen model at the point of yielding. The values of η considered are: 0.25, 0.5, 1.0, 2.0, 4.0 and 8.0. Below 1.0, the roundness of the model may be larger than feasible considering actual isolator hysteresis loops that have been observed in experimental tests. Values less than one were included in this study to get better insight into the effect of η on response. Increasing η progressively moves to a model similar to the bilinear plasticity model. As done for the previous study, the KEPCO E&C horizontal EUR ground motion at the DBE level of excitation was used.

Figure 5.10 to Figure 5.12 present the hysteresis loops for the different Bouc-Wen model parameter values considered. The maximum displacement and force is the same for all cases shown. However, with increasing η the transition from elastic behavior to yielding becomes less gradual.

For Figure 5.13 to Figure 5.16, short segments of the displacement and acceleration time histories are shown for each model. As seen in the previous study, the displacement time history shows negligible differences. Around 5.5 second into the record, the plots show some variation based on the η value, however, the overall maximum displacement remains the same. In terms of acceleration time history, the η values produce three instances of high frequency content. As the isolator moves closer to a bilinear plasticity model (i.e., as η increases), the prominence of the high frequency content increases as highlighted in Figure 5.15. With the decrease in η value, these points of high frequency are almost completely removed. However, the maximum acceleration amplitudes associated with these oscillations at these points is on the order of 0.02g for even large values of η.

Figure 5.17 to Figure 5.19 present the FRS for the η values examined. Higher values of η yield slightly higher spectral accelerations and high frequency content at specific frequencies near the fundamental frequency of the supported structure. The overall maximum spectral acceleration around 1 Hz remains constant. However, between 1 and 10 Hz, the amplitude of pseudo-accelerations in the FRS increases with η value along with an increased localized peak spectral pseudo-acceleration at around 10 Hz. Decreasing η reduces accelerations by approximately 20%. However, the high frequency content remains in an amplitude range of possible concern for components and equipment. Reducing the η value (sharpness of the transition to and from bearing yielding) shows some but not an unduly large improvement in the FRS. Isolator displacement appears to remain constant with very little influence from η parameter used in the model. Thus, to better understand and possibly reduce the peak in the FRS near the fundamental period of the supported structure, other parameters related to the mechanical properties of the bearing need to be considered.

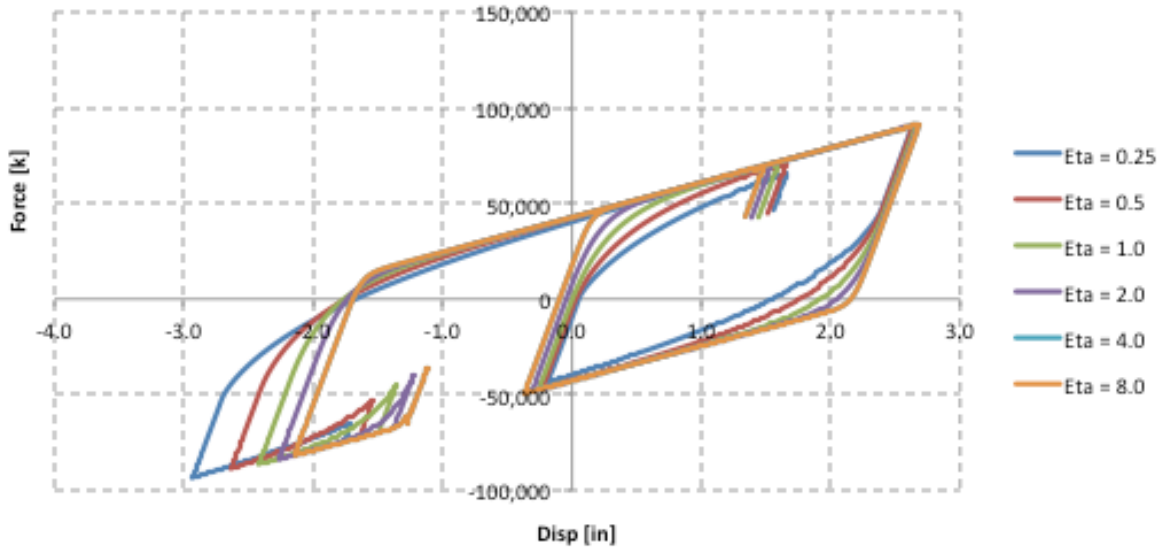

Figure 5.10 Hysteresis Loops for All η Values.

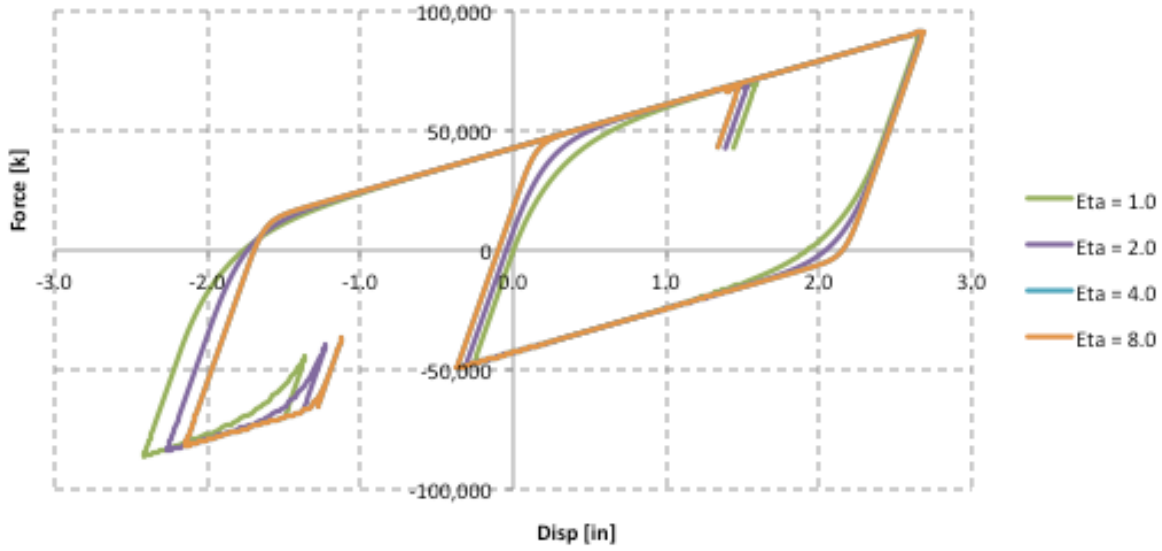

Figure 5.11 Hysteresis Loops for η = 1.0, 2.0, 4.0 and 8.0.

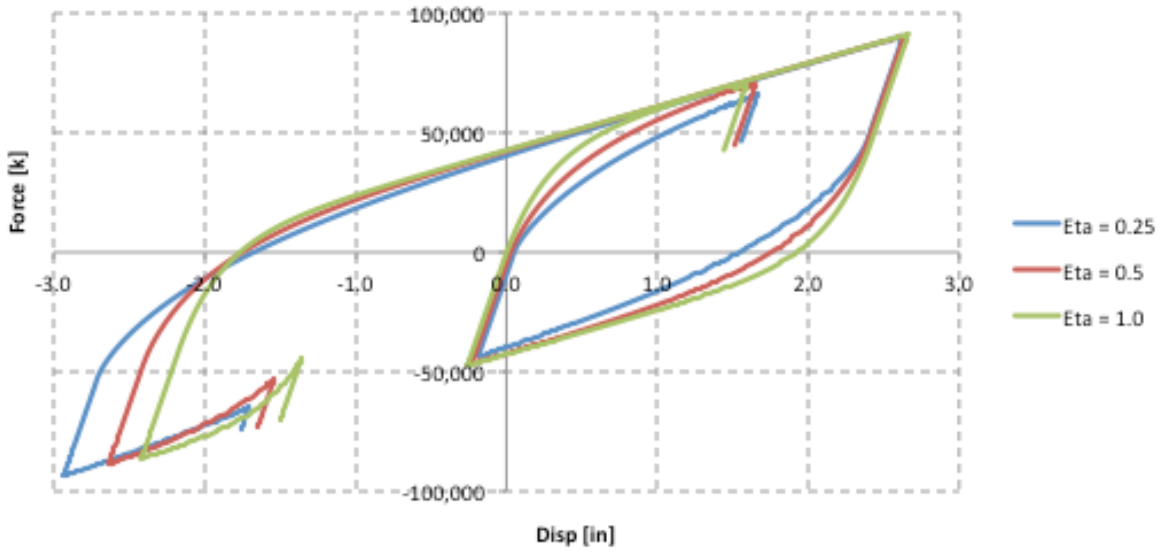

Figure 5.12 Hysteresis Loops for η = 0.25, 0.5 and 1.0.

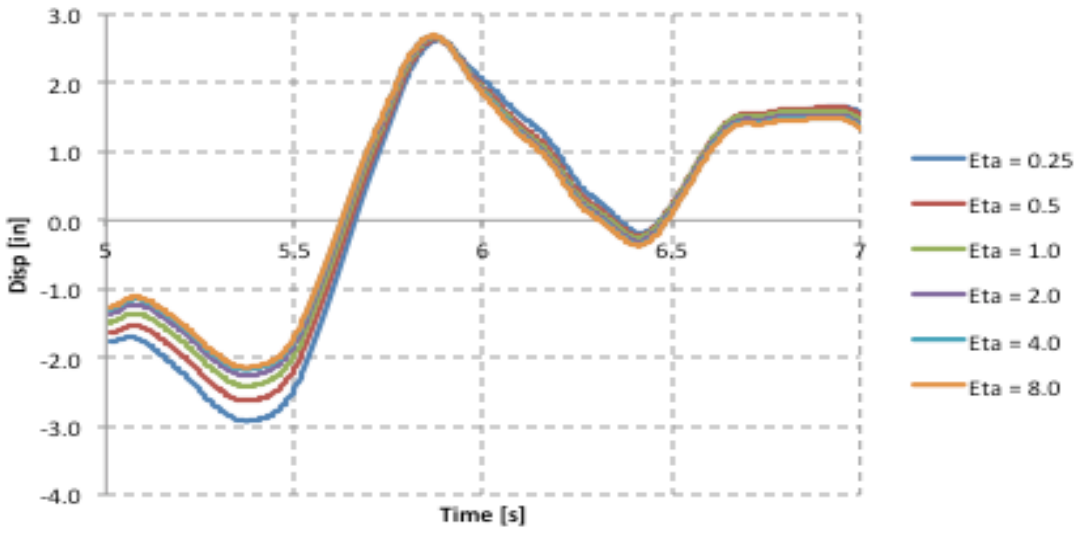

Figure 5.13 Displacement Time History Segment for η Values.

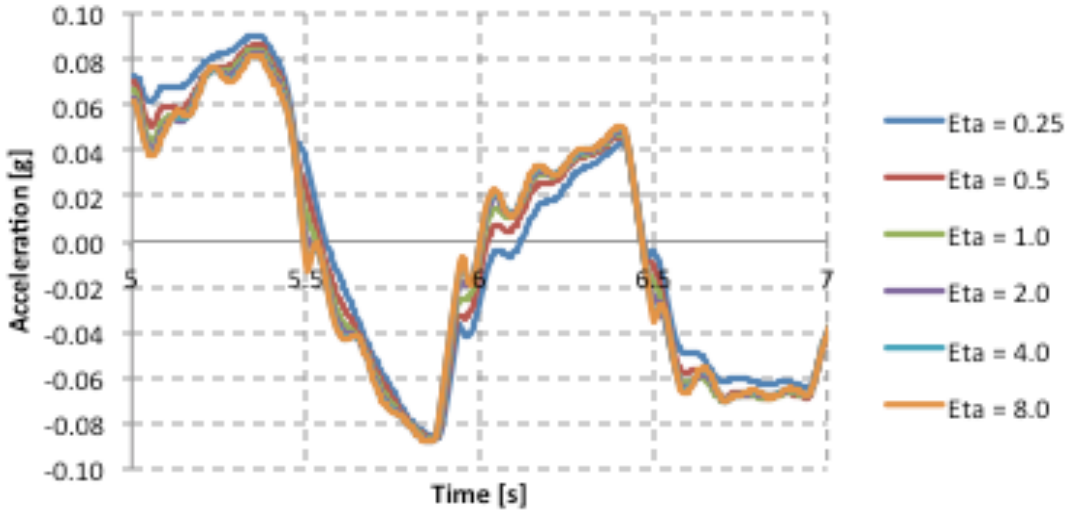

Figure 5.14 Acceleration Time History Segment for All η Values.

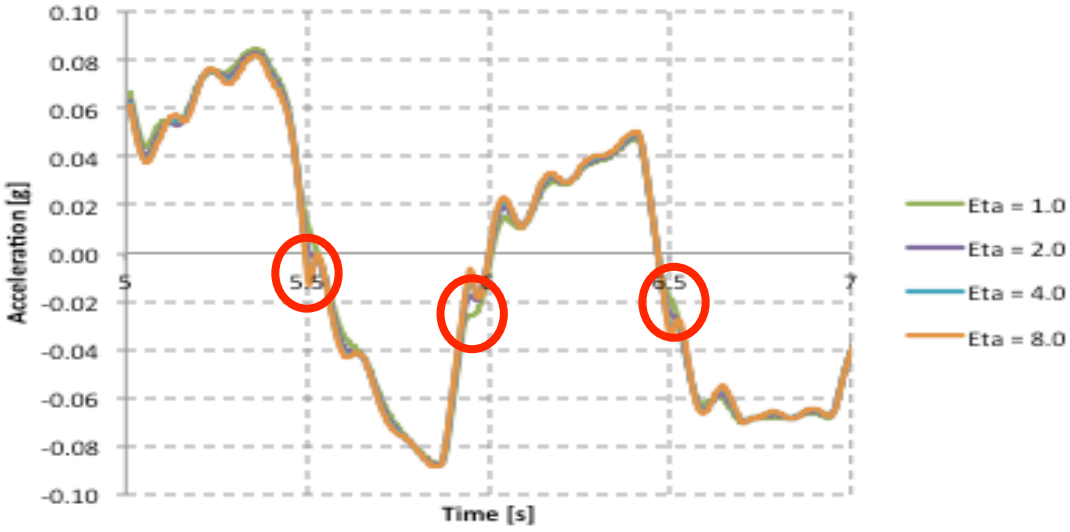

Figure 5.15 Acceleration Time History Segment for η = 1.0, 2.0, 4.0 and 8.0.

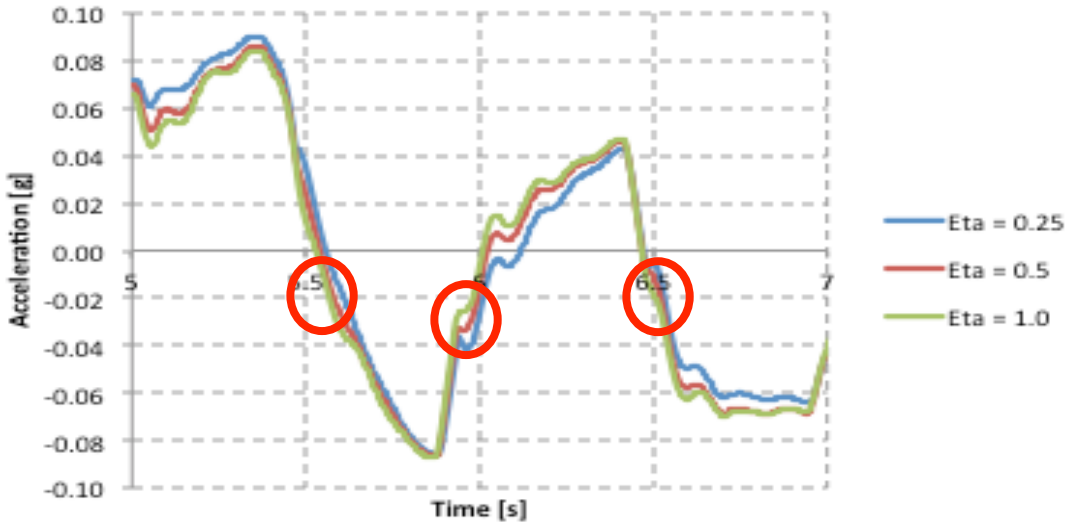

Figure 5.16 Acceleration Time History for η = 0.25, 0.5 and 1.0.

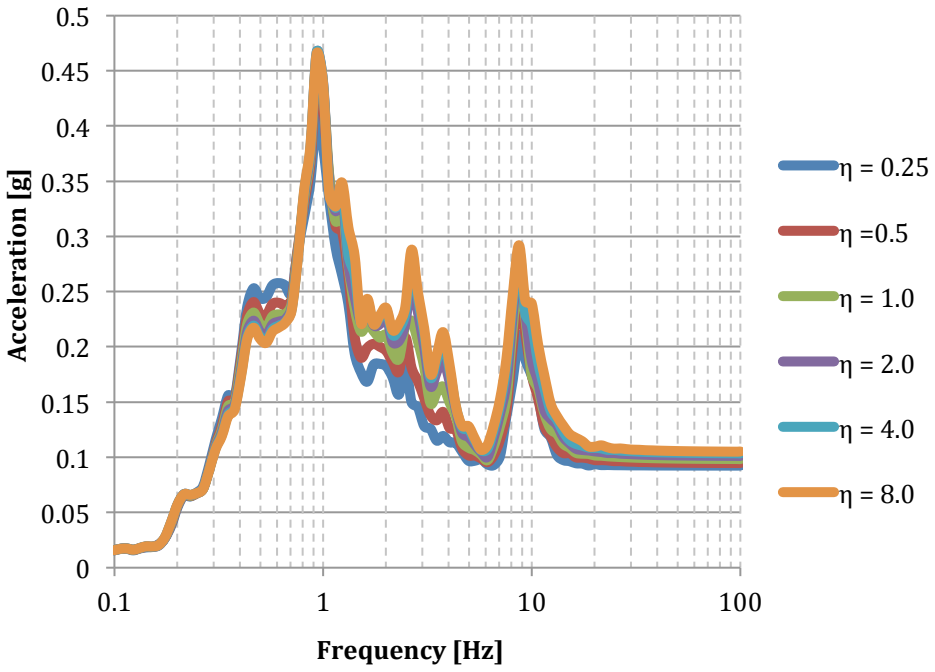

Figure 5.17 FRS at Elev. 156' of Primary Shield Wall for All η Values.

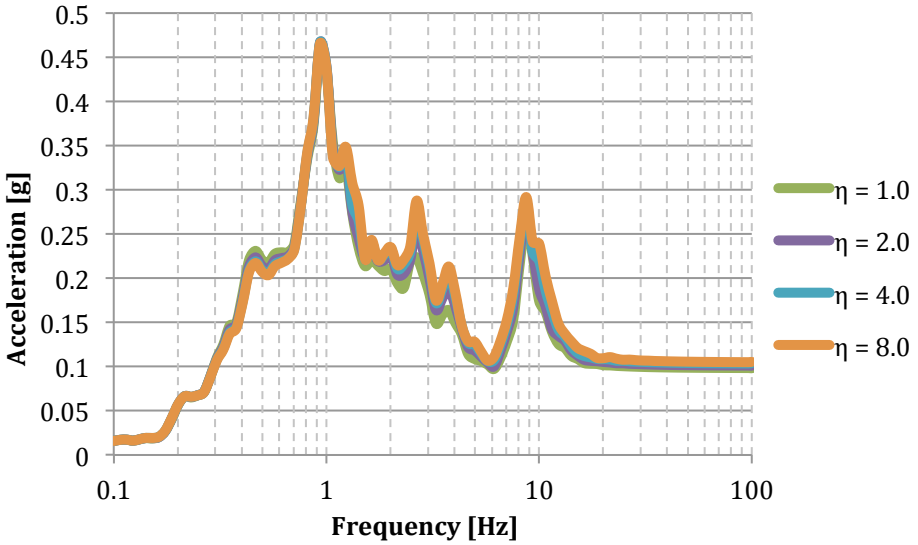

Figure 5.18 Acceleration Time History for η = 1.0, 2.0, 4.0, and 8.0.

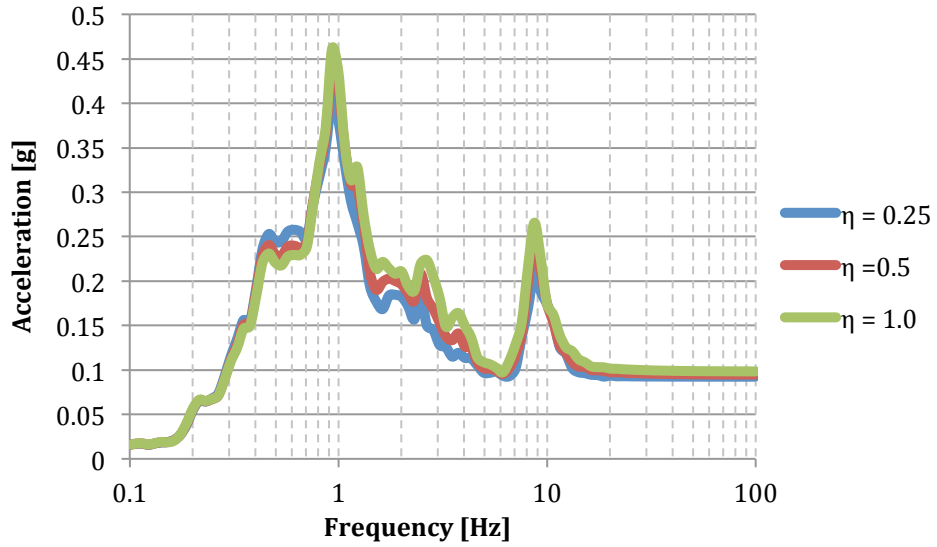

Figure 5.19 Acceleration Time History for η = 0.25, 0.5 and 1.0.

5.2.4 Sensitivity Analysis

The analyses in this sub-section seek to identify nonlinear isolator properties having the greatest influence on the FRS. For this study, key parameters are identified including initial stiffness (K_1) and isolator strength (Q_d) of the bilinear plasticity model.

To understand how parametric variations in these parameters influence response, a range of values is used. The original values for initial stiffness (K_1) are scaled to 25%, 50%, 100%, 200%, and 400% of the initial baseline values. The range of values for the isolator strength is scaled over a smaller range, to 90%, 95%, 97%, 100%, 103%, 105%, and 110%, compared to the

initial baseline values. Not all of the particular values and combinations of parameters may be realizable.

Figure 5.20 and Figure 5.21 show the results of this analysis for the bilinear plasticity model. From these plots, the greatest influence on FRS is from the initial stiffness. By shifting the value of the stiffness, the peak response decreases with a reduction in high frequency content. For example, by decreasing the initial stiffness, the peak acceleration in the high frequency range decreases significantly, especially near the natural frequency of the supported structure. However, while pseudo-accelerations decrease at high frequencies, the accelerations in the lower frequency range dominate. Thus, there is a tradeoff between having large pseudo-accelerations in the high or low frequency ranges. This tradeoff can be made considering the frequencies of critical components in the structure. A balanced design with relatively low pseudo-accelerations in the high and low frequency ranges appears to have a value of K_1 between 100% and 50% of the baseline values for the bilinear plasticity bearing model. It may be possible to also reduce the high frequency amplification of response near the natural period of the structure by a combination of reducing K_1 and providing a more gradual transition from the initial stiffness to the yield behavior (by reducing η in a Bouc-Wen type bearing model). By adjusting the physical dimensions and properties of the components in a BL-P or placing a SF-C bearing on a more flexible pedestal or using multistage pendulum friction bearings, it may be possible to optimize bearing properties to achieve FRS that will achieve performance desired for acceleration-sensitive components.

When the isolator yield strength (Q_d) increases, it can be seen in Figure 5.21 that the pseudo-accelerations increase slightly. In this case, only small variations in Q_d are considered. However, this illustrates that such small variations in the average properties of bearings that may result as a consequence of variations in material proprieties and manufacturing techniques may have little effect on FRS. Larger changes in Q_d, based on deliberate decisions in the design process should be explored, but other results (Morgan and Mahin, 2012) also suggest that bearing strength has limited effect on peak forces and accelerations. In the results presented, there is a small difference between the effects of altering strength. That is, for cases increasing strength, the FRS ordinates increase for frequencies greater than the effective frequency of the isolation system, but decrease slightly for frequencies less than the isolation frequency.

Based on these observations, adjusting the initial stiffness of the isolator is the most effective means of shifting the peak response of the FRS. Overall, there is a tradeoff between where the peak responses occur. Changing a modeling parameter tends to increase the FRS in one frequency range while decreasing it in another.

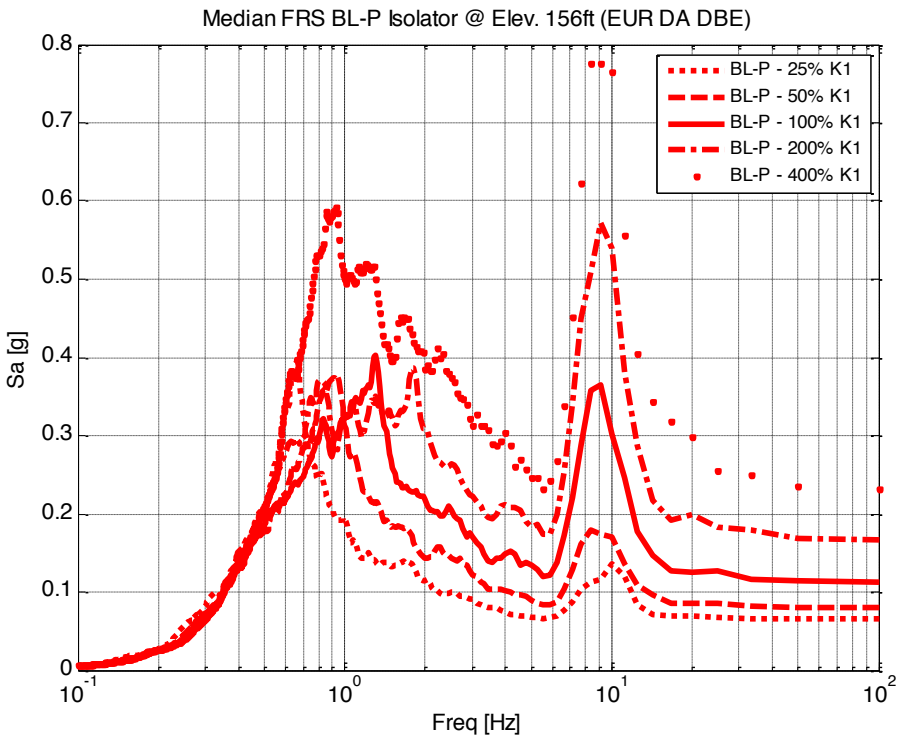

Figure 5.20 Median FRS with Initial Stiffness Variation (Elev. 156', DBE).

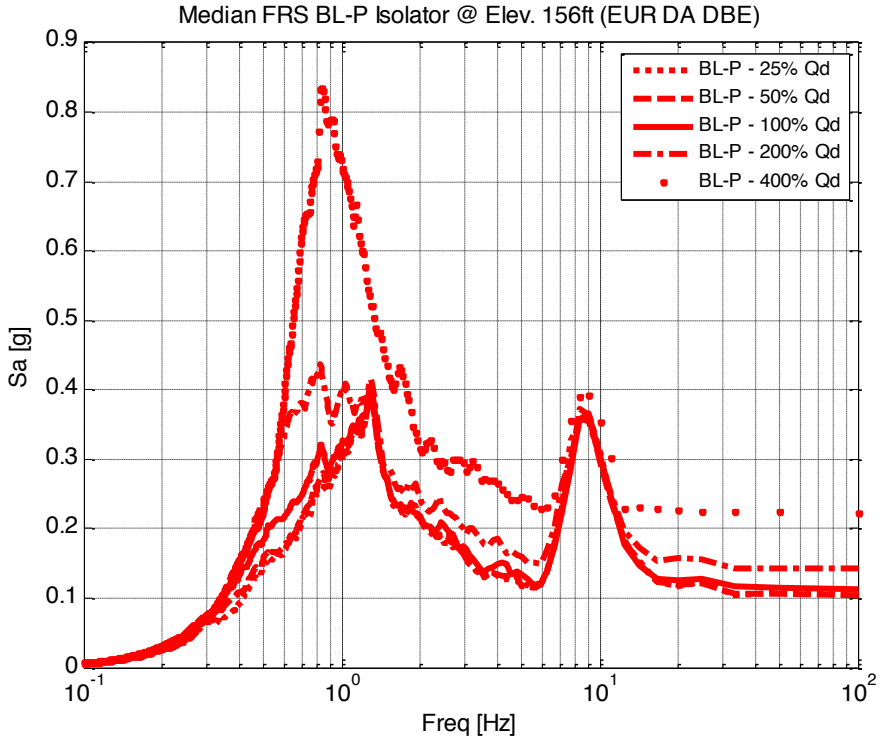

Figure 5.21 Median FRS with Isolator Strength Variation (Elev. 156', DBE).

5.3 CONCLUSIONS FOR STUDY 2

The studies covered in this section provide data and information on the isolation of the APR1400 plant for horizontal input motion.

Firstly, the isolator type and model characteristics affect the FRS. With nonlinear models, high frequency content is introduced into the system especially near the fundamental frequency of the isolator system and of the supported structure. The initial stiffness of the isolator has a large effect on the amplitude of the peaks in the floor spectra, followed by the post yield tangent stiffness and the roundness of the hysteretic loops. The results presented indicate that small changes in bearing strength, as might be seen during production of large numbers of bearings, does not have a substantial effect on the floor spectrum. Further study is needed to understand how the high frequency content that is introduced with nonlinearity can be reduced or adjusted.

Secondly, for the ground motion set considered, the selection of the bearing type and model did not have substantial effect on the peak bearing displacement. All of the bearings had essentially the same effective period and damping, but different $K_1$and Q_d values. As a result, the bearings developed different maximum shear forces. In particular, while K_1 had a very large effect on the FRS, it had little or no apparent effect on the peak isolator shear forces or displacements.

These studies on horizontal motion provide insight into a number of ways isolator parameters influence performance. The next studies explore how these results and trends change with the inclusion of vertical motion.

6 Study 3: Vertical Motion (Part A)

6.1 INTRODUCTION

The vertical component of motion is frequently disregarded in the design of buildings, including ones that are seismically isolated. The purpose of this study is to investigate how results from nonlinear analysis of different seismic isolation systems are affected by the use of vertical and vertical-horizontal ground motions.

6.2 ANALYSIS SET-UP

Research focuses on the 3D model of the APR1400 shown in Figure 6.1. The rigid mat foundation was removed and replaced with a brick element system consistent with the material properties of the concrete foundation. As a result, the model was allowed to experience pitch, roll, and torsion. The thickness of the mat varies from 10 ft underneath the auxiliary building to approximately 33 ft under the reactor building.[3]

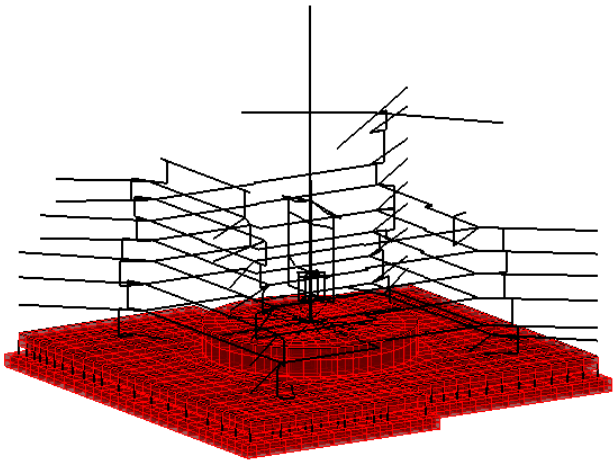

Figure 6.1 3D APR1400 OpenSees Model.

[3] Refer to, *Review and Improve Numerical Models*, Schellenberg et al. 2014 for additional details on the model definition in OpenSees.

Nonlinear response history analyses were conducted in OpenSees. Seismic motions were applied under two scenarios, vertical motions only and full three-dimensional motion, using all 20 Baker motions. The horizontal FRS are computed using SRSS to present the combined horizontal result. Several seismic isolation systems are considered in this study including linear bearings, bilinear elastomeric bearings and simple friction bearings.

6.3 RESULTS

As a first investigation, the model is subjected only to the vertical component of excitation. As seen in Figure 6.2, the vertical FRS for one location is chosen and plotted with the input motion (vertical only) and for the fixed base and isolated systems. For the fixed base system, the vertical floor spectrum is amplified for frequencies above 2 or 3 Hz compared to the input ground motion spectrum, with peaks at about 25 and 10 Hz. These peaks correspond to natural frequencies in the vertical and horizontal directions of the structure. For both NRC and EUR records, the bilinear models generally have higher pseudo-acceleration ordinates in the high frequency range than does the fixed base system. There is a noticeable peak acceleration around 14 Hz for the bilinear models. The vertically stiff friction bearings have spectral ordinates similar to or in some cases lower. Both bearings have some vertical stiffness that shift the vertical frequency of the structure away from 25 Hz and result for the friction bearings a significantly lower spectral response at this frequency.

These results contrast observations from horizontal only motions, which saw significant decreases in acceleration with isolation especially at the higher frequency range. This is because the isolation systems considered do not isolate in the vertical direction, but can shift the periods and perhaps amplify the response in the vertical direction.

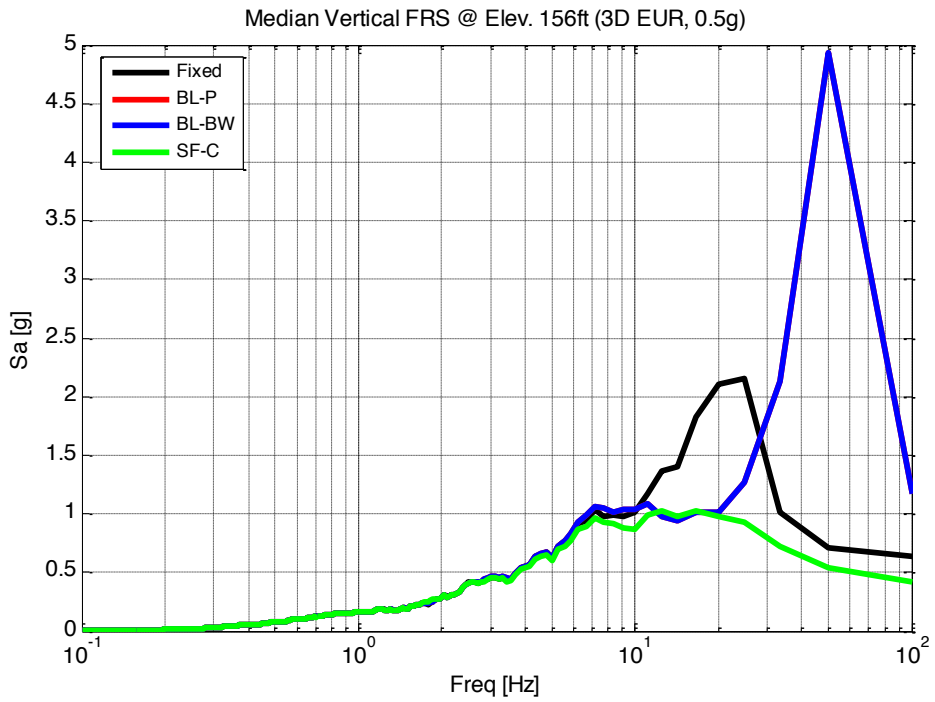

(a)

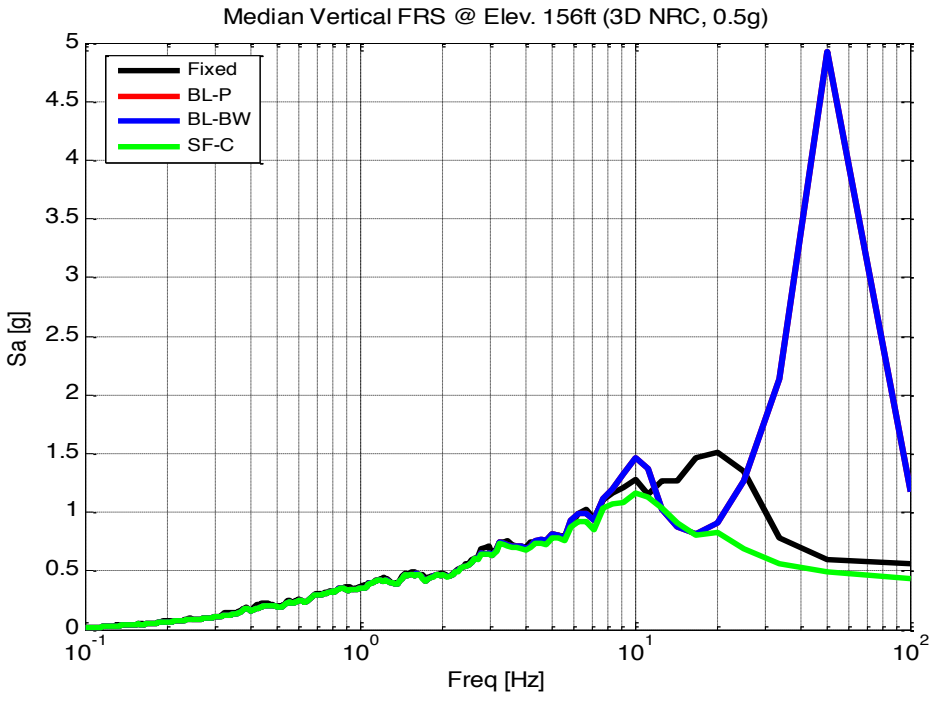

(b)

Figure 6.2 Median Vertical FRS in primary shield wall for different isolation types: vertical motion only (a) EUR and (b) NRC– elev. 156'.

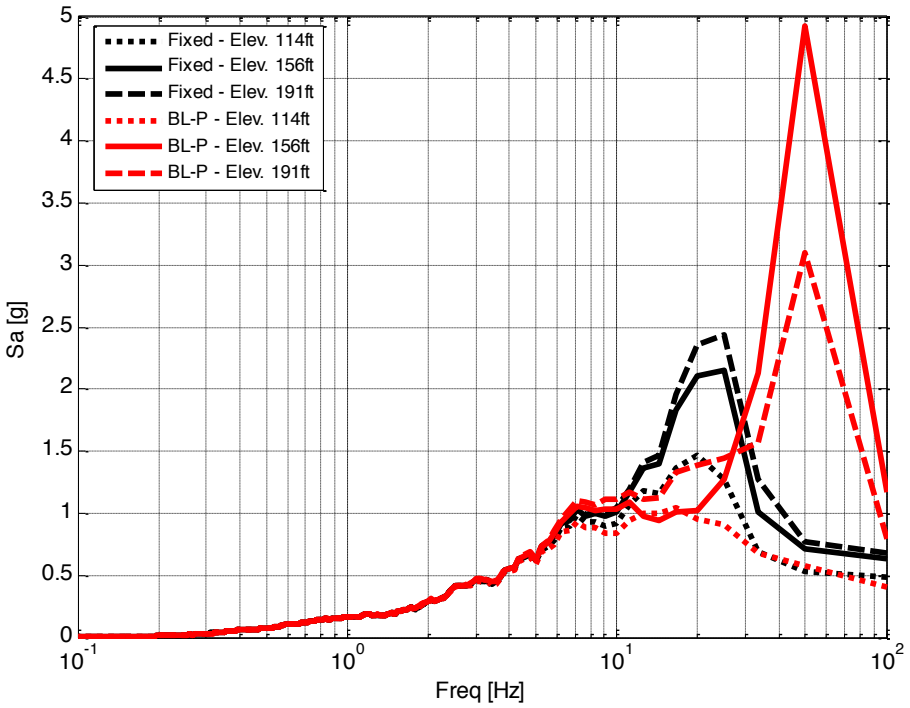

(a)

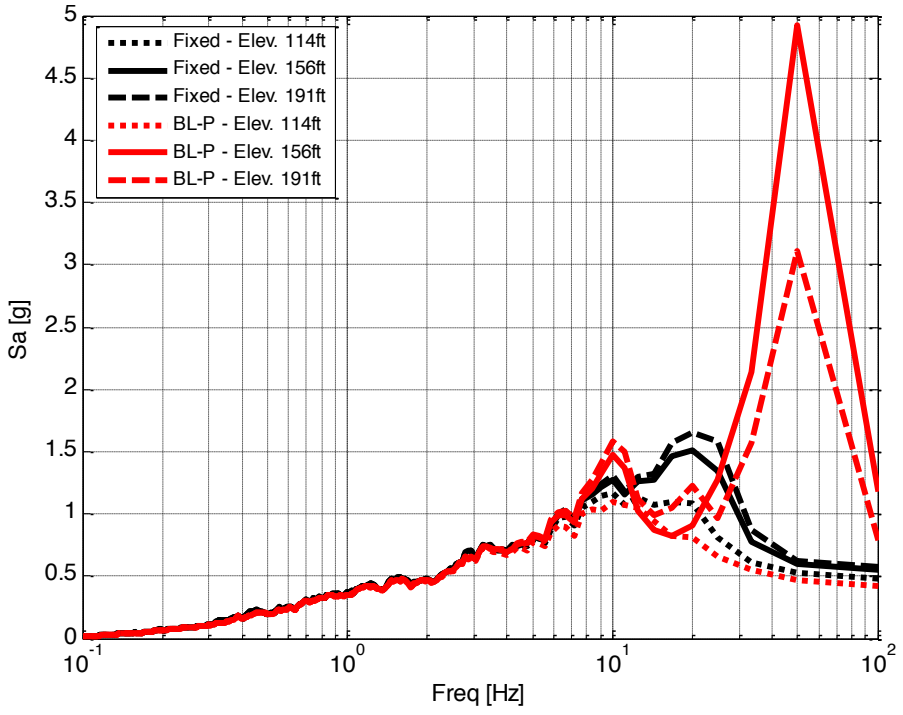

(b)

Figure 6.3 Median Vertical FRS at different elevations in primary shield wall: vertical motion only (a) EUR and (b) NRC.

The FRS are consistent for the three elevations in the primary shield wall shown in Figure 6.3. The spectra for the isolated and fixed base structures at all elevations are about nearly the same for frequencies below 10 Hz. For higher frequencies, the FRS for the isolated structure represented by the bilinear plasticity generally are larger than for the fixed base structure. The exception at the lowest elevation observed on the structure, where this isolation system reduces the spike in the FRS observed for the fixed base structure, especially when it is subjected to the NRC records. The other localized peaks in fixed base FRS, however, remain present and increased by isolation.

Next, the same analyses were carried out, but using two components of horizontal excitation combined with the vertical component. As seen in Figure 6.4 for the bilinear plasticity isolator, results show the vertical spectra for the horizontal-vertical motion are almost exactly the same as with vertical only motion.

Figure 6.5 to Figure 6.8 show the horizontal FRS for various scenarios. The fixed base case displays significant accelerations across the majority of the spectra. However, there is no significant difference between the spectra with the introduction of the vertical component of motion for the fixed base model.

For the isolated structures the FRS are sensitive to the isolation system and ground motion used. As will be seen later, the horizontal displacements and shears developed by the bearings vary even though both are anchored to a 0.5g PGA. In the plots below for the bilinear models, there is a clear impact of the inclusion of vertical motion around the frequency of the structure. At this frequency, the 3D motion results in higher spectral accelerations across the height of the structure. The increase ranges from 0.2g to 1.0g with the greatest increases occurring at the upper portion of the structure. This shows there is an impact on the horizontal FRS with the inclusion of vertical motion. As a result, the vertical component of motion cannot be ignored and should be included in FRS analysis to fully characterize the response of the structure at various elevations.

In contrast to the bilinear models, the simple friction bearing appears not to have the same sensitivity to the input motion. Rather, the results show the FRS are nearly similar with some tolerance allowed at the various elevations. This presents a case such that elastomers may be more sensitive to the input motions used in analysis compared to the friction or pendulum like isolators.

Additional results presented in Appendix C.

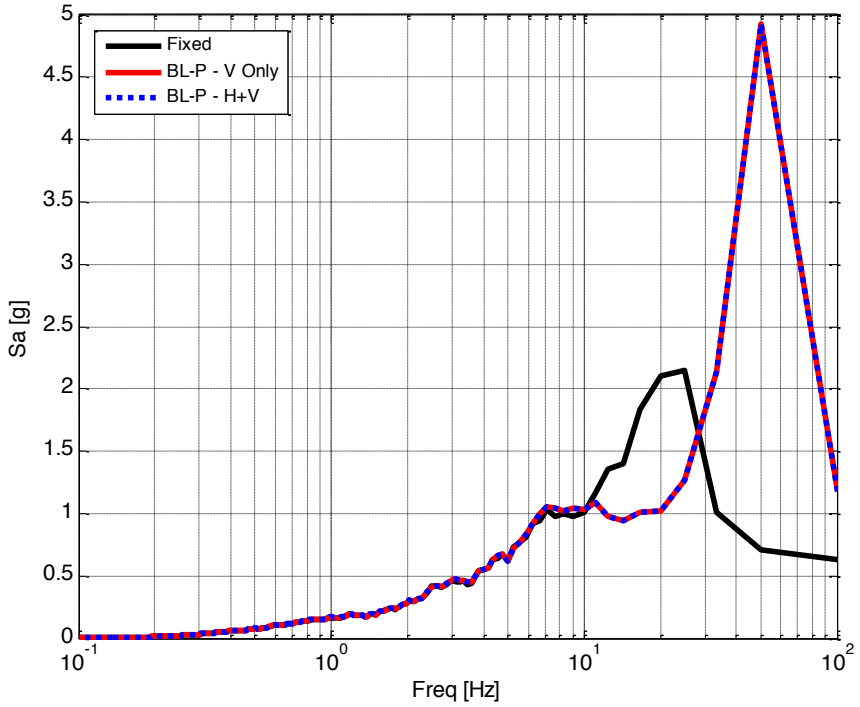

(a)

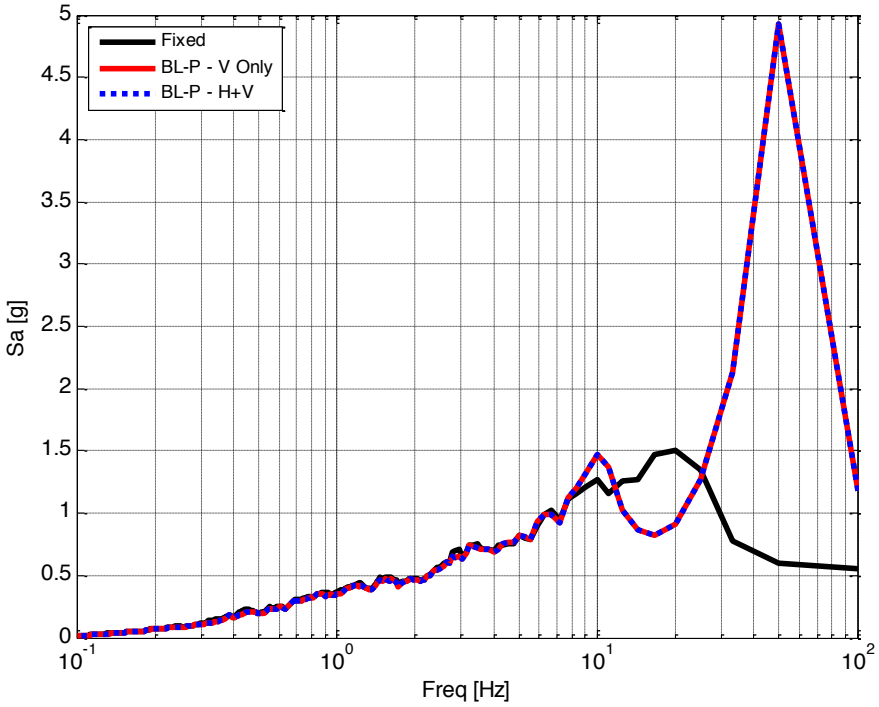

(b)

Figure 6.4 Median vertical FRS primary shield wall with bilinear plasticity isolators: vertical and vertical-horizontal motions (a) EUR and (b) NRC at Elev. 156'.

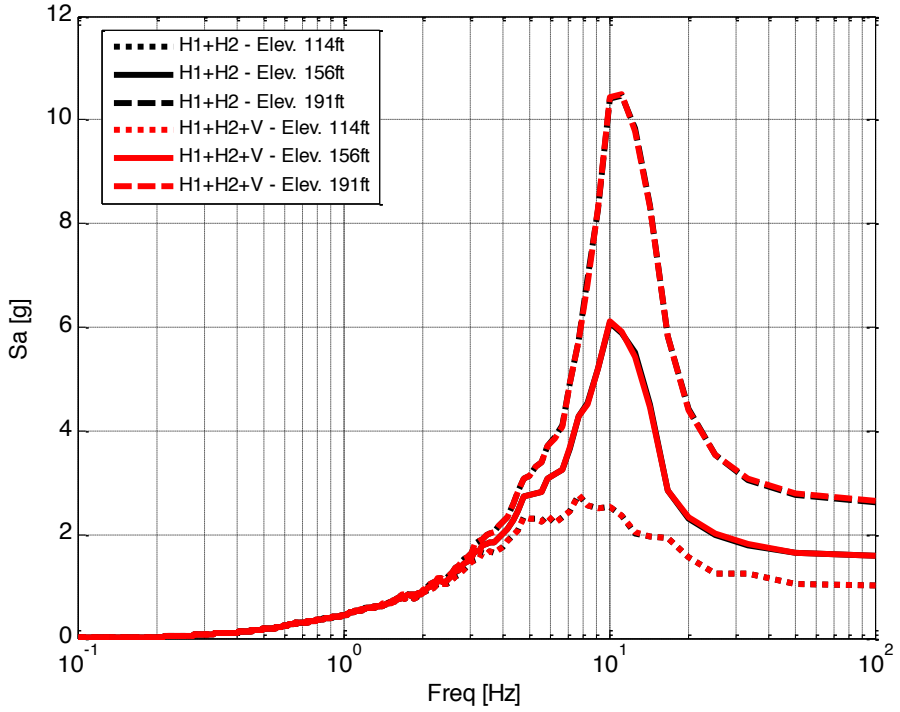

(a)

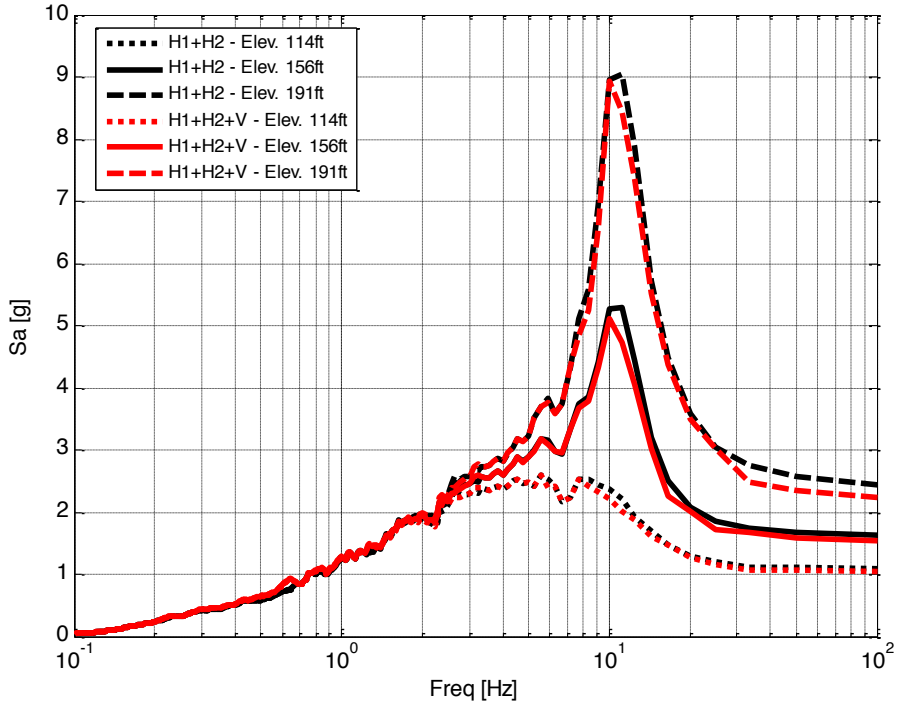

(b)

Figure 6.5 Median Horizontal FRS primary shield wall with fixed base: horizontal and vertical-horizontal (a) EUR and (b) NRC.

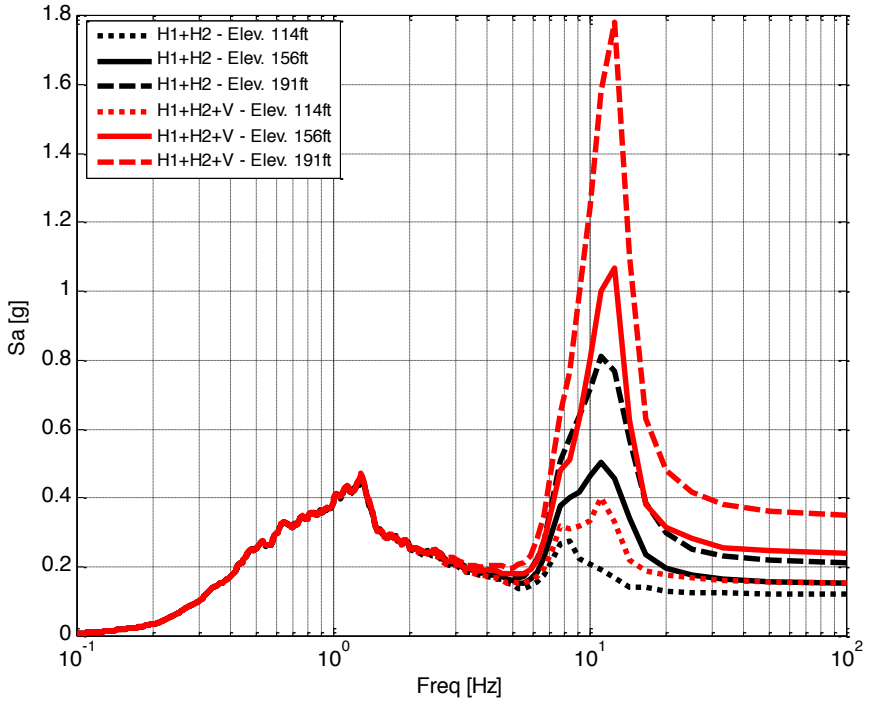

(a)

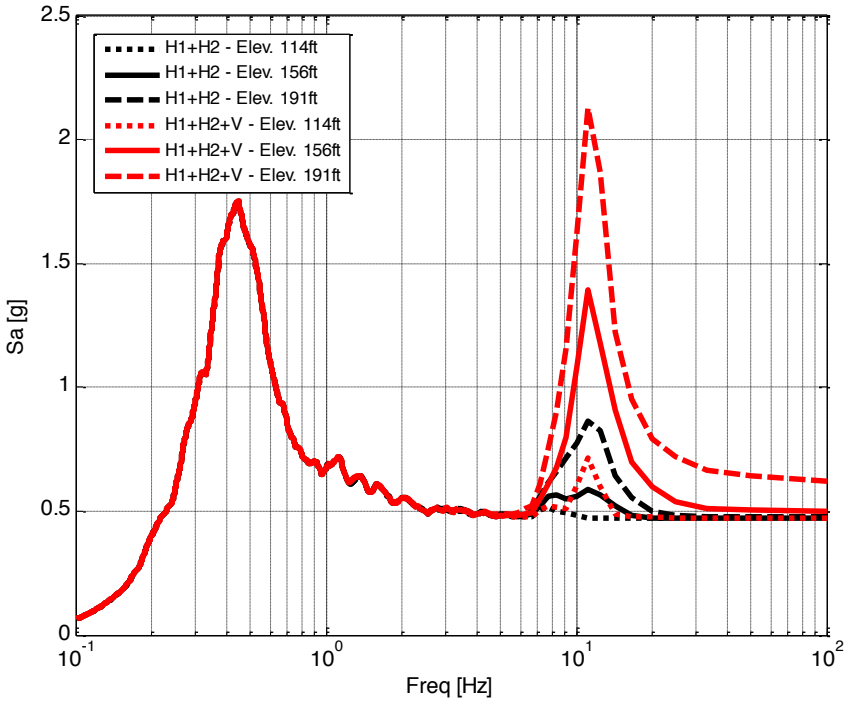

(b)

Figure 6.6 Median Horizontal FRS primary shield wall with bilinear plasticity isolators: vertical and vertical-horizontal motions (a) EUR and (b) NRC – elev. 156'.

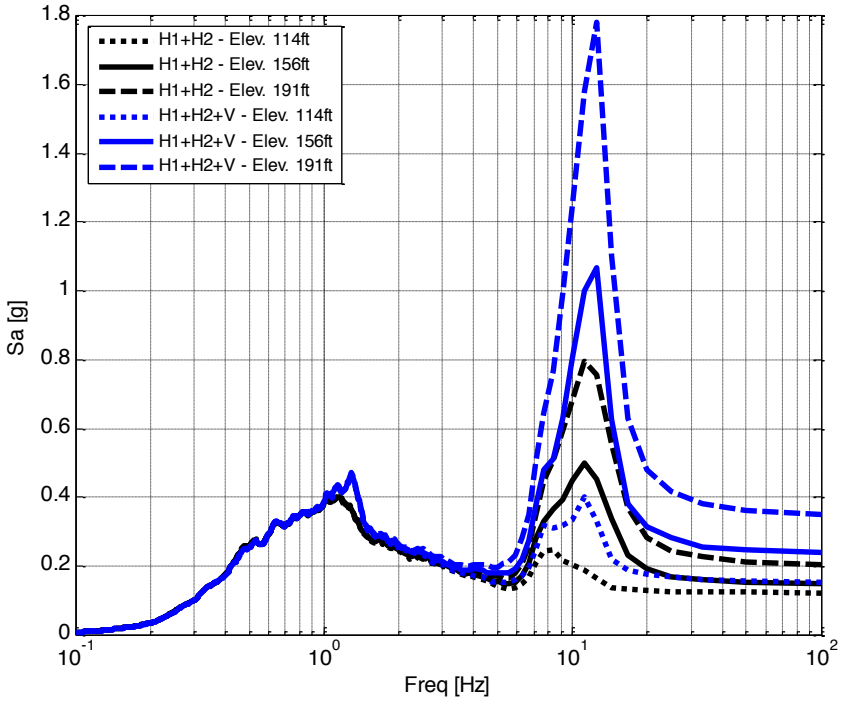

(a)

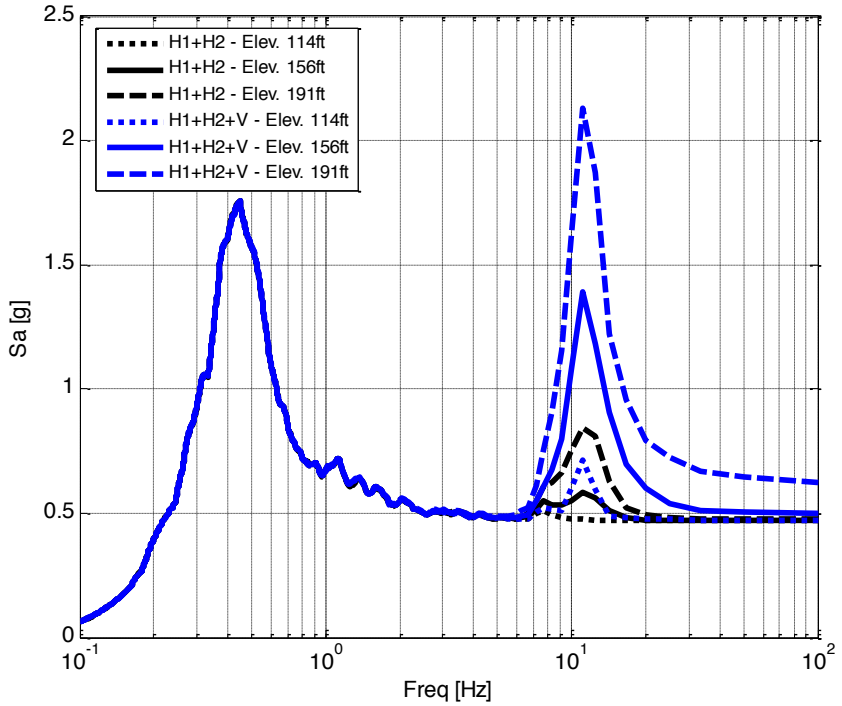

(b)

Figure 6.7 Median Horizontal FRS primary shield wall with bilinear Bouc-Wen isolators: vertical and vertical-horizontal motions (a) EUR and (b) NRC – elev. 156'.

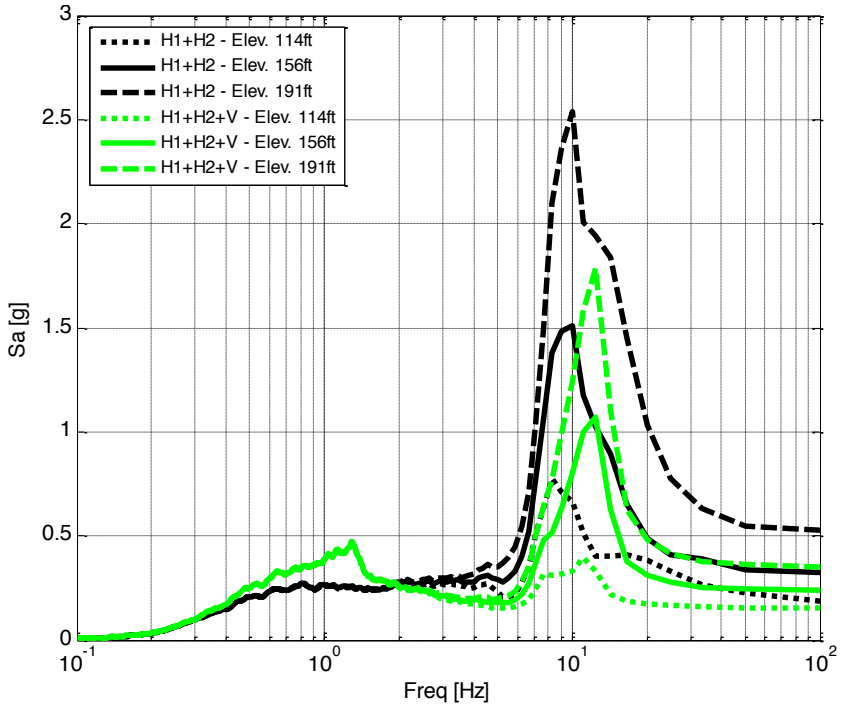

(a)

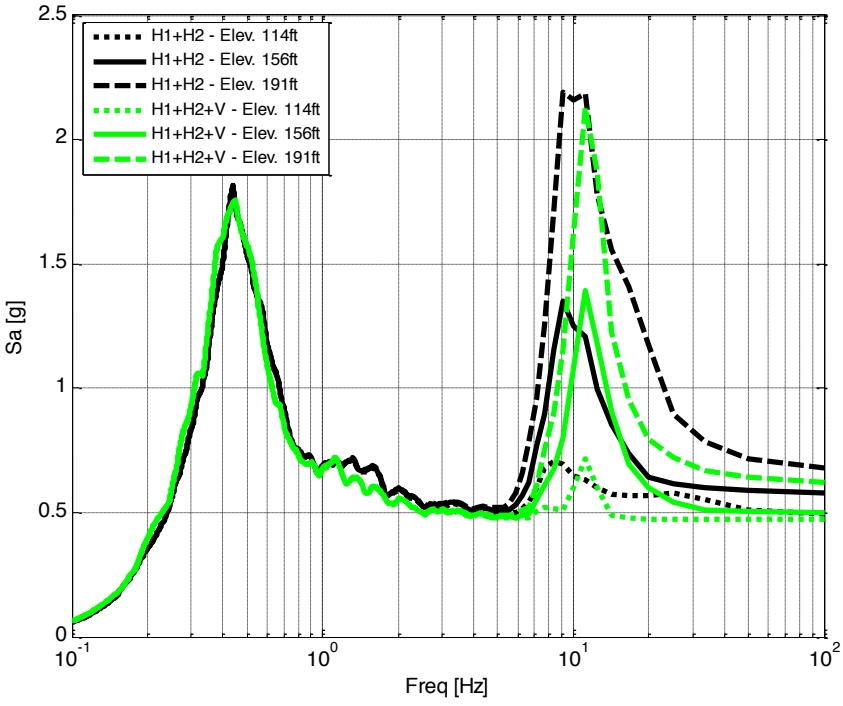

(b)

Figure 6.8 Median Horizontal FRS primary shield wall with constant friction isolators: vertical and vertical-horizontal motions (a) EUR and (b) NRC – elev. 156'.

6.4 CONCLUSIONS FOR STUDY 3

This study yields a number of important results. Although, isolation reduces horizontal accelerations, when focus is turned to the vertical component of motion, the beneficial effect of isolation is not as noticeable. Vertically, the isolation system is performing at the same level of the fixed base case both when the vertical motion is used alone and along with horizontal ground motions.

The largest increases in FRS accelerations were observed for the elastomeric bearing models. In this case, the bearing was quite stiff in the vertical direction. Vertical motion can be problematic for sensitive equipment thus additional work is needed to determine whether current isolation design can be adapted or if secondary isolation devices must be added to help protect critical components. In contrast, the simple friction bearings showed less sensitivity to the input motion with the 2D and 3D analysis nearly similar in value. However, this is important as it shows that horizontal response cannot be based only on a horizontal 2D analysis.

7 Study 4: Vertical Motion (Part B) – Sensitivity Analysis

7.1 INTRODUCTION

This study explores the sensitivity of structural response with the inclusion of 3 components of motion. As discussed in the previous chapter, the vertical component is capable of altering the response. Given this result, the question becomes whether the methods of adaptation observed from the horizontal only sensitivity analysis are still valid. Additionally, the previous sensitivity analysis study used ground motions without the vertical component of motion. Goal of this study is to reconfirm the results of the previous sensitivity analysis and present ways in which the vertical component motion changes the options for isolator design.

7.2 STUDY APPROACH

To allow for efficient analysis, a single isolator model was used with the following isolator parameters considered: initial stiffness (K_1), isolator strength (Qd), vertical stiffness (K_V) and coefficient of friction (μ). These elements were scaled by 25%, 50%, 100%, 200% and 400% of the original value. The only exception taken was for the isolator strength, as such a wide range of values is not expected. The range used for this case was 90%, 95%, 97%, 100%, 103%, 105% and 110%. The simple friction isolator with constant friction was used for the study of variations in coefficient of friction. All other cases used the bilinear plasticity model and the dispersion appropriate EUR DBE motions.

7.3 RESULTS

The results from this study presented some interesting findings not observed with the previous sensitivity analysis.

Firstly, in the initial study, there was a shift in the FRS due to changes in the initial stiffness which presented a situation where a compromise can be made in terms of where the overall peak response occurs. In this case, a similar situation arises, but mainly as a result of the change in elevation as seen in Figure 7.1. As the node of interest shifts upward, the overall maximum spectral acceleration moves from the low to high frequency range. Secondly, depending on the frequency, there is a different response to the stiffness change. In the low frequency range, spectral accelerations increase and decrease based on respective increase and

decreases to the initial stiffness. Changing the initial stiffness increases the spectral acceleration by almost 2.5 times maximum compared to the base line stiffness. In terms of the peak response in the high frequency range (occurring around the structure's natural frequency), there appears to be a similar influence such that as the isolator's stiffness increases so do the spectral accelerations. However, the difference between the accelerations is not as substantial in the high frequency range compared to the low frequency range. Overall, FRS show some high frequency content as the isolator's stiffness increases. This tends to be located in the frequency range between 1 and 10 Hz. Although the initial stiffness does not shift the peak response, these results present potential means of controlling the magnitude of the response.

With the changes in isolator strength for the elastomeric, as shown in Figure 7.2, there is a very consistent response that is independent of this parameter. The strength shows some variation around the overall peak response, however, it is within a +/- 10% range from the original value. As a result, the isolator strength does not show a significant influence on the FRS. Additionally, unlike the initial stiffness, the FRS do not shift with increasing height. However, as the elevation increases the localized peak in the high frequency range becomes more apparent. This appears to show a tuning effect occurring between the structure and isolation as a function of elevation.

For the coefficient of friction, Figure 7.3 shows the friction coefficient does have an affect on response but not necessarily a significant one. The current value appears to present the highest spectral accelerations with the result decreasing both with an increase and decrease in the value. As this parameter shows the greatest influence in the frequency range for most equipment, the friction may present a means of adaptation to the design performance. Unlike the isolator strength, a low frequency peak is not introduced with the increase in elevation. However, the overall peak spectral acceleration does increase tremendously with change in height for all cases of the friction coefficient. Between an elevation of 114 ft to 191 ft, the spectral acceleration increases by 3.5 times.

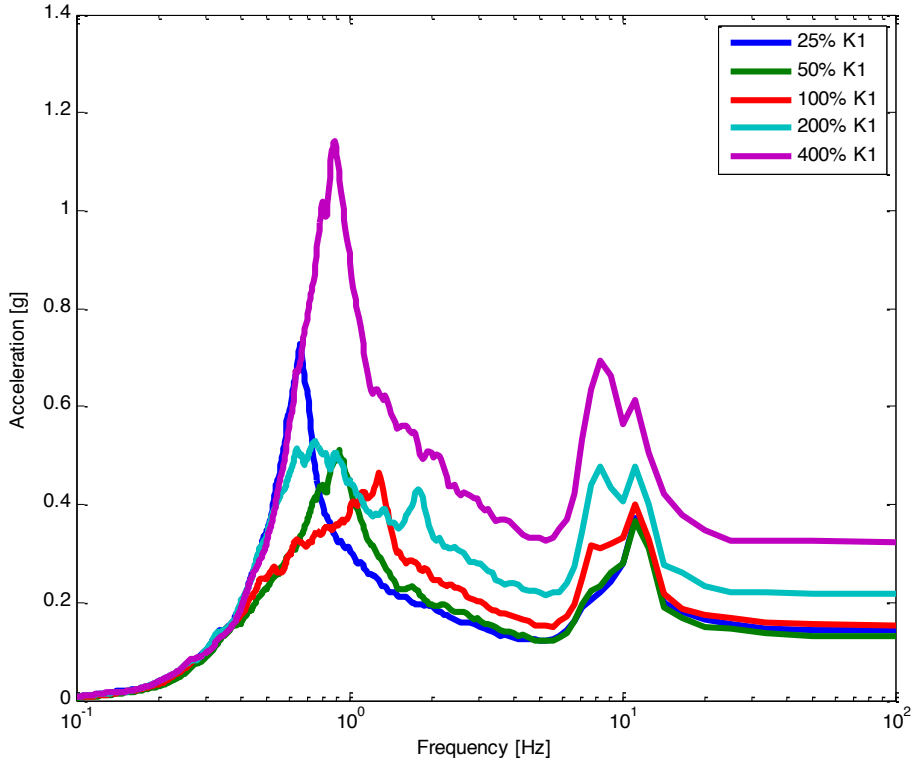
25% K1
50% K1
100% K1
200% K1
400% K1
Acceleration [g]
Frequency [Hz]
0
0.2
0.4
0.6
0.8
1
1.2
1.4
10^-1
10^0
10^1
10^2

(a)

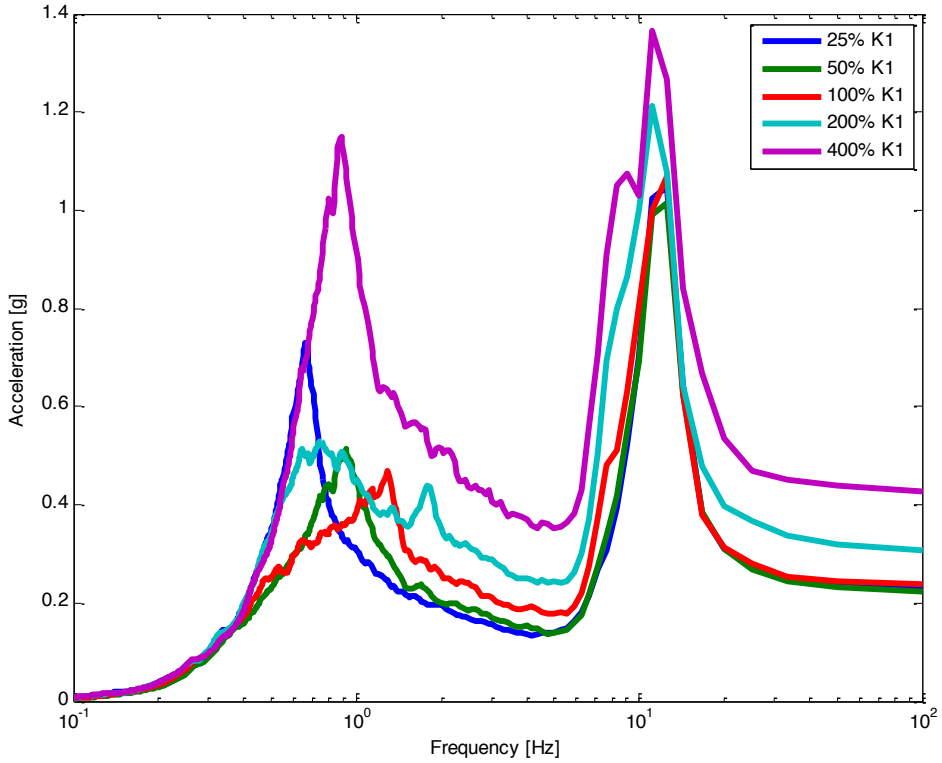
25% K1
50% K1
100% K1
200% K1
400% K1
Acceleration [g]
Frequency [Hz]
0
0.2
0.4
0.6
0.8
1
1.2
1.4
10^-1
10^0
10^1
10^2

(b)

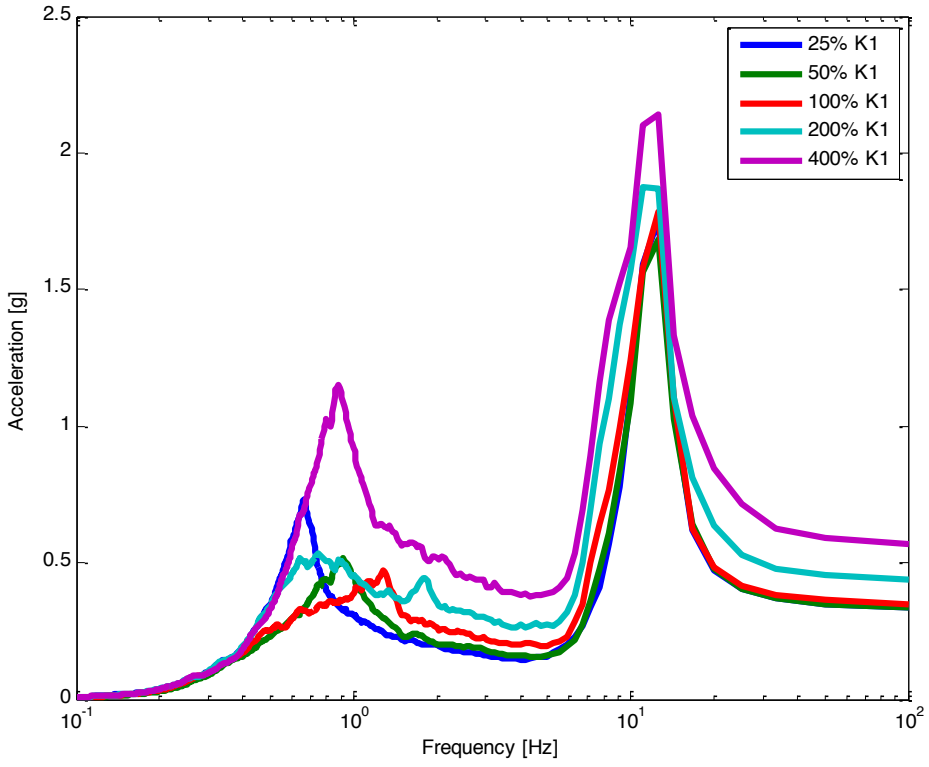

(c)

Figure 7.1 Median FRS for BL-P Comparing Effects of K1 Variations for EUR DBE for Primary Shield Wall Elevations: 114' (a), 156' (b), and 191' (c).

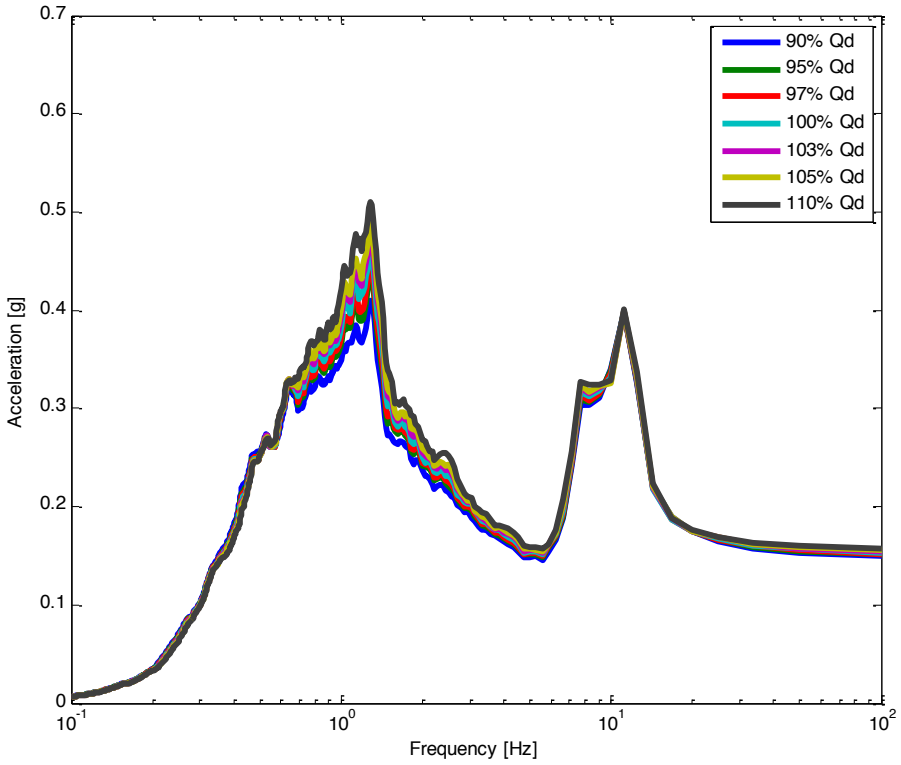
90% Qd
95% Qd
97% Qd
100% Qd
103% Qd
105% Qd
110% Qd
Acceleration [g]
Frequency [Hz]
0
0.1
0.2
0.3
0.4
0.5
0.6
0.7
10^-1
10^0
10^1
10^2

(a)

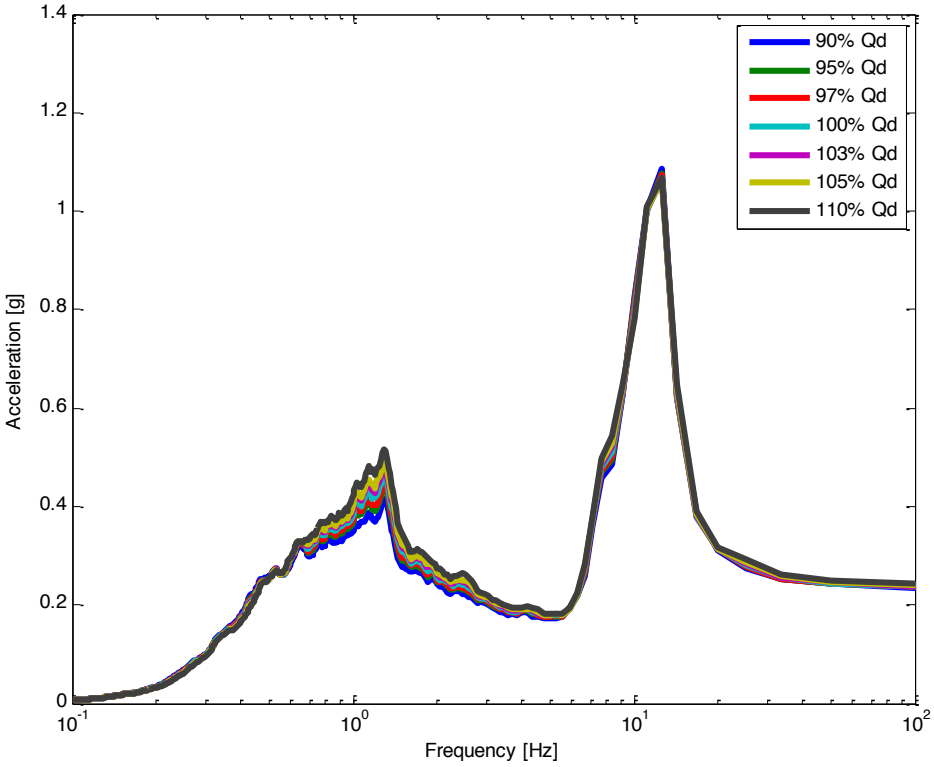
90% Qd
95% Qd
97% Qd
100% Qd
103% Qd
105% Qd
110% Qd
Acceleration [g]
Frequency [Hz]
0
0.2
0.4
0.6
0.8
1
1.2
1.4
10^-1
10^0
10^1
10^2

(b)

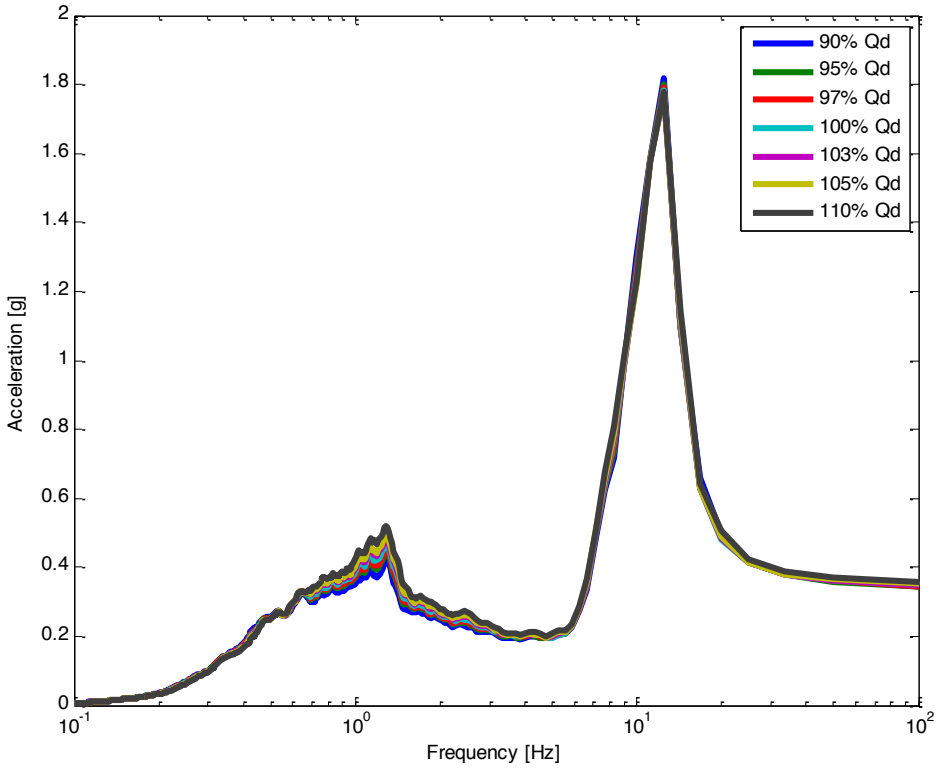

(c)

Figure 7.2 Median FRS for BL-P Comparing Effects of Qd Variations for EUR DBE for Primary Shield Wall Elevations: 114' (a), 156' (b), and 191' (c).

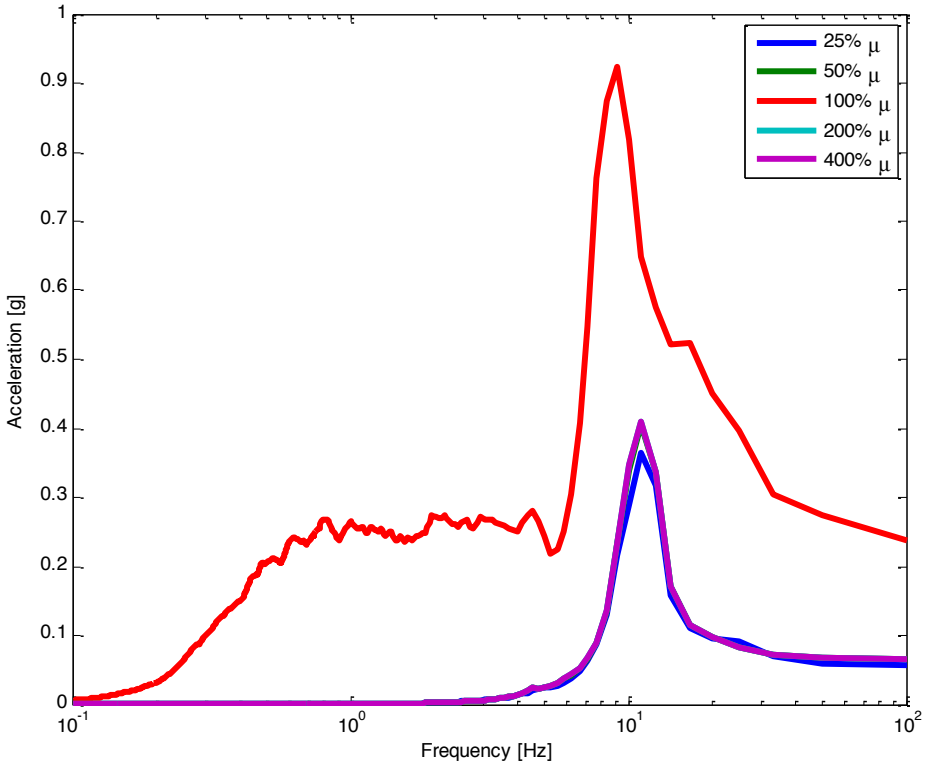
25% μ
50% μ
100% μ
200% μ
400% μ
Acceleration [g]
Frequency [Hz]
0
0.1
0.2
0.3
0.4
0.5
0.6
0.7
0.8
0.9
1
10^-1
10^0
10^1
10^2

(a)

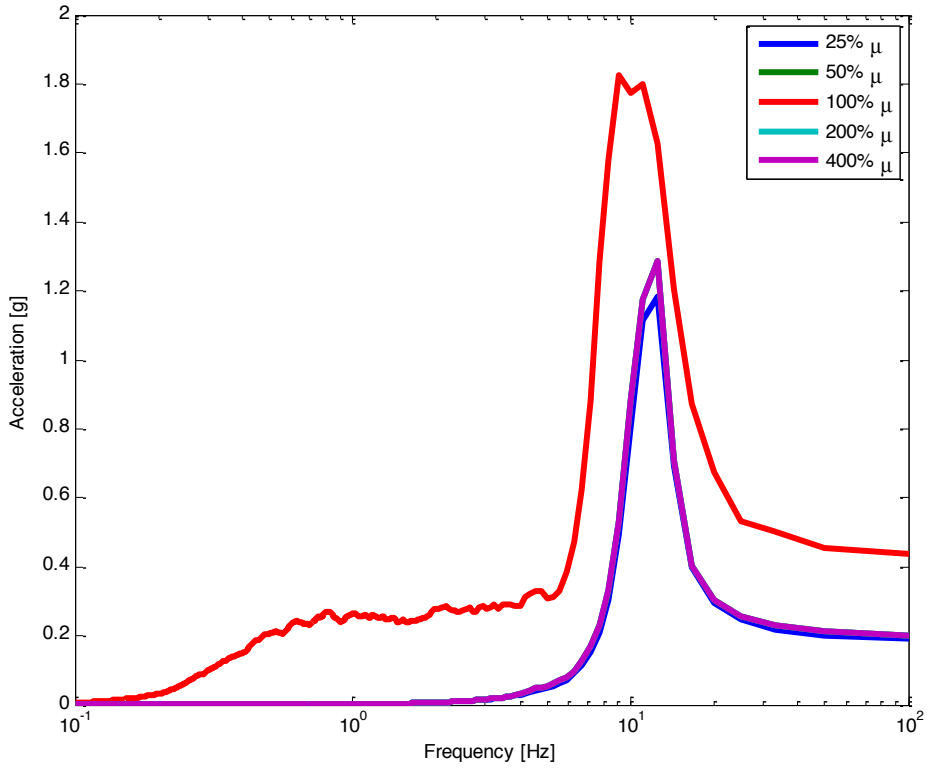
25% μ
50% μ
100% μ
200% μ
400% μ
Acceleration [g]
Frequency [Hz]
0
0.2
0.4
0.6
0.8
1
1.2
1.4
1.6
1.8
2
10^-1
10^0
10^1
10^2

(b)

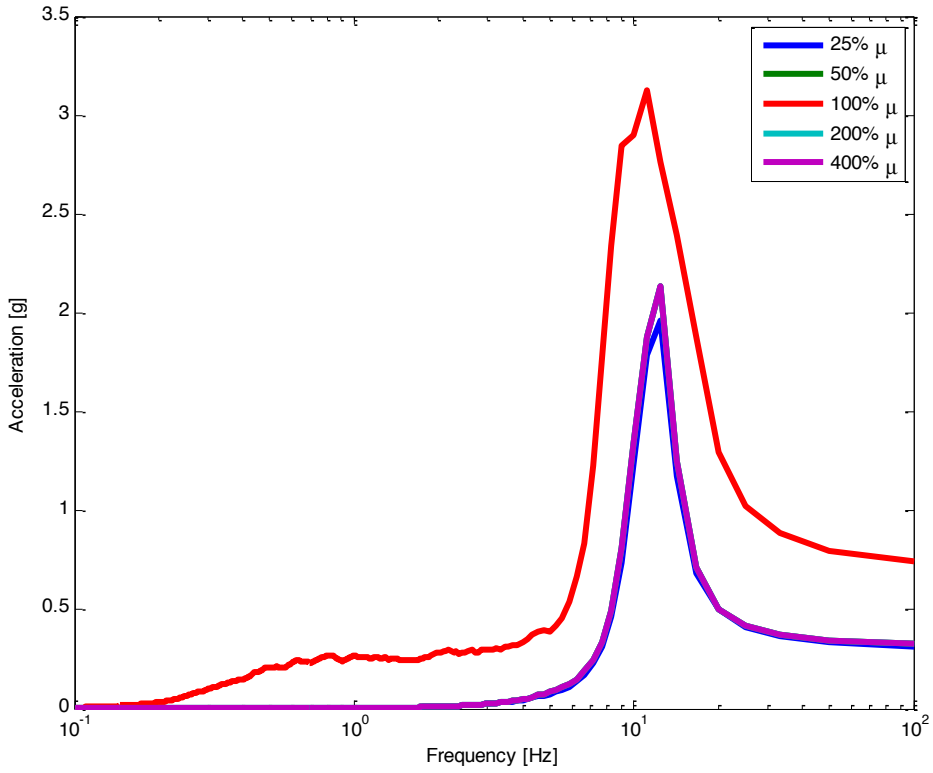

(c)

Figure 7.3 Median FRS for SF-C Comparing Effects of μ Variations for EUR DBE for Primary Shield Wall Elevations: 114' (a), 156' (b), and 191' (c).

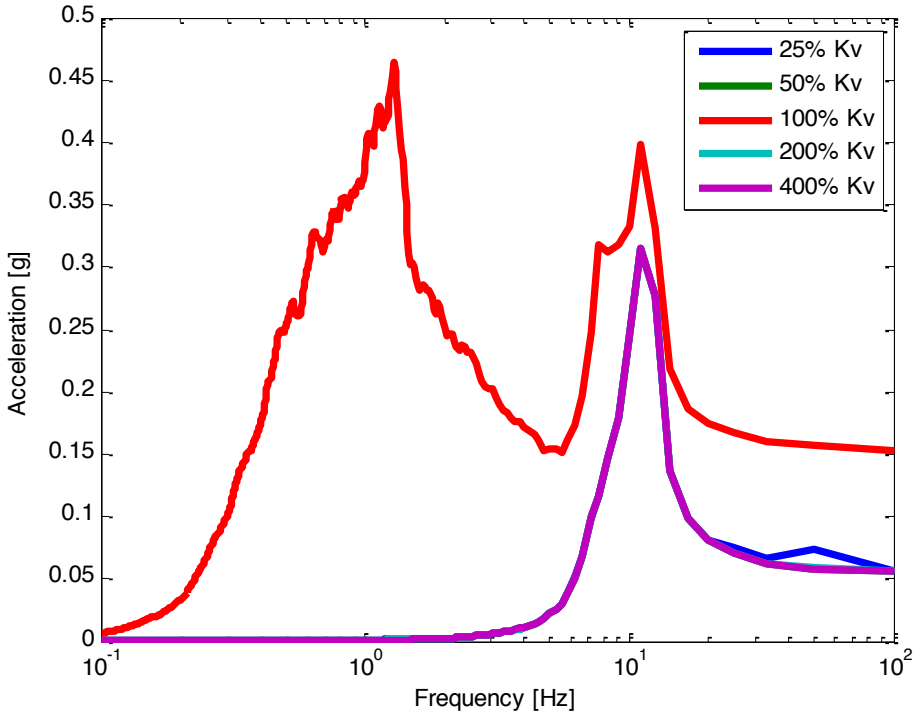
25% Kv
50% Kv
100% Kv
200% Kv
400% Kv
Acceleration [g]
Frequency [Hz]
0.5
0.45
0.4
0.35
0.3
0.25
0.2
0.15
0.1
0.05
0
10^-1
10^0
10^1
10^2

(a)

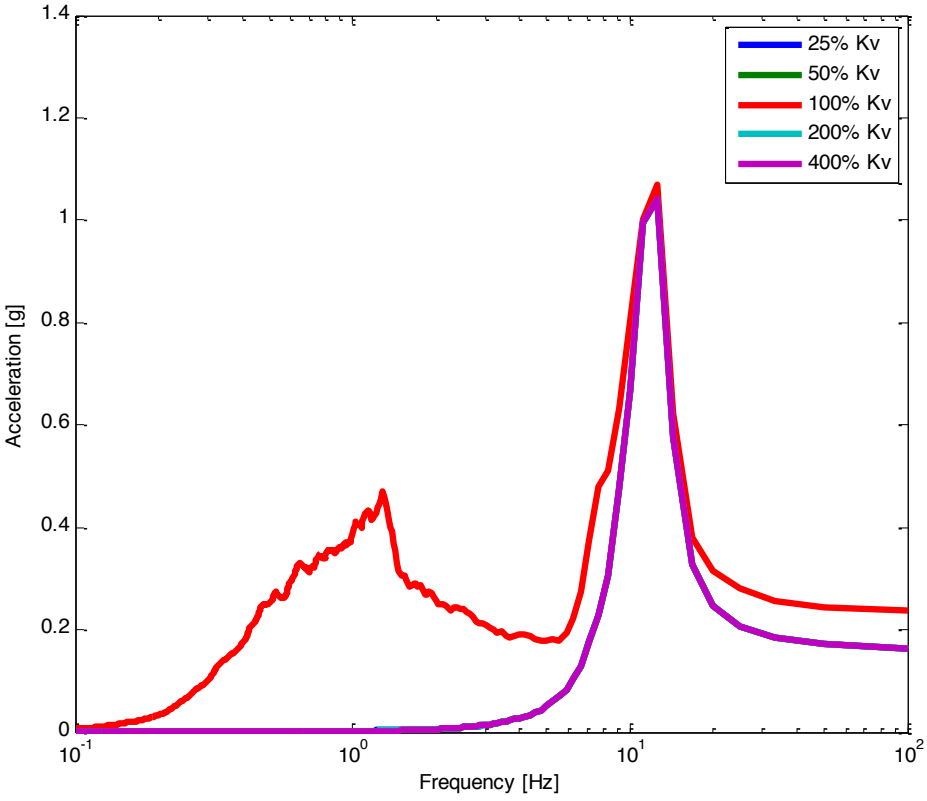
25% Kv
50% Kv
100% Kv
200% Kv
400% Kv
Acceleration [g]
Frequency [Hz]
1.4
1.2
1
0.8
0.6
0.4
0.2
0
10^-1
10^0
10^1
10^2

(b)

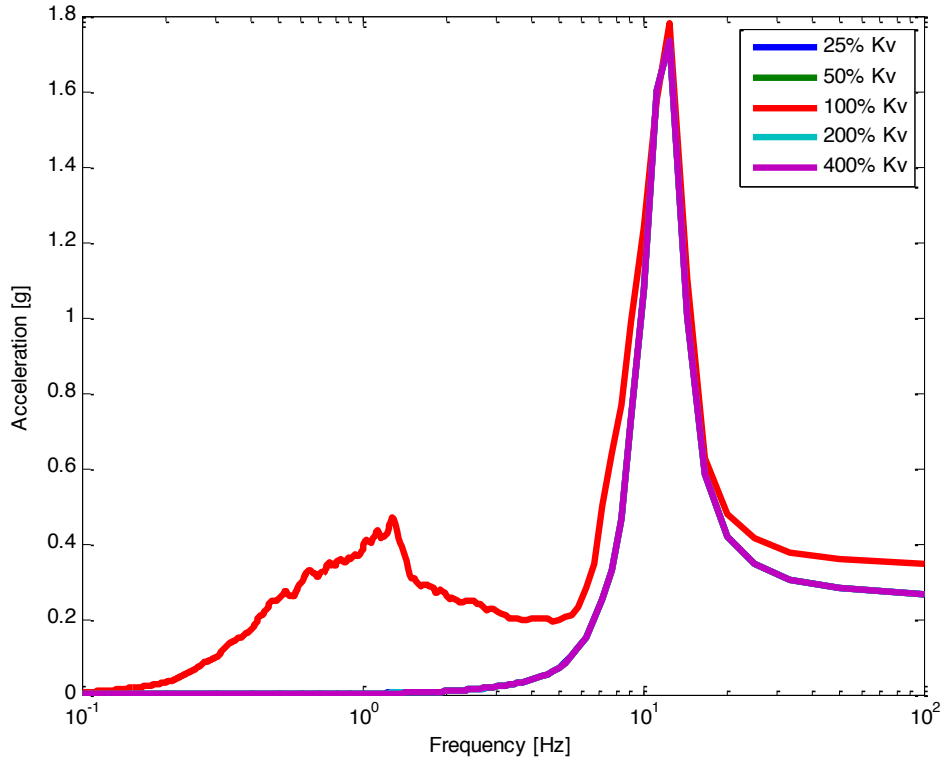

(c)

Figure 7.4 Median FRS for BL-P Comparing Effects of Kv Variations for EUR DBE for Primary Shield Wall Elevations: 114' (a), 156' (b), and 191' (c).

Figure 7.4 presents the FRS for changes in the vertical stiffness of the isolator. There is not a lot of variation between the responses at a given elevation. Again, as seen with the coefficient of friction the current vertical stiffness produces the largest spectral acceleration with approximately 10% decrease with an increase or decrease in the stiffness. However, in the low frequency range, there is a localized peak due to the current stiffness, which is reduced dramatically with a change in value. The reasoning for this peak response needs to be further studied in order to determine the mechanism behind this response. Similar to previous observations, the spectral accelerations increase with elevation.

7.4 CONCLUSIONS FOR STUDY 4

The studies covered in this section provide data and information on the isolation of the APR1400 plant for horizontal motion.

The parameters explored in this study present various means of adapting the isolator design to meet performance requirements. The initial stiffness remains to be the most influential parameter for the FRS. However, changes in isolator strength, coefficient of friction, or vertical stiffness may be needed to control the magnitude of FRS peaks. Thus again, the results show that for any change in parameters a compromise must be made. Unlike previous studies, elevation played an influential role in the results. With horizontal only analysis, the magnitude of response from one location to the next did not change significantly. However, in this case, the response is

increasing 2-3 times from the lowest elevation. Further study is needed to understand the mechanisms behind the change in response between 2D horizontal and 3D analysis. Overall, this study on 3D motion provides insight into a number of ways isolator parameters influence performance.

8 Study 5: Vertical Motion (Part C) – Fixed Base-Isolated FRS Comparison

8.1 INTRODUCTION

This section reviews another means of comparing results for fixed base and isolated plant designs and discusses the variation in response depending on the use of individual versus median results.

8.2 STUDY APPROACH

This study used the EUR DBE set of ground motions (dispersion appropriate, spectral matched, and spectral matched multi-damping). The model used was the APR1400 structure isolated using a single representative plasticity, Bouc-Wen, and simple friction (constant) bearing with a foundation that restricted torsion and pitch.

The plots for the FRS were computed two different ways. Plots of individual ground motions, in terms of the ratio of the FRS of the isolated plant to that for the fixed base case. This was then compared against the median result for the set of 20 ground motions.

8.3 RESULTS

Figure 8.1 presents the ratio of isolated to fixed base FRS for a given elevation in the Primary Shield Wall. In this plot, both the isolated and fixed base plants were subjected to bi-directional DBE earthquake records. Thus, the solid black line presents the case where the pseudo-acceleration values at a given frequency are the same for the isolated and fixed base cases. Assuming components and systems attached to the fixed base structure were adequate for 0.3g PGA, they would be adequate for the case where the ratio in the plot is (0.5g/0.3g =) 1.67 or lower. Thus, systems and components in a standard plant qualified for spectra anchored at 0.3g should be acceptable for all of the isolated systems for ground motions of 0.5g PGA, except near 0.45 Hz, which is close to the natural frequency of the isolation system.

From both plots, there are a number of additional observations. Firstly, in the lower frequency range the isolated FRS present higher responses compared to the fixed base case. However, the accelerations are small in magnitude. Above 0.6 Hz, the isolated response dramatically decreases its FRS in comparison to the fixed base displaying the improvement.

Between the two plots, there are some variations between the isolators. Firstly, while the same general trend is observed, the results for the single ground motion selected (Figure 2.47a) are higher in comparison to the median values in Figure 2.47b. The individual plot presents a 25% higher peak ratio in the low frequency range compared to the median plots. Additionally, the median ratios presents a slightly more accentuated difference between the plasticity and Bouc-Wen bearings with the simple friction bearing. The median plot shows lower ratios and a lower frequency at which the isolated FRS improve over the fixed base. The differences in response are a part of the median taken the various ground motions.

Dispersion appropriate motions are the preferred method of analysis according to draft NRC guidelines for analysis of seismically isolated NPPs. Nonetheless, results for spectral matched results are presented in **Figure 8.2** and **Figure 8.3**, considering matching to a single damping value or multiple damping values, respectively. When a single ground motion is observed, there is variation in the magnitudes of the FRS for the dispersion appropriate, spectrally matched, and spectrally matched multi-damping. This difference in magnitude is then reduced with the median response. This is a reasonable result given the definition of a median response and how it incorporates the variation and dispersion of results for a given set of motions. However, the spectrally matched FRS for a single damping ratio presents the least amount of high frequency content around the peak response. As a result, these plots show the need to use dispersion appropriate or spectrally matched for multi-damping responses. This will present the most information for a median response considering the variation in peak responses for the low frequency range of an isolated system. .

8.4 CONCLUSIONS FOR STUDY 5

Although median results present a means of aggregating the results from a number of analyses, there is the potential for individual results to differ in magnitude and overall trend. Thus, it is important to not only analyze the median values but also examine the variation of results obtained with individual records to identify undesired response characteristics.

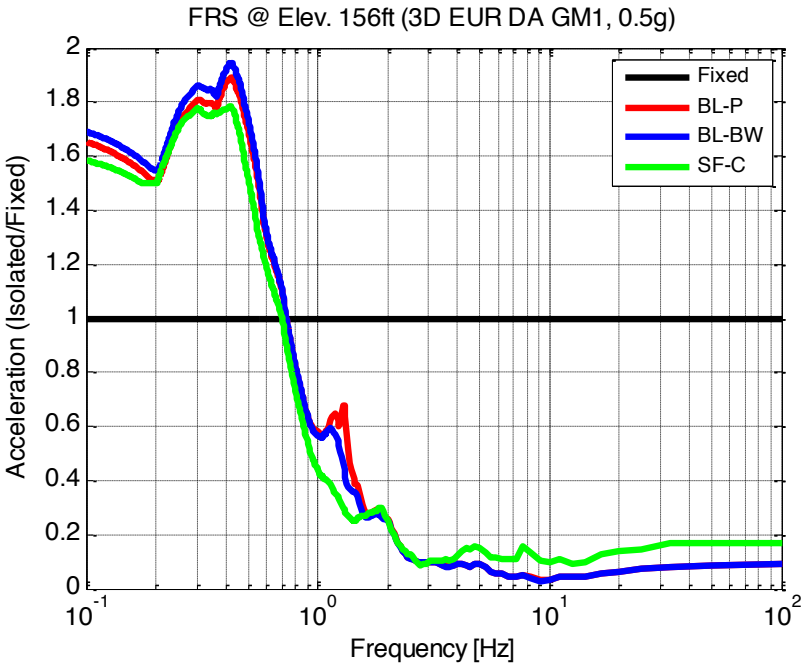

(a)

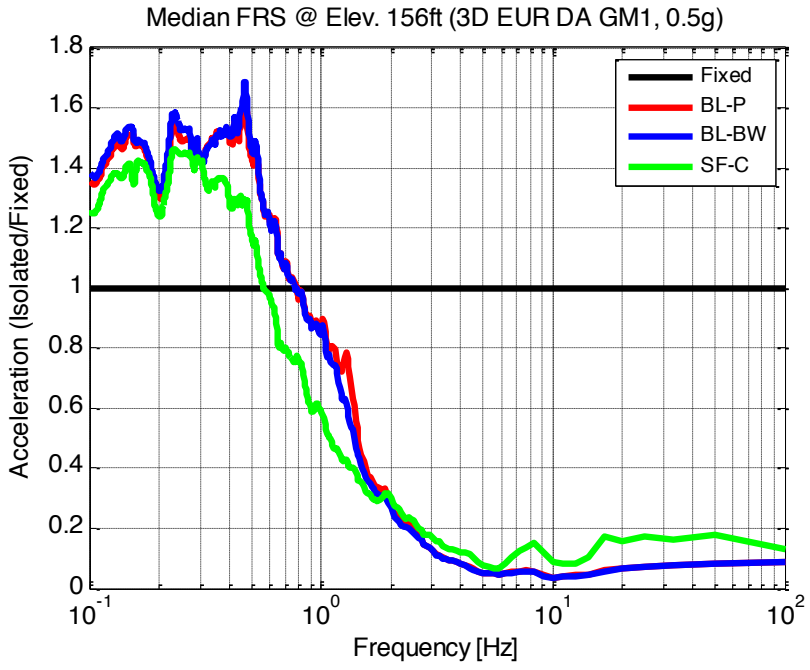

(b)

Figure 8.1 Ratio of Isolated to Fixed Base FRS for primary shield wall with plasticity, Bouc-Wen, and simple friction bearings: 3D EUR Dispersion Appropriate DBE motions (a) Ground Motion 1 and (b) Median across all Ground Motions – elev. 156'.

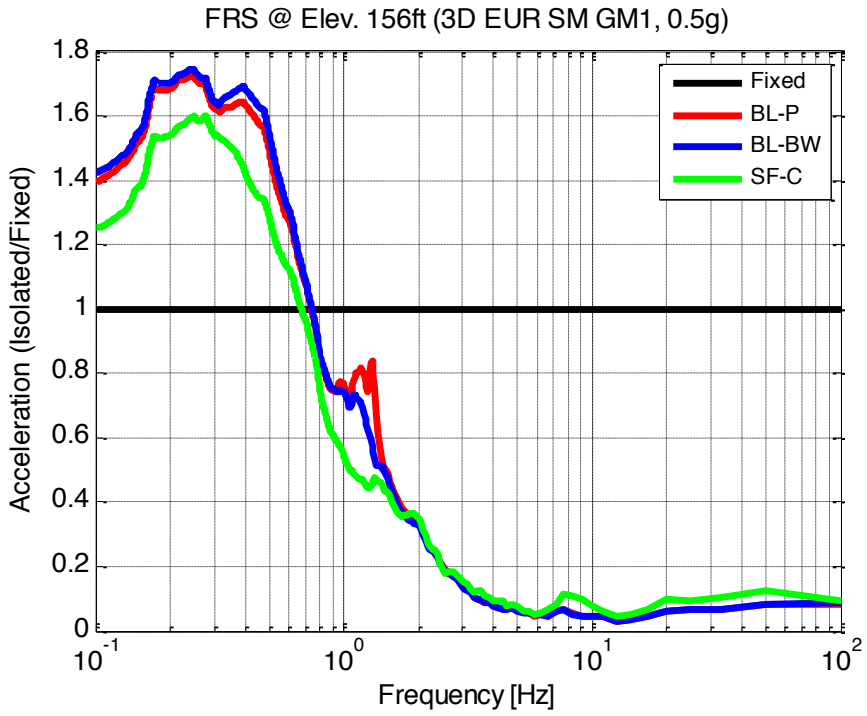

(a)

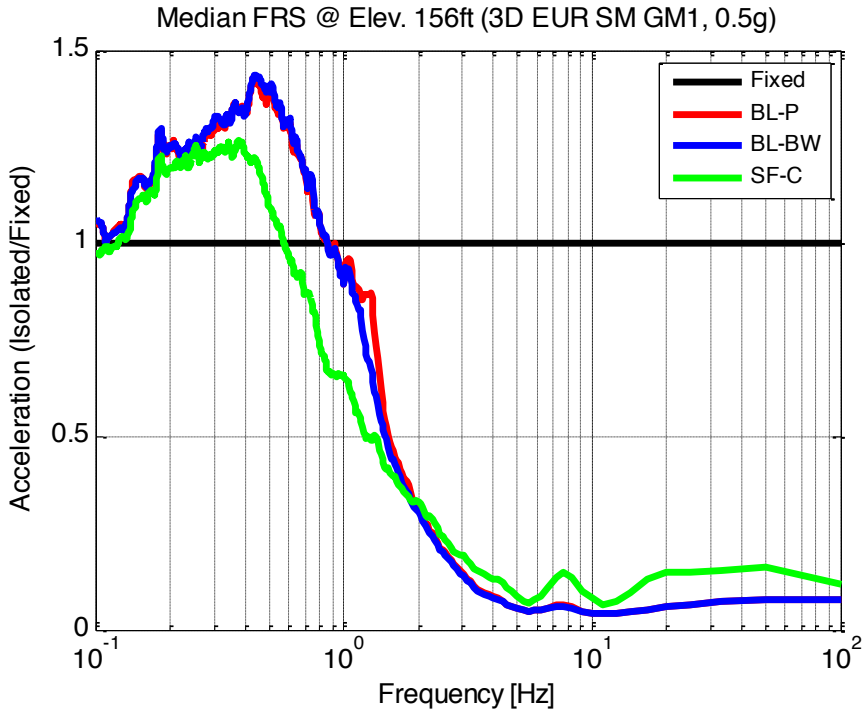

(b)

Figure 8.2 Ratio of Isolated to Fixed Base FRS for primary shield wall with plasticity, Bouc-Wen, and simple friction bearings: 3D EUR Spectral Matched DBE motions (a) Ground Motion 1 and (b) Median across all Ground Motions – elev. 156'.

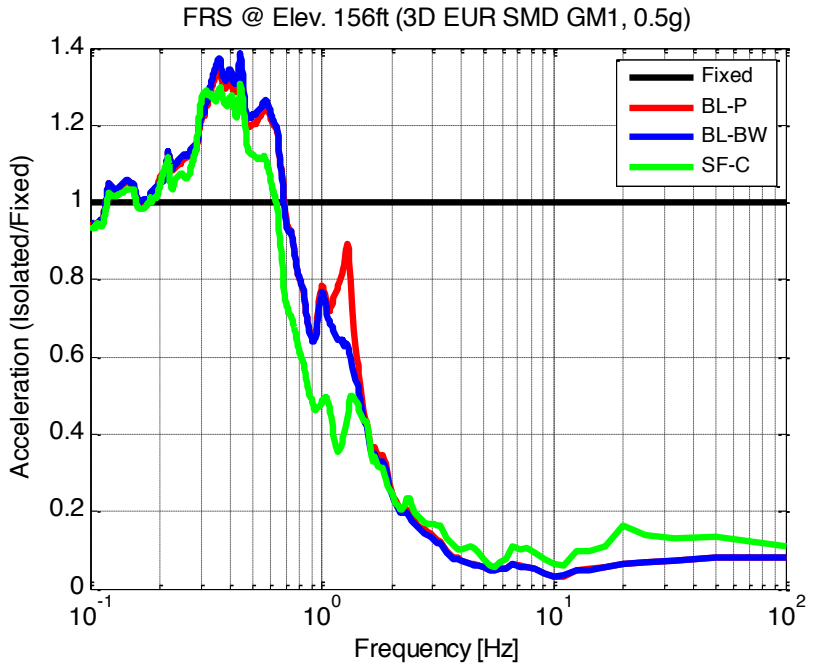

(a)

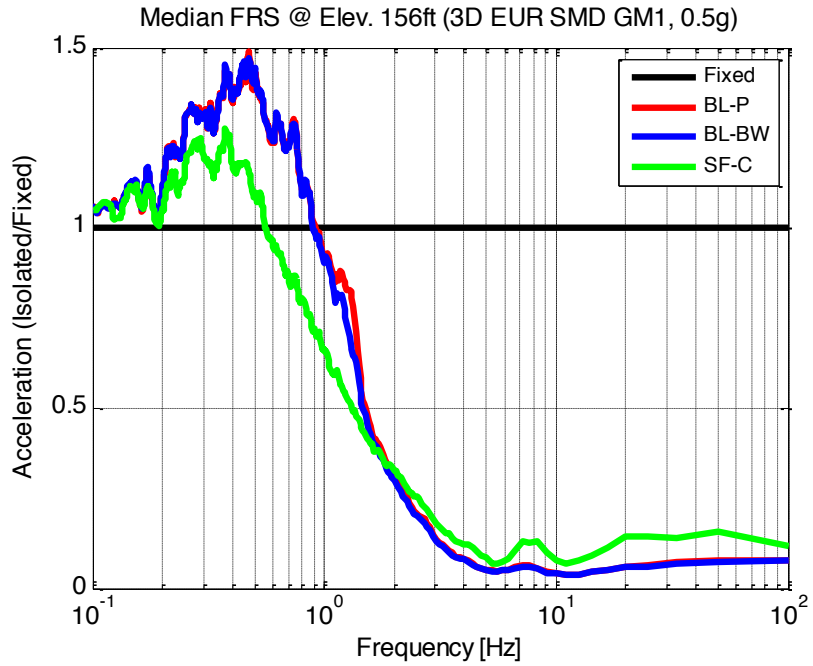

(b)

Figure 8.3 Ratio of Isolated to Fixed Base FRS for primary shield wall with plasticity, Bouc-Wen, and simple friction bearings: 3D EUR Spectral Matched Multi-Damping DBE motions (a) Ground Motion 1 and (b) Median across all Ground Motions – elev. 156'.

9 Study 6: Identify Factors Controlling Seismic Gap Size

9.1 INTRODUCTION

The lateral movement of the isolated structure is accommodated using a seismic gap. This seismic gap or moat is a space provided around the entire perimeter of the structure. Its width is controlled by the ultimate permitted lateral displacement of the isolation system (Taylor and Takeru 2004).

The major factor controlling seismic gap size is the isolator displacement. In the case of the US NRC NUREG, there is an expected level of performance for a controlled hard stop, such as a moat wall. Table 9.1 is a summary of requirements included in the draft NRC guidelines. The moat wall is expected to withstand a hard stop impact with very little damage. This can be achieved in three ways: 1) ensure that the seismic gap is large enough that the probability of impact is very low; 2) design the moat wall to withstand an impact loading; and 3) include a lateral displacement limiting system.

For options 2 and 3, the moat wall design can be achieved using various methods and the addition of devices such as bumpers. These two options can be further studied in future research if considered viable.

For option 1, this involves determining the expected maximum isolator displacement. The following study explores the confidence levels described in Table 9.1 are explored for the APR1400.

9.2 STUDY APPROACH

To focus attention on the isolator displacement, the model was simplified to a single representative isolator supported underneath the APR1400 (similar to model in Chapter 3). Note, results from this simplification are consistent with those found using a full-scale isolation system.[4] This study uses sets of dispersion appropriate, spectrally matched, and spectrally matched at multi-damping EUR and NRC ground motions applied in three dimensions.

Isolator models observed include bilinear elastomeric (plasticity and Bouc-Wen model), constant and velocity dependent single friction pendulum bearing, and constant and velocity dependent EQS bearing. The properties of these bearings are best matched to the updated values

[4] Refer to Volume 5, *Sensitivity Assessment of a Seismically Isolated Nuclear Power Plant*, Terzic et al., 2014

Table 9.1 Performance Matrix for Isolated NPP [Kammerer et al 2011]

Ground motion levels	Isolation system				
	Isolation unit and system design and performance criteria	Approach to demonstrating acceptable performance of isolator unit	Superstructure design and performance	Umbilical line design and performance	Moat or hard stop design and performance
GMRS+[2] The envelope of the RG1.208 GMRS and the minimum foundation input motion[3] for each spectral frequency	No long-term change in mechanical properties. 100% confidence of the isolation system surviving without damage when subjected to the mean displacement of the isolator system under the GMRS+ loading.	Production testing must be performed on each isolator for the mean system displacement under the GMRS+ loading level and corresponding axial force.	The superstructure design and performance must conform to NUREG-0800 under GMRS+ loading.	Umbilical line design and performance must conform to NUREG-0800 under GMRS+ loading.	The moat is sized such that there is less than 1% probability of the superstructure contacting the moat or hard stop under GMRS+ loading.
EDB[4] **GMRS** The envelope of the ground motion amplitude with a mean annual frequency of exceedance of $1x10^{-5}$ and 167% of the GMRS+ spectral amplitude	90% confidence of each isolator and the isolation system surviving without loss of gravity-load capacity at the mean displacement under EDB loading.	Prototype testing must be performed on a sufficient number of isolators at the CHS[5] displacement and the corresponding axial force to demonstrate acceptable performance with 90% confidence. Limited isolator unit damage is acceptable but load-carrying capacity must be maintained.	There should be less than a 10% probability of the superstructure contacting the moat or hard stop under EDB loading.	Greater than 90% confidence that each type of safety-related umbilical line, together with its connections, remains functional for the CHS displacement. Performance can be demonstrated by testing, analysis or a combination of both.[6]	CHS displacement must be equal to or greater than the 90th percentile isolation system displacement under EDB loading. Moat or hard stop designed to survive impact forces associated with 95th percentile EDB isolation system displacement.[7] Limited damage to the moat or hard stop is acceptable but the moat or hard stop must perform its intended function.

1. Analysis and design of safety-related components and systems should conform to NUREG-0800, as in a conventional nuclear structure.
2. 10CFR50 Appendix S requires the use of an appropriate free-field spectrum with a peak ground acceleration of no less than 0.10g at the foundation level. RG1.60 spectral shape anchored at 0.10g is often used for this purpose.
3. The analysis can be performed using a single composite spectrum or separately for the GMRS and the minimum spectrum.
4. The analysis can be performed using a single composite spectrum or separately for the 10^{-5} MAFE response spectrum and 167% GMRS.
5. CHS=Clearance to the Hard Stop
6. Seismic Category 2 SSCs whose failure could impact the functionality of umbilical lines should also remain functional for the CHS displacement.
7. Impact velocity calculated at the displacement equal to the CHS assuming cyclic response of the isolation system for motions associated with the 95th percentile (or greater) EDB displacement.

provided for use in the University of California, San Diego (UCSD) Shake Table experimental portion of this project.[5]

The OpenSees data presented is post-processed in Matlab. For each ground motion, the maximum isolator displacement is recorded for each isolator. Then for each scenario, isolator and earthquake level, a lognormal distribution is fitted to the data. From this distribution, a mean and standard deviation value are determined. The 90 and 99 percentage confidence levels about the mean isolator displacement are computed. However, for each earthquake level, there is a specific confidence interval that must be considered for NRC acceptance. The seismic gap size for the DBE must meet the 99 percent confidence interval while the EDB earthquake needs to satisfy the 90 percent confidence interval.

9.3 RESULTS

The isolator displacements observed in this study provide a basis from which the seismic gap size can be approximated. Results for the bilinear plasticity and simple friction constant friction isolators are summarized in Table 9.2 to Table 9.9 for all isolators and two earthquake levels (DBE and EDB).

Results show a large range in isolator displacement demands. At the respective confidence levels, the maximum mean isolator displacements range from 3 to 20 in. for the DBE and 6 to 45 in. for the EDB earthquake. This range is extensive due to the NRC ground motions. If only the EUR ground motions are considered, the ranges for maximum mean displacements reduces to 3-5 in. for the DBE and 6-9 in. for the EDB earthquake. The EUR results are a significant reduction in the possible displacement range with the maximum isolator displacement falling within the design displacement of the isolator.

The statistical data of these results is presented in Figure 9.1 to Figure 9.8 for the bilinear plasticity model. From cumulative density functions (CDFs), trends in the displacement are observed. Firstly, the slope of the curve provides information on the dispersion of the results. A more gradual slope indicates data that is more dispersed while the steeper slopes indicate less dispersion with a smaller range in values. Spectrally matched values have less dispersion than the dispersion appropriate results. The dispersion is also observed through the width of the probability density functions (PDFs). Wider PDFs have higher dispersion corresponding to the same results seen in the slopes of the CDFs.

Statistically, it is important to note one item observed from the PDFs. The displacement range requirement is based on a confidence interval about the mean displacement. It does not consider the displacement percentile. The difference between confidence interval and percentile is sometimes misunderstood which can lead to very different results. For example, if the isolators are required to reach 99-percentile displacements, then this results in significantly higher values than those tabulated. This is especially true for the EDB level earthquake for the NRC motions. The 99-percentile displacement results in nearly 120 in. of displacement. This difference in value is significant and understanding the difference between these two measurements is very important to accurately approaching the seismic gap design.

[5] Refer to *Hybrid Simulation Tests of Seismically Isolated Nuclear Power Plant* (Schellenberg et al. 2014)

As observed in previous results, the isolator type does not have a significant influence on displacements. The current results suggest that ultimately, the ground motion input influences the overall displacements. Designers can select a seismic gap size and isolator arrangement with the option of changing the isolator used at a later time.

Additional results are presented in Appendix D.

Table 9.2 Isolator Displacements for the Bilinear Plasticity Isolator (EUR, DBE) .

(1 inch = 2.54cm)	Mean	Std	99% Lower Bound	99% Upper Bound	90% Lower Bound	90% Upper Bound
Dispersion Appropriate	3.6 in	1.5 in	2.8 in	4.6 in	3.1 in	4.2 in
Spectral Matched	2.9 in	1.3 in	2.5 in	3.3 in	2.6 in	3.2 in
Spectral Matched (Multi-Damp)	2.5 in	1.2 in	2.2 in	2.8 in	2.3 in	2.7 in

Table 9.3 Isolator Displacements for the Bilinear Plasticity Isolator (EUR, EDB).

(1 inch = 2.54cm)	Mean	Std	99% Lower Bound	99% Upper Bound	90% Lower Bound	90% Upper Bound
Dispersion Appropriate	7.5 in	1.5 in	5.9 in	9.5 in	6.5 in	8.7 in
Spectral Matched	6.2 in	1.2 in	5.5 in	7.1 in	5.8 in	6.7 in
Spectral Matched (Multi-Damp)	5.3 in	1.2 in	4.7 in	5.9 in	4.9 in	5.7 in

Table 9.4 Isolator Displacements for the Bilinear Plasticity Isolator (NRC, DBE).

(1 inch = 2.54cm)	Mean	Std	99% Lower Bound	99% Upper Bound	90% Lower Bound	90% Upper Bound
Dispersion Appropriate	21.5 in	1.6 in	15.9 in	28.9 in	17.9 in	25.7 in
Spectral Matched	18.2 in	1.1 in	16.7 in	19.9 in	17.3 in	19 in
Spectral Matched (Multi-Damp)	18.11 in	1.3 in	15.4 in	21.3 in	16.4 in	20 in

Table 9.5 Isolator Displacements for the Bilinear Plasticity Isolator (NRC, EDB).

(1 inch = 2.54cm)	Mean	Std	99% Lower Bound	99% Upper Bound	90% Lower Bound	90% Upper Bound
Dispersion Appropriate	43.9 in	1.6 in	32.8 in	58.8 in	36.8 in	52.4 in
Spectral Matched	40.7 in	1.2 in	36.9 in	44.9 in	38.3 in	43.2 in
Spectral Matched (Multi-Damp)	39.0 in	1.3 in	32.6 in	46.6 in	35 in	43.4 in

Table 9.6 Isolator Displacements for the Simple Constant Friction Isolator (EUR, DBE).

(1 inch = 2.54cm)	Mean	Std	99% Lower Bound	99% Upper Bound	90% Lower Bound	90% Upper Bound
Dispersion Appropriate	2.4 in	1.4 in	2.7 in	4.2 in	2.9 in	3.9 in
Spectral Matched	2.5 in	1.3 in	2.2 in	3.0 in	2.3 in	2.8 in
Spectral Matched (Multi-Damp)	2.0 in	1.2 in	1.8 in	2.3 in	1.9 in	2.2 in

Table 9.7 Isolator Displacements for the Simple Constant Friction Isolator (EUR, EDB).

(1 inch = 2.54cm)	Mean	Std	99% Lower Bound	99% Upper Bound	90% Lower Bound	90% Upper Bound
Dispersion Appropriate	7.4 in	1.4 in	5.9 in	9.3 in	6.4 in	8.5 in
Spectral Matched	6.2 in	1.2 in	5.5 in	7.1 in	5.8 in	6.7 in
Spectral Matched (Multi-Damp)	4.9 in	1.2 in	4.3 in	5.4 in	4.5 in	5.2 in

Table 9.8 Isolator Displacements for the Simple Constant Friction Isolator (NRC, DBE).

(1 inch = 2.54cm)	Mean	Std	99% Lower Bound	99% Upper Bound	90% Lower Bound	90% Upper Bound
Dispersion Appropriate	19.7 in	1.5 in	15.3 in	25.5 in	16.9 in	23.0 in
Spectral Matched	17.1 in	1.1 in	15.7 in	18.6 in	16.2 in	17.9 in
Spectral Matched (Multi-Damp)	17.0 in	1.3 in	14.7 in	19.6 in	15.5 in	18.5 in

Table 9.9 Isolator Displacements for the Simple Constant Friction Isolator (NRC, EDB).

(1 inch = 2.54cm)	Mean	Std	99% Lower Bound	99% Upper Bound	90% Lower Bound	90% Upper Bound
Dispersion Appropriate	43.9 in	1.6 in	32.8 in	58.8 in	36.8 in	52.4 in
Spectral Matched	32.7 in	1.1 in	31.0 in	34.6 in	32.7 in	33.8 in
Spectral Matched (Multi-Damp)	32.1 in	1.2 in	28.7 in	35.8 in	30.0 in	34.3 in

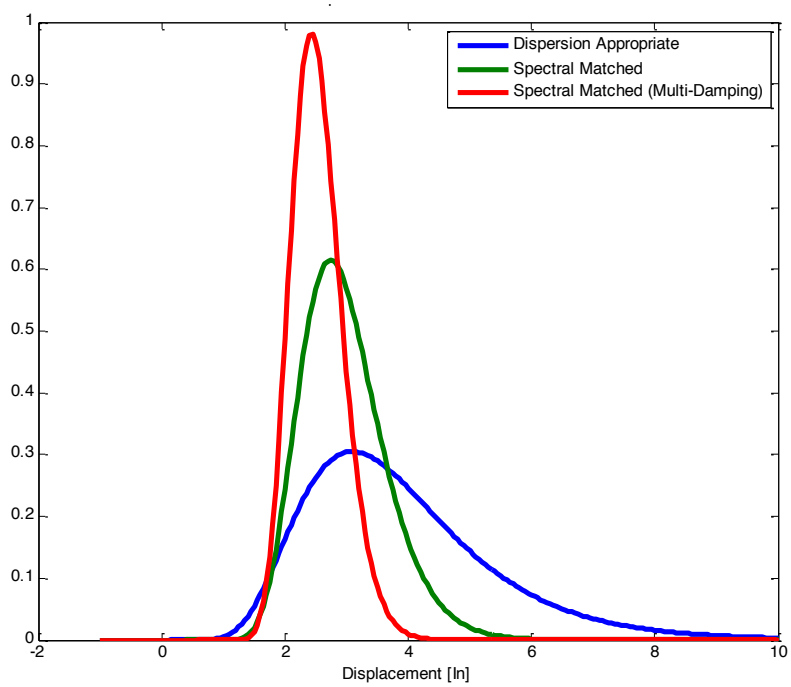

Figure 9.1 PDF for Bilinear Plasticity Model (EUR, DBE).

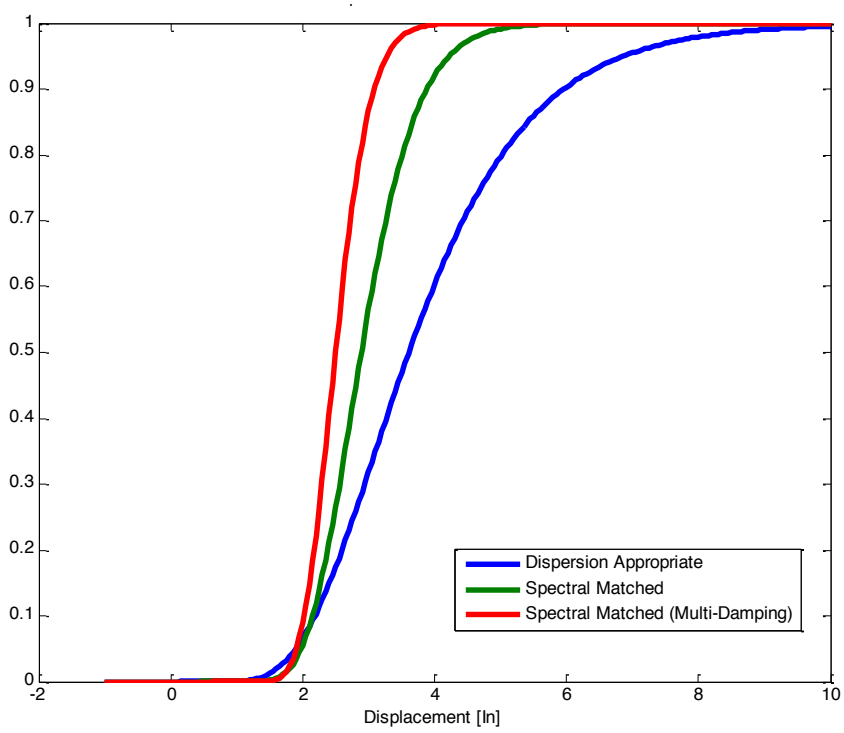

Figure 9.2 CDF for Bilinear Plasticity Model (EUR, DBE).

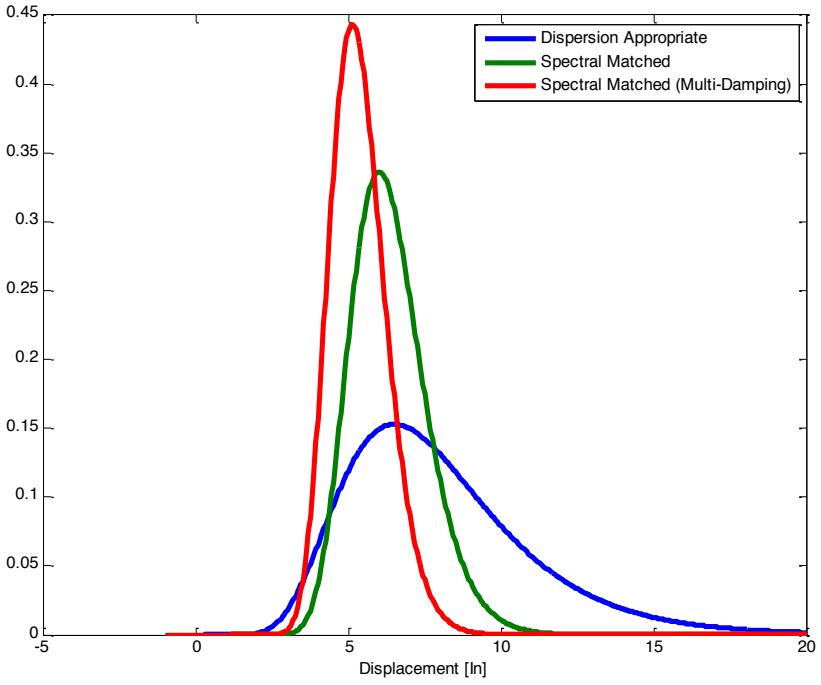

Figure 9.3 PDF for Bilinear Plasticity Model (EUR, EDB).

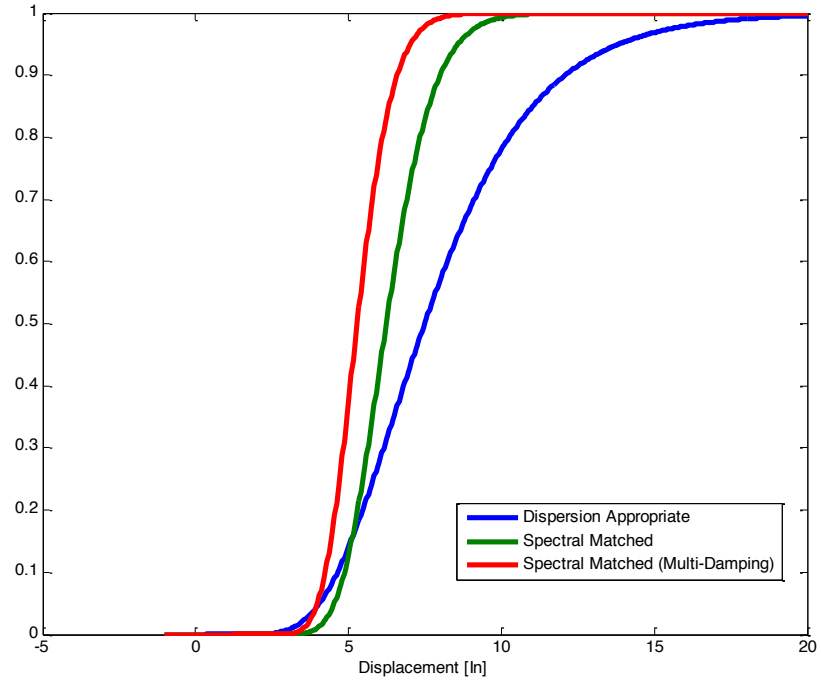

Figure 9.4 CDF for Bilinear Plasticity Model (EUR, EDB).

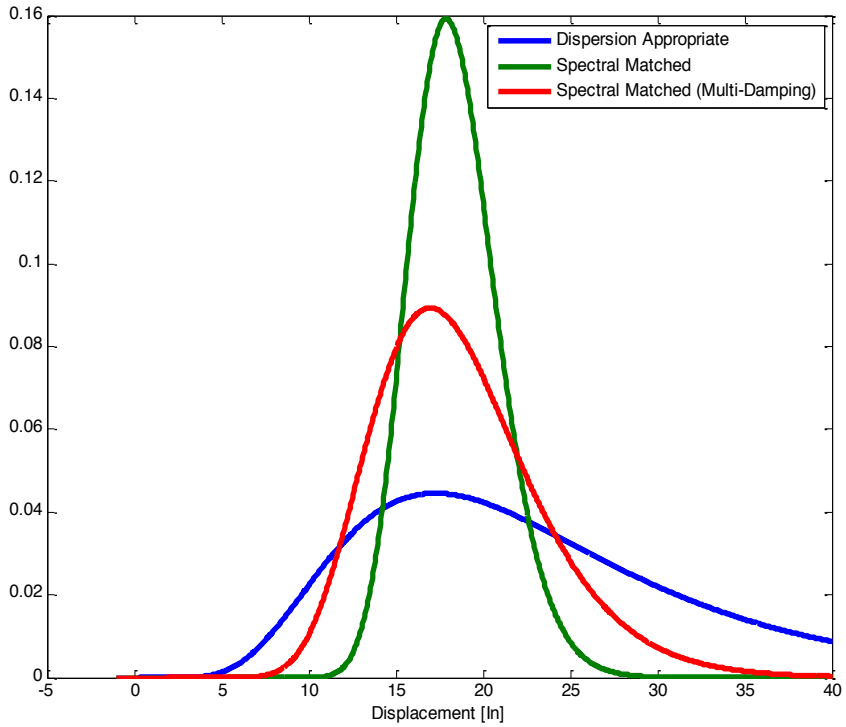

Figure 9.5 PDF for Bilinear Plasticity Model (NRC, DBE).

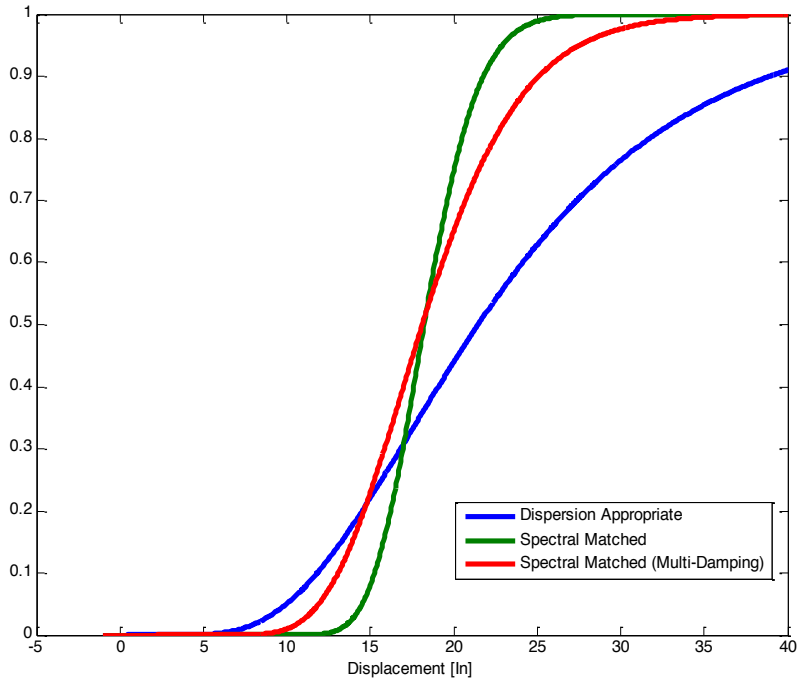

Figure 9.6 CDF for Bilinear Plasticity Model (NRC, DBE).

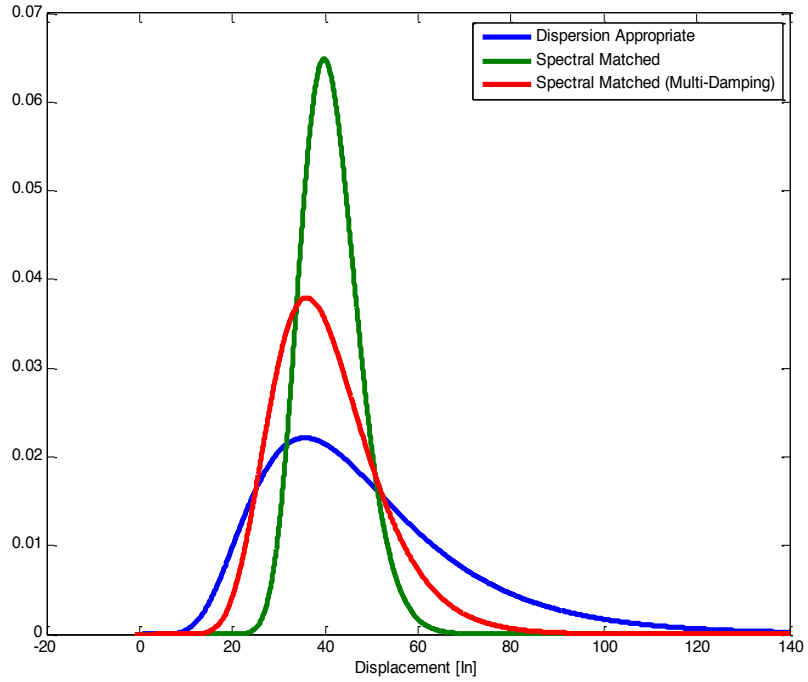

Figure 9.7 PDF for Bilinear Plasticity Model (NRC, EDB).

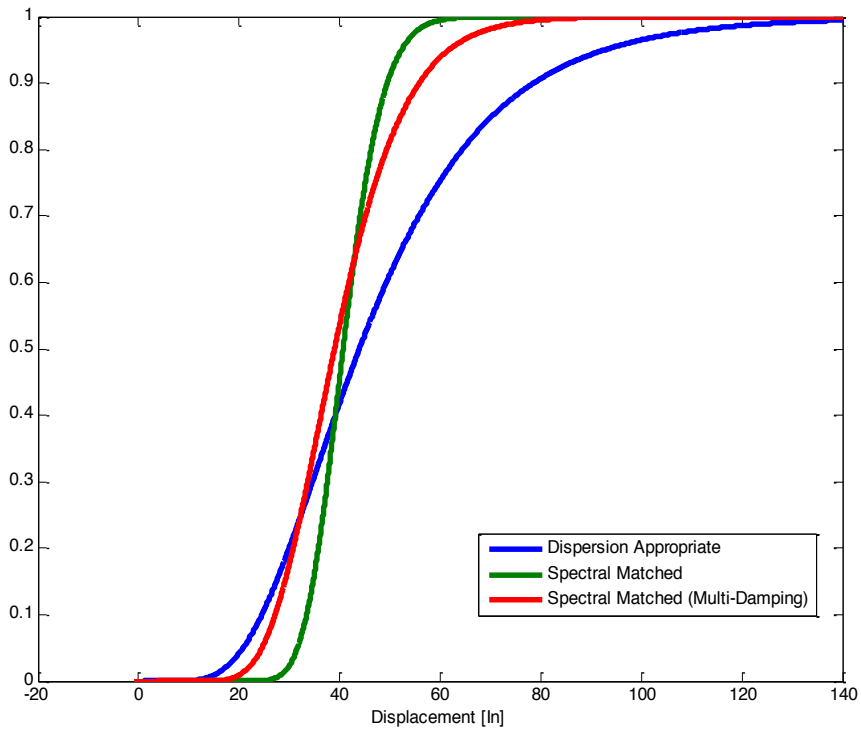

Figure 9.8 PDF for Bilinear Plasticity Model (NRC, EDB).

The tables presented in this section require an extensive amount of analysis and post-processing. For each isolator type (i.e. dispersion appropriate), the OpenSees model is run for all 20 ground motions. On a standard laptop computer, the analysis for a single isolator type is approximately 45-50 minutes. Once this is completed, the data is post-processed in MATLAB. Overall, a single table can take anywhere between 1-2 hours depending on the resources available.

An isolation system design may undergo numerous iterations due to changes in conditions, arrangements, isolation parameters, etc. However, dedicating this amount of time for each change in design may not be feasible. For this reason, based on the data from this study, equations were developed to approximate isolators based on several known values. This will reduce the amount of post-processing required because these equations will only require the use of a single known value.

From Equation 9.1, the 90 and 99 percent confidence level isolator displacements can be estimated knowing the mean isolator displacement (D_{mean}). The X factors for this equation are given in Table 9.10. From these factors, it shows that the isolator displacements are within +/- 20 percent of the mean displacement with the exception of the 99 percent upper bound factor for the dispersion appropriate motions.

$$\mathbf{D_{90\%,99\%} = X * D_{mean}} \qquad \textbf{(9.1)}$$

Table 9.10 X Factors for Equation 2.1 to Calculate the 90% and 99% Confidence Level Isolator Displacements Given the Mean Displacement.

X Factors	99% Lower Bound	99% Upper Bound	90% Lower Bound	90% Upper Bound
Dispersion Appropriate	0.8	1.3	0.9	1.2
Spectral Matched	0.9	1.1	0.9	1.1
Spectral Matched (Multi-Damp)	0.9	1.1	0.9	1.1

For Equation 2.2, the isolator displacements for the spectral matched and spectral matched (multi-damping) motions can be computed knowing the respective dispersion appropriate value (D_{DA}).

Table 9.11 presents the X factors for this equation. Based on these values, the spectral matched displacements are approximately +/- 30 percent of D_{DA}. The range is slightly larger than about the mean since dispersion appropriate motions result in larger isolator ranges as shown in the results presented earlier in this section.

$$\mathbf{D_{SM,SMD} = X * D_{DA}} \qquad \textbf{(9.2)}$$

Table 9.11 X Factors for Equation 2.2 to Calculate the Spectrally Matched Isolator Displacements Given the Dispersion Appropriate Displacement.

X Factors	99% Lower Bound	99% Upper Bound	90% Lower Bound	90% Upper Bound
Spectral Matched	1.0	0.7	0.9	0.8
Spectral Matched (Multi-Damp)	0.9	0.7	0.8	0.7

Finally, the last two Equations 9.3 and 9.4 allow for the calculation of the mean and 90 percent, 99 percent confidence level respectively.

(9.3) $$\mathbf{D_{mean,90\%} = X * D_{99\%}}$$

Table 9.12 X Factors for Equation 2.3 to Calculate the Mean or 90% Confidence Level Displacements Given the 99% Confidence Level Displacement.

X Factors	Mean from Lower Bound	Mean from Upper Bound	90% Lower Bound	90% Upper Bound
Dispersion Appropriate	1.3	0.8	1.1	0.9
Spectral Matched	1.1	0.9	1.0	1.0
Spectral Matched (Multi-Damp)	1.1	0.9	1.1	1.0

(9.4) $$\mathbf{D_{mean,99\%} = X * D_{90\%}}$$

Table 9.13 X Factors for Equation 2.3 to Calculate the Mean or 99% Confidence Level Displacements Given the 90% Confidence Level Displacement.

X Factors	Mean from Lower Bound	Mean from Upper Bound	99% Lower Bound	99% Upper Bound
Dispersion Appropriate	1.2	0.8	0.9	1.1
Spectral Matched	1.1	0.9	1.0	1.0
Spectral Matched (Multi-Damp)	1.1	0.9	0.9	1.1

These equations are useful and provide insight on the relationship between the various available displacements. All of the displacements are within a +/- 30 percent range from each other. However, 30 percent can be a significant amount if the base displacement is 30 in. versus 6 in. Nevertheless, utilizing these equations can provide engineers a means of estimating the isolation displacements knowing a single value. This can reduce computation and post-processing time. For the final design, it is recommended that full analysis be conducted to determine the isolator displacements at all required confidence levels.

9.4 CONCLUSIONS FOR STUDY 6

The results presented illustrate a number of important issues. Firstly, per the NRC guidelines, spectral matched ground motions tend to underestimate median responses and dispersion by a significant amount compared to dispersion appropriate sets of motion. In this case, results for the dispersion appropriate motions are higher than the spectral matched results.

10 Study 7: Ground Motion Subset

10.1 INTRODUCTION

The computation of the inelastic response of complex systems requires substantial effort. This is true not only in terms of analysis time but also in terms of data management and post-processing. Thus, it is of interest to identify how well smaller of subsets of motions can estimate response quantities such as isolator displacement at the 50%, 90% and 99% confidence level.

10.2 STUDY APPROACH

To explore this idea, the following approach was taken for the bilinear plasticity elastomeric. Firstly, in our study, geometric mean spectra for the full set of 20 dispersion appropriate ground motions at the DBE level were used for both the EUR and NRC. From these spectra, 4 periods were selected (T = 0.5, 2, 5 and 10 s). The selection of these periods was based on the attempt to cover the frequency span of interest. Next, at these periods, a lognormal distribution as fitted to the spectral values and the mean and standard deviation were computed using functions available in MATLAB. These mean and standard deviation values were the basis for the selection criteria of the subsets.

With the selection criteria set, the next step was to define the number of subsets to investigate. The study looked at generating subsets of 3, 7, 11 and 15 ground motions. Using predefined functions in MATLAB, all possible combinations for these subsets were generated. Next, each combination went through the same process as for the 20 ground motions where lognormal distributions were fitted at the designated periods with the mean and standard deviations computed. For each combination, the approximation error between the subset and the full set was computed using Equation 10.1 where v was the mean and standard deviation respectively. Based on this error, the combinations were ordered with the subset with the minimized error selected.

$$\epsilon = \left|\boldsymbol{\nu} - \boldsymbol{\nu}_{\mathbf{approx}}\right| \qquad \textbf{(10.1)}$$

10.3 RESULTS

Table 10.1 summarizes the subsets selected.

Table 10.1 Ground Motion Subsets for DBE Level Selected Based on the Minimized Error between Subset and Full Set of 20 Dispersion Appropriate Geometric Mean Spectra.

3 Ground Motions	EUR Subset: 4 7 10
	NRC Subset: 2 3 18
7 Ground Motions	EUR Subset: 3 4 6 7 10 16 17
	NRC Subset: 3 8 13 15 17 18 19
11 Ground Motions	EUR Subset: 2 3 4 6 7 10 11 15 16 17 18
	NRC Subset: 1 2 3 6 8 12 13 15 17 18 19
15 Ground Motions	EUR Subset: 1 2 3 4 5 6 7 9 10 11 12 15 16 17 18
	NRC Subset: 1 2 3 5 6 7 8 9 12 13 15 16 17 18 19

Based on these selections, the isolator displacement for the subsets were calculated using a similar process as done in the previous Chapter. Table 10.2 below provides the isolator displacements with Table 10.3 showing the error between the results of the subset and full set of motions. Results for the NRC DBE results are presented in Table 10.4 and Table 10.5.

Table 10.2 BL-P Isolator Displacements for the DBE EUR Motions for the Optimized Subsets (1 inch = 2.54cm).

	Mean	Std	99% Lower Bound	99% Upper Bound	90% Lower Bound	90% Upper Bound
3 GMs	2.4 in	1.3 in	0.5 in	10.7 in	1.5 in	3.7 in
7 GMs	3.1 in	1.7 in	1.6 in	6.3 in	2.2 in	4.5 in
11 GMs	3.3 in	1.5 in	2.3 in	4.9 in	2.7 in	4.2 in
15 GMs	3.4 in	1.5 in	2.5 in	4.6 in	2.9 in	4.1 in
20 GMs	3.6 in	1.5 in	2.8 in	4.6 in	3.1 in	4.2 in

Table 10.3 Errors as Percentages between the Results for the Subset and Full Set of Ground Motion Spectra of DBE EUR.

	Mean	Std	99% Lower Bound	99% Upper Bound	90% Lower Bound	90% Upper Bound
3 GMs	-35%	-12%	-81%	130%	-51%	-13%
7 GMs	-13%	12%	-45%	36%	-30%	8%
11 GMs	-7%	1%	-19%	6%	-14%	-0.8%
15 GMs	-5%	-0.3%	-10%	-0.6%	-8%	-3%

Table 10.4 BL-P Isolator Displacements for the DBE NRC Motions for the Optimized Subsets (1 inch = 2.54cm).

	Mean	Std	99% Lower Bound	99% Upper Bound	90% Lower Bound	90% Upper Bound
3 GMs	12.7 in	1.3 in	2.8 in	57.3 in	8.1 in	19.8 in
7 GMs	22.7 in	1.5 in	12.7 in	40.4 in	16.7 in	30.7 in
11 GMs	17.8 in	1.6 in	11.3 in	28 in	13.7 in	23 in
15 GMs	20.1 in	1.6 in	13.9 in	29 in	16.1 in	25 in
20 GMs	21.5 in	1.6 in	15.9 in	29 in	17.9 in	25.7 in

Table 10.5 Errors as Percentages between the Results for the Subset and Full Set of Ground Motion Spectra of DBE NRC.

	Mean	Std	99% Lower Bound	99% Upper Bound	90% Lower Bound	90% Upper Bound
3 GMs	-41%	-18%	-82%	99%	-55%	-23%
7 GMs	6%	-5%	-20%	39%	-7%	19%
11 GMs	-17%	1%	-29%	-3%	-23%	-10%
15 GMs	-6%	2%	-13%	0.6%	-10%	-3%

From Equation 10.6, the isolator displacements for 20 ground motions can be estimated knowing the respective isolator displacement for 3, 7, 11, or 15 ground motions respectively ($D_{\#GM}$). The X factors for this equation are given in Table 10.6. From these factors, it shows that the isolator displacements for 20 ground motions are best estimated as the number of ground motions increase. The greatest difference is between 3 and 7 ground motions where the X factors

reduce significantly. These factors were generated using similar methods from the previous Chapter.

$$D_{20\,GM} = X * D_{\#\,GM} \quad (10.2)$$

Table 10.6 X Factors for Equation 2.1 to Estimate the Isolator Displacements for 20 Ground Motions Given the Respective Isolator Displacements for 3, 7, 11, or 15 Ground Motions.

X Factors	Mean	99% Lower Bound	99% Upper Bound	90% Lower Bound	90% Upper Bound
3 GMs	1.6	5.6	0.5	2.1	1.2
7 GMs	1.1	1.5	0.7	1.2	0.9
11 GMs	1.1	1.3	1.0	1.2	1.1
15 GMs	1.1	1.1	1.0	1.1	1.0

10.4 CONCLUSIONS FOR STUDY 7

Results show that at least 11 ground motions are needed to determine the isolator displacements. Less ground motions can be used to provide more "conservative" results but they can also produce unrealistic displacements given the lack of information. The use of 11 ground motions has been suggested by (Huang et al. 2009). However, technically, there appears to be an opportunity to use less than 11 ground motions since the increase between the 7 and 11 subsets appears to show a still relatively acceptable error. One major consideration for the future is the actual tolerance that will be considered acceptable by the client. This is meant for a first-level estimate as full ground motion analysis is required to verify the final design. However, by using a smaller set of ground motions, these results show that you do not necessarily have to have 20 motions to get reasonable results. The error must be accounted for but this would be within a tolerance set This is very useful as some locations may not have access to a wide set of seismic events. Another situation is that the given conditions for that the site do not match many other locations with seismic occurrences. Although this does introduce a level of uncertainty, which is discussed in Chapter 6, estimates are still possible with reasonable numbers. But using too few motions can and does show that there is a major error introduced which cannot accurately provide displacements.

11 Characterize Epistemic and Aleatoric Uncertainties

Two sources of uncertainty are epistemic and aleatoric. Epistemic uncertainty pertains to the scientific uncertainty in the model of the process due to limited data and knowledge (Abrahamson). This type of uncertainty can be reduced with the introduction of additional data or knowledge about the system (Sandomeer, 2008). Aleatoric uncertainty, on the other hand, is associated with intrinsic randomness in a process, which cannot be reduced. In this study, both types of uncertainties are encountered.

11.1 EPISTEMIC

The most significant source of epistemic uncertainty is in the models used for the structure and the isolators. All these systems are complex in terms of their material properties and behavior. As a result, elements are used that generate similar behavior to the actual structural elements.

The APR1400 model is a lump-stick model that gives very basic information on the mass and stiffness distribution along with general arrangement. This type of model is significantly more simplified than a finite element model (FEM). Additionally, from the original SAP2000 model there have been changes in the elements and materials for usage in the OpenSees program. Future studies should consider the use of a FEM to capture detail in the structural response.

A secondary part of the system is the isolation. There are two major elements for uncertainty. Firstly, the isolator arrangement was simplified for a number of studies conducted. This is done to reduce computation time and allow the study to focus on the parameters of interest. Due to these simplifications, results do not account for torsion or rocking. This uncertainty is considered in the 3D studies. Secondly, the isolator elements used linear and nonlinear models that approximate the experimental behavior. These models do not take into account temperature and rate change, which should be considered in future studies. This uncertainty is considered by studying a number of isolator devices with varying hysteretic behavior and conducting sensitivity analysis to determine isolator properties with greatest influence on response.

Finally, the generation and selection of ground motions introduce an epistemic uncertainty due to their selection. This study used dispersion appropriate as well as spectrum-matched motions. For the vertical component of motion, there is a secondary level of uncertainty introduced. The vertical component of motion is two-thirds of the horizontal motions. Although

this is considered an acceptable practice it still retains a level of uncertainty due to the dependence on the accuracy of the horizontal components. Additionally, this component is then put through the process of spectral matching which introduces another potential for error in computation or estimation. Overall, it may be plausible to research the effect of using only spectrally matched the horizontal components of motion. Generally, epistemic uncertainty can be reduced with the increase in data; however, this may be difficult for ground motions. In this study's case, a site was not specified allowing for more flexibility in the selection process. If a specific site is specified, it may be difficult to obtain a large selection of motions to choose from6.

11.2 ALEATORIC

Randomization of parameters in this study tries to account for the aleatoric uncertainty. For the sensitivity analysis, using a variety of values randomizes the isolator parameters. The values were selected by increasing and decreasing the parameters by a percentage. For future studies, it is recommended to study the use of dispersed parameters based on a distribution to reduce the amount of randomness introduced. The ground motions are another source of aleatoric uncertainty. However, through the use of dispersed appropriate motions accounts for the randomness present in the ground motion selection. This type of uncertainty is harder to reduce but there are methods of reducing it by using distributed and dispersed quantities.

[6] Uncertainty in ground motion selection and generation is discussed in more detail in Volume 2, *Selection of Ground Motions*.

12 Overall Findings and Recommendations

A large number of nuclear facilities are in operation worldwide. As the number and complexity of regulations and codes needed for certification of new plants has increased over the past few decades, reactor designers are increasingly considering the use of standardized plant designs. However, these designs must account for a great variation in seismic conditions that can be expected worldwide. To avoid the need to re-design and create one-of-a-kind plants, seismic isolation is being considered as a safe and economical means of adapting standard plant designs to a wide variety of seismic conditions.

Seismic isolation is used in various applications for both traditional structures and industry. Isolation is known for its ability to reduce forces and displacements in structures due to horizontal ground motions. However, studies of the application of seismic isolation to nuclear facilities are limited with few practical applications to modern plant design.

12.1 STUDY FINDINGS

This report's goal was to summarize the work in assessing the effectiveness of applying isolation systems to a nuclear power plant by exploring the APR1400 model. The APR1400 is a substantial structure capable of remaining elastic per regulatory guidelines for earthquakes having peak ground accelerations of at least 30%g. In researching the performance of an isolated APR1400 plant at a DBE of 0.5g, a number of factors were taken into account. Firstly, not only must the structure remain in adequate conditions post-seismic event but the equipment must also be operable. Thus, the isolation system must protect both the structure and its contents. Secondly, the equipment is a major challenge for interpretation of results. General knowledge suggests critical equipment in a NPP has a frequency of 2 Hz and higher. However, a wide variety of important equipment can be found in NPPs so a more general assessment of the effect of seismic isolation over a broad range of frequencies should be considered.

With these two major factors in mind, the research provides an overview from reinforcement of isolation's capabilities with horizontal ground motions to analytical models and studies focusing on variations in response for different isolator types, models, and ground motion inputs.

The initial study examined the abilities of isolation to reduce horizontal floor accelerations and explored the effects of multiple components of horizontal ground motions. It was effectively shown that with seismic isolation (for all types and models) there was a significant reduction in the FRS at frequencies in excess of 1 Hz at all locations investigated compared to a fixed base situation. The isolated structure did have accelerations higher than the fixed base structure in the low frequency range, but the values were comparatively low to the overall responses observed. The overall maximum floor acceleration for the isolated and fixed base structures occurred at the structures fundamental frequency. The analyses showed results were sensitive to the number of horizontal ground motion components used. As a result, it is recommended that 2D horizontal analysis be used to capture the full structural response. Between the isolator systems, there was variation in performance. The linear elastomeric bearing used in combination with 20% supplemental viscous damping reduced accelerations and presented relatively low high frequency content. Nonlinear isolators performed well in the analyses but introduced high frequency content in FRS near the fundamental frequency of the structure.

The next study explored the effects of isolator hysteretic characteristics on performance. For the bilinear elastomeric, a difference in results was expected between the FRS of the plasticity and Bouc-Wen models due to their hysteretic characteristics. This was not observed. When a segment from a time history of response was examined, the associated displacement time history showed no changes in the response for the two models. However, the acceleration time history captured instances of high frequency oscillation in the acceleration time histories at the points of yielding and unloading. The peak amplitude of these high frequency acceleration oscillations were comparatively small (about 0.02g) resulting in the negligible appearance of this behavior in the system's FRS. Nevertheless, these instances of amplified acceleration were reduced with the Bouc-Wen model.

Since amplified accelerations were observed, the next subject involved understanding the influence of the Bouc-Wen hysteretic parameters. Approximately, how much change in the roundness of the Bouc-Wen hysteresis was needed to create a more significant difference in response? Research showed that the displacement time history is not affected by changes in the model's hysteresis. The Bouc-Wen model would need a η less than 1.0 to observe a significant change in response compared to the plasticity model. Thus, this parameter of the model is not as influential in changing the response considering the other given parameters for the current design.

The next study investigated which parameters do have a significant influence on the response. Results showed the greatest affect on the FRS coming from changes in the initial stiffness of the isolator. When the initial stiffness is a fraction of the original value, the peak accelerations at this level are found in the low frequency range, which is out of the typical range of equipment of 2-10 Hz. But if the initial stiffness is significantly higher than the original stiffness, there is a shift of peaks to higher frequency ranges. The structure and its equipment must be well understood so that the initial stiffness of the isolator device can be selected to avoid or minimize these peaks in the high frequency range of the FRS. Before isolation design takes place, a thorough understanding of the structural system and equipment is needed to properly select the isolation parameters for optimized response.

With the completion of the 2D studies, the next studies explored the effect of 3D input motion. For vertical FRS, there was no difference in the response between the use of vertical only and vertical-horizontal input motion. Most notably, the accelerations were comparable to

the fixed base case suggesting that additional means of controlling vertical accelerations is needed. For the horizontal structural response, the inclusion of the vertical component of motion increased the horizontal FRS. The amount of increased acceleration was dependent on the ground motion input and the isolator type. However, it should be noted that the models used for elastomeric bearings did not include coupling of horizontal and vertical response. These results emphasized the necessity of 3D analysis to fully capture the structural response in order to characterize system performance.

Beyond the FRS, a major factor on the system performance will depend on the interaction of the isolated system with the fixed based buildings on the nuclear island. These two entities are separated by the seismic gap that is designed based on the ultimate lateral displacement. From the perspective of the draft US NRC NUREG, there should be less than a 10% probability of the isolated structure contacting the hard stop under the EDB event and less than 1% probability of contact for the DBE. Thus, studies herein focused on the 90 and 99 percent confidence intervals for the mean isolator displacement. Considering both the EUR and NRC motions, the mean displacements ranged from 2-20 in. for the DBE and 6-45 in. for the EDB earthquake. Ground motion selection was very influential in the results. Dispersion appropriate motions used to get a realistic estimate of the dispersions of response results produced the largest displacements with the most dispersion. The EUR motions resulted in maximum displacements substantially lower than computed for the NRC motions. Current isolator designs considered would have difficulty achieving the displacements predicted with the NRC motions at the targeted dispersion level. This would be not so difficult for the EUR motions. Understanding the extent of isolator displacement is essential as it not only will control the seismic gap size but it directly effects the design of the isolators.

12.2 RECOMMENDATIONS FOR FUTURE RESEARCH

The results from this report's studies have created an excellent foundation for further research and development of seismic isolation for NPPs. A number of future studies are recommended.

Improved bearing modeling is needed to explore rate and temperature effects and the mechanisms of failure/rupture. Means of determining the time and temperature dependency of the properties will greatly enhance numerical analysis, as it will better represent in-situ conditions. However, being able to observe changes in the material properties can provide insight into how isolator hysteresis and resulting structural responses change.

Additionally, the current model cannot provide information on the failure and rupture event of the isolators. At the point of failure, there are a myriad of questions raised. Does the isolator failure transmit forces into the structure and if so, are these forces similar to impact loadings? Under what conditions, can we expect this failure and how many isolators would be lost? And most importantly, given the failure of X number of isolators, what is the expected performance level of the structure? These answers will aide in developing the most effective isolation system.

For vertical motion, there are a number of areas for future study. Isolation is not as effective vertically compared to horizontal studies. Sensitivity analysis is needed to determine which parameters affect this response and can be used to reduce the accelerations while still maintaining optimal responses both vertically and horizontally. The differences in response between the vertical only and uncoupled motion need to be explored further. Results suggest a consideration of P- Δ effects and their possible influence on response.

Current studies involve the use of a single isolator type for the whole isolation system. However, a system technically could be comprised of multiple isolator types. To have such a system, will require an understanding of the structural response due to certain layouts and combinations of isolators. Situations where axial or torsional issues are identified may be resolved through the use of a specific isolator type along the perimeter. Information such as this can be useful in optimizing the system and possibly reducing costs by utilizing specialized isolators only at specific locations.

One area of research that has been raised in numerous conferences, meetings, and a few research studies is the effect of aircraft impact on a seismically isolated NPP. Current US standards require this analysis for certification. Worldwide there is some level of impact study required. Because the isolated system is allowed to move laterally, there is concern about how impact forces should be handled and whether auxiliary systems need to be used as an initial barrier.

Aircraft impact involves sudden, fast loading on the system and, the DBE and EDB earthquakes involve strong earthquake motions. What happens when you experience motions on the other side of the spectrum such as low seismic events? The isolation system is meant to initiate at a given level of motion. Up until this point, the isolation system will have a given stiffness. Research should investigate whether this additional stiffness at the structure's base is detrimental or non-influential to the response at these seismic levels. If there is a negative interaction, studies should explore means of reducing this behavior while maintaining the performance level at the DBE and EDB.

Finally, the research involved with NPP analysis is extensive. The computation and the data acquisition require a tremendous amount of time and data storage. Consideration and use of simplified designs as used in this report provide excellent estimates to the expected responses. However, the final design work should include a full-scale analysis to verify performance levels.

12.3 CONCLUSION

Seismic isolation is a very adaptable technology available on today's market for satisfying seismic requirements of nuclear facilities. To utilize isolation's abilities to the fullest extent, engineers must understand the inherent behavior of these systems and response sensitivity. This research initiated this work, provided recommendations, and has created a foundation for future development of seismic isolation for NPP application.

REFERENCES

AASHTO. 2010. *Guide Specification for Seismic Isolation Design*. American Association of State Highway and Transportation Officials, Washington, D.C.

Abrahamson, Norm. "Aleatory Variability and Epistemic Uncertainty." Print.

ASCE (2005). Seismic Design Criteria for Structures, Systems and Components in Nuclear facilities, Standards ASCE/SEI 43-05, American Society of Civil Engineers, Reston, VA.

ASCE. 1998. *Seismic Analysis of Safety-Related Nuclear Structures and* Commentary. American Society of Civil Engineers, Standards ASCE 4-98, Reston VA.

Bensusan, Zachary . "Expansion Joints Dampen Harmful Vibration in Emergency Diesel Generators." *Nuclear Power International Magazine* July 2011. Print.

Blandford E., Keldrauk E., Laufer M., Mieler M., Wei J., Stojadinovic B., Peterson P.F. (2009). Advanced seismic base isolation methods for modular reactors, *Technical Report No. UCBTH-09-004*, University of California, Berkeley, CA.

Bouc, R. (1967). "Forced vibration of mechanical systems with hysteresis". *Proceedings of the Fourth Conference on Nonlinear Oscillation*. Prague, Czechoslovakia. p. 315.

Bouc, R. (1971). "Modèle mathématique d'hystérésis: application aux systèmes à un degré de liberté". *Acustica* (in French) **24,**: 16–25.

Chopra, Anil K.. *Dynamics of structures: theory and applications to earthquake engineering*. 3rd ed. Upper Saddle River, N.J.: Pearson/Prentice Hall, 2007. Print.

Constantinou, M.C., I. Kalpakidis, A. Filiatrault, and R.A. Ecker Lay. "LRFD-Based Analysis and Design Procedures for Bridge Bearings and Seismic Isolators." *MCEER* MCEER-11-0004 (2011). Print.

Diaz, S. 2010. "The Anti-Seismic Bearings of ITER & JHR," *Proceedings, 1st Kashiwazaki International Symposium on Seismic Safety of Nuclear Installations*. Niigata Institute of Technology, Kashiwazaki, Niigata, Japan.

Drosos, V., Sitar, N., Zhou, Z. and Mahin, S. (2014). Investigation of Seismic Isolation Technology Applied to the APR1400 Nuclear Power Plant: Volume 3 -- Effects of Soil-Structure Interaction on Isolated NPP, Technical Report to KEPCO Engineering and Construction, Pacific Engineering Research Center, University of California, Berkeley, CA.

Dynamic Isolation Systems, Inc. (2012). <http://www.dis-inc.com>.

FEMA. 2011. Reducing the Risks of Nonstructural Earthquake Damage. FEMA E- 74. Federal Emergency Management Agency, Washington, D.C.

Germane, L. 2010 "Seismic Isolation of the Jules Horowitz Reactor," *Proceedings, 1st Kashiwasaki International Symposium on Seismic Safety of Nuclear Installation, Workshop 2 – Seismic Isolation of Nuclear Facilities*. Kashiwaskai, Niigata, Japan.

Higashino, M. and Okamoto, S. (2006). Response Control and Seismic Isolation of Buildings, State of the Art Report, Task Group TG44, International Council of Building Research Organizations, Taylor and Francis, New York.

Huang Y-N., Whittaker A.S., Luco N. (2008). Performance assessment of conventional and base-isolated nuclear power plants for earthquake and blast loadings*, MCEER Technical Report No. 08-0019*, State University of New York, Buffalo, NY.

Huang, Y-N. and Whittaker, A.S. (2009). Assessment of Base-Isolated Nuclear Structures for Design and Beyond-Design Basis Earthquake Shaking, *MCEER Technical Report No. 09-0008*, State University of New York, Buffalo, NY.

JEA (2000). *Design and Technical Guideline of Seismic Isolation Structure for Nuclear Power Plant*, Japan Electric Association, *JEAG 4614-2000* (in Japanese).

JEAG (2000). *Design Guideline of Seismic Isolation System for Nuclear Power Plants, JEAG 4614-2000*, Japan Electric Association.

Kammerer A.M., Whittaker A.S., Constantinou M.C. (2011). *Technical Considerations for Seismic Isolation of Nuclear Facilities (DRAFT)*. Office Nuclear Regulatory Research Division of Engineering, U.S. Nuclear Regulatory Commission, Washington, D.C. (Draft Version for Review).

Kelly J.M. (1997). *Earthquake-resistant Design with Rubber*, London: Springer.

Konstantinidis, D., and F. Nikfar. "Seismic Performance of Sliding Contents in Base-Isolated Buildings." Proc. of Tenth U.S. National Conference on Earthquake Engineering, Anchorage, Alaska. N.p.: n.p., 2014. N. pag. Print.

Lee, Sang-Hoon . "Seismic Analysis on the APR1400 with Seismic Isolation." KEPCO E&C and PEER Meeting. KEPCO E&C. UC Berkeley, Berkeley. Jan. 2013. Lecture.

Marin-Artieda, C.C. "Case Studies on the Seismic Protection of Equipment in Essential Buildings." Proc. of Tenth U.S. National Conference on Earthquake Engineering, Anchorage, Alaska. N.p.: n.p., 2014. N. pag. Print.

MATLAB and Statistics Toolbox Release 2013b, The MathWorks, Inc., Natick, Massachusetts, United States.

McKenna, Frank, and G. L. Fenves, "Open system for earthquake engineering simulation." *University of California, Berkeley, CA* (2000).

Morgan, T. and Mahin, S. (2011). The Use of Base Isolation Systems to Achieve Complex Seismic Performance Objectives, PEER Report PEER 2011/06, Pacific Earthquake Engineering Research Center, University of California, Berkeley, CA.

Motosaka, Masato, and Kazuya Mitsuji. "Building Damage during the 2011 off the Pacific Coast of Tohoku Earthquake." *Soils and Foundations* (2012): 929-44. Web.

Naeim F, Kelly J.M (1999). *Design of Seismic Isolated Structures: From Theory to Practice*, John Wiley and Sons, Inc., Chichester, U.K.

Nuclear Regulatory Commission, (1973).Regulatory Guide 1.60 (Rev. 1, December 1973), Design Response Spectra for Seismic Deign of Nuclear Power Plants, U.S. Nuclear Regulatory Commission, NUREG-1.60, Washington, D.C.

Russell, Pam R. "Nuclear Rebirth." *Engineering News-Record* 6 Dec. 2010: 30-37. Web.

Sandomeer, Markus K. . "Aleatoric or epistemic? Does it matter?." presentation on the paper of Kiureghian and Ditlevsen, 2008. ETH, IBK. Lecture.

Schellenberg, A., Drosos, V., Mahin, S. and Sitar, N. (2014a). Investigation of Seismic Isolation Technology Applied to the APR1400 Nuclear Power Plant - Volume 1: Review and Improve Numerical Models, Technical Report to KEPCO Engineering and Construction, Pacific Engineering Research Center, University of California, Berkeley, CA.

Schellenberg, A., Baker, J., Mahin, S. and Sitar, N. (2014b). Investigation of Seismic Isolation Technology Applied to the APR1400 Nuclear Power Plant - Volume 2: Selection of Ground Motions, Technical Report to KEPCO Engineering and Construction, Pacific Engineering Research Center, University of California, Berkeley, CA.

Spie Batignolles and Electricité de France. 1985. *Protection of Nuclear Power Plants Against Earthquakes (Aseismic Bearings)*, movie.

Taylor, A. W., and Takeru Igusa. *Primer on seismic isolation*. Reston, VA: American Society of Civil Engineers, 2004. Print.

Terzic, V., Schellenberg, A., McKenna, F., Mahin, S. and Sitar, N. (2014), Investigation of Seismic Isolation Technology Applied to the APR1400 Nuclear Power Plant, Volume 5: Sensitivity Assessment of a Seismically Isolated Nuclear Power Plant, Technical Report to KEPCO Engineering and Construction, Inc., Pacific Earthquake Engineering Research Center, University of California, Berkeley, June 2014.

"The Great East Japan Earthquake Damage Report." *Building Research Institute* (2011): 22-27. Web.

Wen, Y. K. (1976). "Method for random vibration of hysteretic systems". *Journal of Engineering Mechanics* (American Society of Civil Engineers) **102** (2): 249–263.

Wong, J. and Mahin, S. (2012). Background information on seismically isolated facilities at nuclear power stations, Project Report on Task 1.2 to KEPCO E&C, Seismic Isolation of Nuclear Power Plants (Phase 1), Pacific Earthquake Engineering Research Center, University of California, Berkeley, May 2012.

Wong, J., Zhou, Z. and Mahin, S. (2012). On-going research activities for seismically isolated facilities at nuclear power stations, Project Report on Task 1.3 to KEPCO E&C, Seismic Isolation of Nuclear Power Plants (Phase 1), Pacific Earthquake Engineering Research Center, University of California, Berkeley, May 2012.

Wong, J., Zhou, Z. and Mahin, S. (2012). Design criteria, regulatory guidelines, and code requirements for seismically isolated facilities at nuclear power stations, Project Report on Task 1.4 to KEPCO E&C, Seismic Isolation of Nuclear Power Plants (Phase 1), Pacific Earthquake Engineering Research Center, University of California, Berkeley, May 2012.

Wong, J., Zhou, Z. and Mahin, S. (2012). Brief summary of the advantages and disadvantages of seismic isolation of NPPs, Project Report on Task 1.6 to KEPCO E&C, Seismic Isolation of Nuclear Power Plants (Phase 1), Pacific Earthquake Engineering Research Center, University of California, Berkeley, May 2012.

Wong, J. and Mahin, S. (2013a). Preliminary analysis of floor response spectra of a seismically base isolated nuclear power plant, Transactions, SMIRT-22, International Association for Structural Mechanics in Reactor Technology, San Francisco, CA, August 2013.

Wong, J., Zhou, Z., and Mahin, S. (2013b). Seismic Isolation of Nuclear Power Plants, Report 3002000561, Electric Power Research Institute, Palo Alto, CA, August 2013.

Wong, J., Schellenberg, A. and Mahin, S. (2013c). Effects of isolator modeling on floor response spectra of seismically base isolated nuclear power plant, 13th World Conference on Seismic Isolation, Japan Society for Seismic Isolation, Sendai Japan, September 2013.

Zhou, Z., Sitar, N. and Mahin, S. (2013a). Effects of Soil-Structure Interaction on Seismically Isolated Nuclear Power Plant, Transactions, SMIRT-22, International Association for Structural Mechanics in Reactor Technology, San Francisco, CA, August 2013.

Zhou, Z., Wong, J. and Mahin, S. (2013b). Vertical and 3D isolation Systems: A review with emphasis on their use in nuclear structures, Transactions, SMIRT-22, International Association for Structural Mechanics in Reactor Technology, San Francisco, CA, August 2013.

Zhou, Z., Sitar, N. and Mahin, S. (2013c). Effects of changing soil and isolator properties on seismic response of an isolated nuclear power plant, 13th World Conference on Seismic Isolation, Japan Society for Seismic Isolation, Sendai Japan, September 2013.

Appendix A

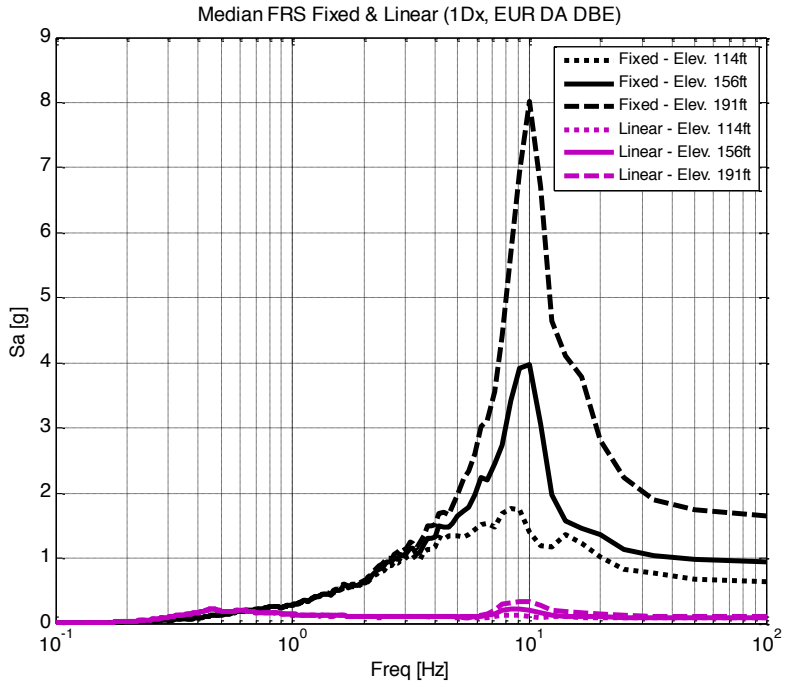

Figure A.1 Median FRS Primary Shield Wall H1 Only-Fixed vs Linear (EUR DBE).

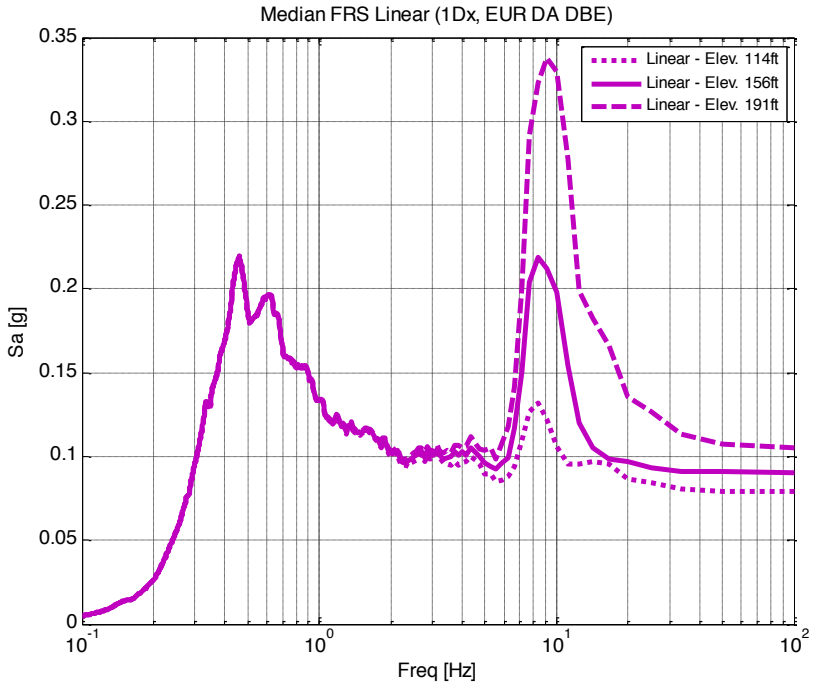

Figure A.2 Median FRS Primary Shield Wall H1 Only- Linear (EUR DBE).

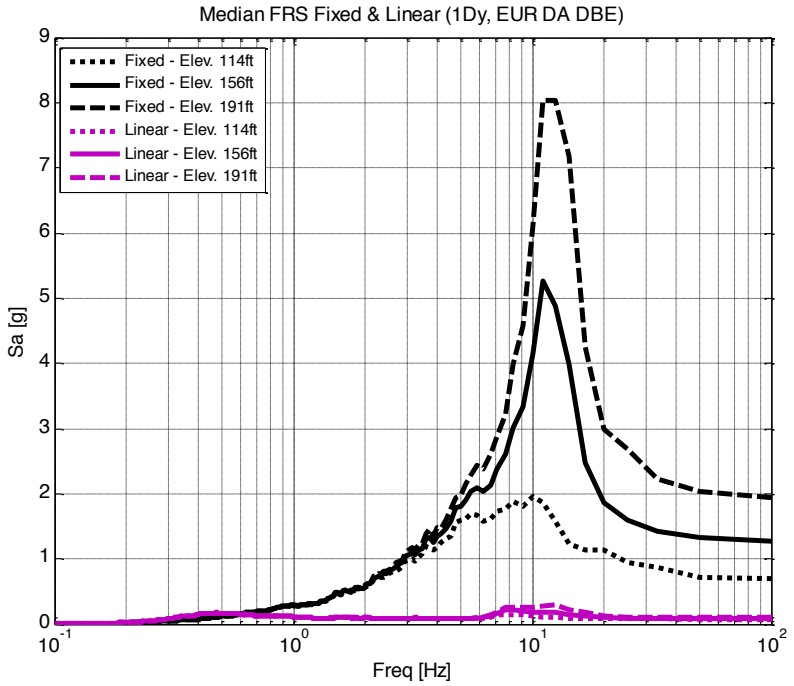

Figure A.3 Median FRS Primary Shield Wall H2 Only- Fixed vs Linear (EUR DBE).

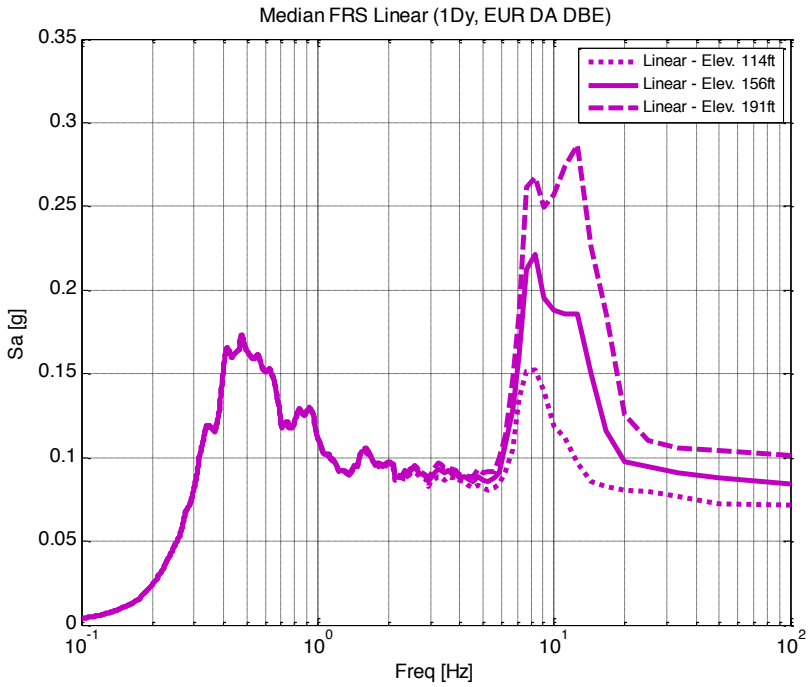

Figure A.4 Median FRS Primary Shield Wall H2 Only- Linear (EUR DBE).

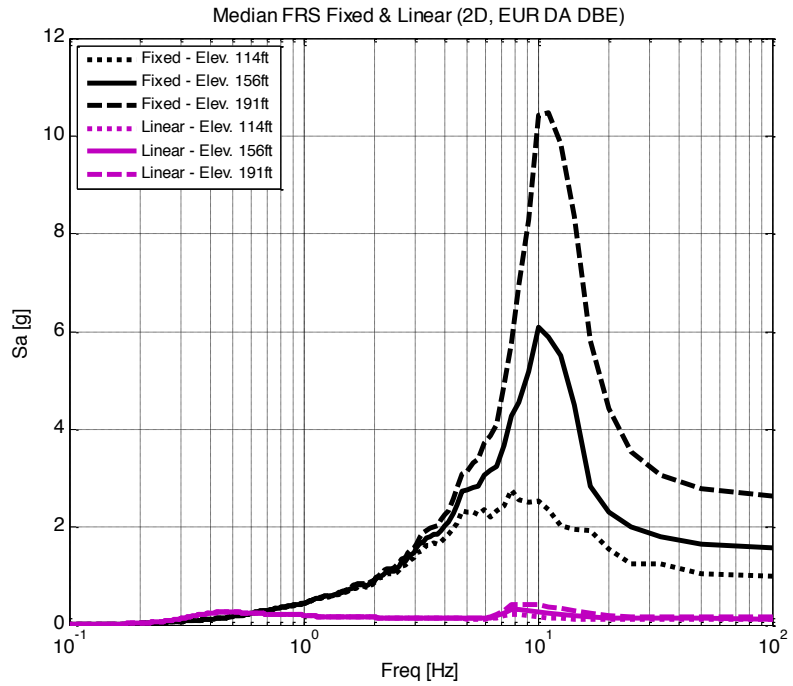

Figure A.5 Median FRS Primary Shield Wall H1+H2 - Fixed vs Linear (EUR DBE).

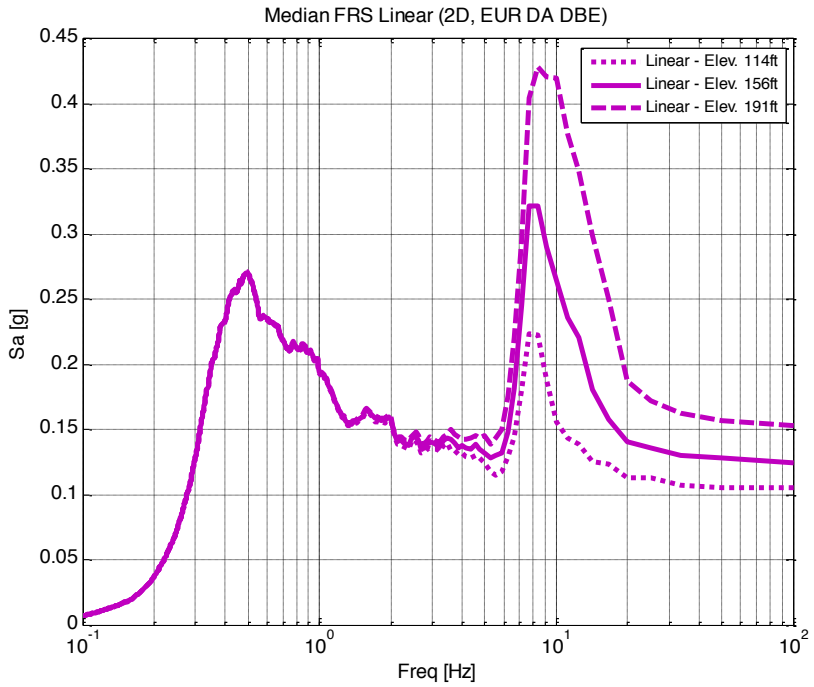

Figure A.6 Median FRS Primary Shield Wall H1+H2 - Linear (EUR DBE).

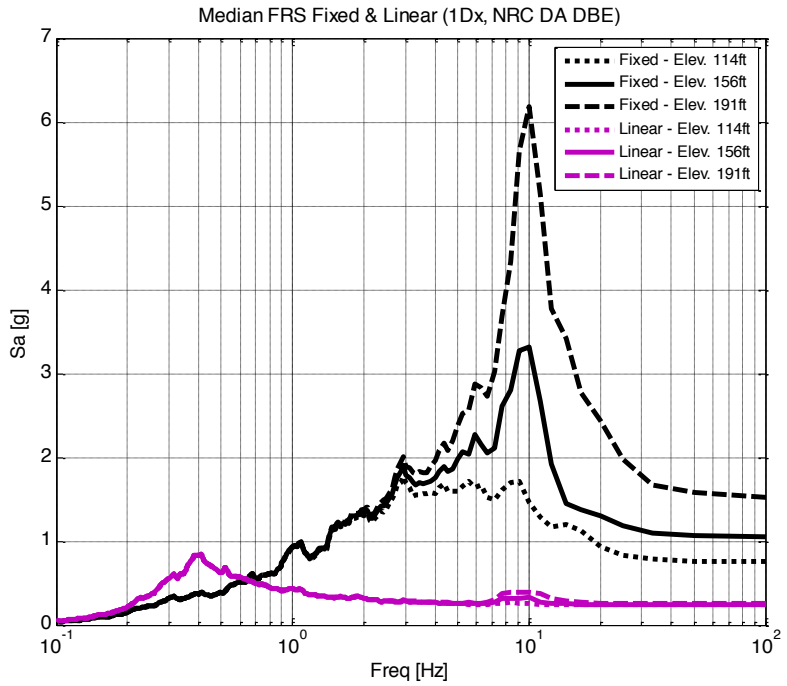

Figure A.7 Median FRS Primary Shield Wall H1 Only – Fixed vs Linear (NRC DBE).

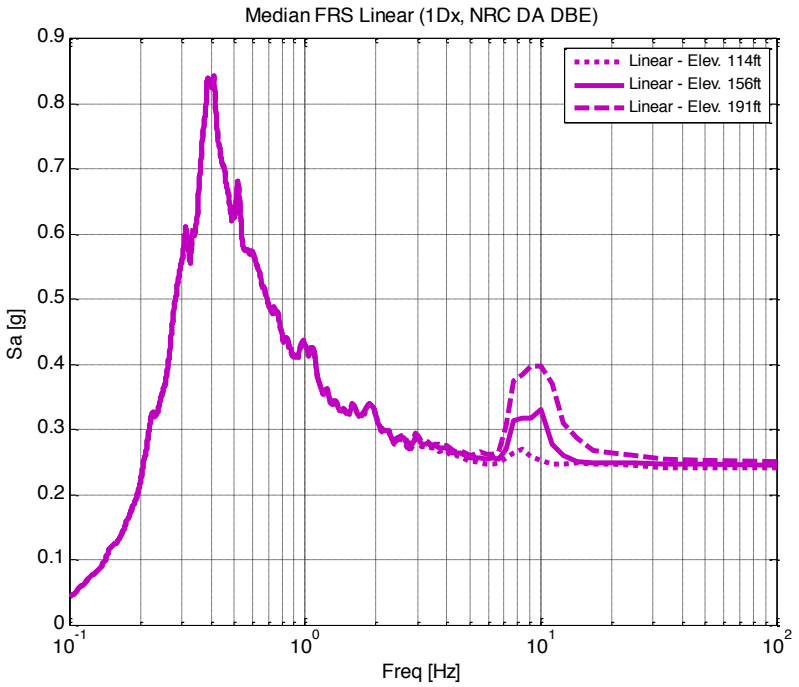

Figure A.8 Median FRS Primary Shield Wall H1 Only –Linear (NRC DBE).

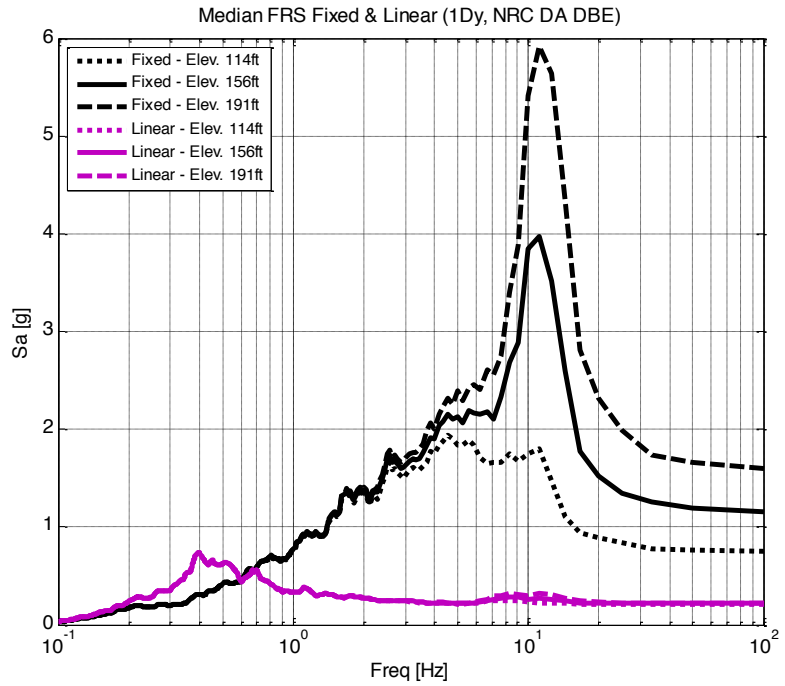

Figure A.9 Median FRS Primary Shield Wall H2 Only –Fixed vs Linear (NRC DBE).

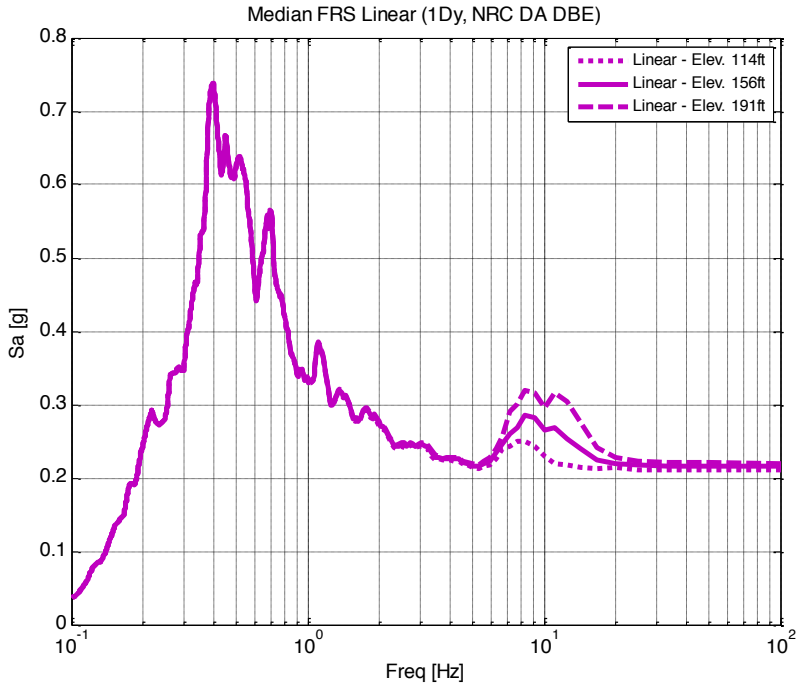

Figure A.10 Median FRS Primary Shield Wall H2 Only –Linear (NRC DBE).

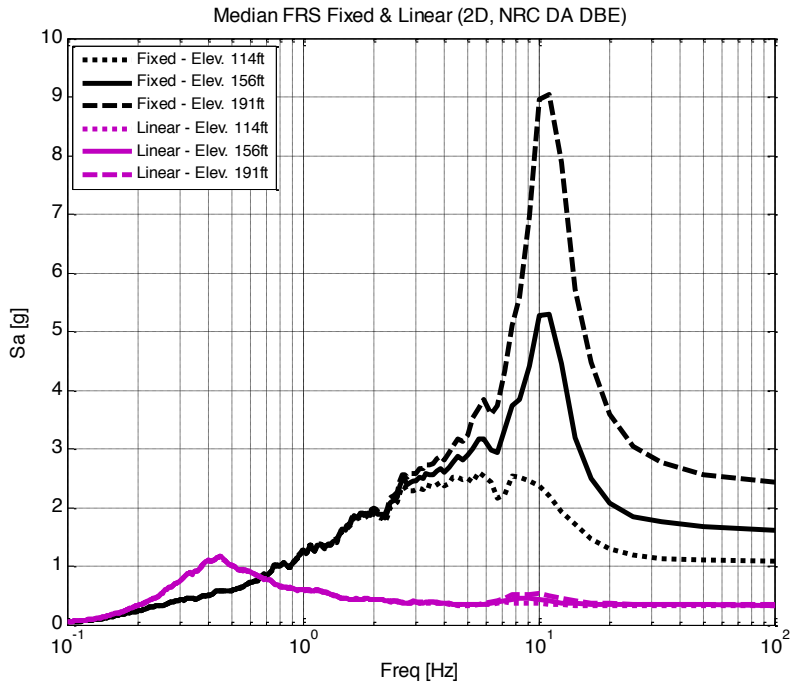

Figure A.11 Median FRS Primary Shield Wall 2D – Fixed vs Linear (NRC DBE).

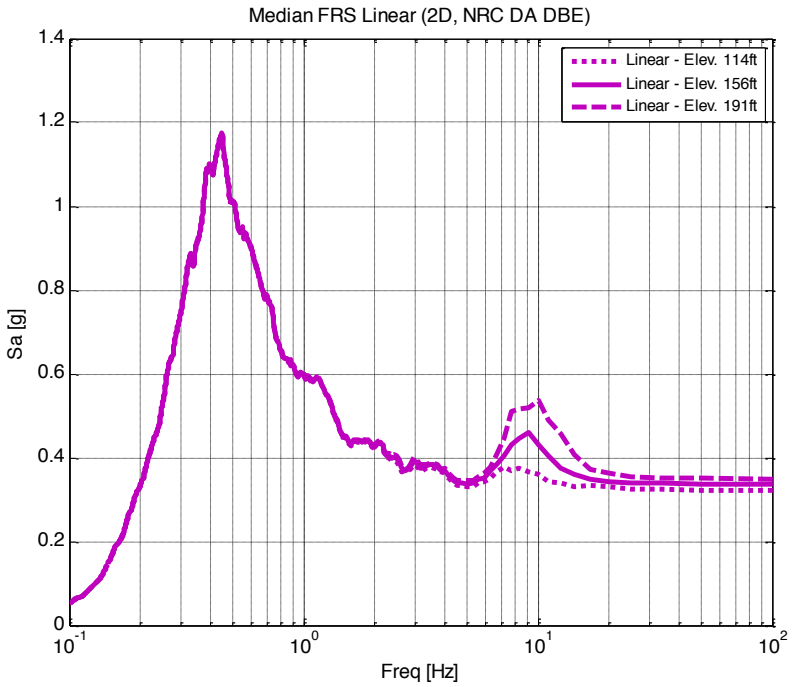

Figure A.12 Median FRS Primary Shield Wall 2D – Linear (NRC DBE).

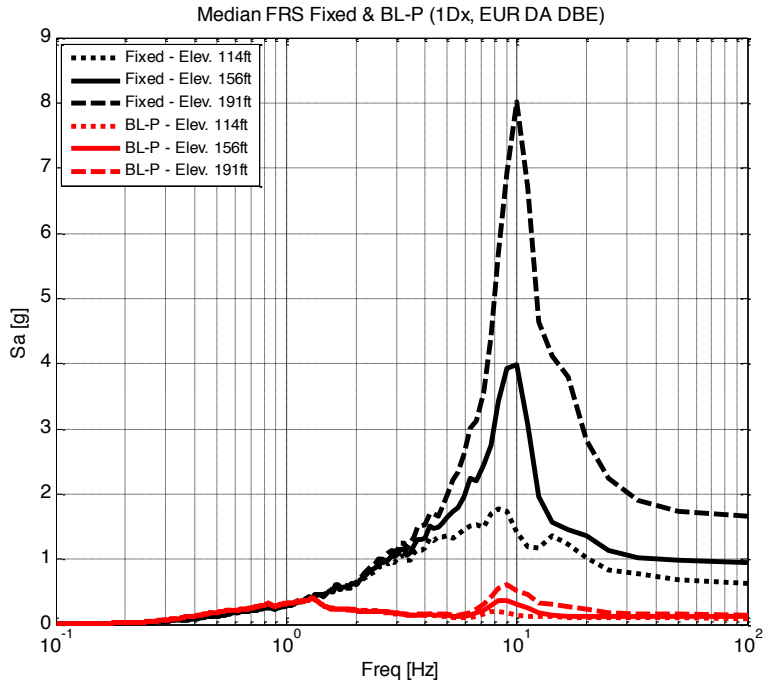

Figure A.13 Median FRS Primary Shield Wall H1 Only – Fixed vs BL-P (EUR DBE).

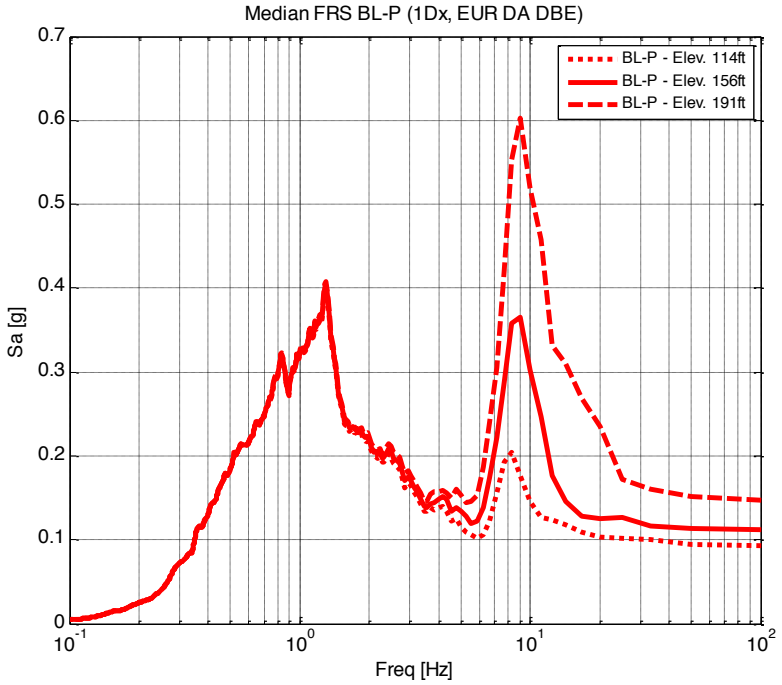

Figure A.14 Median FRS Primary Shield Wall H1 Only –BL-P (EUR DBE).

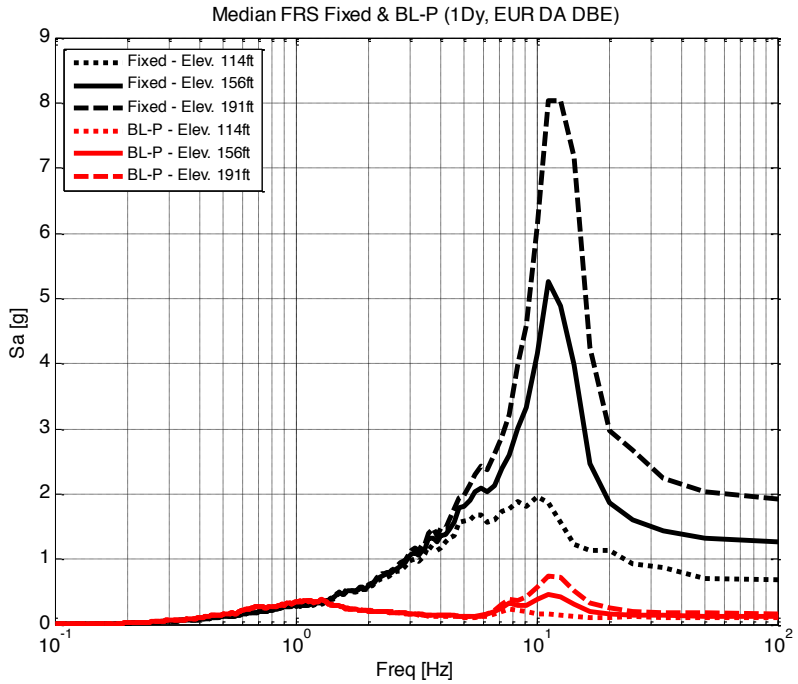

Figure A.15 Median FRS Primary Shield Wall H2 Only – Fixed vs BL-P (EUR DBE).

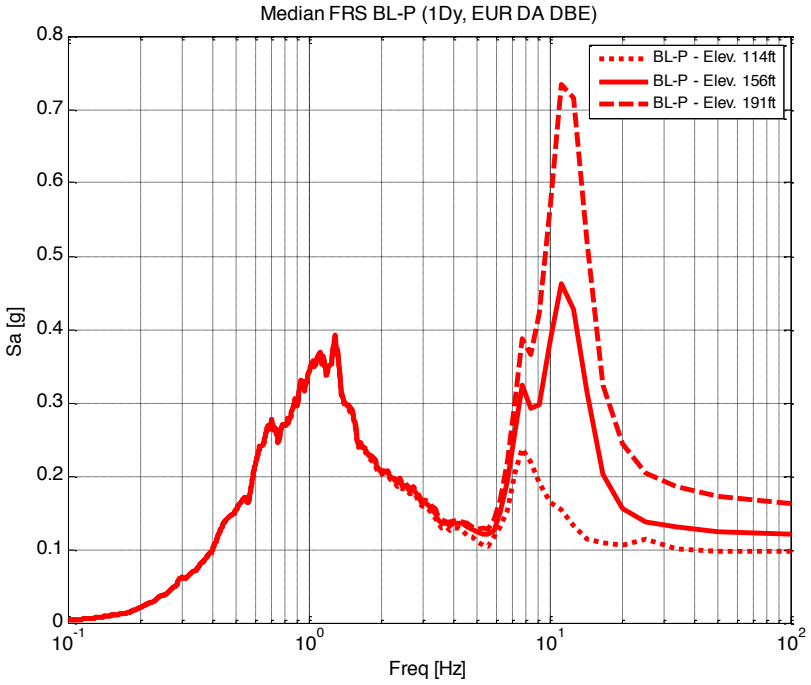

Figure A.16 Median FRS Primary Shield Wall H2 Only –BL-P (EUR DBE).

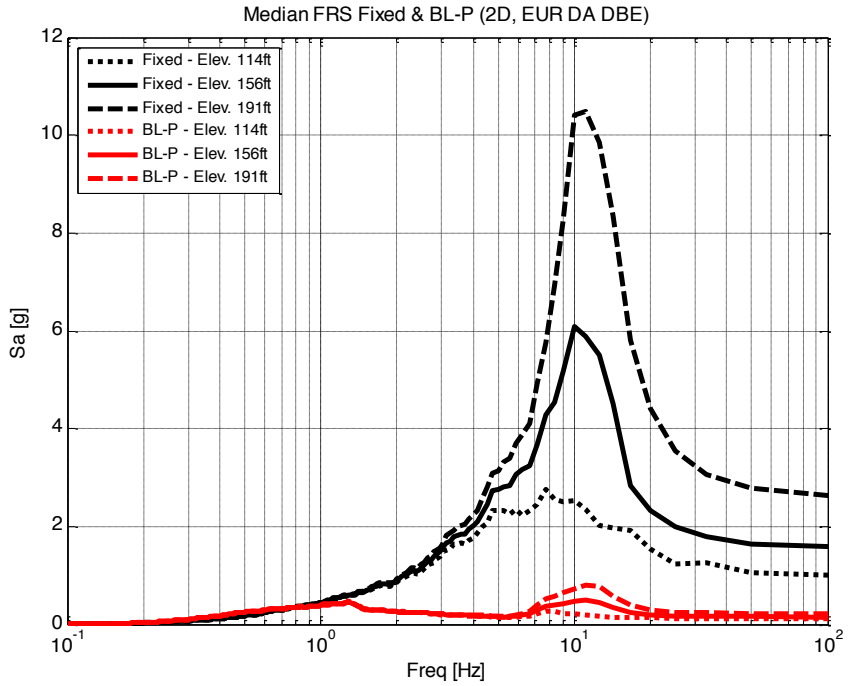

Figure A.17 Median FRS Primary Shield Wall 2D – Fixed BL-P (EUR DBE).

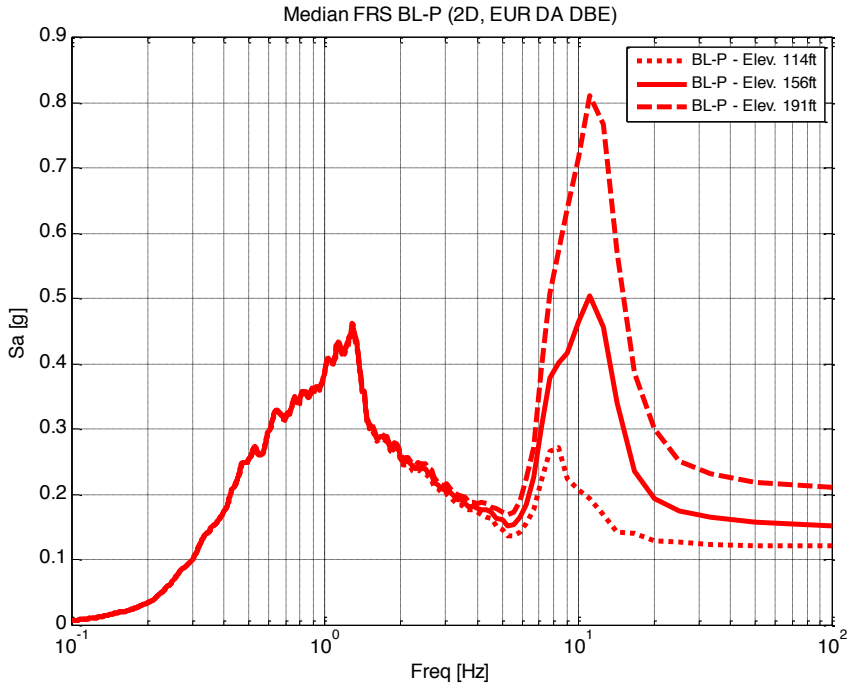

Figure A.18 Median FRS Primary Shield Wall 2D – BL-P (EUR DBE).

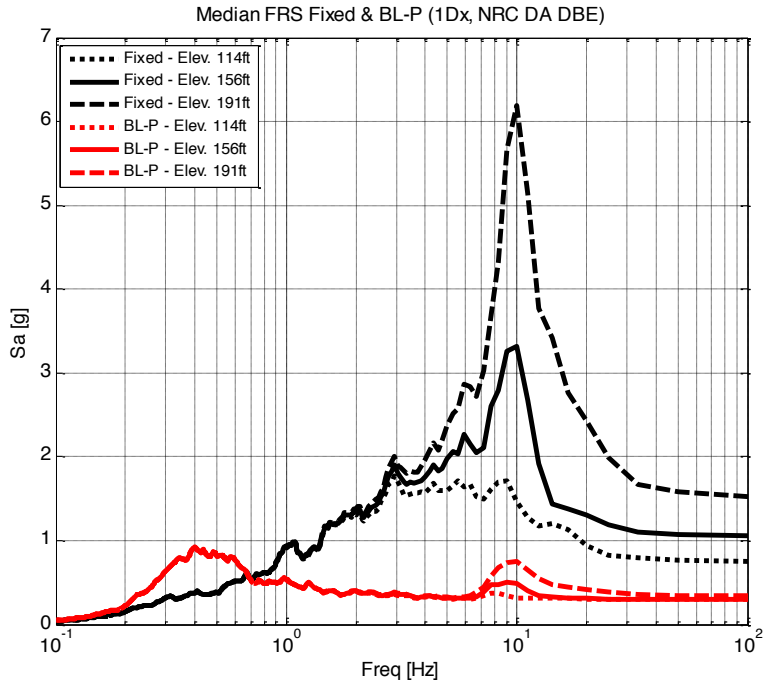

Figure A.19 Median FRS Primary Shield Wall H1 Only – Fixed vs BL-P (NRC DBE).

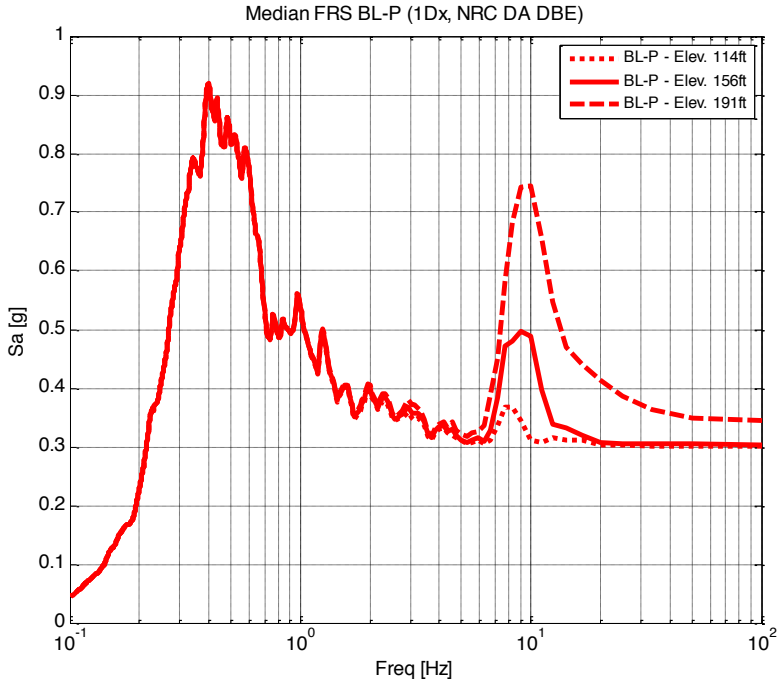

Figure A.20 Median FRS Primary Shield Wall H1 Only –BL-P (NRC DBE).

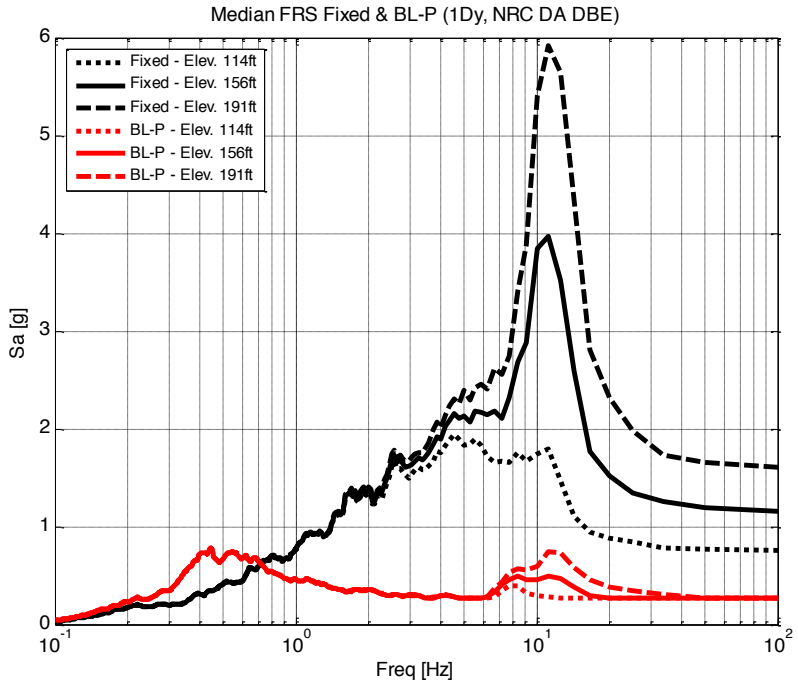

Figure A.21 Median FRS Primary Shield Wall H2 Only – Fixed vs BL-P (NRC DBE).

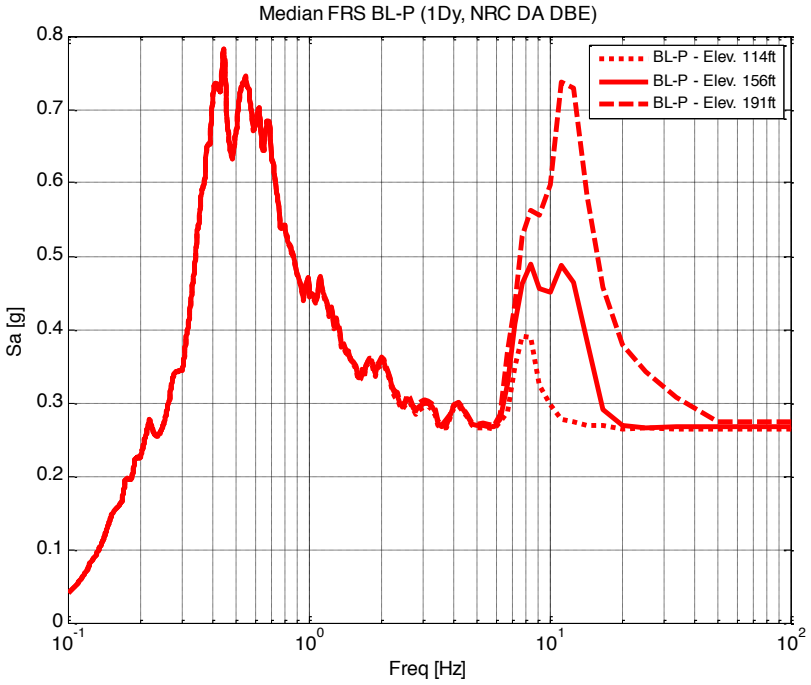

Figure A.22 Median FRS Primary Shield Wall H2 Only –BL-P (NRC DBE).

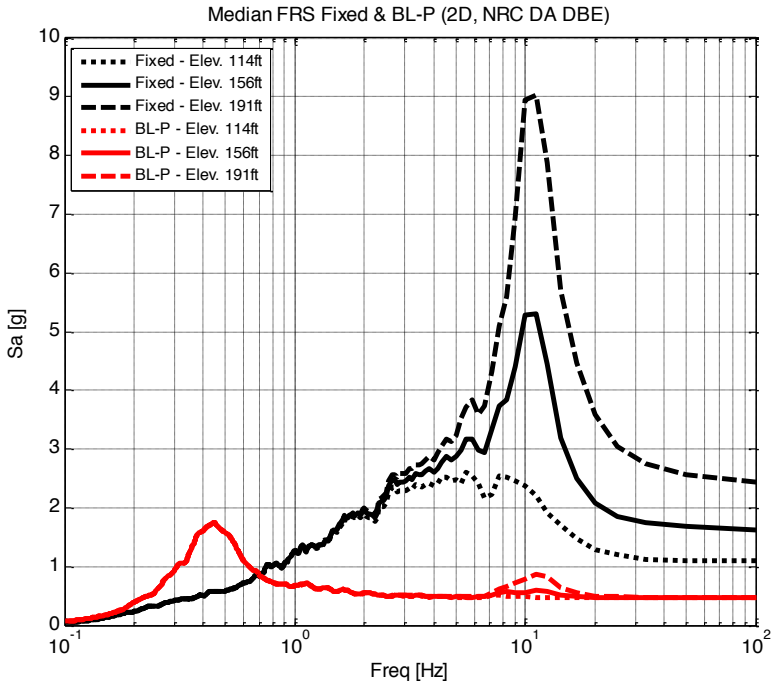

Figure A.23 Median FRS Primary Shield Wall 2D – Fixed vs BL-P (NRC DBE).

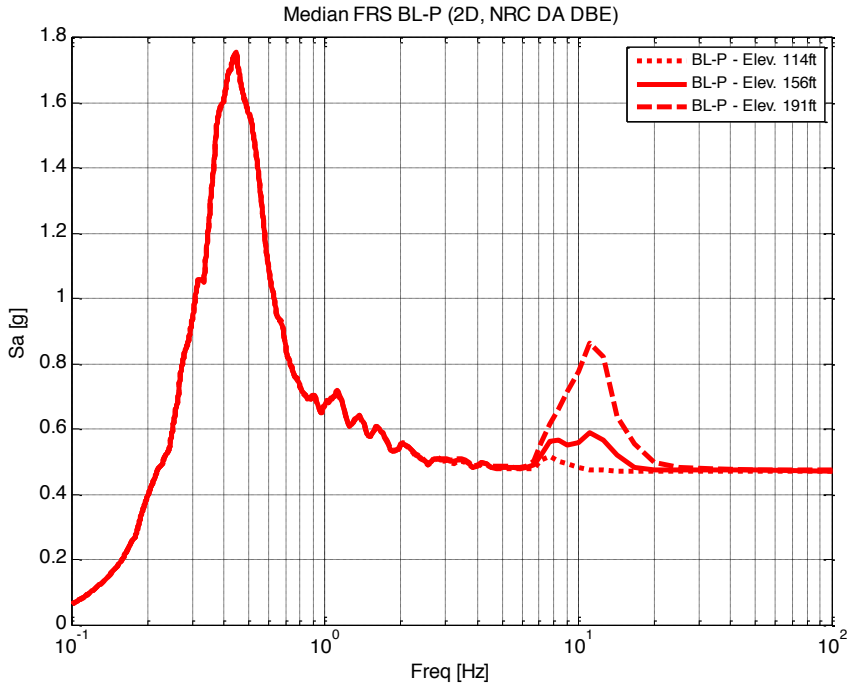

Figure A.24 Median FRS Primary Shield Wall 2D –BL-P (NRC DBE).

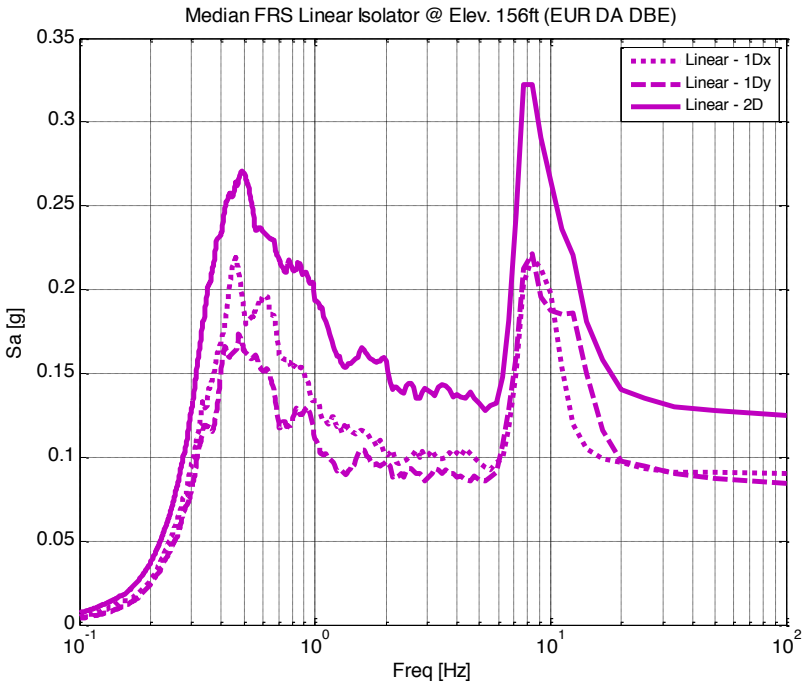

Figure A.25 Median FRS Primary Shield Wall Linear (EUR DBE).

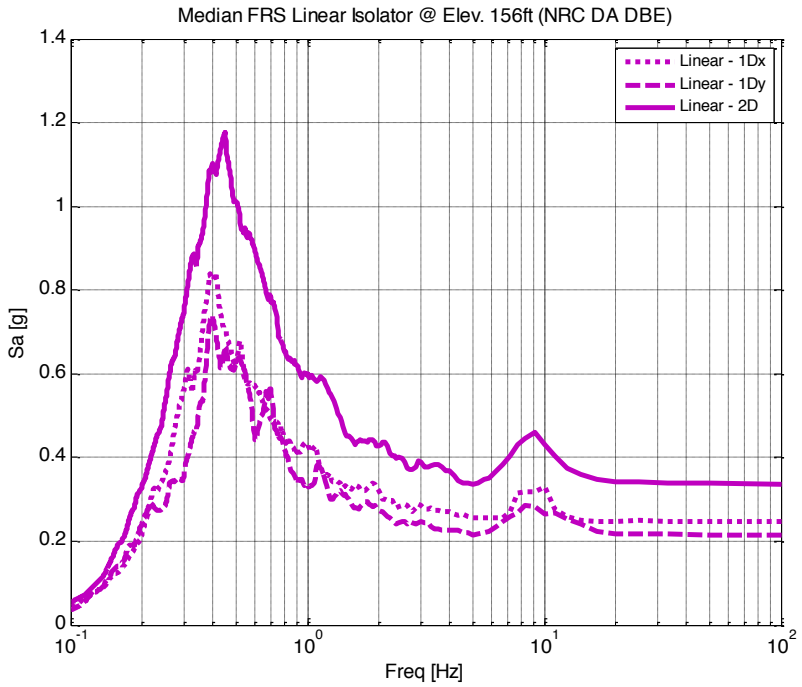

Figure A.26 Median FRS Primary Shield Wall Linear (NRC DBE).

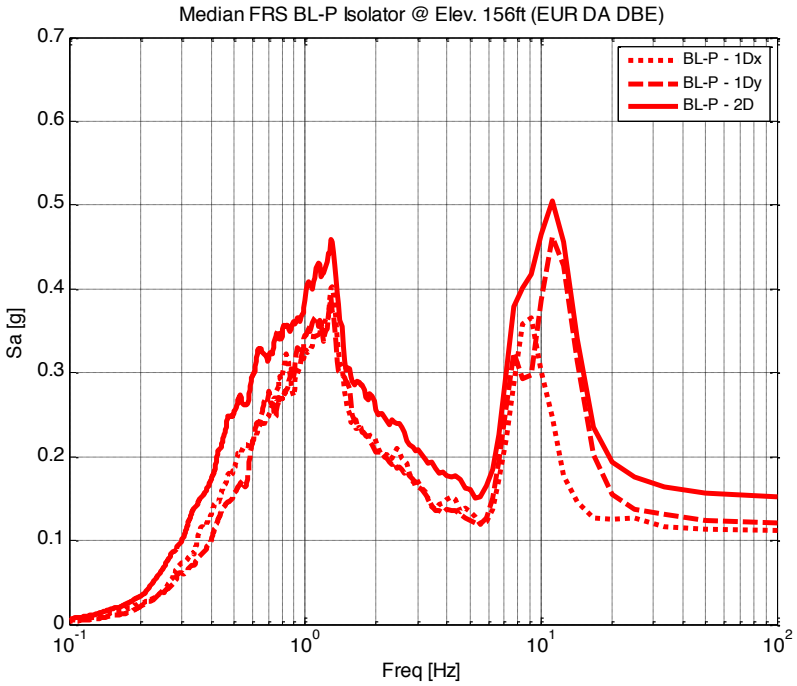

Figure A.27 Median FRS Primary Shield Wall BL-P (EUR DBE).

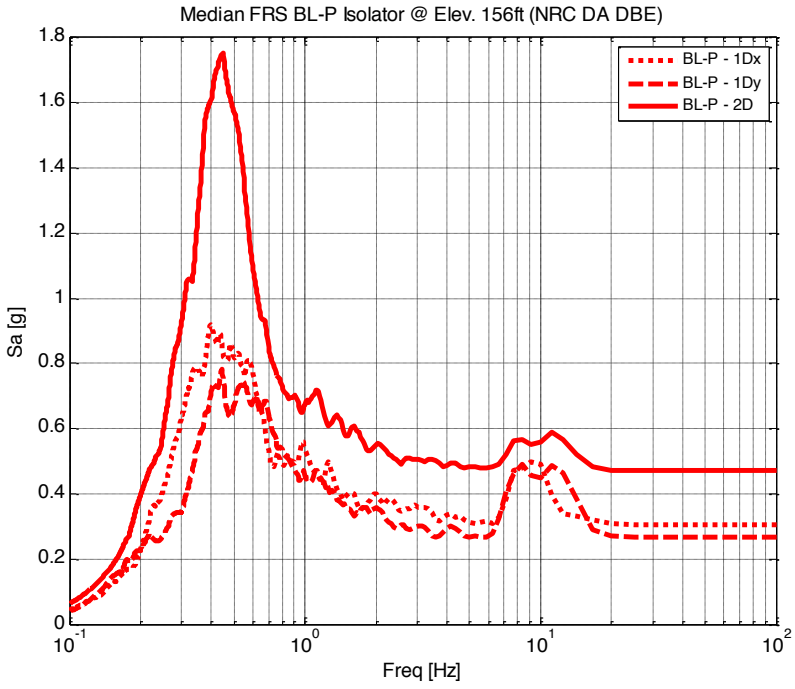

Figure A.28 Median FRS Primary Shield Wall BL-P (NRC DBE).

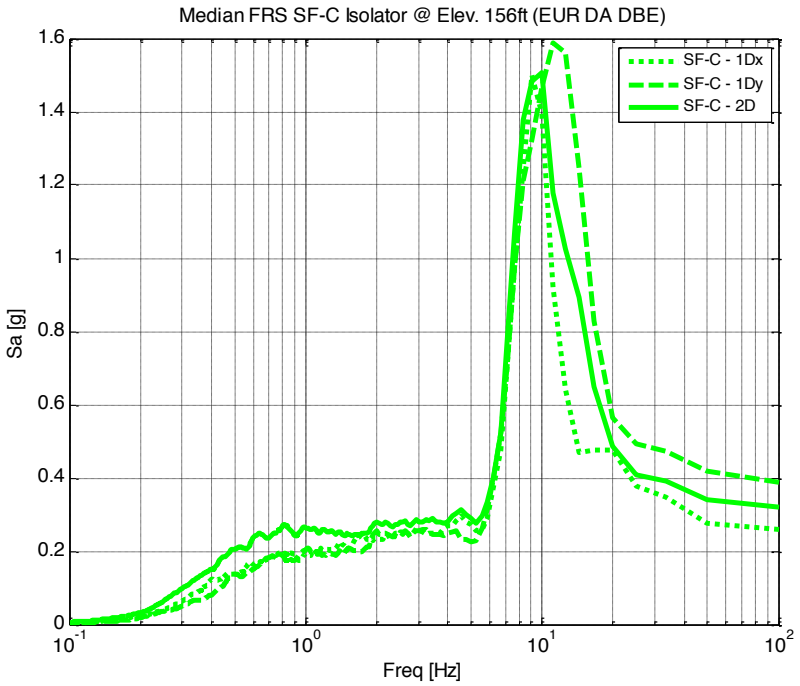

Figure A.29 Median FRS Primary Shield Wall SF-C (EUR DBE).

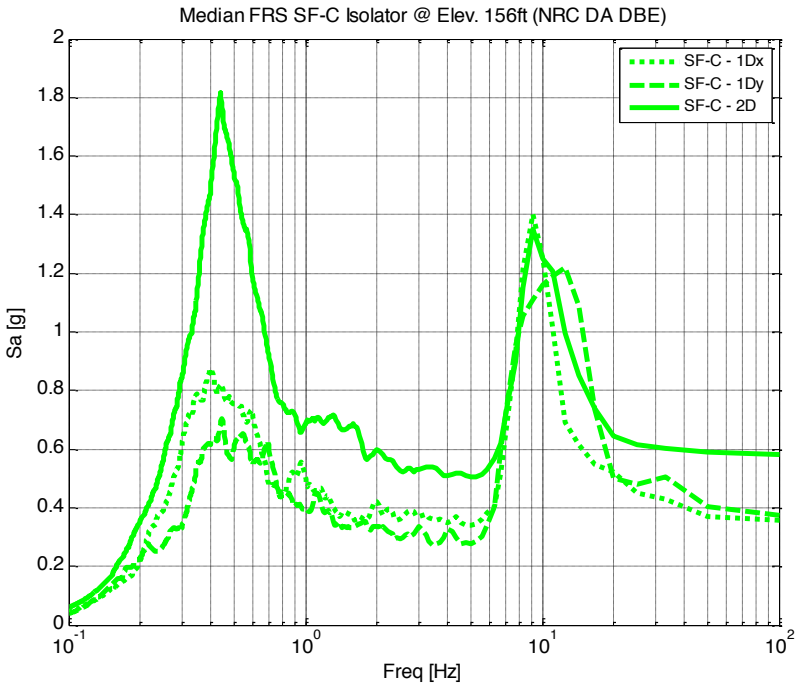

Figure A.30 Median FRS Primary Shield Wall SF-C (NRC DBE).

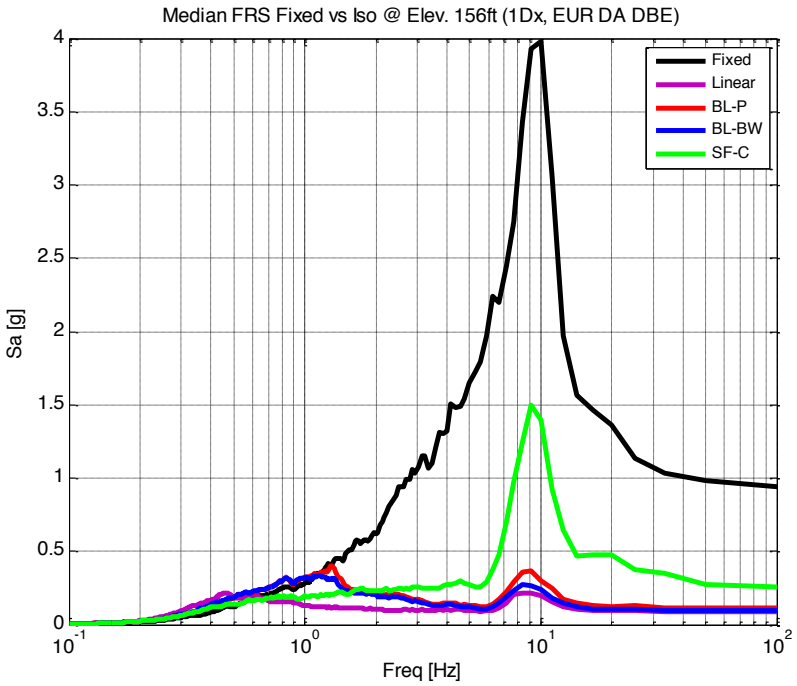

Figure A.31 Median FRS Primary Shield Wall H1 Only - Fixed vs Isolated (EUR DBE).

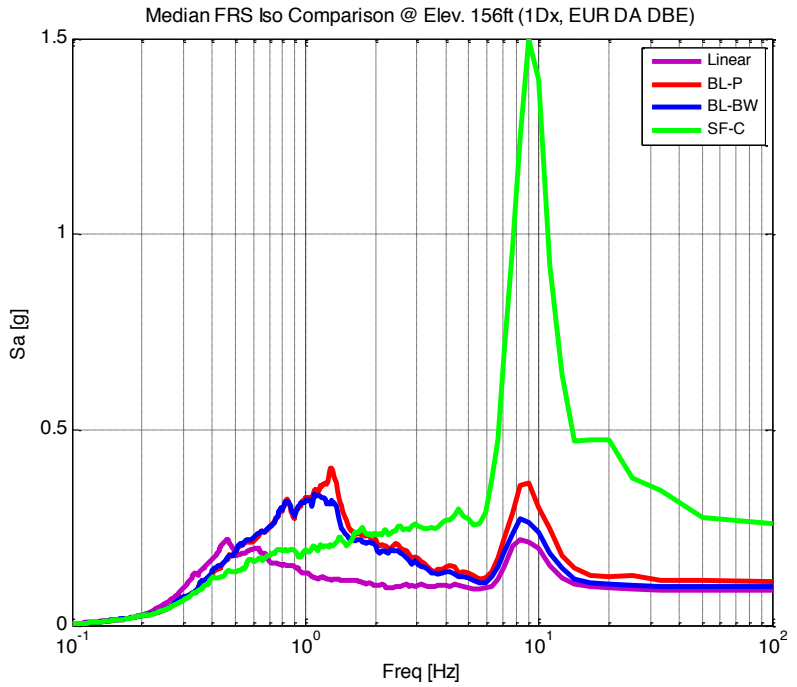

Figure A.32 Median FRS Primary Shield Wall H1 Only - Isolated (EUR DBE).

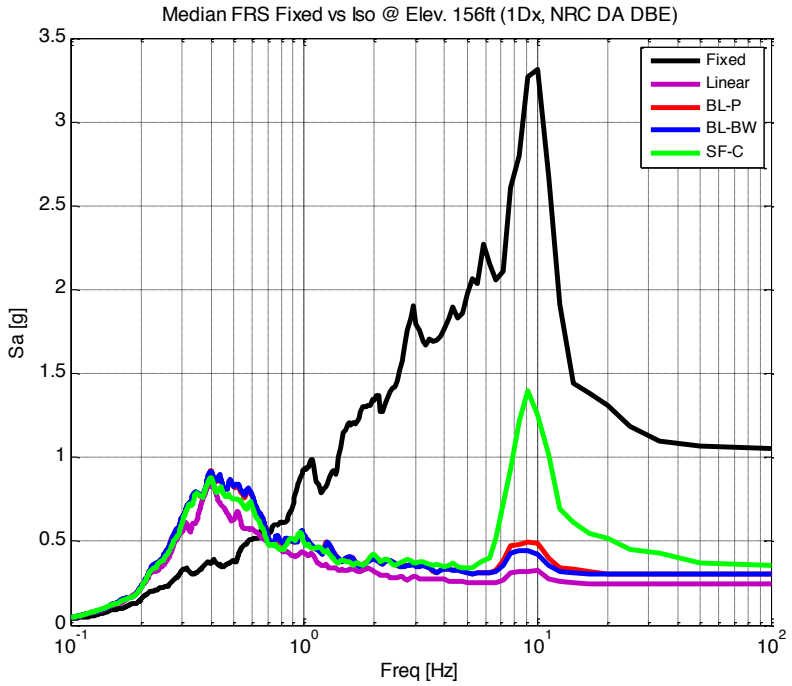

Figure A.33 Median FRS Primary Shield Wall H1 Only – Fixed vs Isolated (NRC DBE).

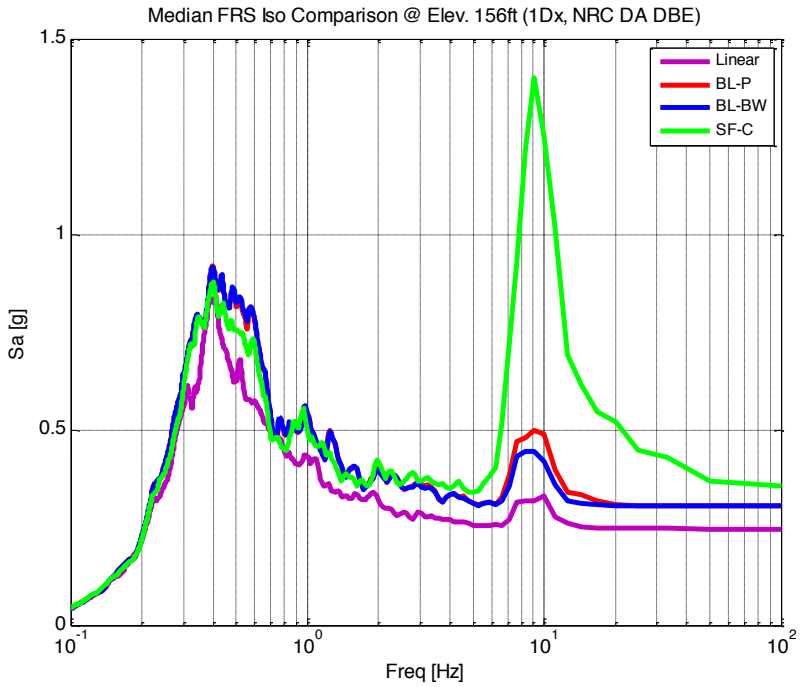

Figure A.34 Median FRS Primary Shield Wall H1 Only –Isolated (NRC DBE).

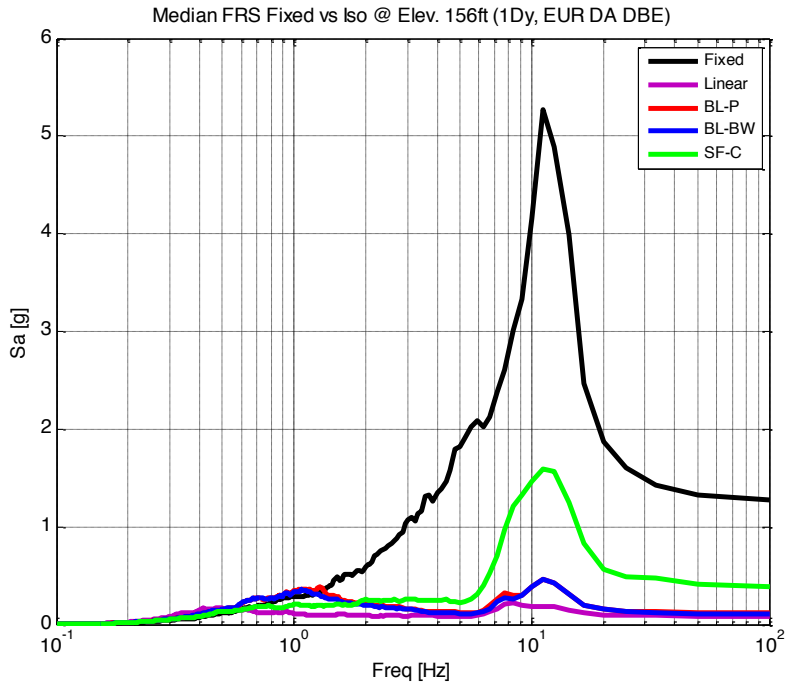

Figure A.35 Median FRS Primary Shield Wall H2 Only –Fixed vs Isolated (EUR DBE).

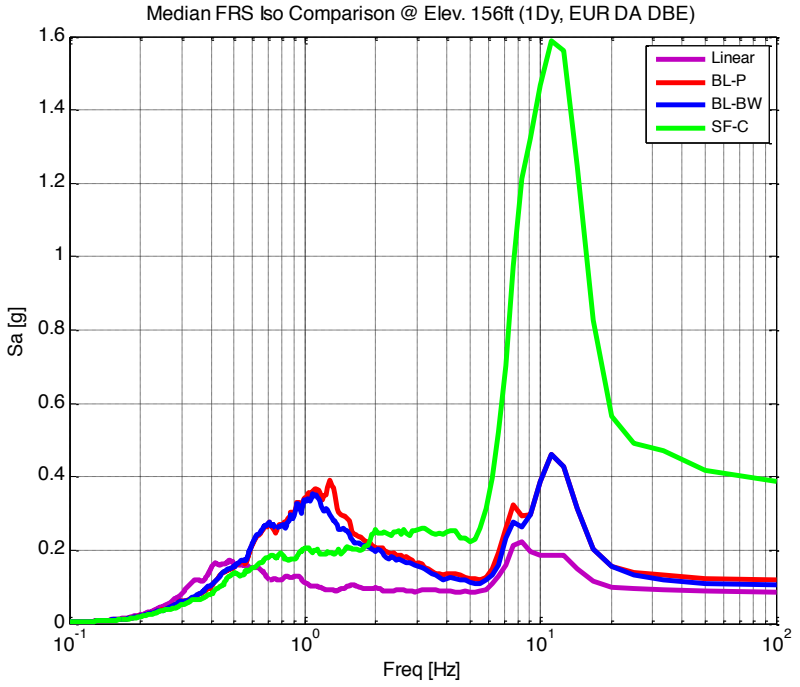

Figure A.36 Median FRS Primary Shield Wall H2 Only –Isolated (EUR DBE).

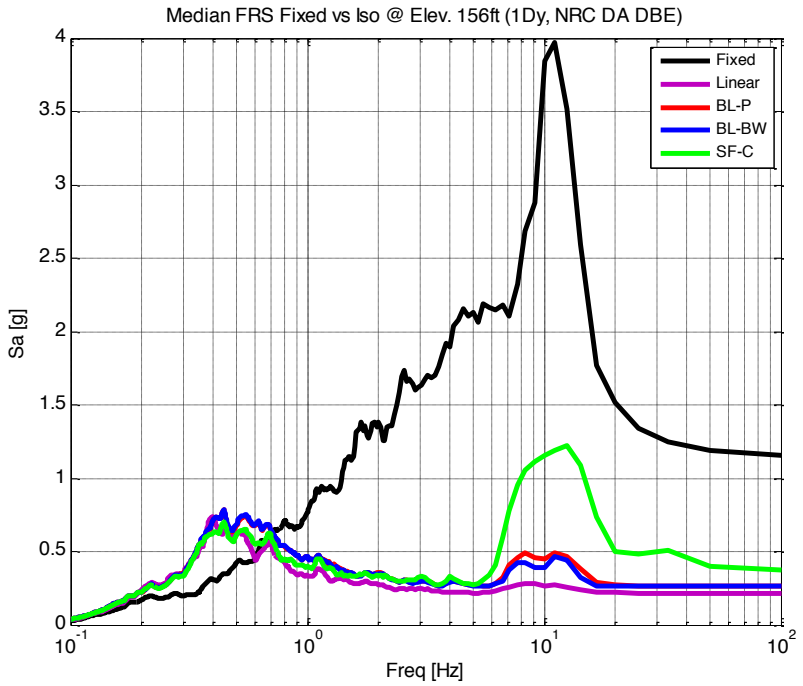

Figure A.37 Median FRS Primary Shield Wall H2 Only – Fixed vs Isolated (NRC DBE).

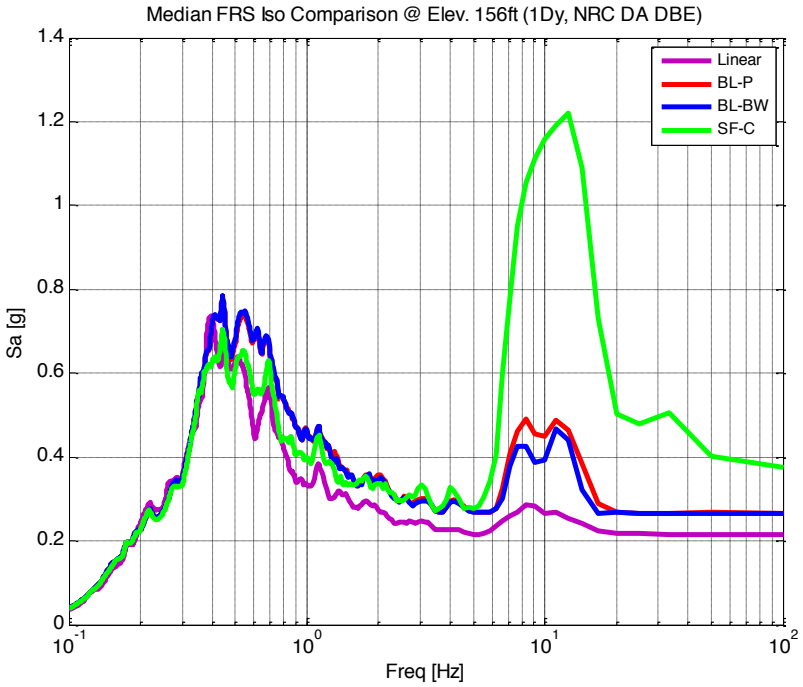

Figure A.38 Median FRS Primary Shield Wall H2 Only – Isolated (NRC DBE).

Appendix B

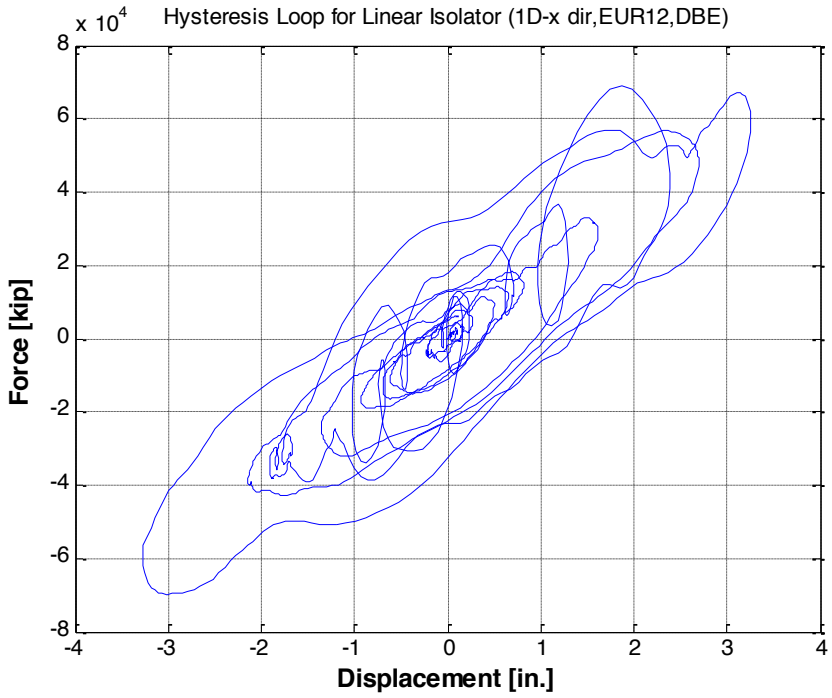

Figure A.39 Hysteresis Loop H1 Only - Linear (EUR 12 DBE).

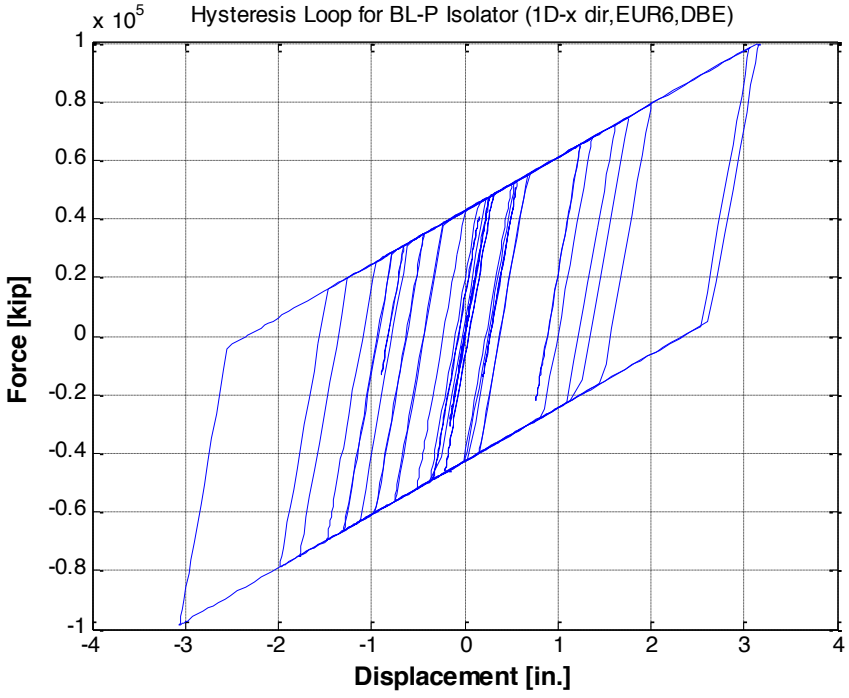

Figure A.40 Hysteresis Loop H1 Only – BL-P (EUR 12 DBE).

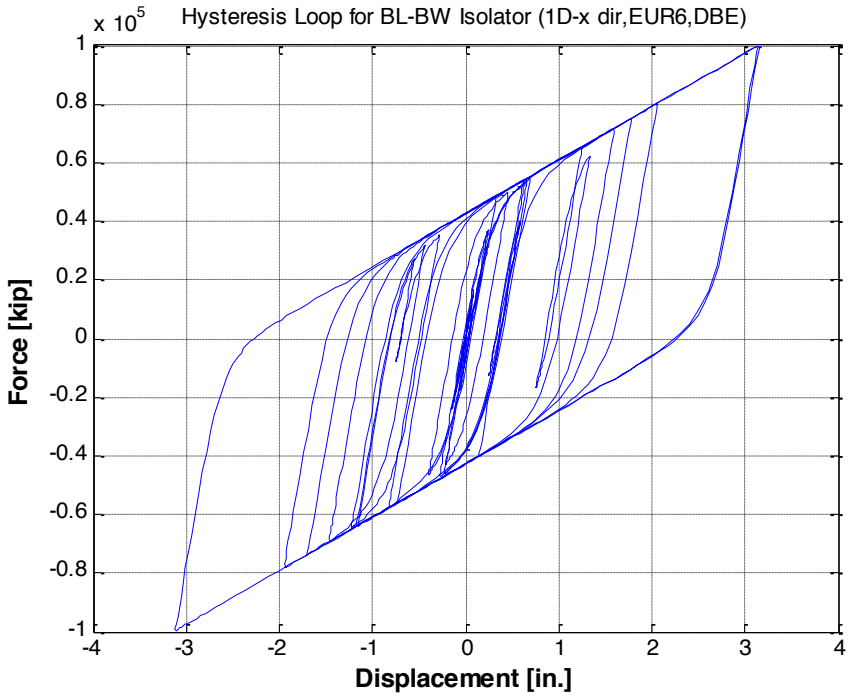

Figure A.41 Hysteresis Loop H1 Only – BL-BW (EUR 12 DBE).

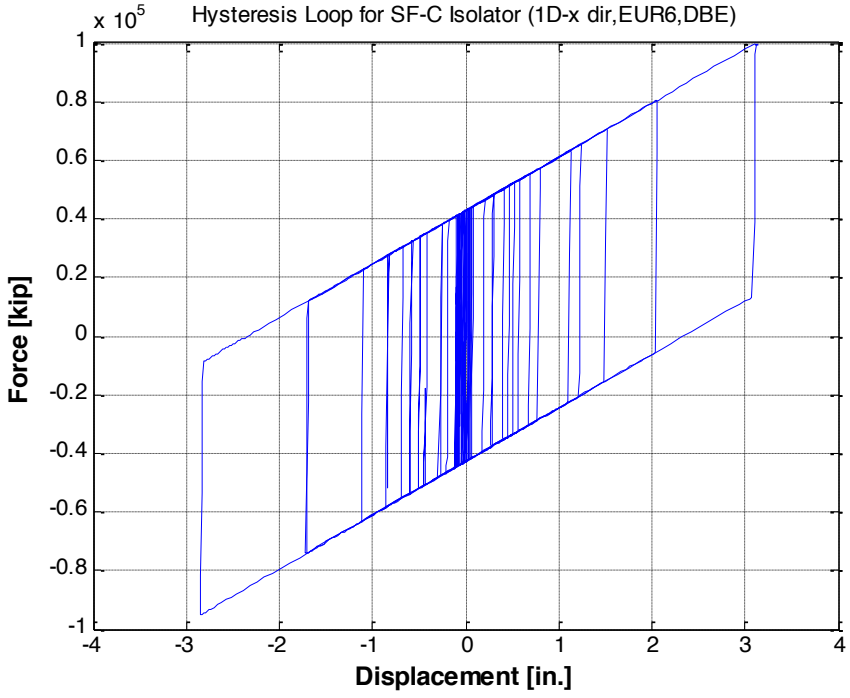

Figure A.42 Hysteresis Loop H1 Only – SF-C (EUR 12 DBE).

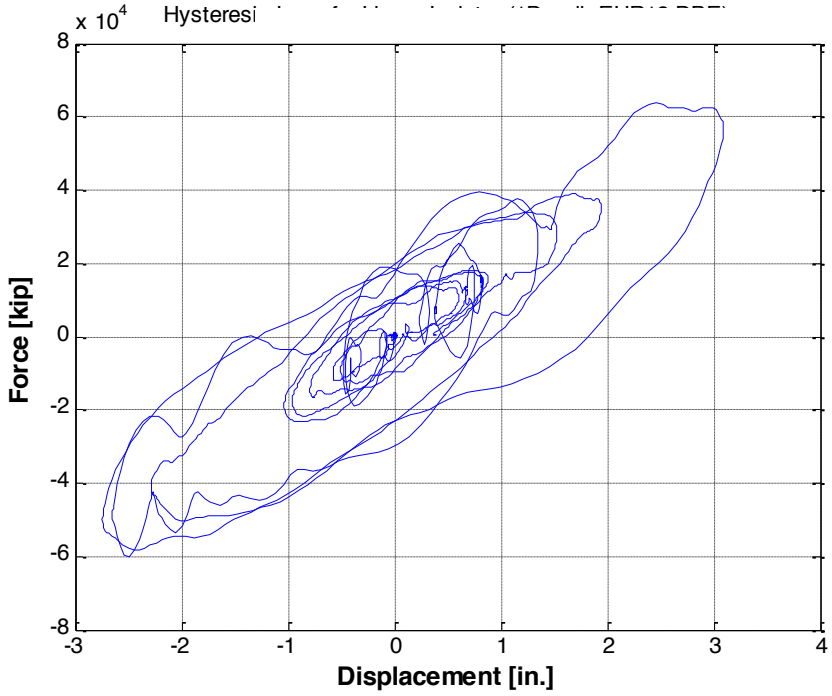

Figure A.43 Hysteresis Loop H1 Only – Linear (EUR 6 DBE).

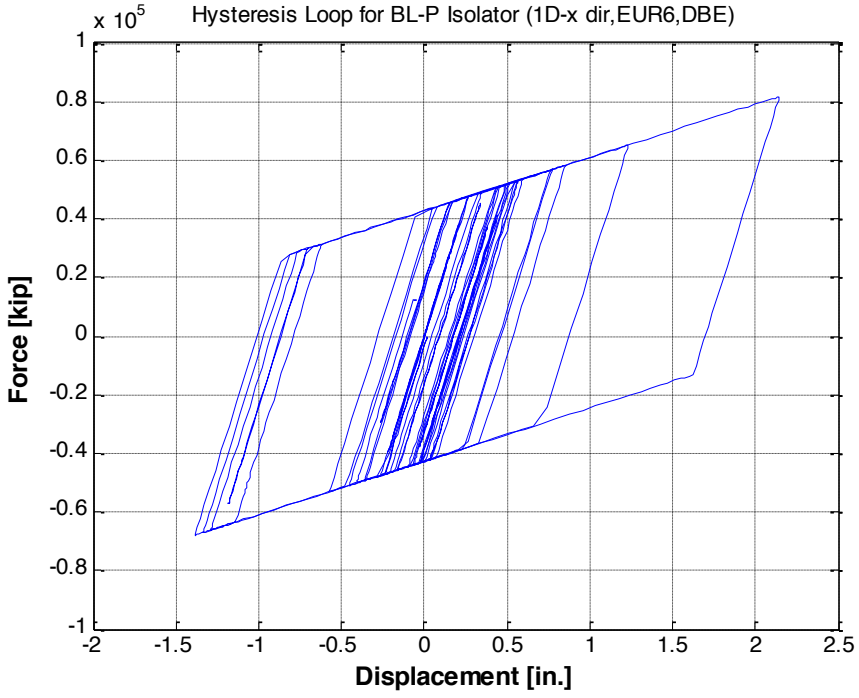

Figure A.44 Hysteresis Loop H1 Only – BL-P (EUR 6 DBE).

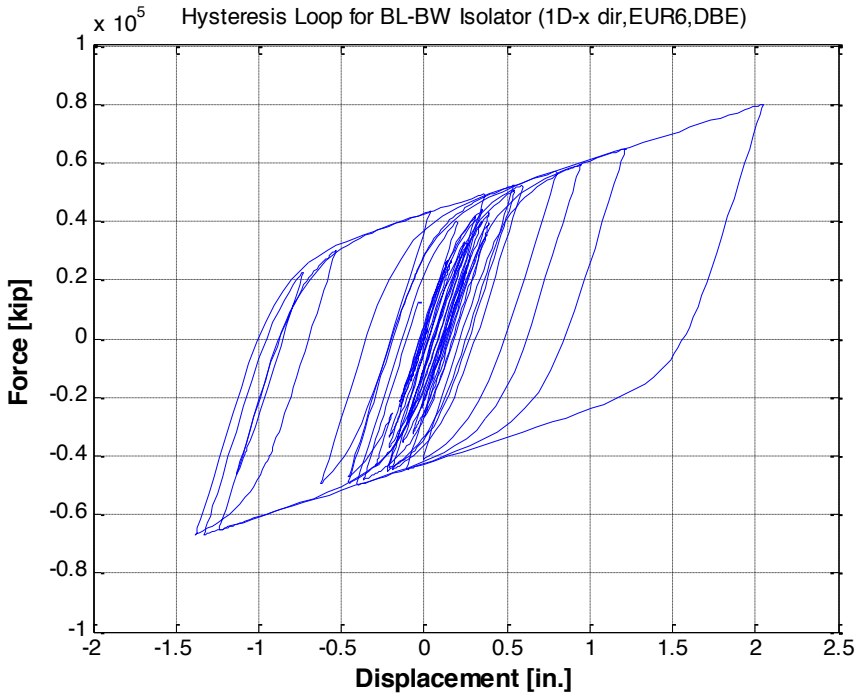

Figure A.45 Hysteresis Loop H1 Only – BL-BW (EUR 6 DBE).

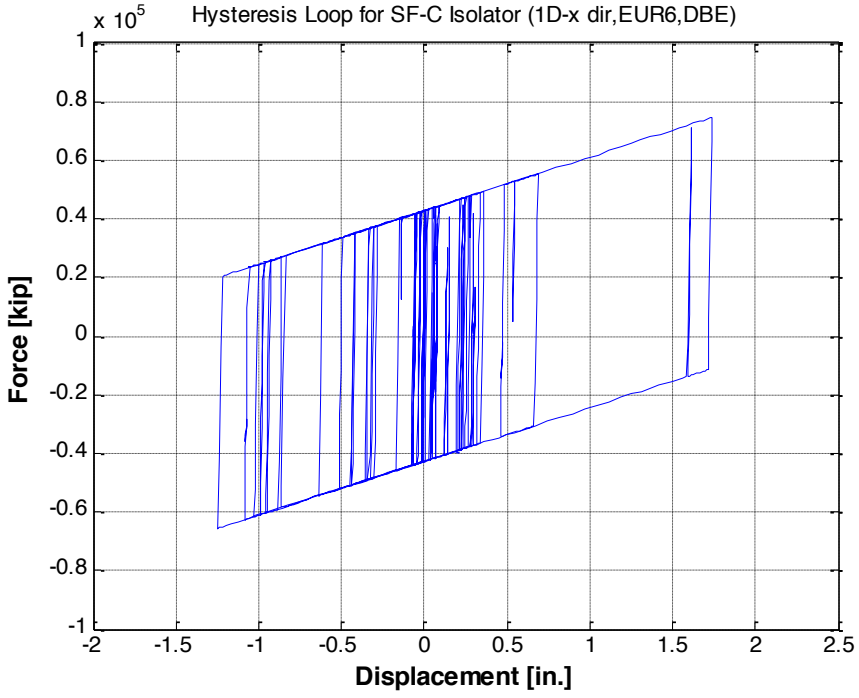

Figure A.46 Hysteresis Loop H1 Only – SF-C (EUR 6 DBE).

KEPCO MOTIONS

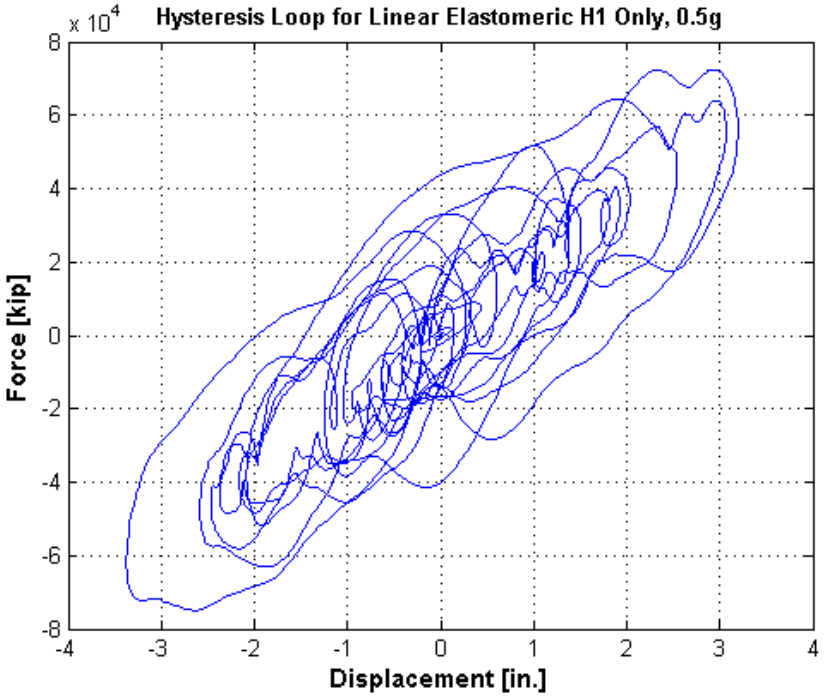

Figure A.47 Hysteresis H1 Only-Linear (DBE)

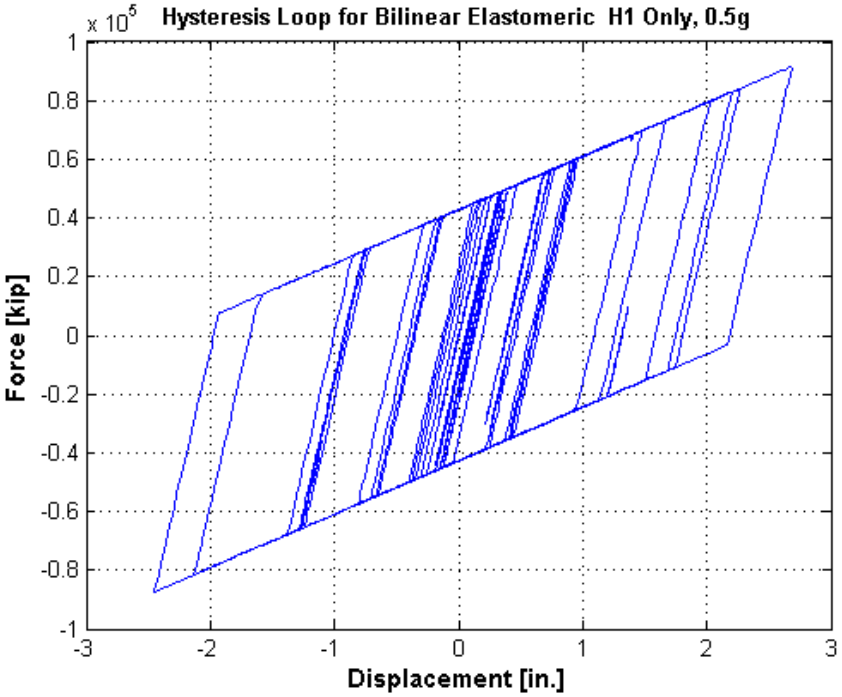

Figure A.48 Hysteresis H1 Only-BL-P (DBE)

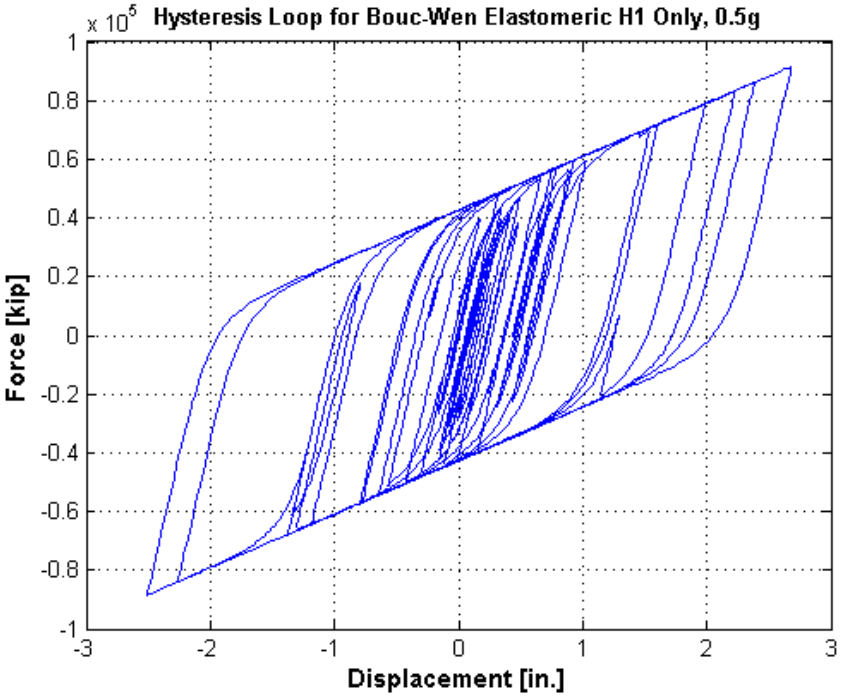

Figure A.49 Hysteresis H1 Only-BL-BW (DBE)

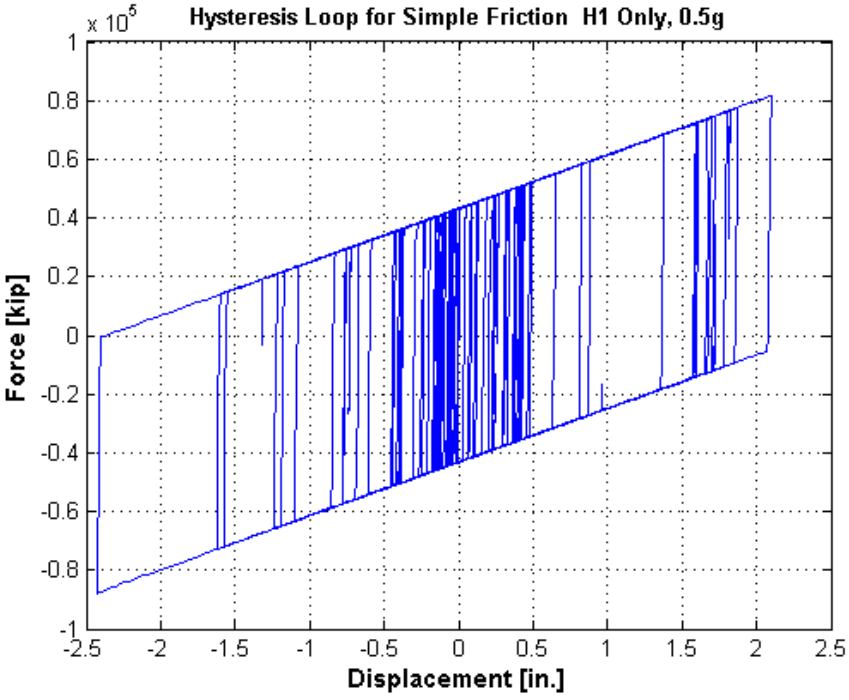

Figure A.50 Hysteresis H1 Only-SF (DBE)

Hysteresis Loops for Isolator Models (DBE, H2 Motion Only)

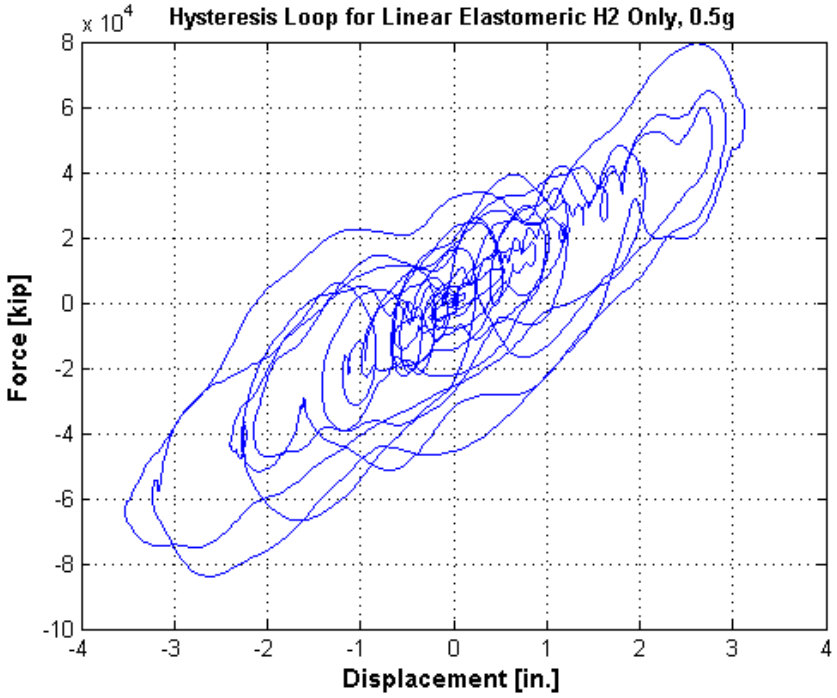

Figure A.51 Hysteresis H2 Only-Linear (DBE)

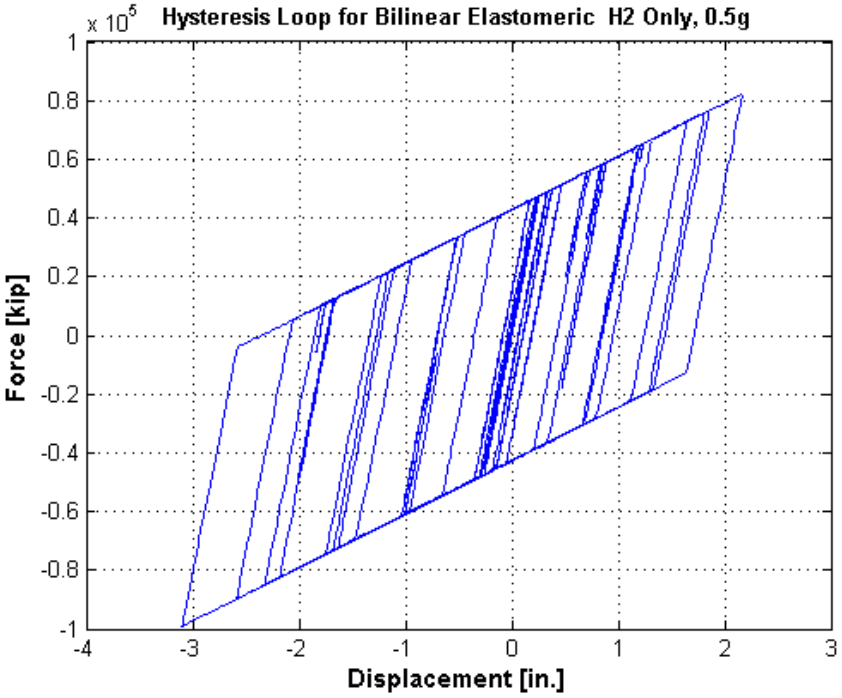

Figure A.52 Hysteresis H2 Only-BL-P (DBE)

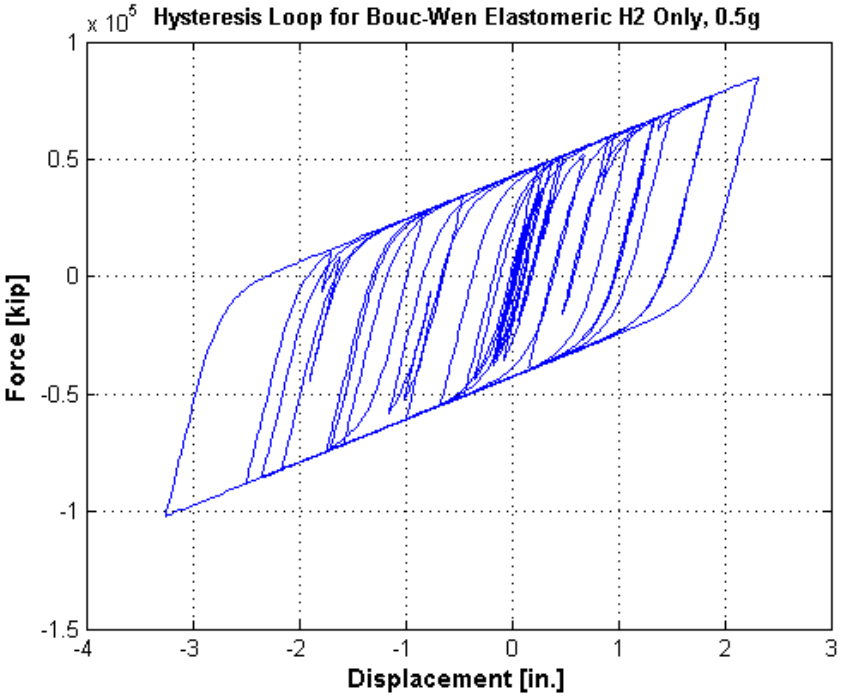

Figure A.53 Hysteresis H2 Only-BL-BW (DBE)

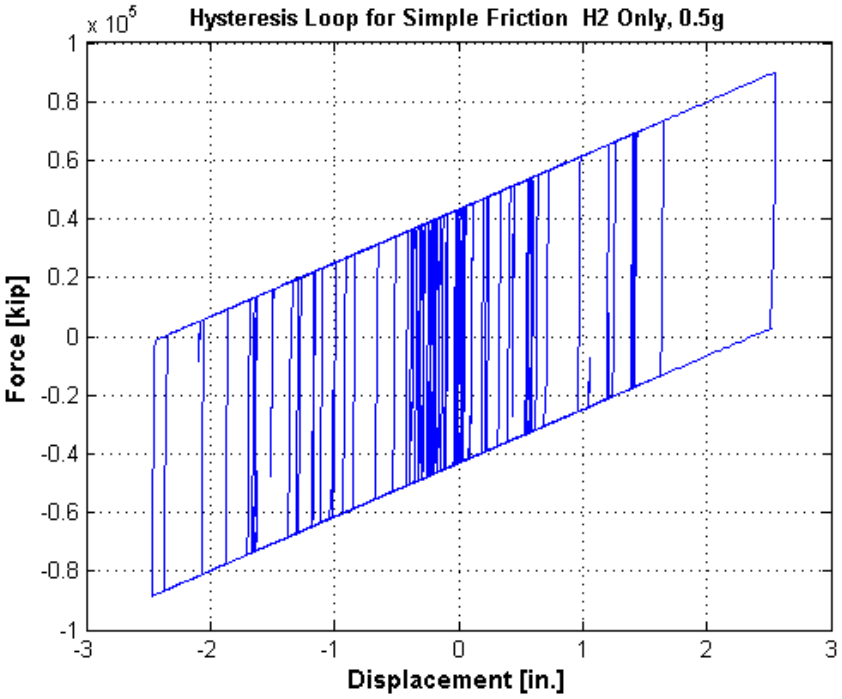

Figure A.54 Hysteresis H2 Only-SF (DBE)

Hysteresis Loops for Isolator Models (DBE, H1 and H2 Motions)

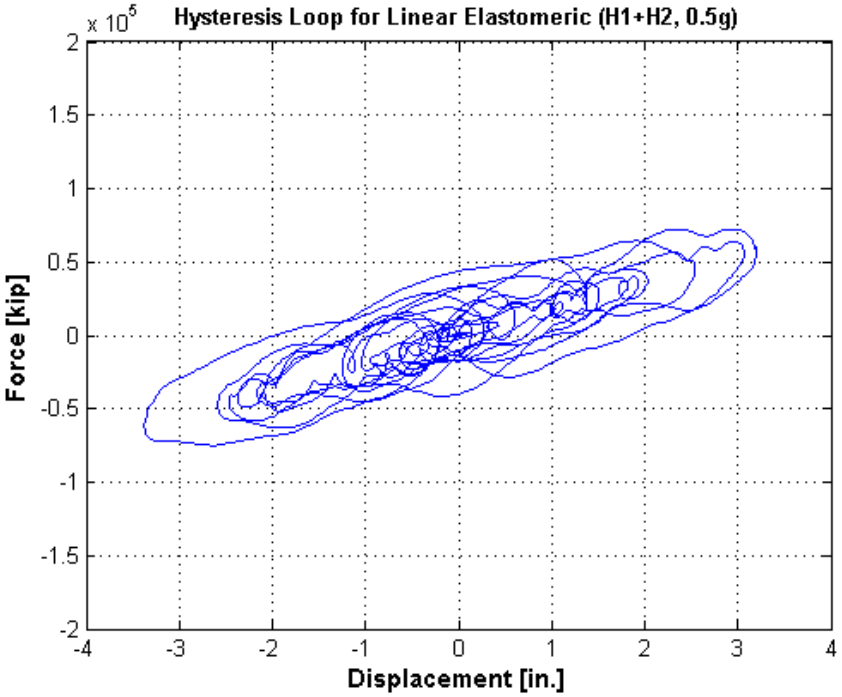

Figure A.55 Hysteresis H1+H2 - Linear (DBE)

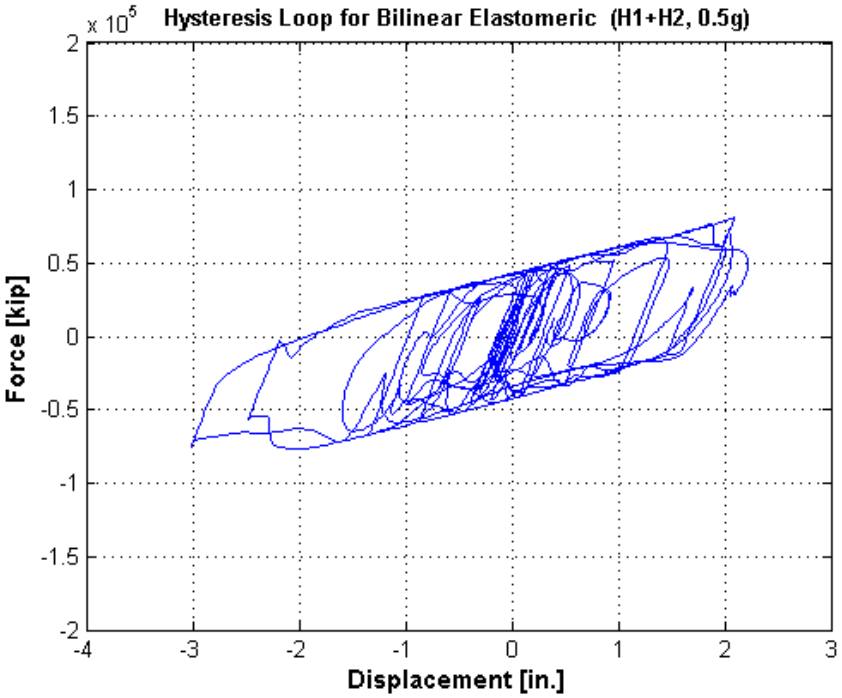

Figure A.56 Hysteresis H1+H2 – BL-P (DBE)

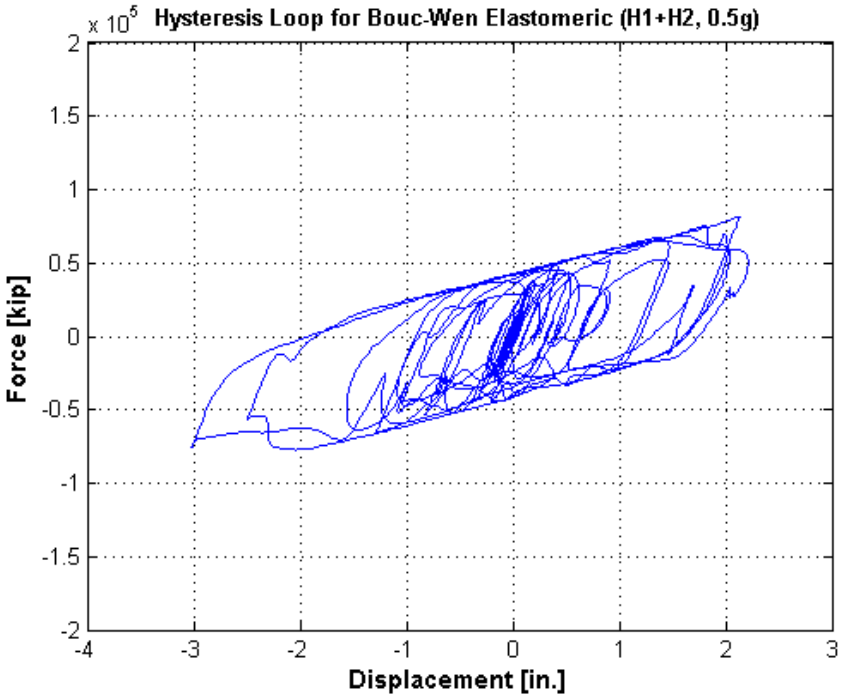

Figure A.57 Hysteresis H1+H2 – BL-BW (DBE)

Response Histories for Isolator Models (DBE, H1 Motion Only)

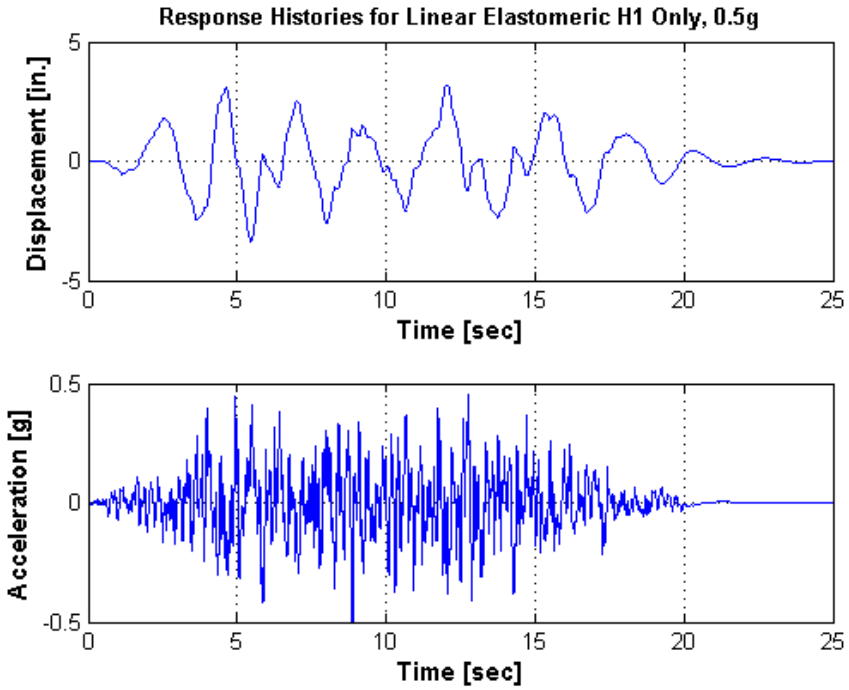

Figure A.58 Displacement and Acceleration. Response Histories H1 Only-Linear (DBE)

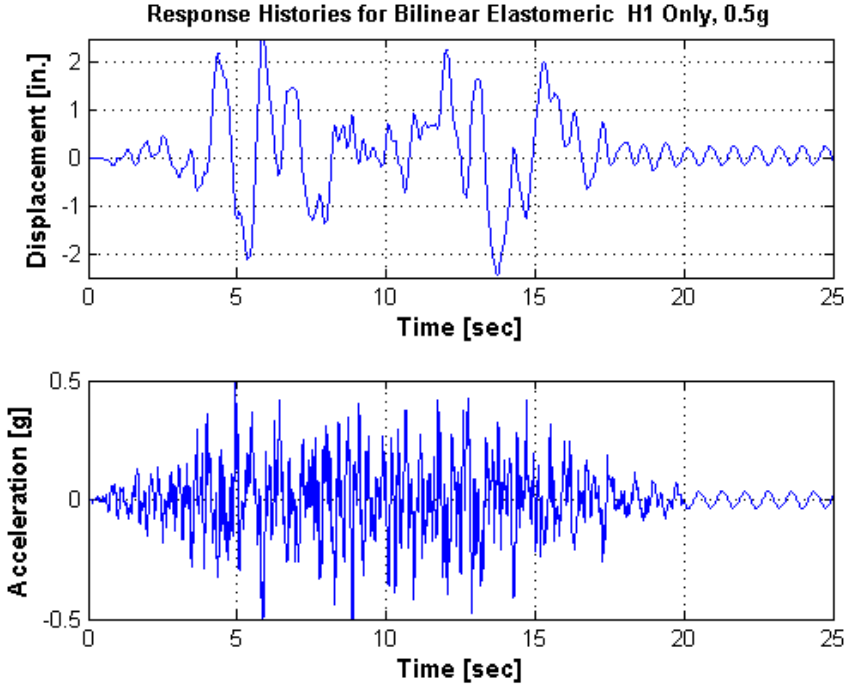

Figure A.59 Displacement and Acceleration Response Histories H1 Only-BL-P (DBE)

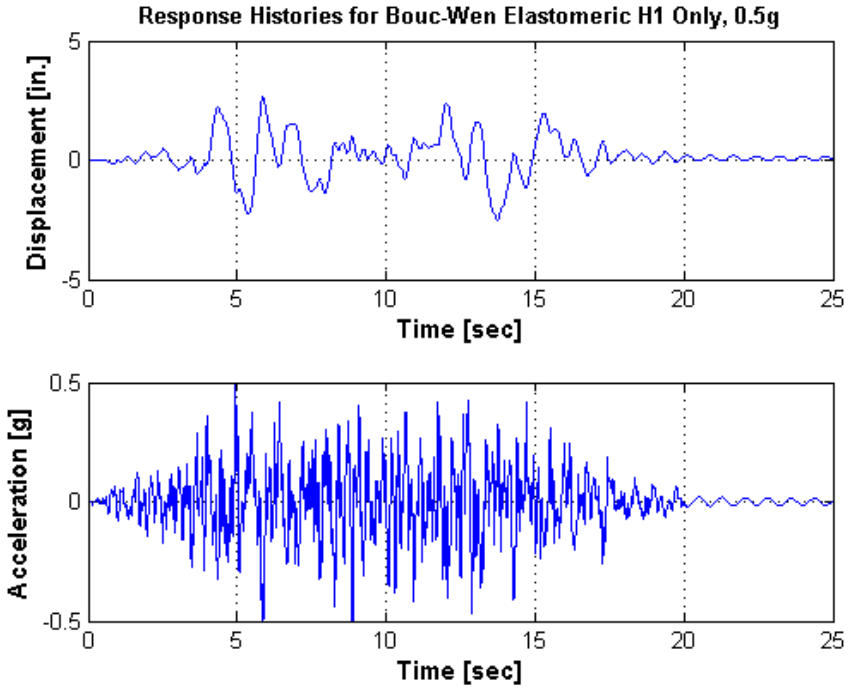

Figure A.60 Displacement and Acceleration Response Histories H1 Only-BL-BW (DBE)

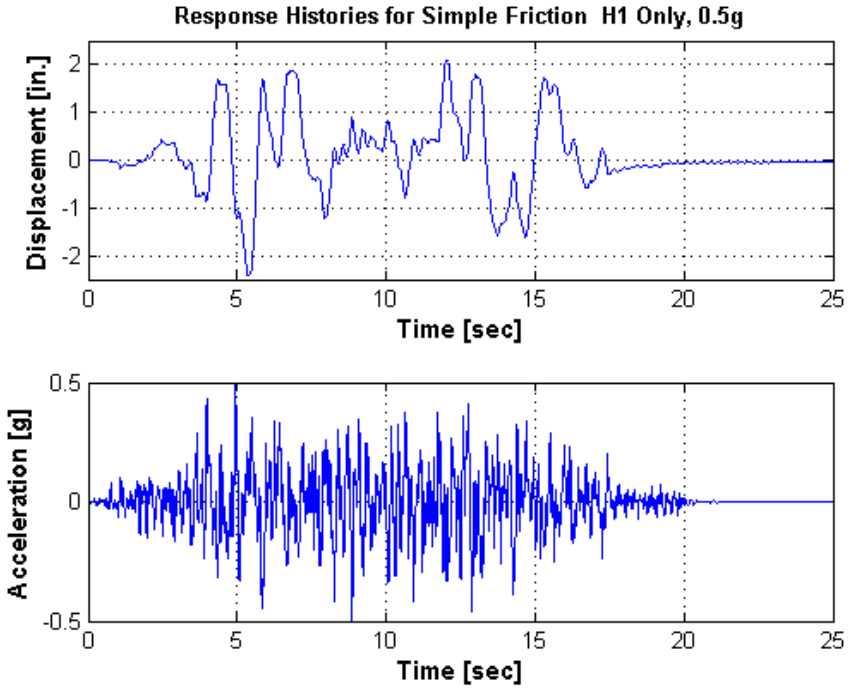

Figure A.61 Displacement and Acceleration Response Histories H1 Only-SF (DBE)

Response Histories for Isolator Models (DBE, H2 Motion Only)

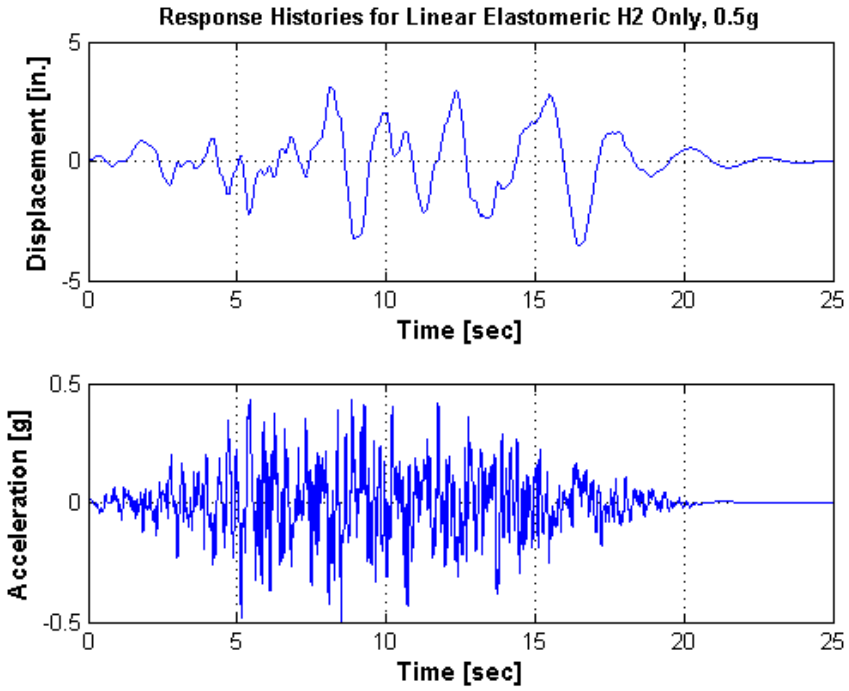

Figure A.62 Displacement and Acceleration. Response Histories H2 Only-Linear (DBE)

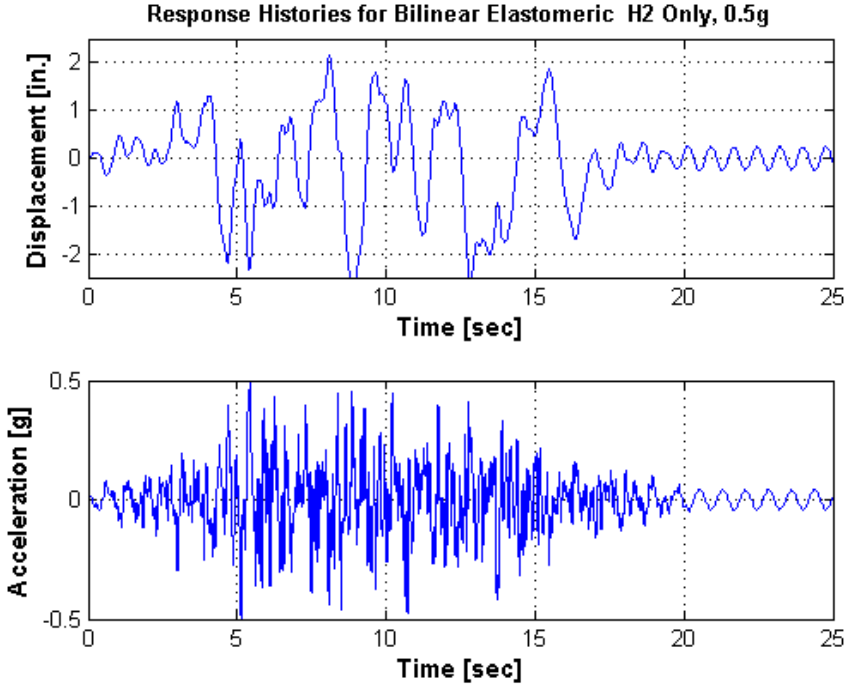

Figure A.63 Displacement and Acceleration. Response Histories H2 Only-BL-P (DBE)

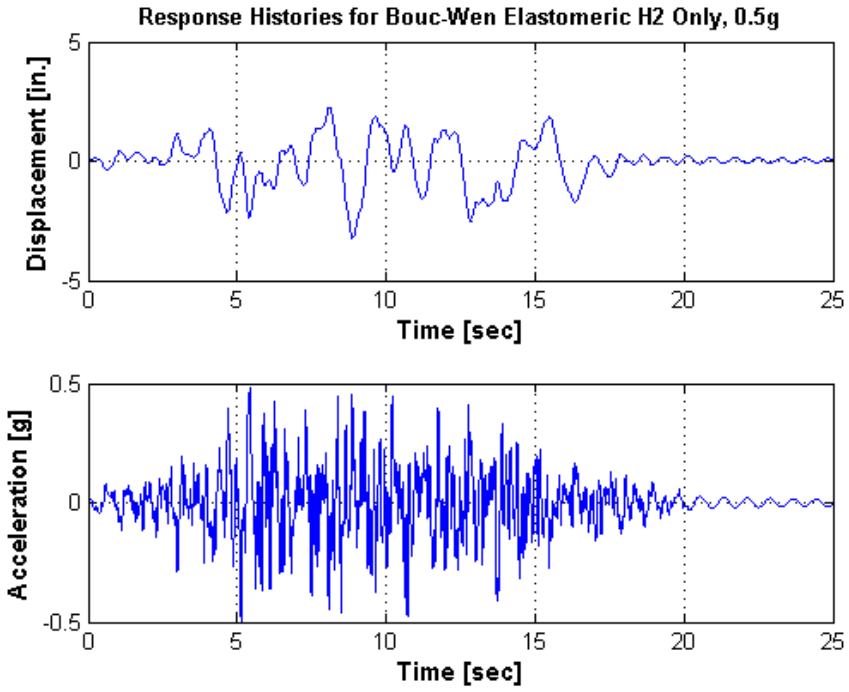

Figure A.64 Displacement and Acceleration. Response Histories H2 Only-BL-BW (DBE)

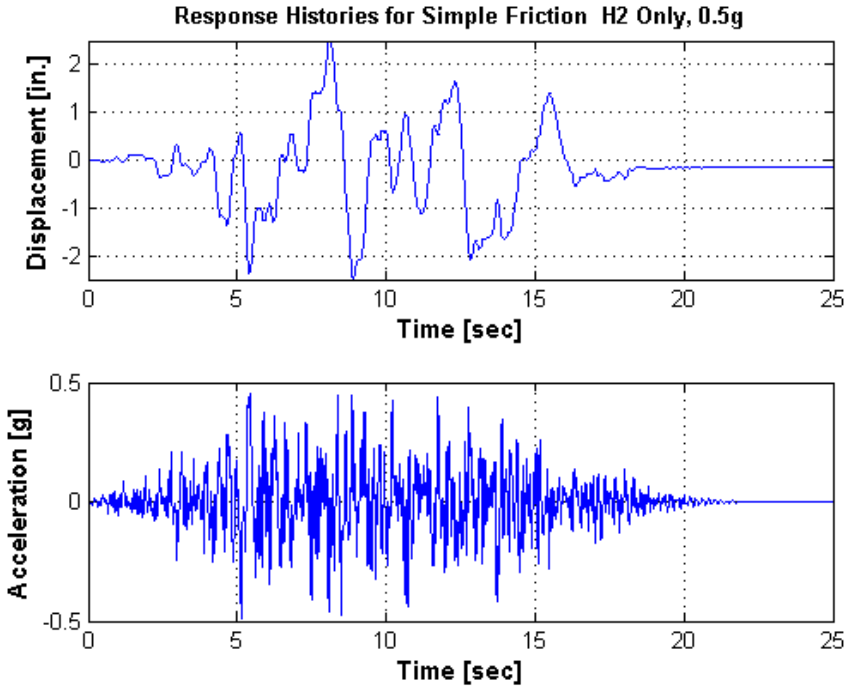

Figure A.65 Displacement and Acceleration. Response Histories H2 Only-SF (DBE)

Response Histories for Isolator Models (DBE, H1 and H2 Motions)

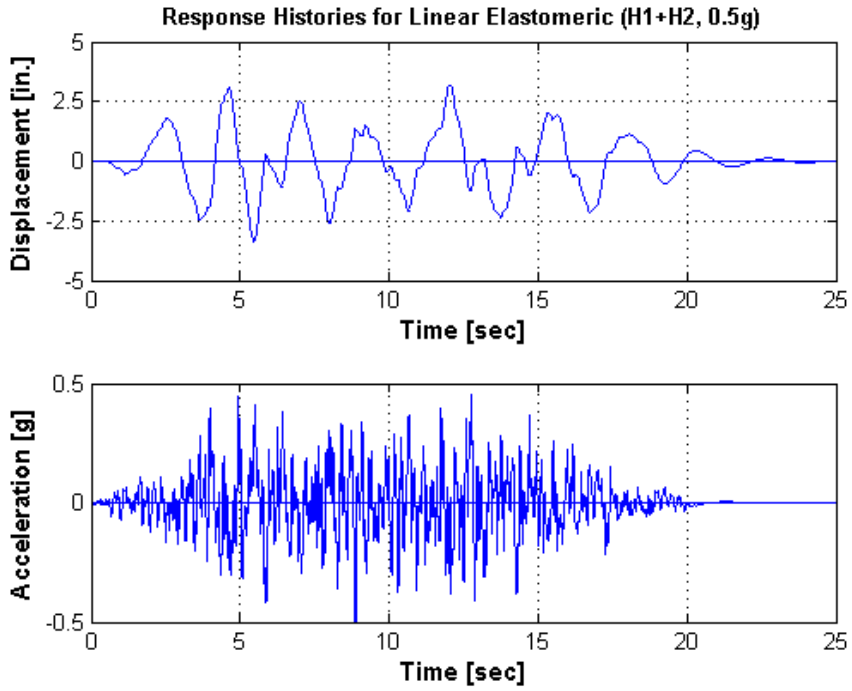

Figure A.66 Displacement and Acceleration. Response Histories (H1+H2) -Linear (DBE)

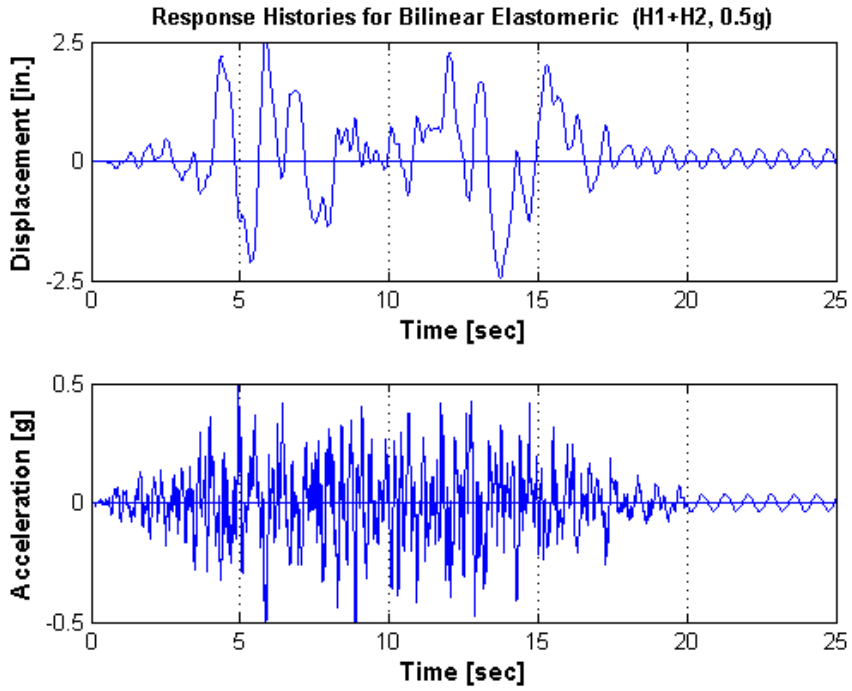

Figure A.67 Displacement and Acceleration. Response Histories (H1+H2) -BL-P (DBE)

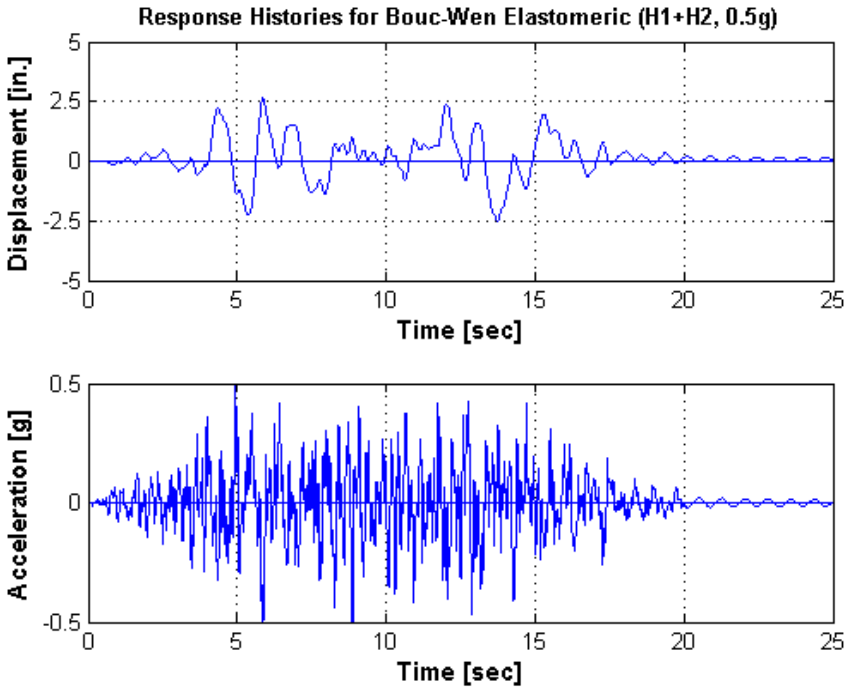

Figure A.68 Displacement and Acceleration. Response Histories (H1+H2) -BL-BW (DBE)

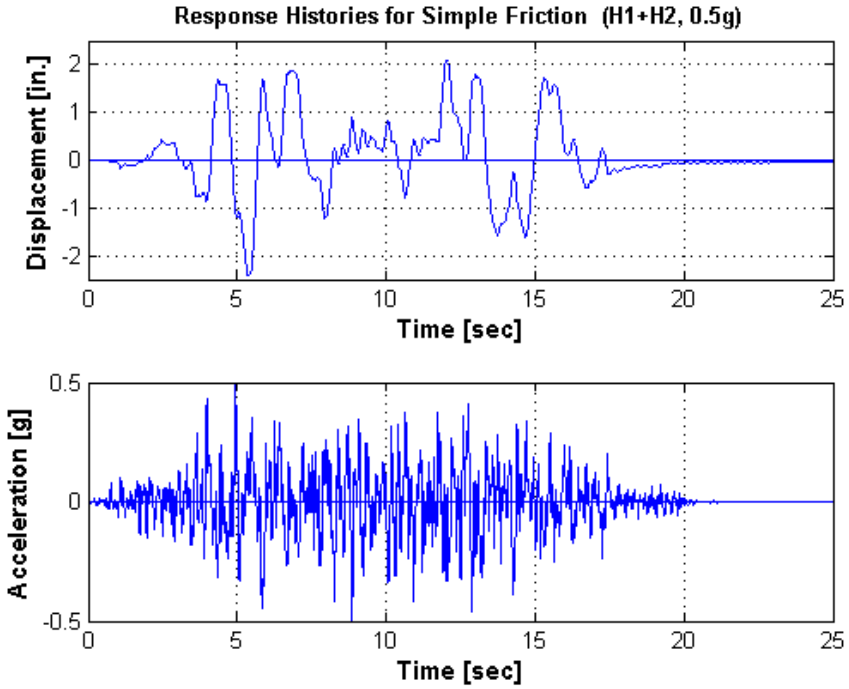

Figure A.69 Displacement and Acceleration. Response Histories (H1+H2)-SF (DBE)

Appendix C

3D DOF Vertical FRS

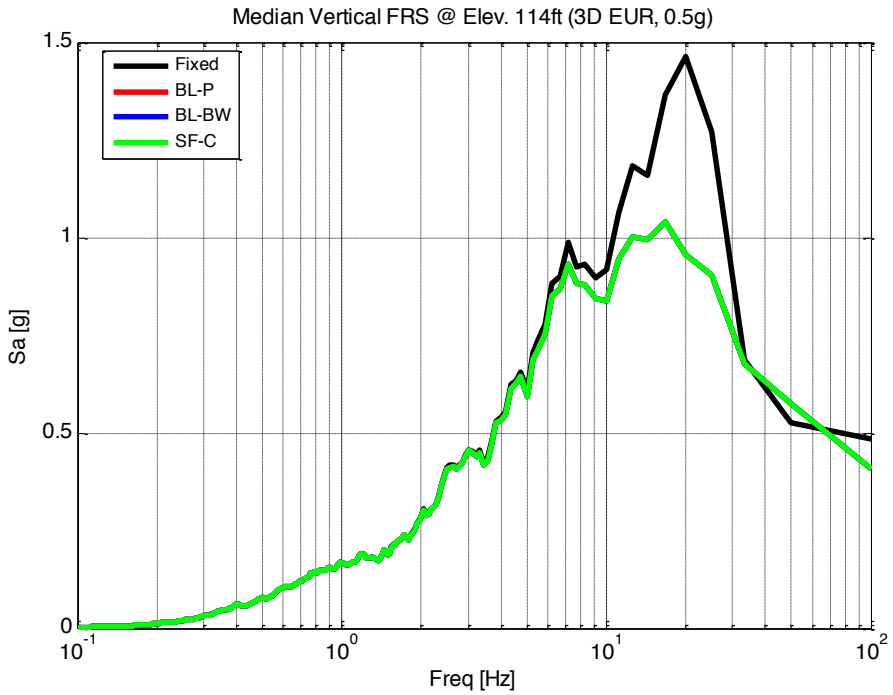

Figure A.70 Median Vertical FRS for Elev. 114ft – EUR 3D, 0.5g

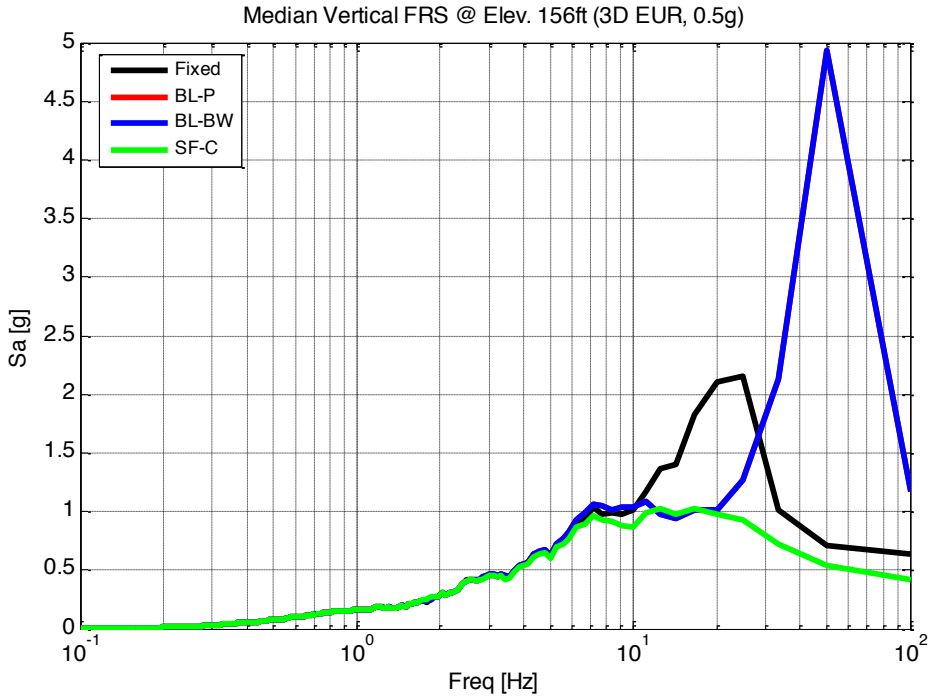

Figure A.71 Median Vertical FRS for Elev. 156ft – EUR 3D, 0.5g

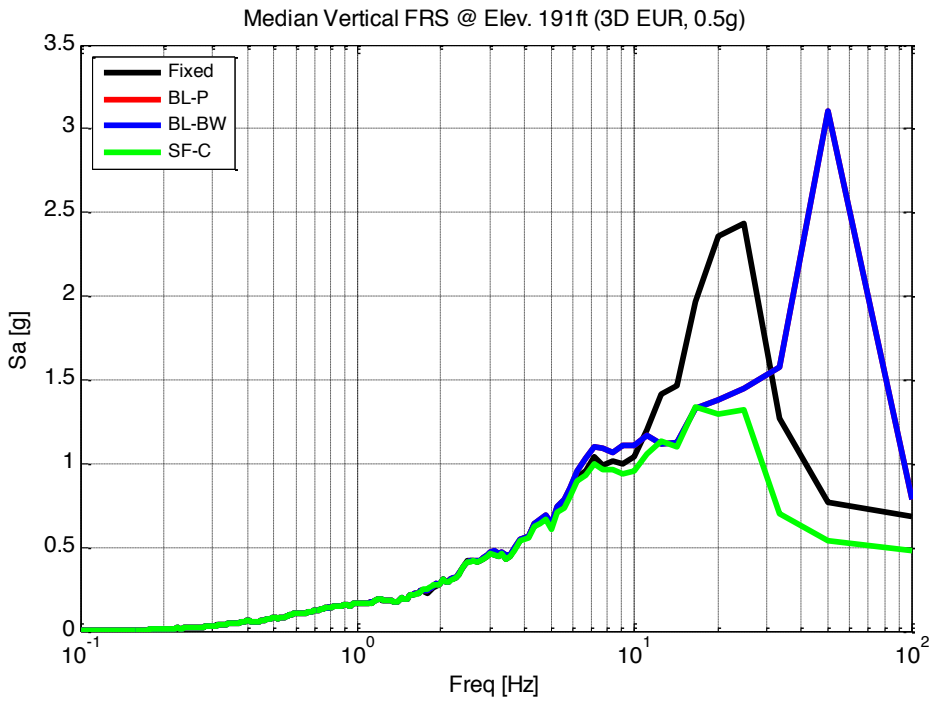

Figure A.72 Median Vertical FRS for Elev. 191ft – EUR 3D, 0.5g

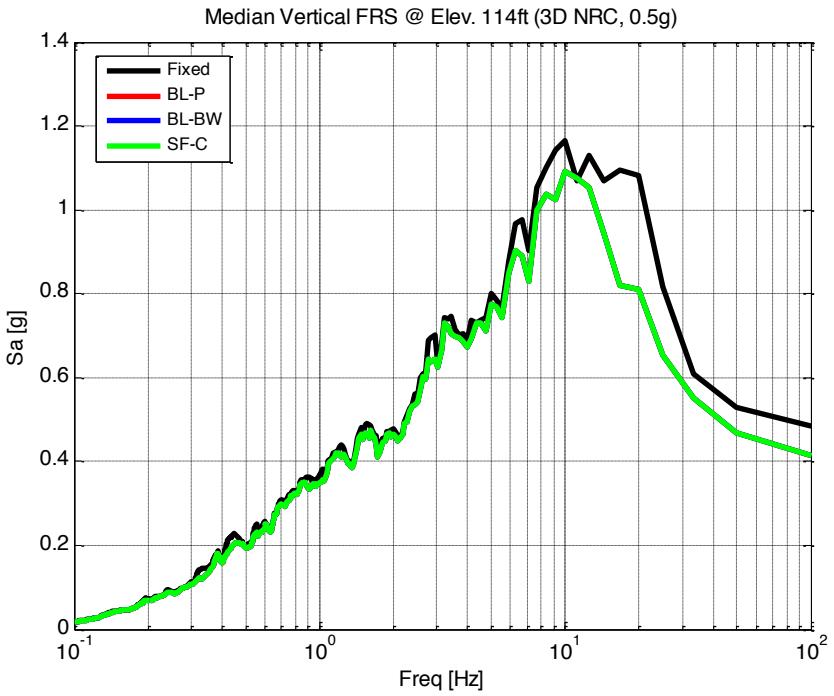

Figure A.73 Median Vertical FRS for Elev. 114ft – NRC 3D, 0.5g

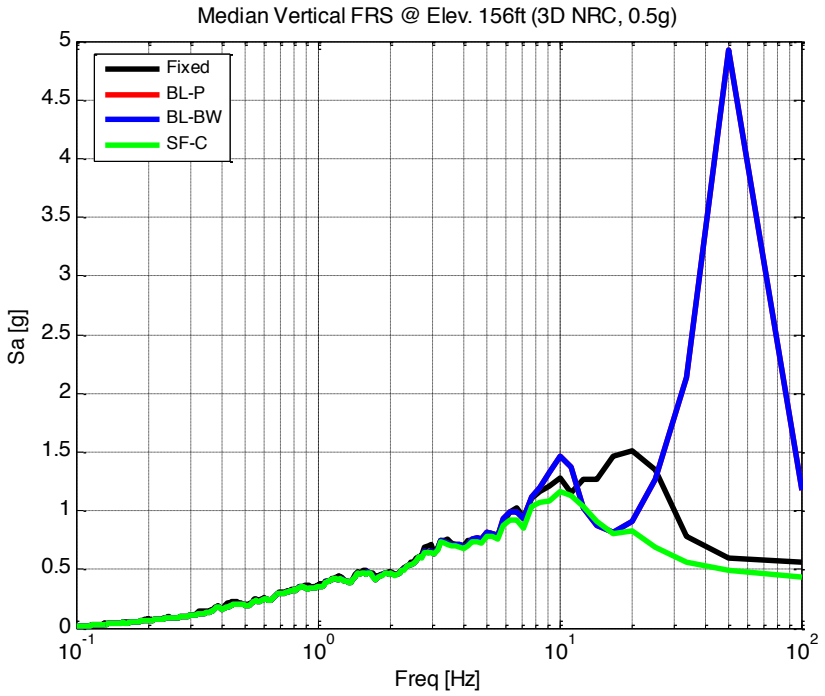

Figure A.74 Median Vertical FRS for Elev. 156ft – NRC 3D, 0.5g

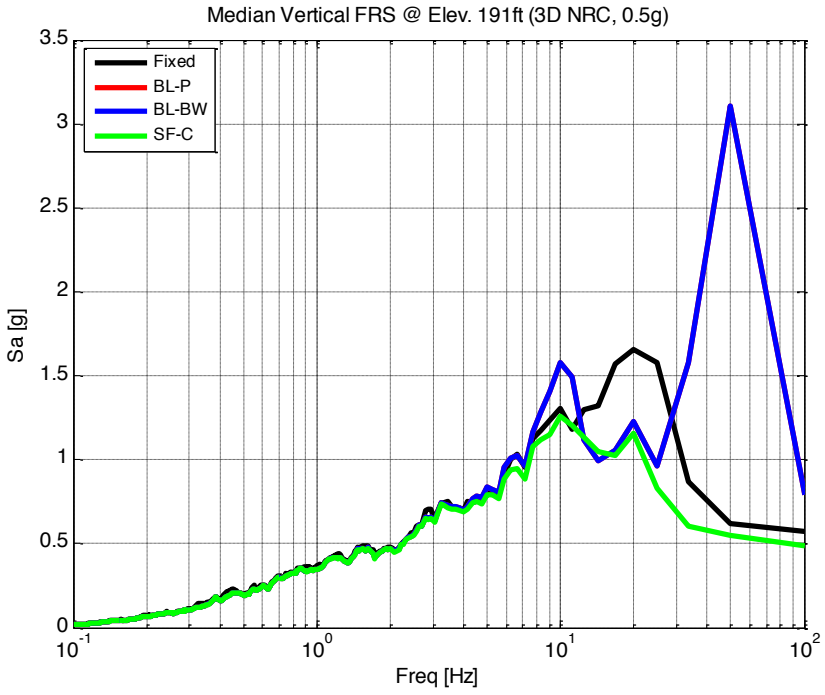

Figure A.75 Median Vertical FRS for Elev. 191ft – NRC 3D, 0.5g

3D DOF Vertical and Vertical Horizontal FRS Comparison

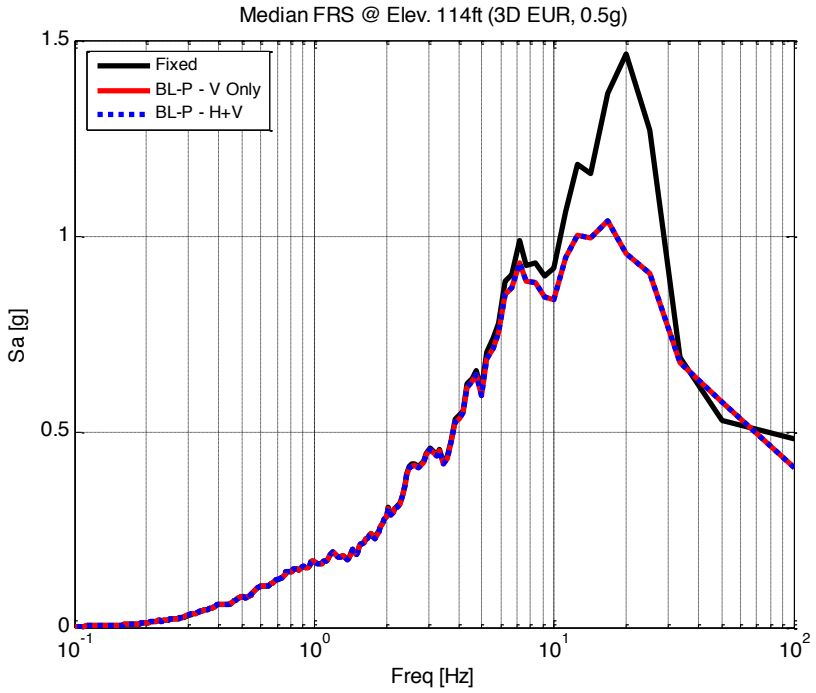

Figure A.76 Median FRS for Elev. 114ft – EUR 3D, 0.5g

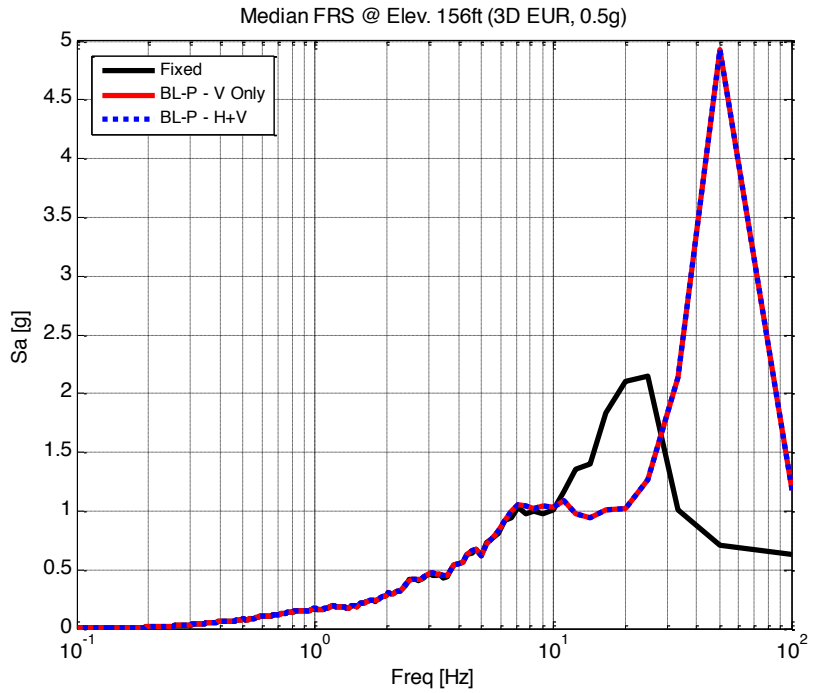

Figure A.77 Median FRS for Elev. 156ft – EUR 3D, 0.5g

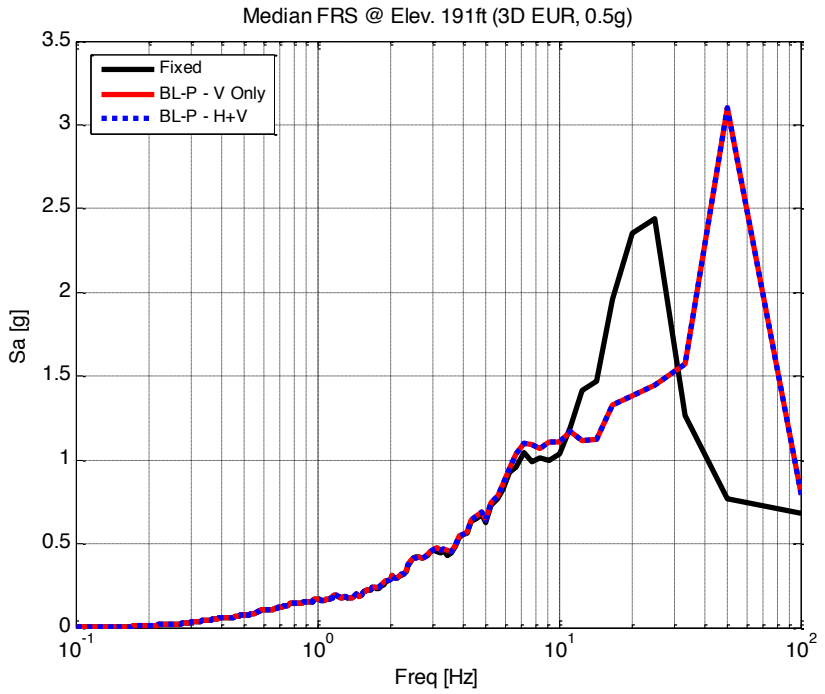

Figure A.78 Median FRS for Elev. 191ft – EUR 3D, 0.5g

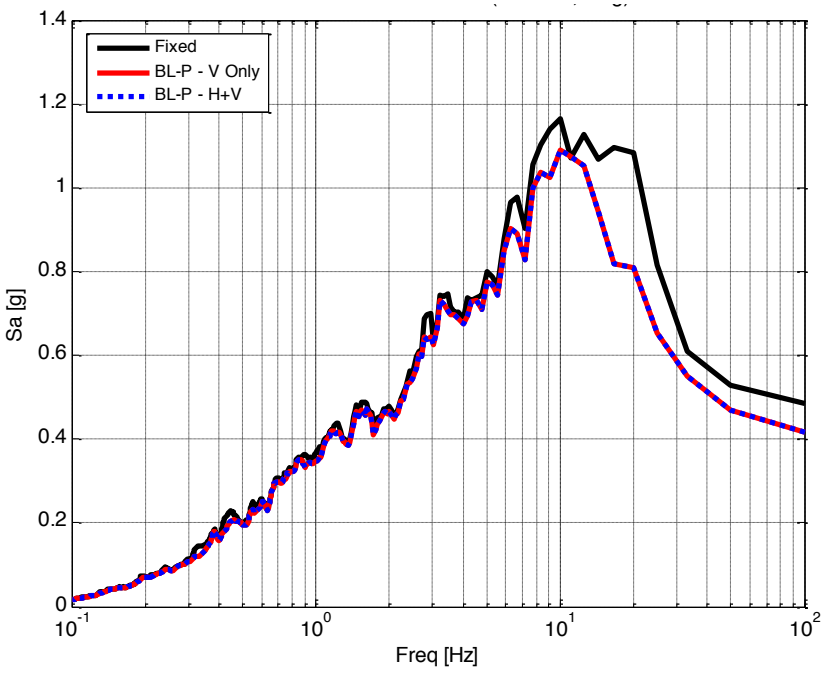

Figure A.79 Median FRS for Elev. 114ft – NRC 3D, 0.5g

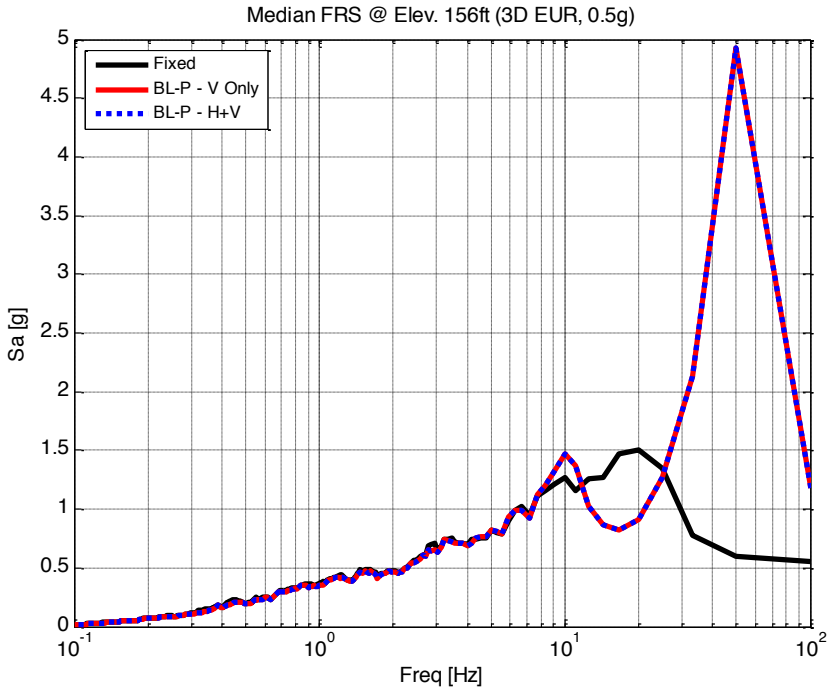

Figure A.80 Median FRS for Elev. 156ft – NRC 3D, 0.5g

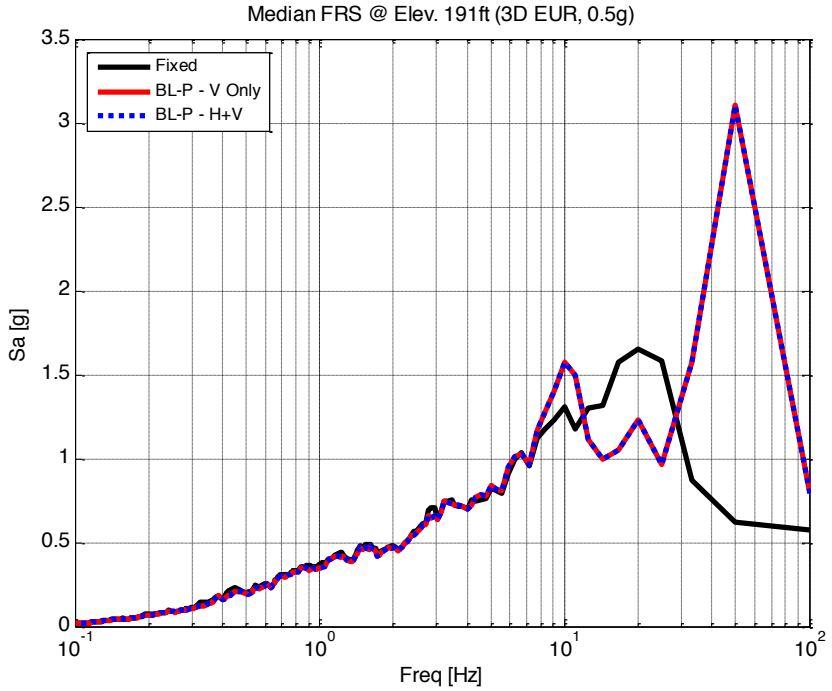

Figure A.81 Median FRS for Elev. 191ft – NRC 3D, 0.5g

Appendix D

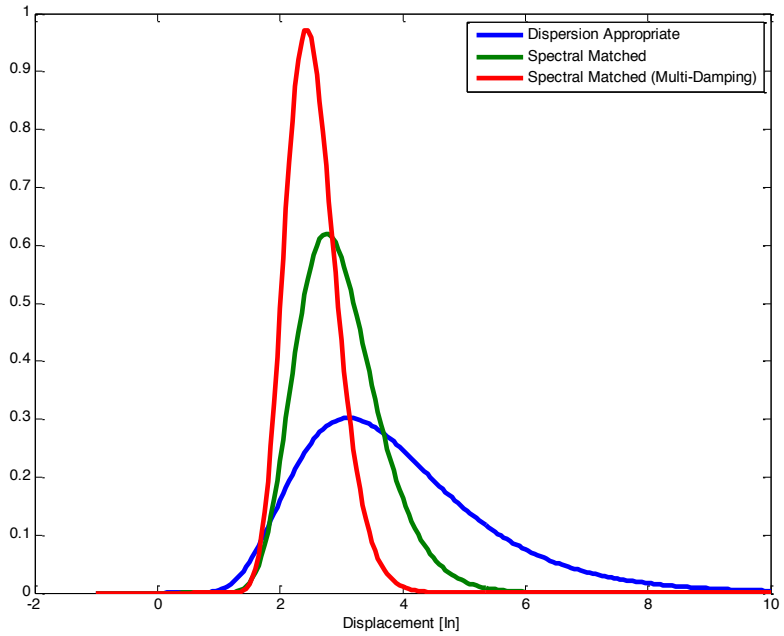

Figure A.82 PDF for Bilinear Bouc-Wen Isolator Presenting the Dispersion of Isolator Displacements for Variety of Ground Motion Inputs (EUR, DBE).

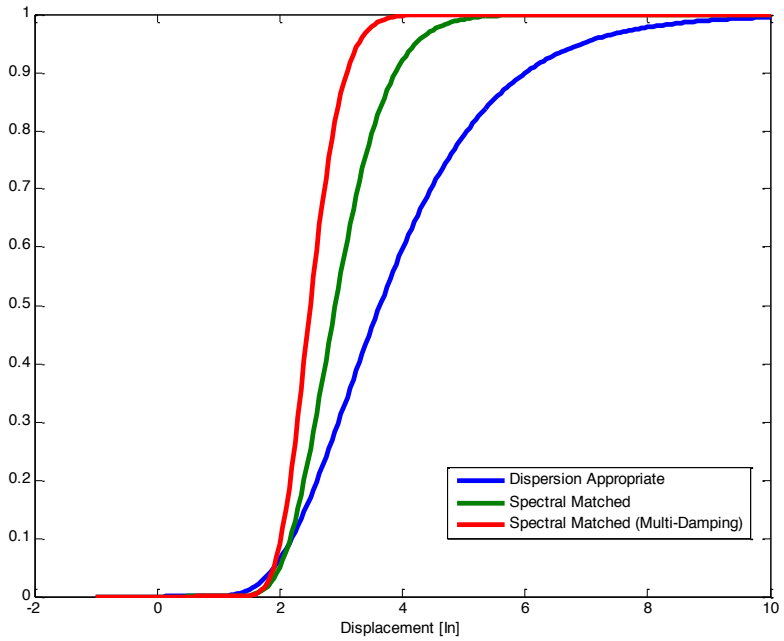

Figure A.83 CDF for Bilinear Bouc-Wen Isolator Presenting the Dispersion of Isolator Displacements for Variety of Ground Motion Inputs (EUR, DBE).

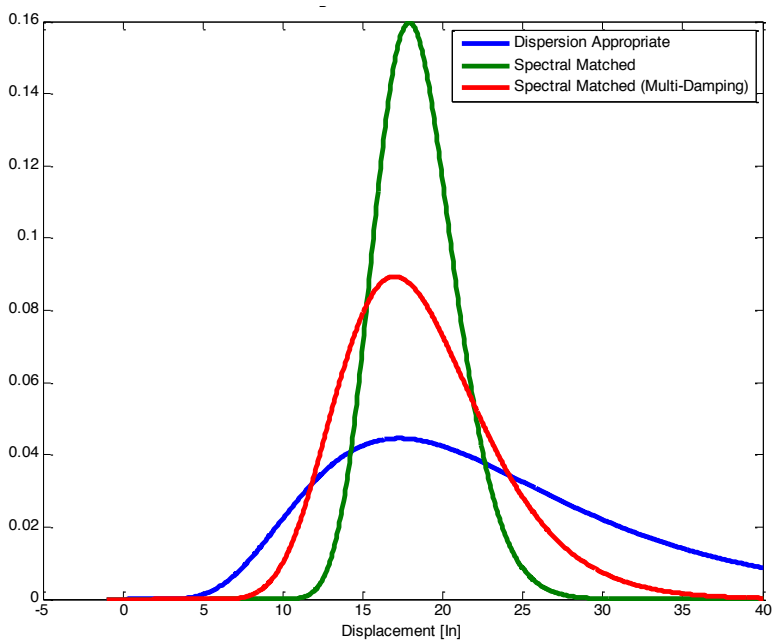

Figure A.84 PDF for Bilinear Bouc-Wen Isolator Presenting the Dispersion of Isolator Displacements for Variety of Ground Motion Inputs (NRC, DBE).

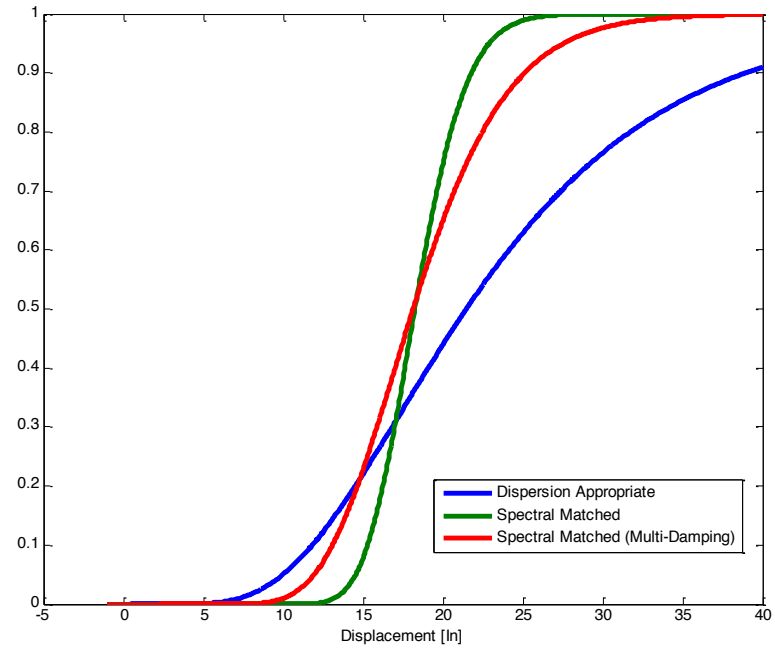

Figure A.85 CDF for Bilinear Bouc-Wen Isolator Presenting the Dispersion of Isolator Displacements for Variety of Ground Motion Inputs (NRC, DBE).

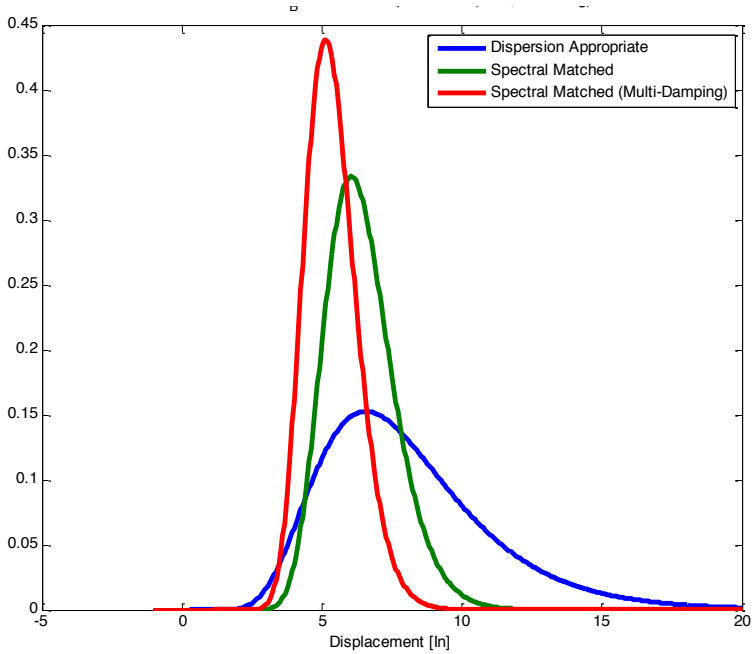

Figure A.86 PDF for Bilinear Bouc-Wen Isolator Presenting the Dispersion of Isolator Displacements for Variety of Ground Motion Inputs (EUR, EDB).

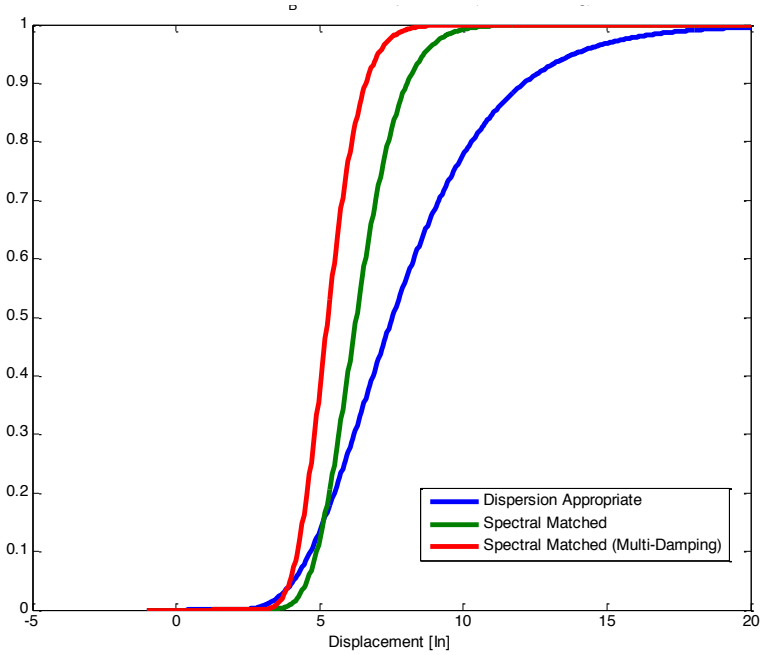

Figure A.87 CDF for Bilinear Bouc-Wen Isolator Presenting the Dispersion of Isolator Displacements for Variety of Ground Motion Inputs (EUR, EDB).

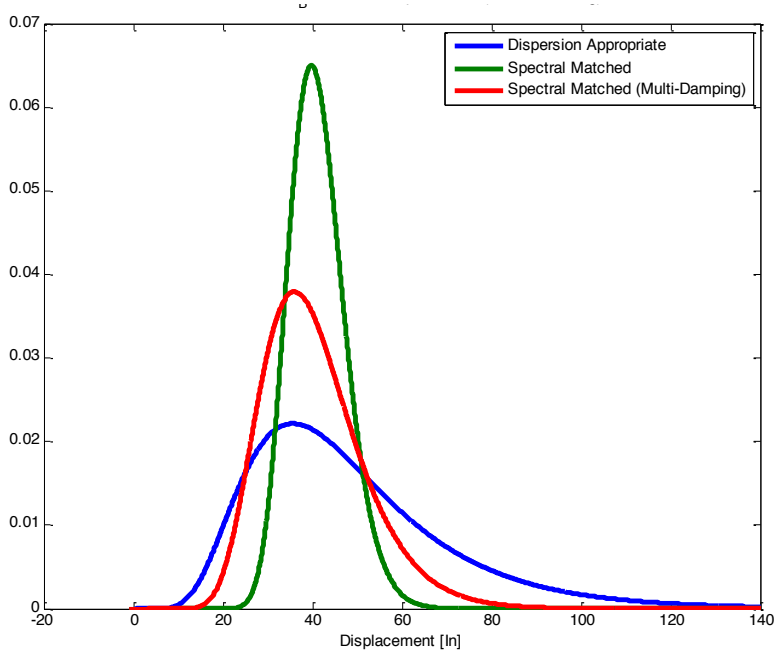

Figure A.88 PDF for Bilinear Bouc-Wen Isolator Presenting the Dispersion of Isolator Displacements for Variety of Ground Motion Inputs (NRC, EDB).

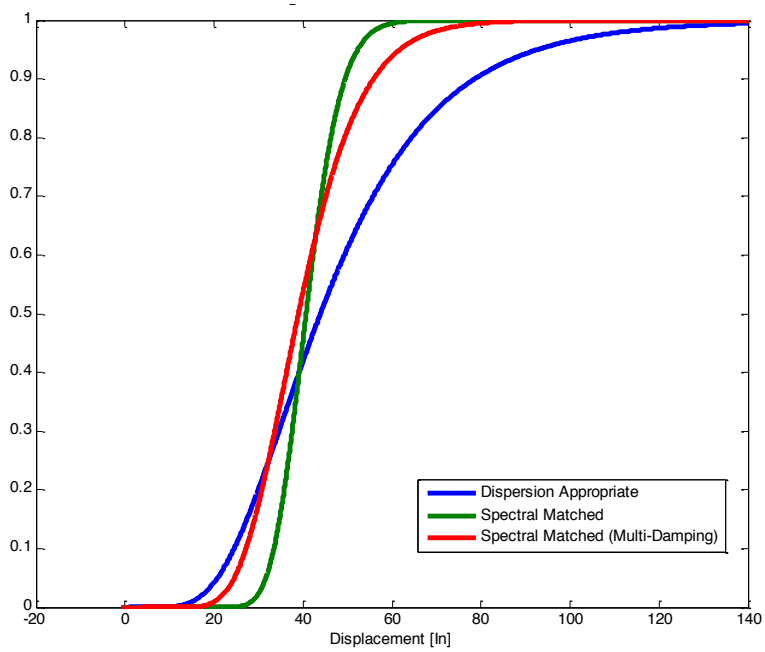

Figure A.89 CDF for Bilinear Bouc-Wen Isolator Presenting the Dispersion of Isolator Displacements for Variety of Ground Motion Inputs (NRC, EDB).

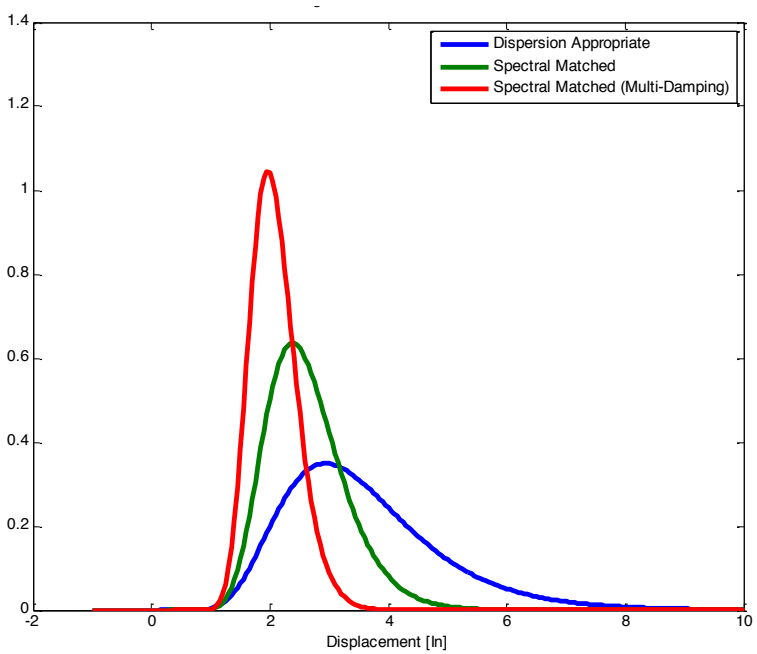

Figure A.90 PDF for Simple Friction Isolator with Constant Friction Presenting the Dispersion of Isolator Displacements for Variety of Ground Motion Inputs (EUR, DBE).

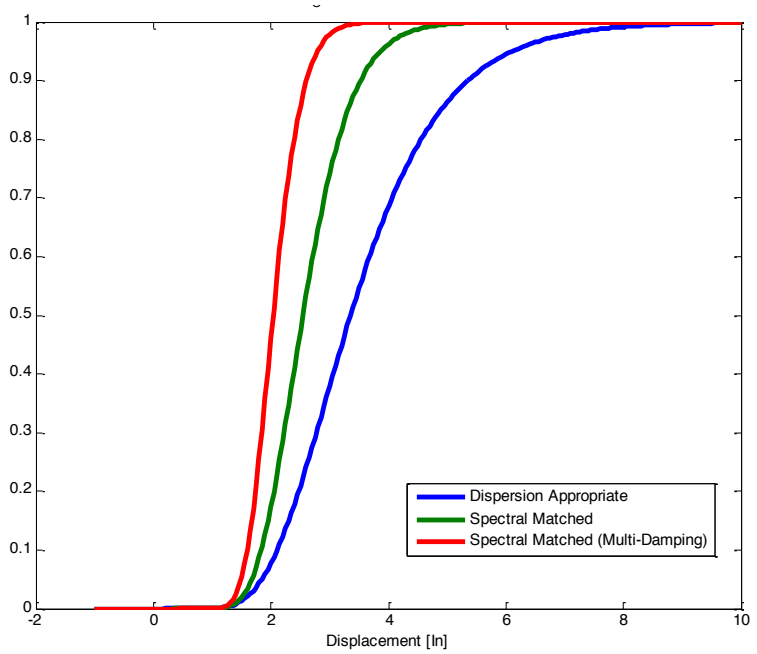

Figure A.91 CDF for Simple Friction Isolator with Constant Friction Presenting the Dispersion of Isolator Displacements for Variety of Ground Motion Inputs (EUR, DBE).

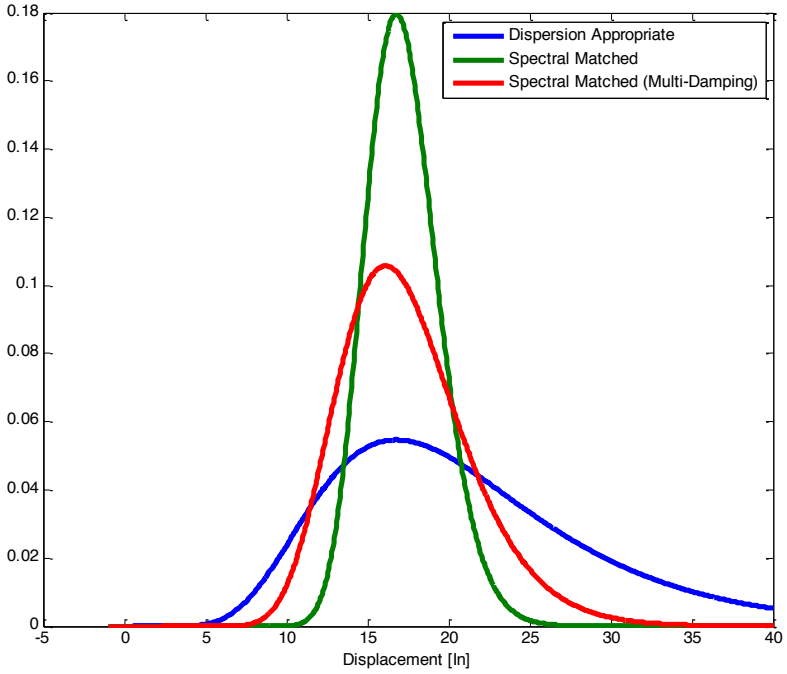

Figure A.92 PDF for Simple Friction Isolator with Constant Friction Presenting the Dispersion of Isolator Displacements for Variety of Ground Motion Inputs (NRC, DBE).

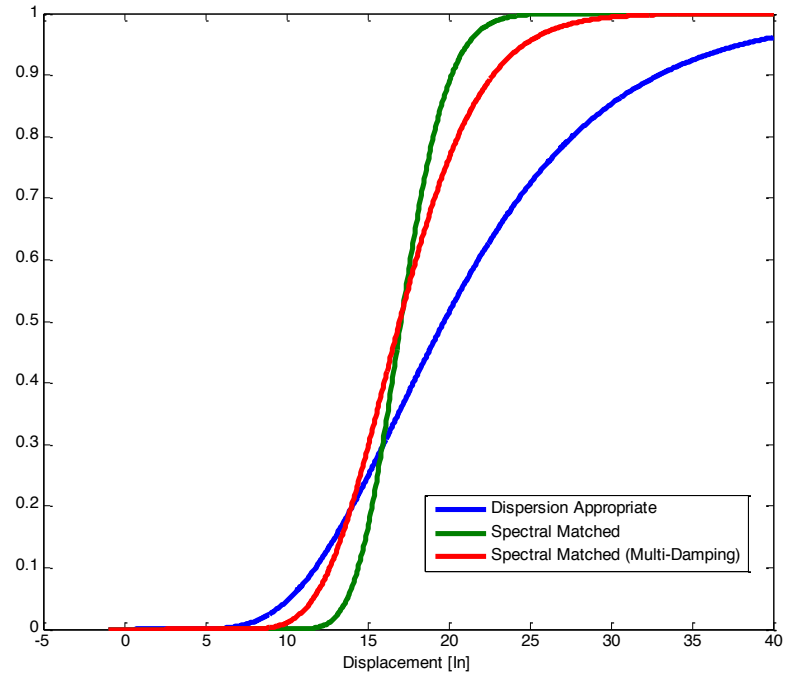

Figure A.93 PDF for Simple Friction Isolator with Constant Friction Presenting the Dispersion of Isolator Displacements for Variety of Ground Motion Inputs (NRC, DBE).

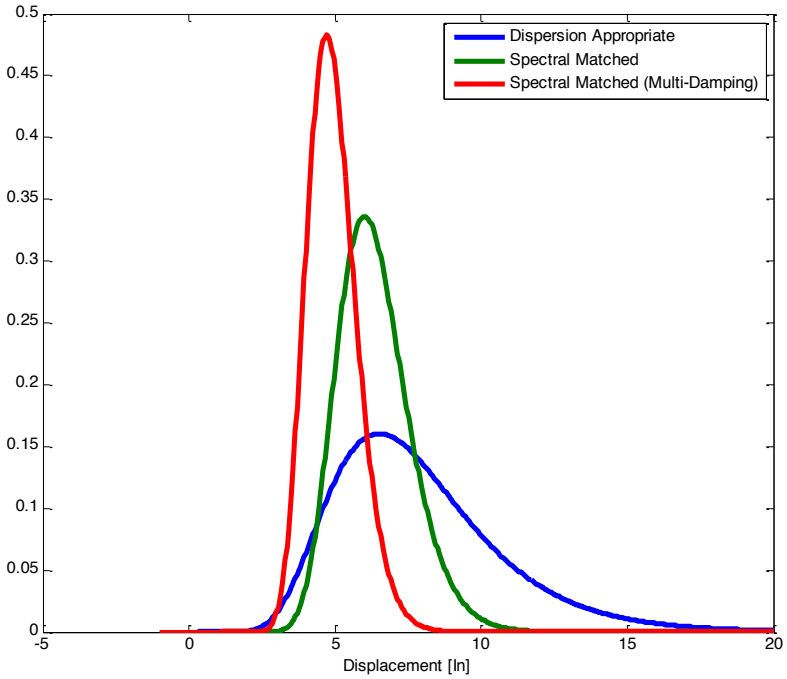

Figure A.94 PDF for Simple Friction Isolator with Constant Friction Presenting the Dispersion of Isolator Displacements for Variety of Ground Motion Inputs (EUR, EDB).

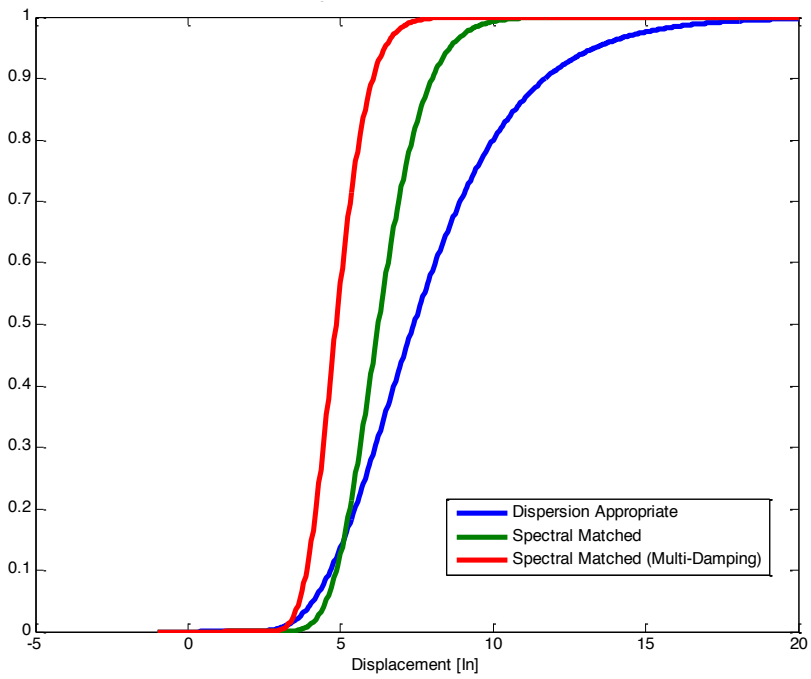

Figure A.95 CDF for Simple Friction Isolator with Constant Friction Presenting the Dispersion of Isolator Displacements for Variety of Ground Motion Inputs (EUR, EDB).

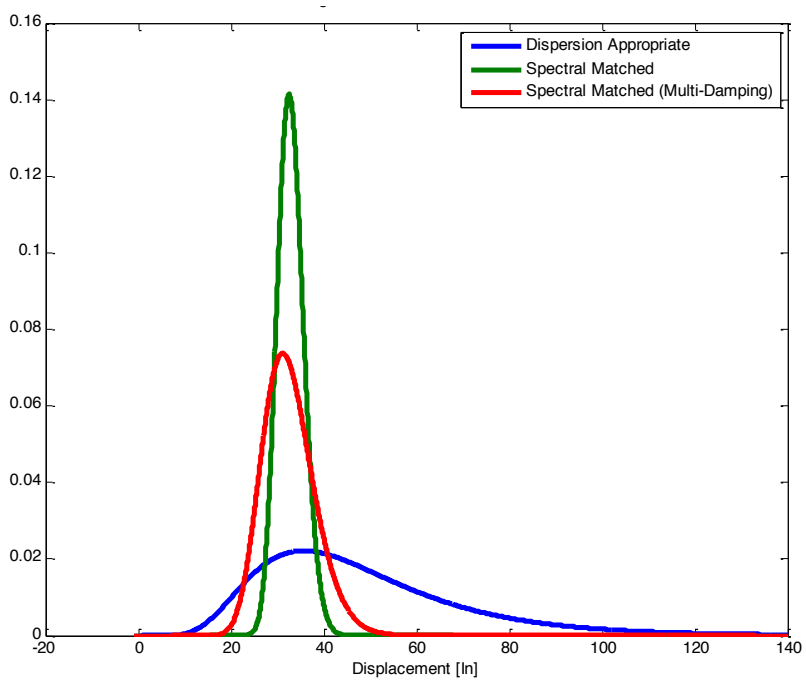

Figure A.96 PDF for Simple Friction Isolator with Constant Friction Presenting the Dispersion of Isolator Displacements for Variety of Ground Motion Inputs (NRC, EDB).

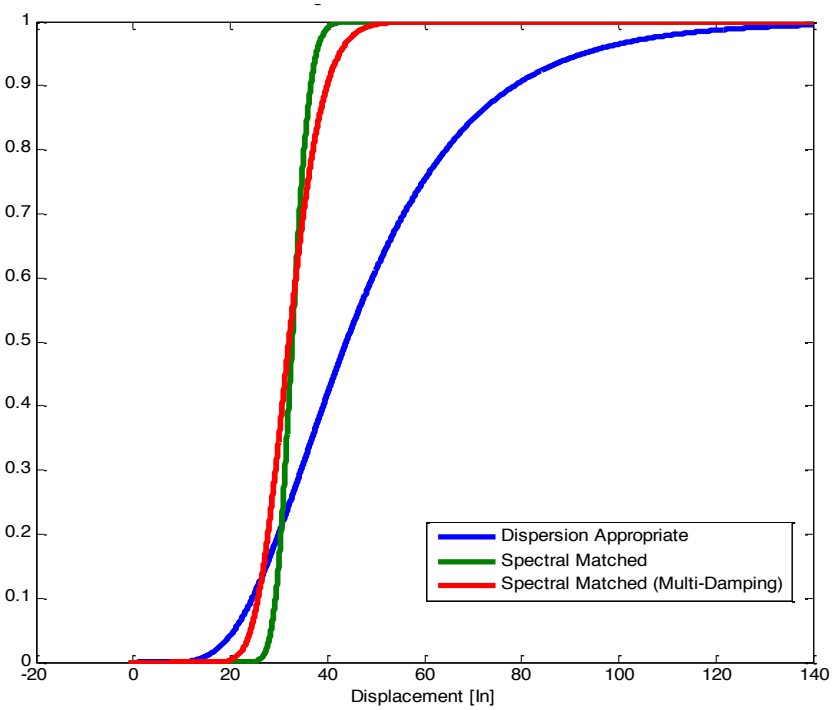

Figure A.97 CDF for Simple Friction Isolator with Constant Friction Presenting the Dispersion of Isolator Displacements for Variety of Ground Motion Inputs (NRC,EDB).

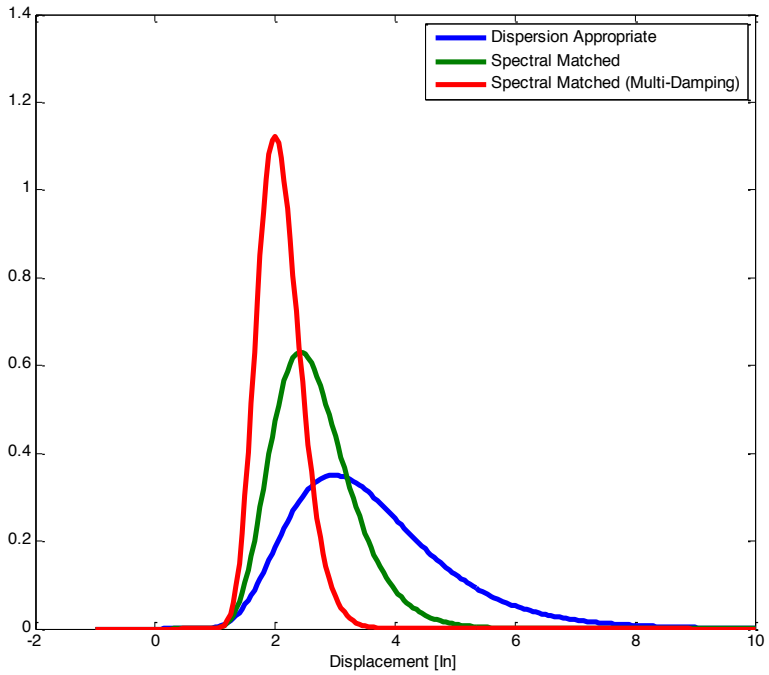

Figure A.98 PDF for Simple Friction Isolator with Velocity Dependent Friction Presenting the Dispersion of Isolator Displacements for Variety of Ground Motion Inputs (EUR, DBE).

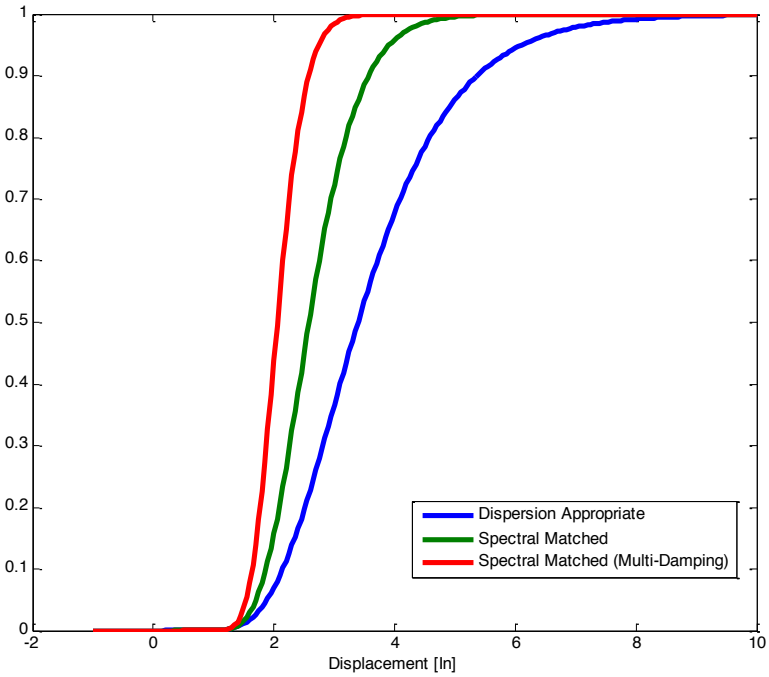

Figure A.99 CDF for Simple Friction Isolator with Velocity Dependent Friction Presenting the Dispersion of Isolator Displacements for Variety of Ground Motion Inputs (EUR, DBE).

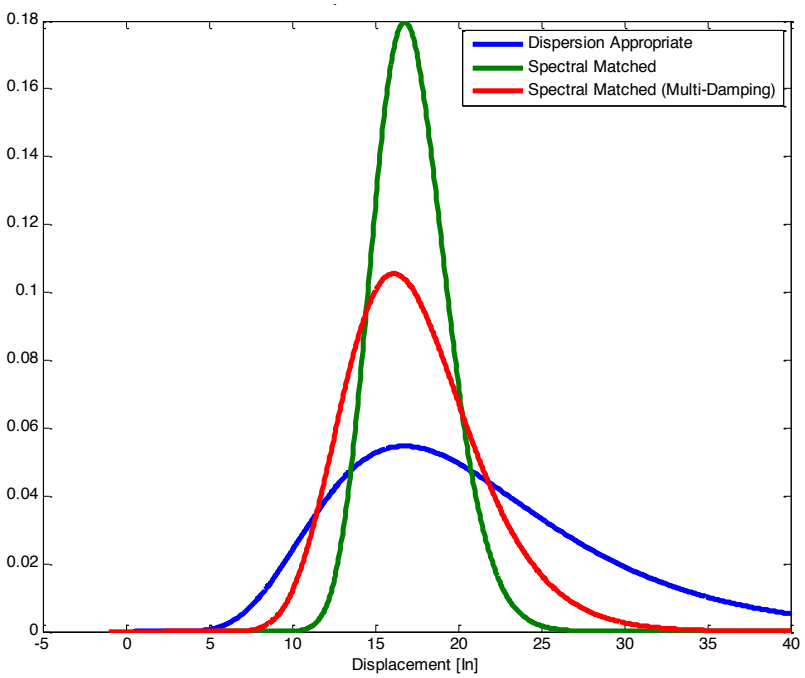

Figure A.100 PDF for Simple Friction Isolator with Velocity Dependent Friction Presenting the Dispersion of Isolator Displacements for Variety of Ground Motion Inputs (NRC, DBE).

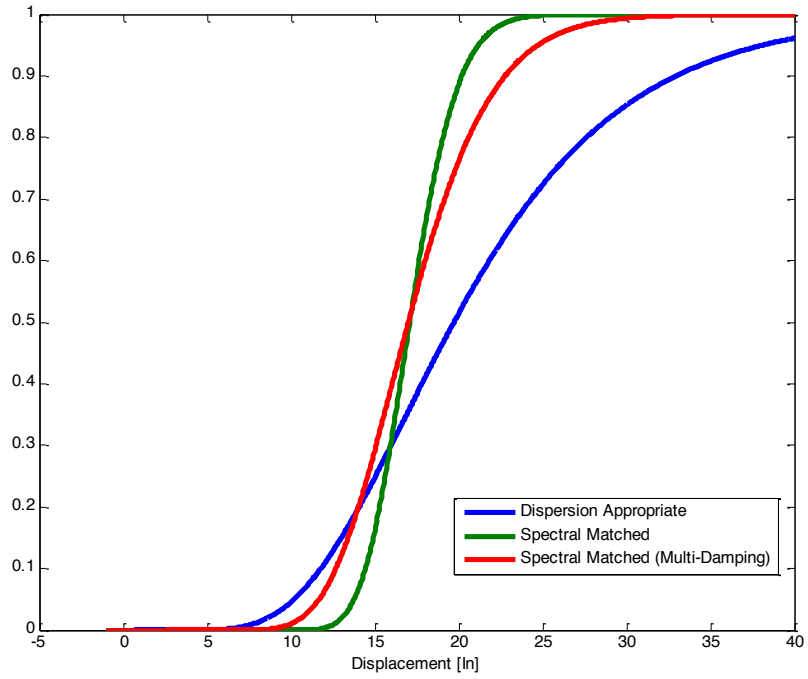

Figure A.101 CDF for Simple Friction Isolator with Velocity Dependent Friction Presenting the Dispersion of Isolator Displacements for Variety of Ground Motion Inputs (NRC, DBE).

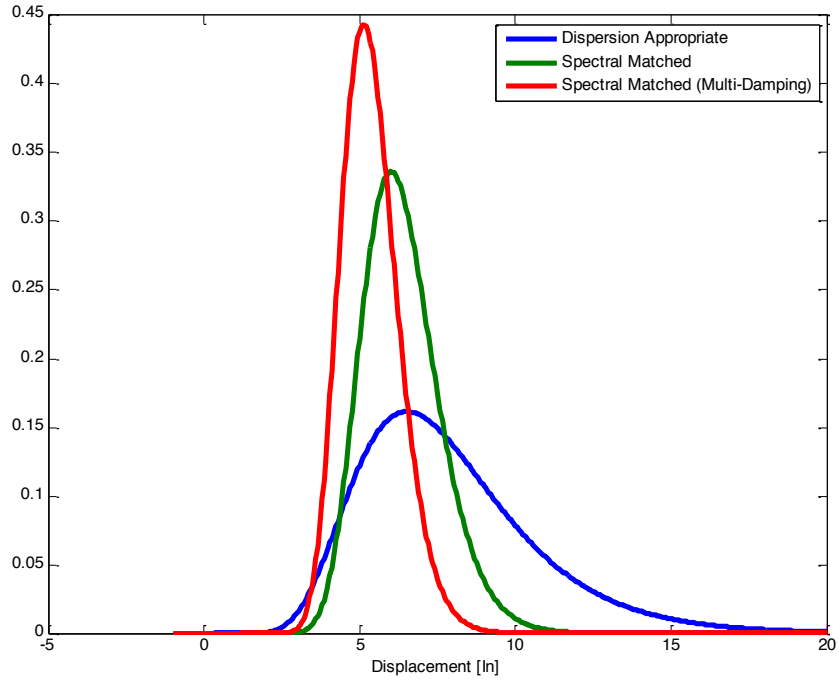

Figure A.102 PDF for Simple Friction Isolator with Velocity Dependent Friction Presenting the Dispersion of Isolator Displacements for Variety of Ground Motion Inputs (EUR, EDB).

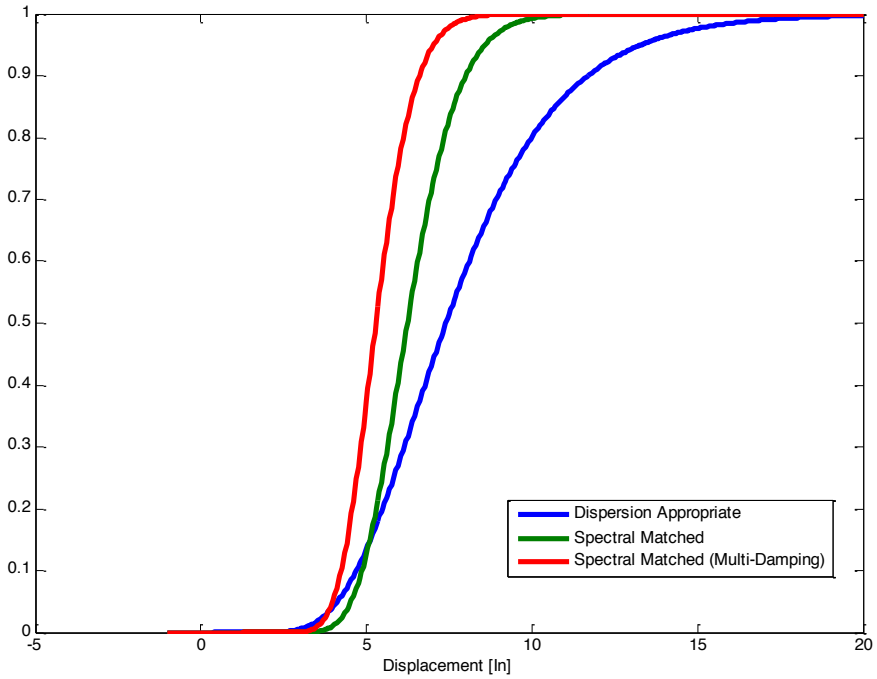

Figure A.103 CDF for Simple Friction Isolator with Velocity Dependent Friction Presenting the Dispersion of Isolator Displacements for Variety of Ground Motion Inputs (EUR, EDB).

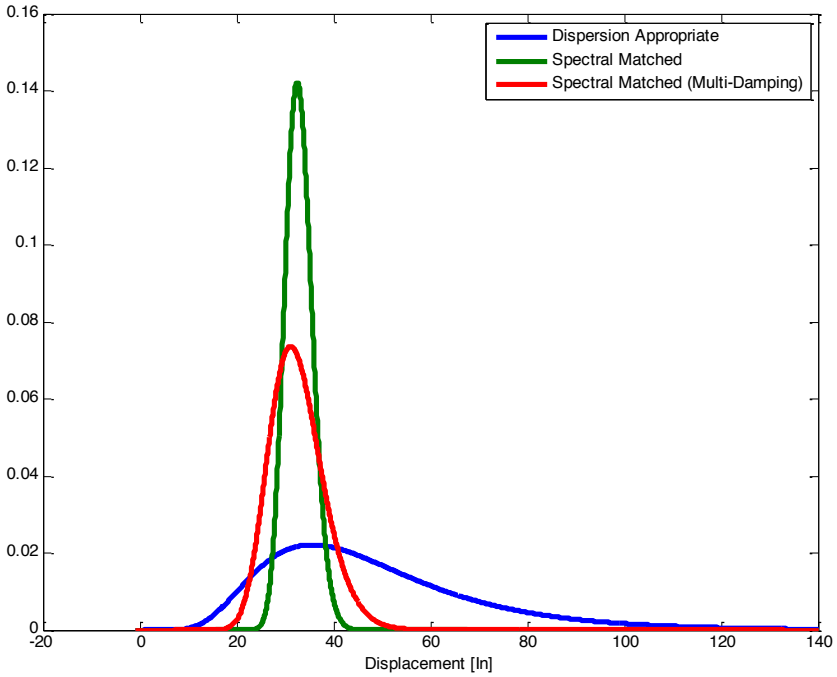

Figure A.104 PDF for Simple Friction Isolator with Velocity Dependent Friction Presenting the Dispersion of Isolator Displacements for Variety of Ground Motion Inputs (NRC, EDB).

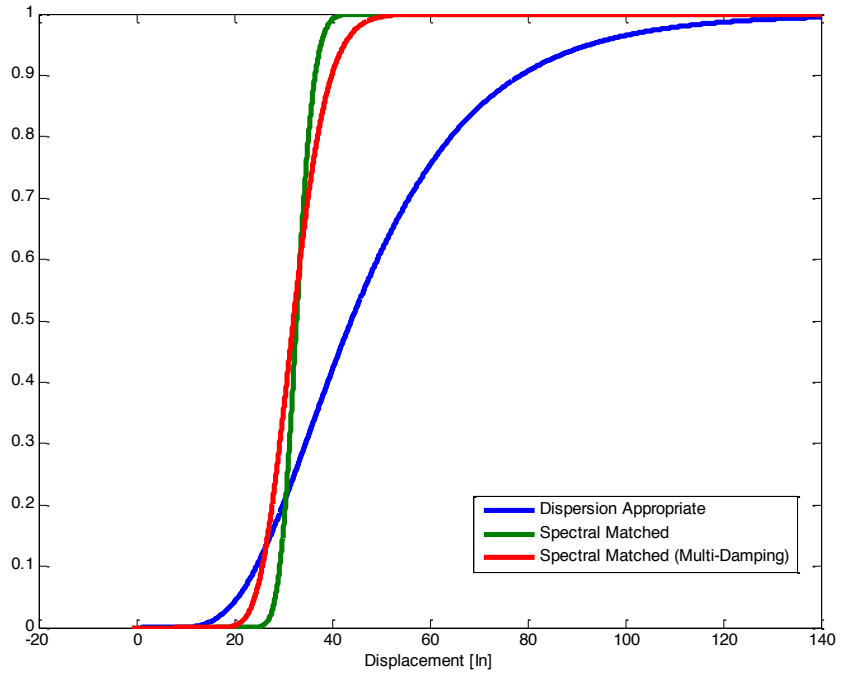

Figure A.105 CDF for Simple Friction Isolator with Velocity Dependent Friction Presenting the Dispersion of Isolator Displacements for Variety of Ground Motion Inputs (NRC, EDB).

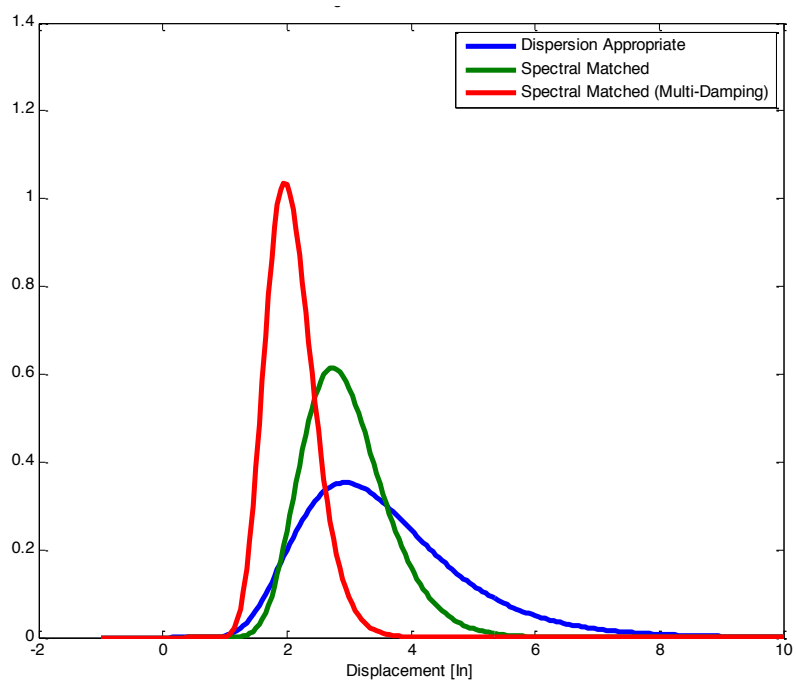

Figure A.106 PDF for EradiQuake System with Constant Friction Presenting the Dispersion of Isolator Displacements for Variety of Ground Motion Inputs (EUR, DBE).

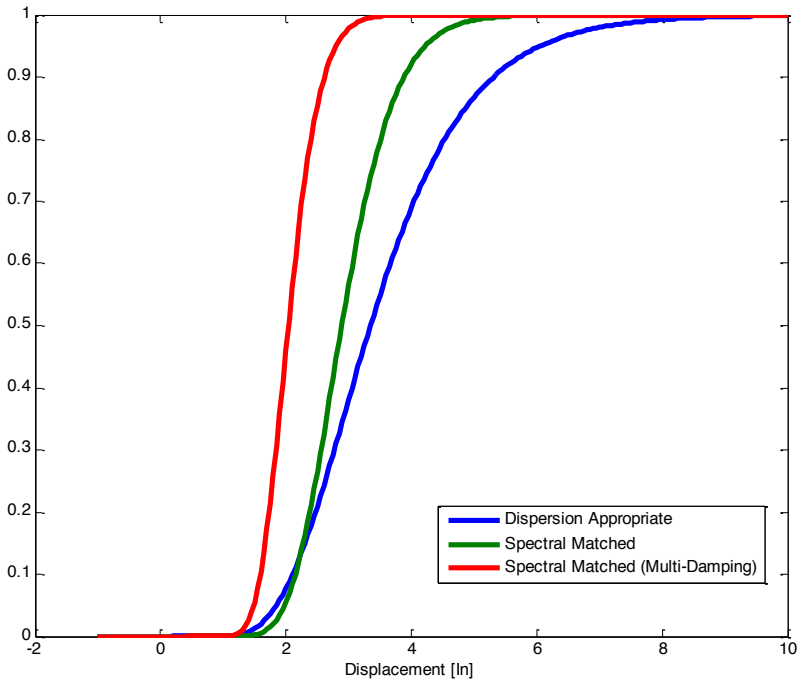

Figure A.107 CDF for EradiQuake System with Constant Friction Presenting the Dispersion of Isolator Displacements for Variety of Ground Motion Inputs (EUR, DBE).

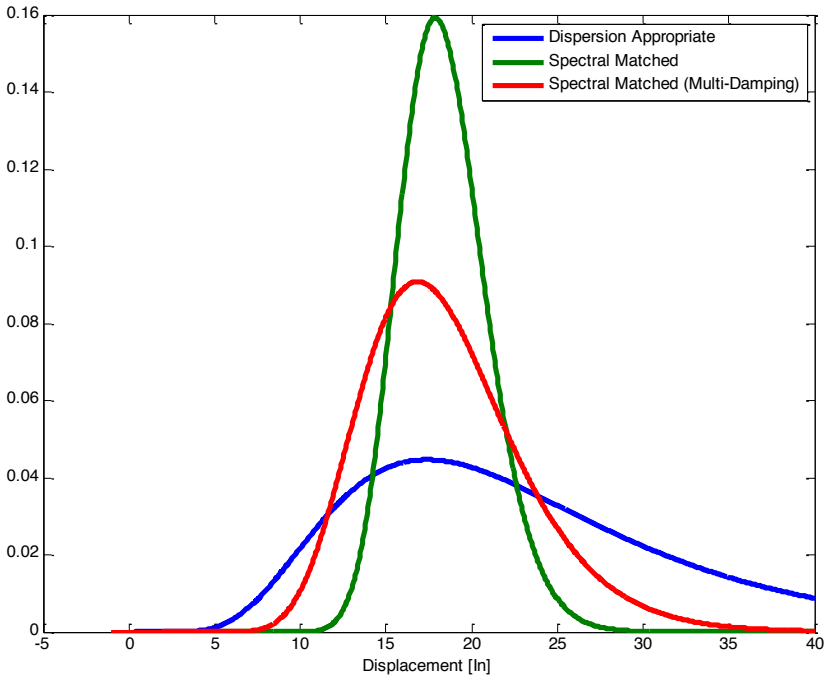

Figure A.108 PDF for EradiQuake System with Constant Friction Presenting the Dispersion of Isolator Displacements for Variety of Ground Motion Inputs (NRC, DBE).

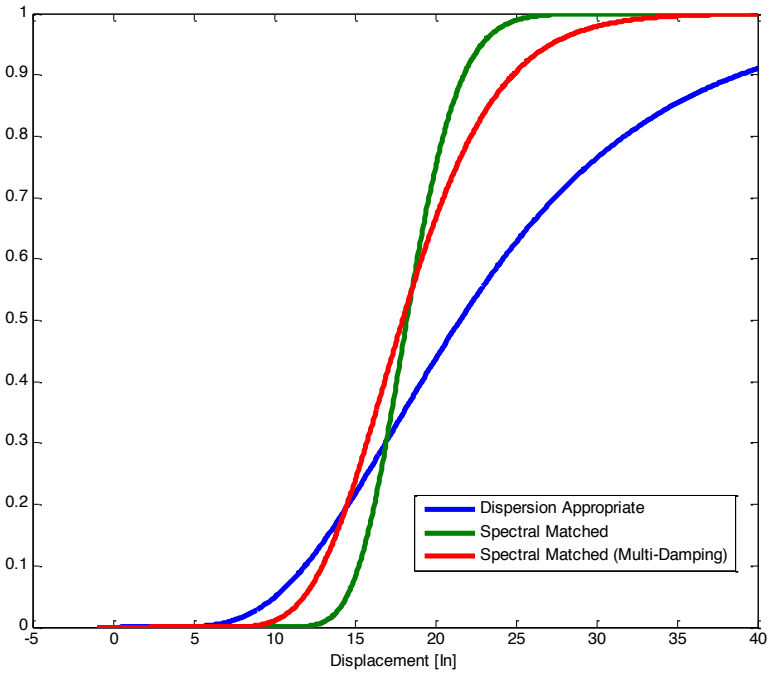

Figure A.109 CDF for EradiQuake System with Constant Friction Presenting the Dispersion of Isolator Displacements for Variet of Ground Motion Inputs (NRC, DBE).

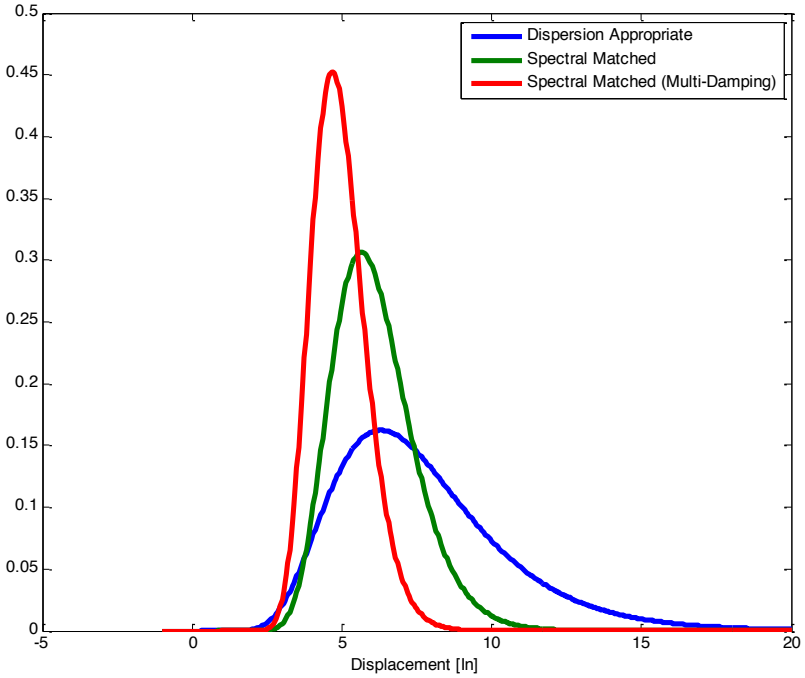

Figure A.110 PDF for EradiQuake System with Constant Friction Presenting the Dispersion of Isolator Displacements for Variety of Ground Motion Inputs (EUR, EDB).

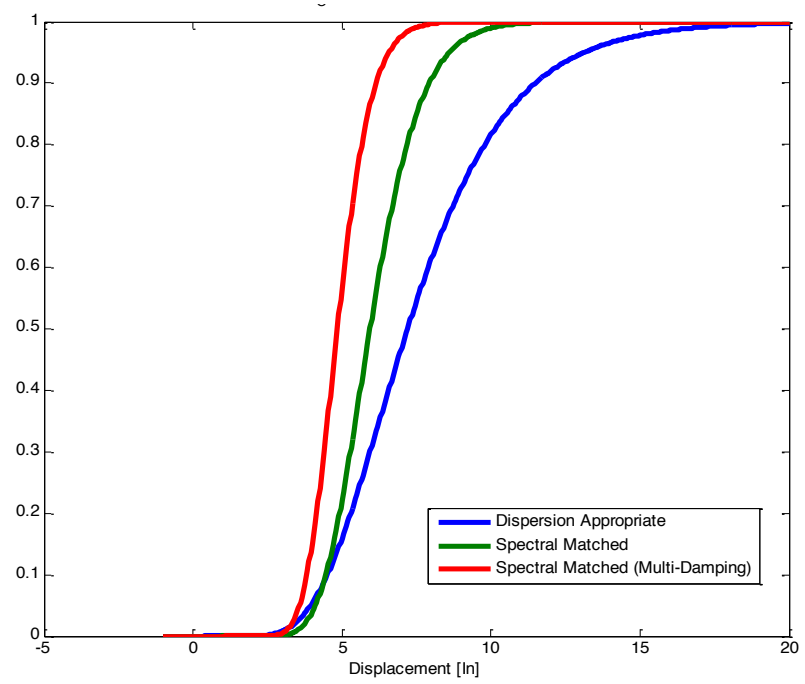

Figure A.111 CDF for EradiQuake System with Constant Friction Presenting the Dispersion of Isolator Displacements for Variety of Ground Motion Inputs (EUR, EDB).

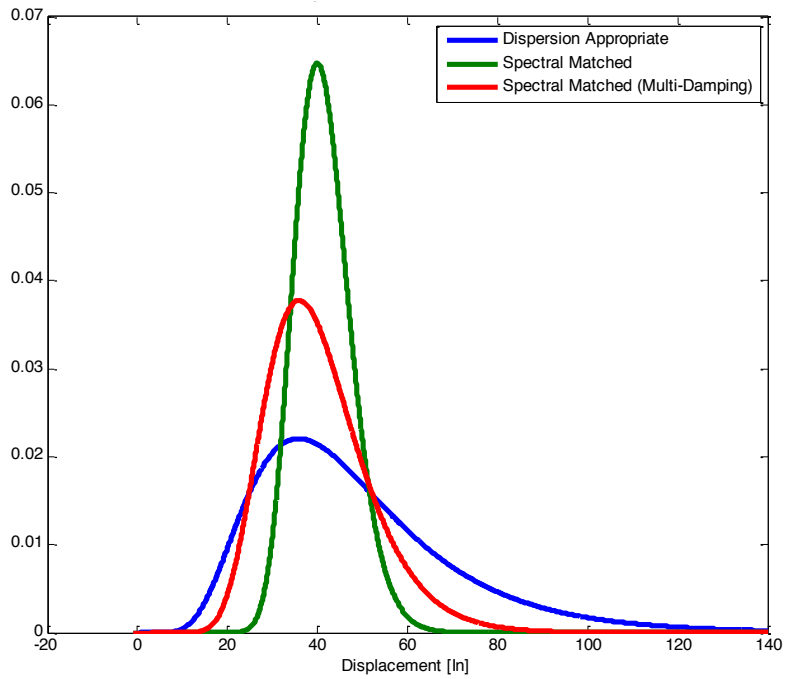

Figure A.112 PDF for EradiQuake System with Constant Friction Presenting the Dispersion of Isolator Displacements for Variety of Ground Motion Inputs (NRC, EDB).

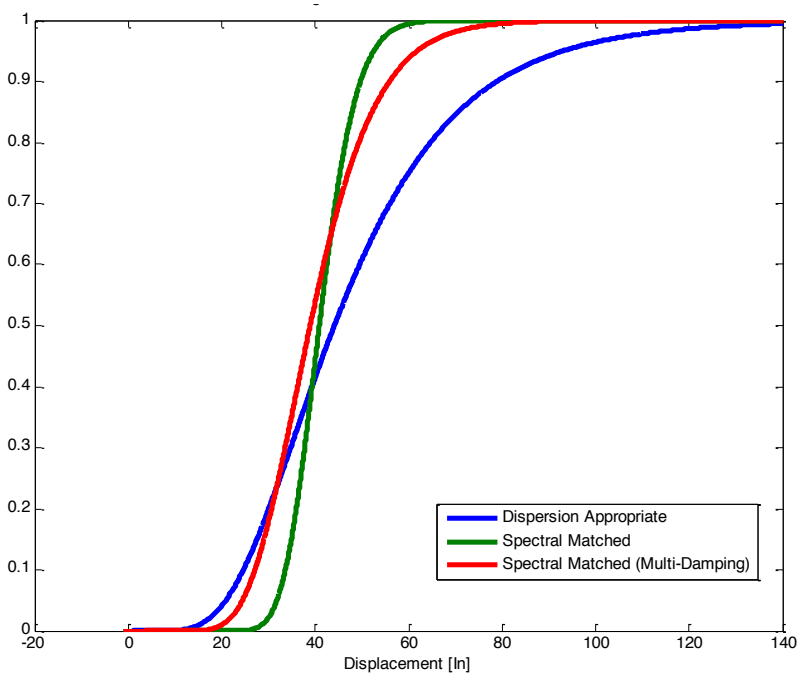

Figure A.113 CDF for EradiQuake System with Constant Friction Presenting the Dispersion of Isolator Displacements for Variety of Ground Motion Inputs (NRC, EDB).

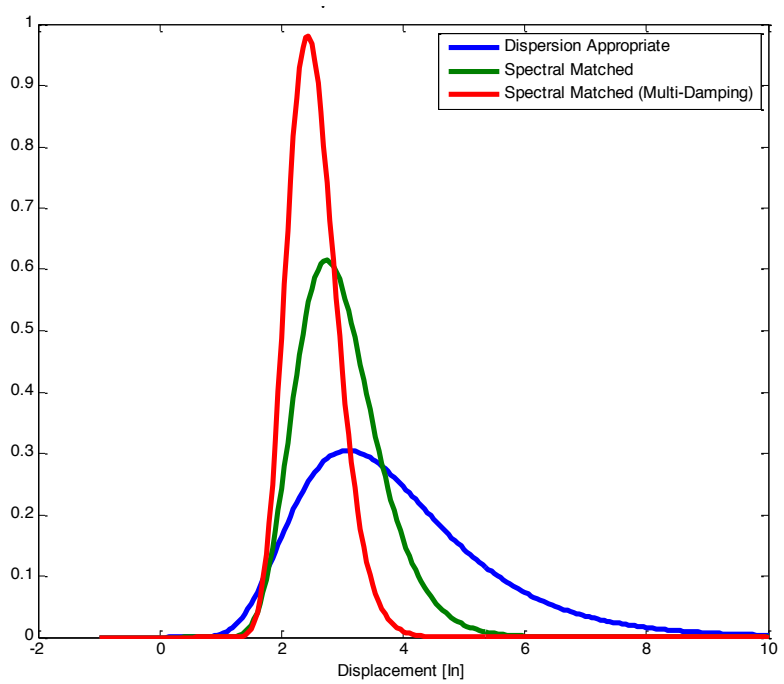

Figure A.114 PDF for EradiQuake System with Velocity Dependent Friction Presenting the Dispersion of Isolator Displacements for Vriety of Ground Motion Inputs (EUR, DBE).

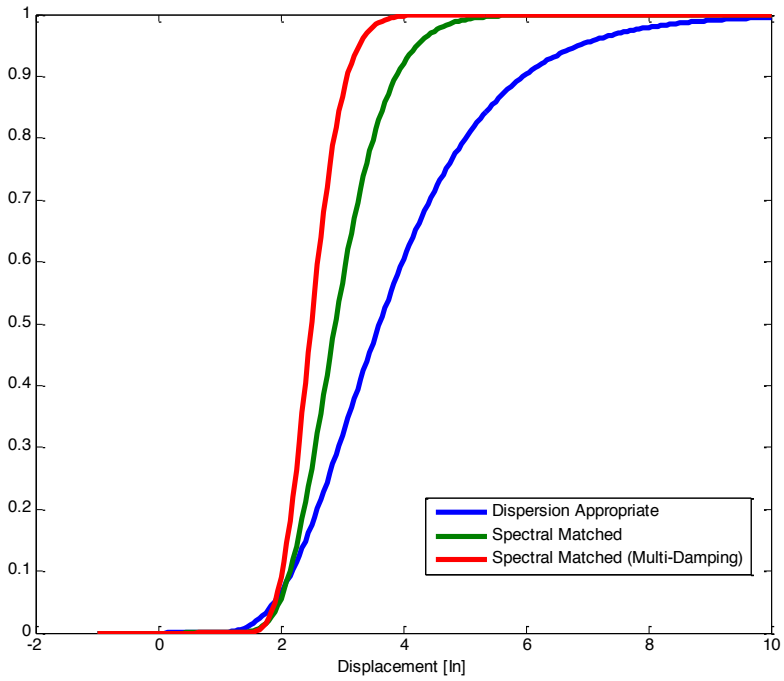

Figure A.115 CDF for EradiQuake System with Velocity Dependent Friction Presenting the Dispersion of Isolator Displacements for Vriety of Ground Motion Inputs (EUR, DBE).

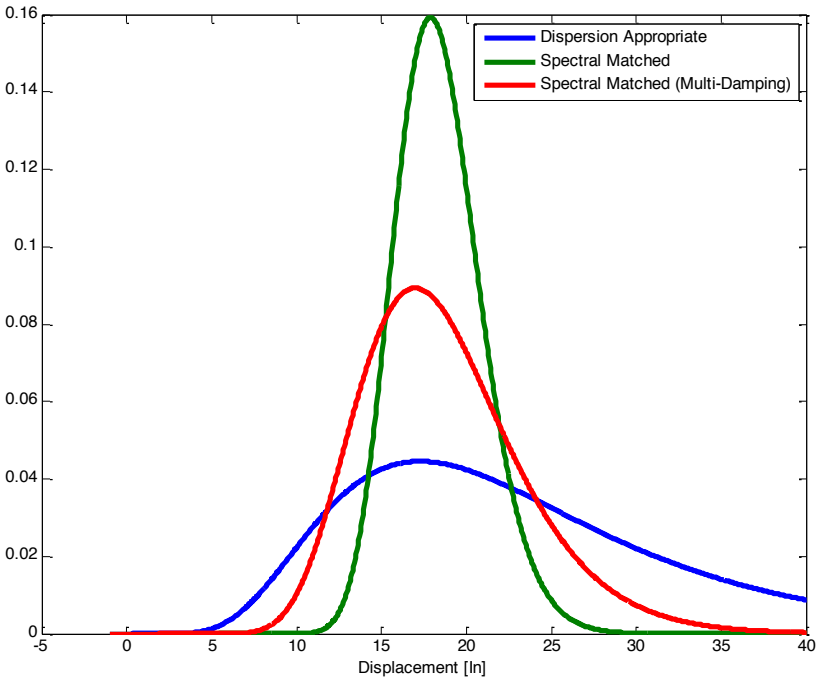

Figure A.116 PDF for EradiQuake System with Velocity Dependent Friction Presenting the Dispersion of Isolator Displacements for Vriety of Ground Motion Inputs (NRC, DBE).

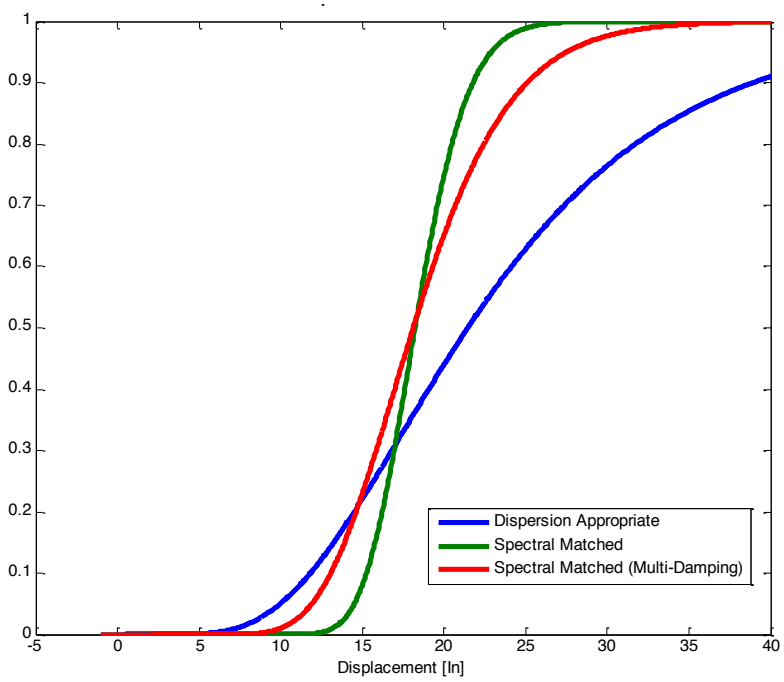

Figure A.117 CDF for EradiQuake System with Velocity Dependent Friction Presenting the Dispersion of Isolator Displacements for Vriety of Ground Motion Inputs (NRC, DBE).

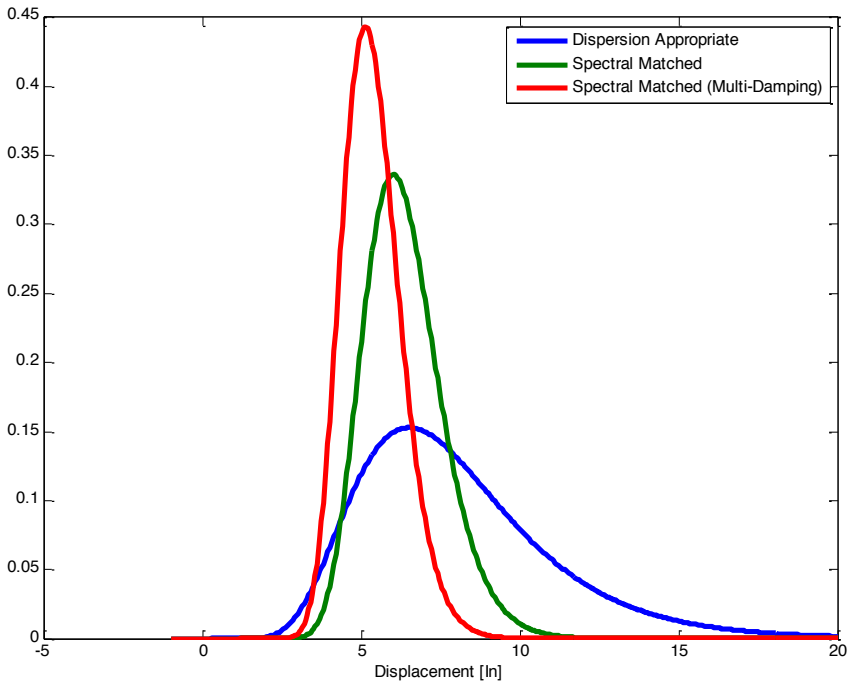

Figure A.118 PDF for EradiQuake System with Velocity Dependent Friction Presenting the Dispersion of Isolator Displacements for Vriety of Ground Motion Inputs (EUR, EDB).

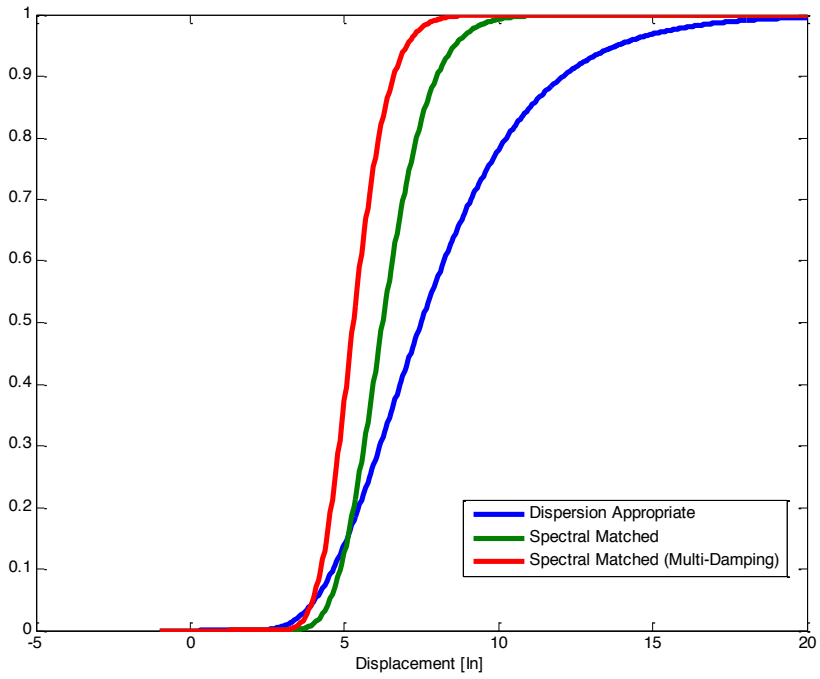

Figure A.119 CDF for EradiQuake System with Velocity Dependent Friction Presenting the Dispersion of Isolator Displacements for Vriety of Ground Motion Inputs (EUR, EDB).

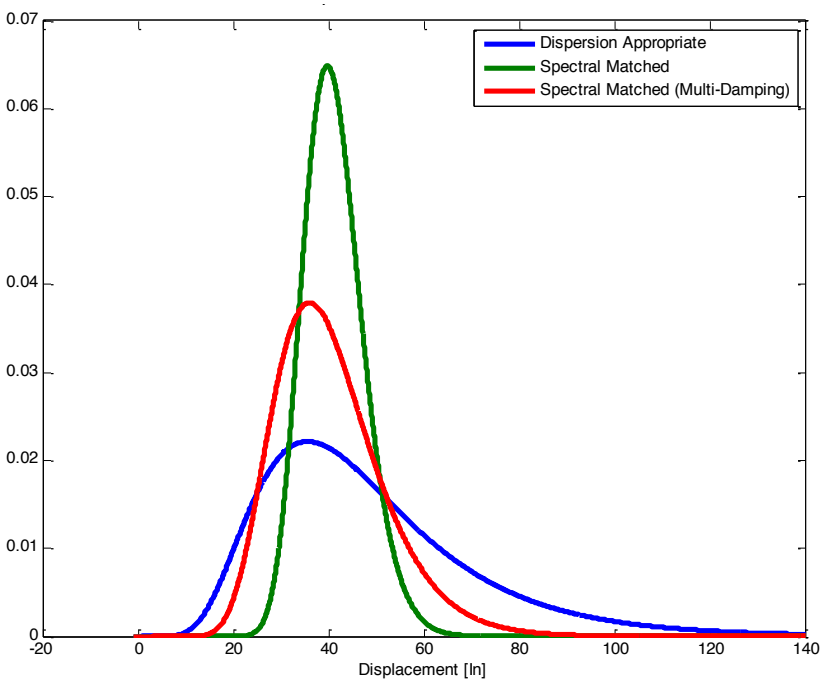

Figure A.120 PDF for EradiQuake System with Velocity Dependent Friction Presenting the Dispersion of Isolator Displacements for Vriety of Ground Motion Inputs (NRC, EDB).

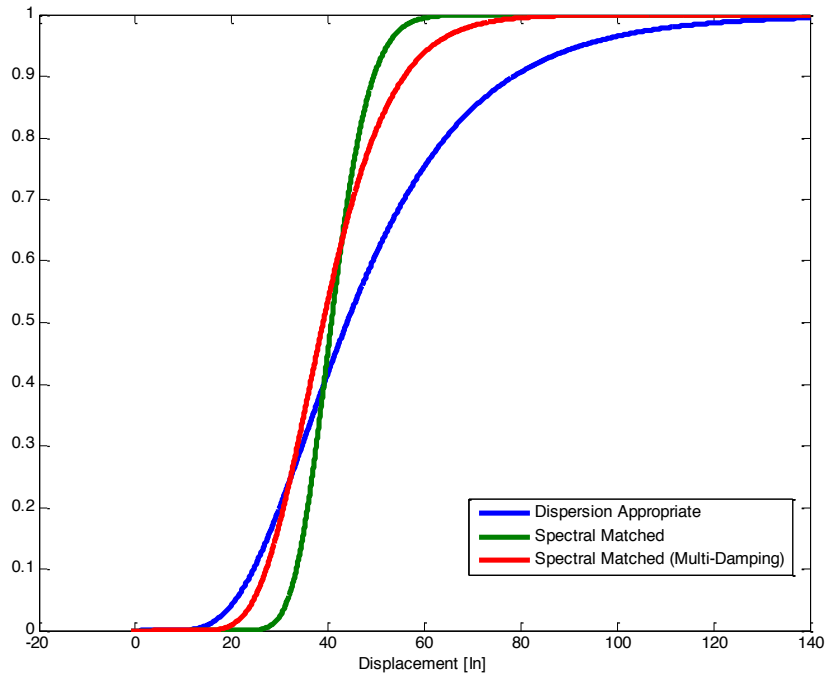

Figure A.121 CDF for EradiQuake System with Velocity Dependent Friction Presenting the Dispersion of Isolator Displacements for Vriety of Ground Motion Inputs (NRC, EDB).

The following tables are the isolator displacements given for the mean, 99% and 90% confidence levels. The standard deviation (std) is also provided. The displacements are tabulated for all ground motion scenarios (dispersion appropriate, spectral matched, and spectral matched multi-damping).

Table A.1 BL-BW (EUR, DBE)

	Mean	Std	99% Lower Bound	99% Upper Bound	90% Lower Bound	90% Upper Bound
Dispersion Appropriate	3.6 in	1.5 in	2.8 in	4.6 in	3.1 in	4.2 in
Spectral Matched	2.9 in	1.3 in	2.5 in	3.4 in	2.7 in	3.2 in
Spectral Matched (Multi-Damp)	2.5 in	1.2 in	2.2 in	2.8 in	2.3 in	2.7 in

Table A.2 BL-BW (EUR, EDB)

	Mean	Std	99% Lower Bound	99% Upper Bound	90% Lower Bound	90% Upper Bound
Dispersion Appropriate	7.5 in	1.4 in	5.9 in	9.5 in	6.5 in	8.7 in
Spectral Matched	6.2 in	1.2 in	5.5 in	7.1 in	5.8 in	6.8 in
Spectral Matched (Multi-Damp)	5.3 in	1.2 in	4.7 in	5.9 in	4.9 in	5.7 in

Table A.3 BL-BW (NRC, DBE)

	Mean	Std	99% Lower Bound	99% Upper Bound	90% Lower Bound	90% Upper Bound
Dispersion Appropriate	21.5 in	1.6 in	15.9 in	28.9 in	17.9 in	25.7in
Spectral Matched	18.2 in	1.1 in	16.7 in	19.9 in	17.3 in	19.2 in
Spectral Matched (Multi-Damp)	18.1 in	1.3 in	15.4 in	21.3 in	16.4 in	20 in

Table A.4 BL-BW (NRC, EDB)

	Mean	Std	99% Lower Bound	99% Upper Bound	90% Lower Bound	90% Upper Bound
Dispersion Appropriate	43.9 in	1.6 in	32.8 in	58.8 in	36.8 in	52.4 in
Spectral Matched	40.7 in	1.2 in	36.9 in	44.9 in	38.4 in	43.2 in
Spectral Matched (Multi-Damp)	39.0 in	1.3 in	32.6 in	46.6 in	35 in	43.4 in

Table A.5 SF-VD (EUR, DBE)

	Mean	Std	99% Lower Bound	99% Upper Bound	90% Lower Bound	90% Upper Bound
Dispersion Appropriate	3.4 in	1.4 in	2.7 in	4.3 in	3.0 in	3.9 in
Spectral Matched	2.6 in	1.3 in	2.2 in	3.0 in	2.3 in	2.8 in
Spectral Matched (Multi-Damp)	2.1 in	1.2 in	1.8 in	2.3 in	1.9 in	2.2 in

Table A.6 SF-VD (EUR, EDB)

	Mean	Std	99% Lower Bound	99% Upper Bound	90% Lower Bound	90% Upper Bound
Dispersion Appropriate	7.4 in	1.4 in	5.9 in	9.3 in	6.5 in	8.5 in
Spectral Matched	6.2 in	1.2 in	5.5 in	7.1 in	5.8 in	6.7 in
Spectral Matched (Multi-Damp)	5.3 in	1.2 in	4.8 in	5.9 in	4.9 in	5.7 in

Table A.7 SF-VD (NRC, DBE)

	Mean	Std	99% Lower Bound	99% Upper Bound	90% Lower Bound	90% Upper Bound
Dispersion Appropriate	19.7 in	1.5 in	15.3 in	25.5 in	16.9 in	23.0 in
Spectral Matched	17.1 in	1.1 in	15.7 in	18.6 in	16.2 in	18.0 in
Spectral Matched (Multi-Damp)	17.0 in	1.3 in	14.7 in	19.7 in	15.6 in	18.6 in

Table A.8 SF-VD (NRC, EDB)

	Mean	Std	99% Lower Bound	99% Upper Bound	90% Lower Bound	90% Upper Bound
Dispersion Appropriate	43.9 in	1.6 in	32.8 in	58.8 in	36.8 in	52.4 in
Spectral Matched	32.7 in	1.1 in	31.0 in	34.6 in	31.7 in	33.8 in
Spectral Matched (Multi-Damp)	32.1 in	1.2 in	28.7 in	35.8 in	30.0 in	34.3 in

Table A.9 EQS-C (EUR, DBE)

	Mean	Std	99% Lower Bound	99% Upper Bound	90% Lower Bound	90% Upper Bound
Dispersion Appropriate	3.3 in	1.4 in	2.7 in	4.2 in	2.9 in	3.8 in
Spectral Matched	2.9 in	1.3 in	2.5 in	3.3 in	2.6 in	3.2 in
Spectral Matched (Multi-Damp)	2.0 in	1.2 in	1.8 in	2.3 in	1.9 in	2.2 in

Table A.10 EQS-C (EUR, EDB)

	Mean	Std	99% Lower Bound	99% Upper Bound	90% Lower Bound	90% Upper Bound
Dispersion Appropriate	7.2 in	1.4 in	5.7 in	9.1 in	6.2 in	8.3 in
Spectral Matched	5.9 in	1.3 in	5.1 in	6.9 in	5.4 in	6.5 in
Spectral Matched (Multi-Damp)	4.8 in	1.2 in	4.3 in	5.5 in	4.5 in	5.2 in

Table A.11 EQS-C (NRC, DBE)

	Mean	Std	99% Lower Bound	99% Upper Bound	90% Lower Bound	90% Upper Bound
Dispersion Appropriate	21.5 in	1.6 in	16.0 in	28.9 in	18.0 in	25.7 in
Spectral Matched	18.2 in	1.1 in	16.7 in	19.9 in	17.3 in	19.2 in
Spectral Matched (Multi-Damp)	18.0 in	1.3 in	15.3 in	21.1 in	16.3 in	19.8 in

Table A.12 EQS-C (NRC, EDB)

	Mean	Std	99% Lower Bound	99% Upper Bound	90% Lower Bound	90% Upper Bound
Dispersion Appropriate	44.1 in	1.6 in	33.0 in	59.0 in	37.0 in	52.6 in
Spectral Matched	40.9 in	1.2 in	37.1 in	45.1 in	38.5 in	43.4 in
Spectral Matched (Multi-Damp)	38.9 in	1.3 in	32.5 in	46.6 in	34.9 in	43.4 in

Table A.13 EQS-VD (EUR, DBE)

	Mean	Std	99% Lower Bound	99% Upper Bound	90% Lower Bound	90% Upper Bound
Dispersion Appropriate	3.6 in	1.5 in	2.8 in	4.6 in	3.1 in	4.2 in
Spectral Matched	2.9 in	1.3 in	2.5 in	3.3 in	2.6 in	3.2 in
Spectral Matched (Multi-Damp)	2.5 in	1.2 in	2.2 in	2.8 in	2.3 in	2.7 in

Table A.14 EQS-VD (EUR, EDB)

	Mean	Std	99% Lower Bound	99% Upper Bound	90% Lower Bound	90% Upper Bound
Dispersion Appropriate	7.5 in	1.5 in	5.9 in	9.5 in	6.5 in	8.7 in
Spectral Matched	6.2 in	1.2 in	5.5 in	7.1 in	5.8 in	6.7 in
Spectral Matched (Multi-Damp)	5.3 in	1.2 in	4.7 in	5.9 in	4.9 in	5.6 in

Table A.15 EQS-VD (NRC, DBE)

	Mean	Std	99% Lower Bound	99% Upper Bound	90% Lower Bound	90% Upper Bound
Dispersion Appropriate	21.5 in	1.6 in	15.9 in	28.9 in	17.9 in	25.7 in
Spectral Matched	18.2 in	1.1 in	16.7 in	19.9 in	17.3 in	19.2 in
Spectral Matched (Multi-Damp)	18.1 in	1.3 in	15.4 in	21.3 in	16.4 in	20.0 in

Table A.16 EQS-VD (NRC, EDB)

	Mean	Std	99% Lower Bound	99% Upper Bound	90% Lower Bound	90% Upper Bound
Dispersion Appropriate	43.9 in	1.6 in	32.8 in	58.8 in	36.8 in	52.4 in
Spectral Matched	40.7 in	1.2 in	36.9 in	44.9 in	38.3 in	43.2 in
Spectral Matched (Multi-Damp)	39.0 in	1.3 in	32.6 in	46.6 in	35.0 in	43.4 in

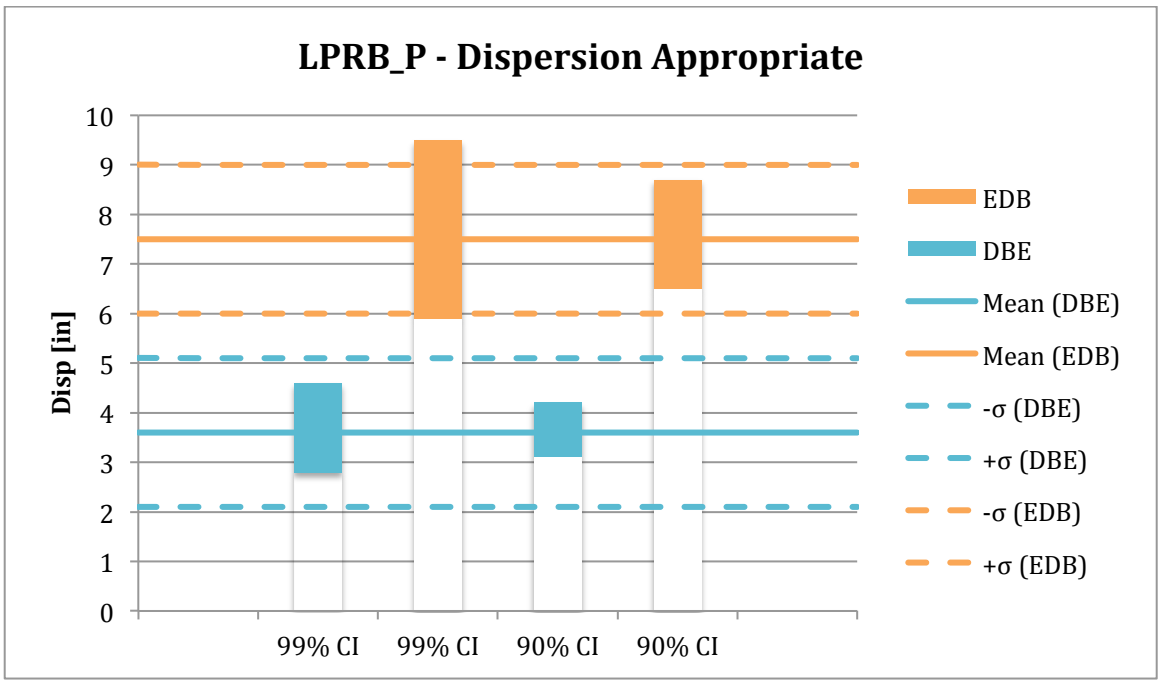

Figure A.122 Graphical Presentation of the Isolator Displacements for the 90- and 99-percent confidence intervals for the DBE and EDB levels with respect to the Standard Deviation and Mean Isolator Displacements – Bilinear Plasticity Dispersion Appropriate Disp. (EUR).

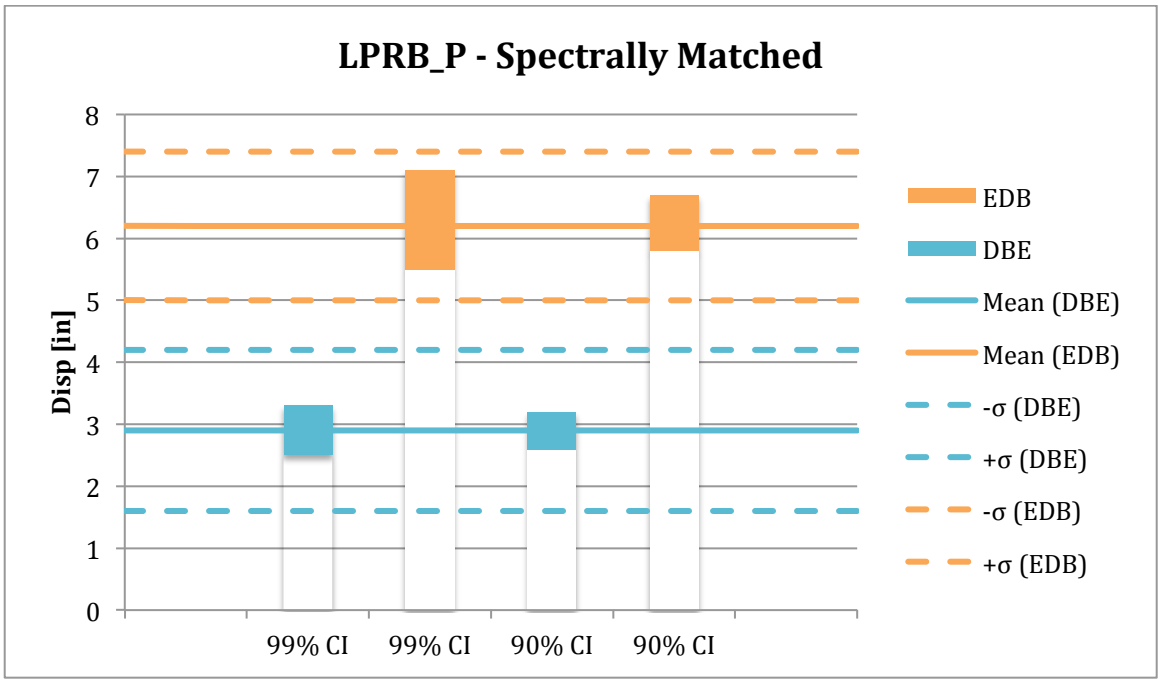

Figure A.123 Graphical Presentation of the Isolator Displacements for the 90- and 99-percent confidence intervals for the DBE and EDB levels with respect to the Standard Deviation and Mean Isolator Displacements – Bilinear Plasticity Spectrally Matched Disp. (EUR).

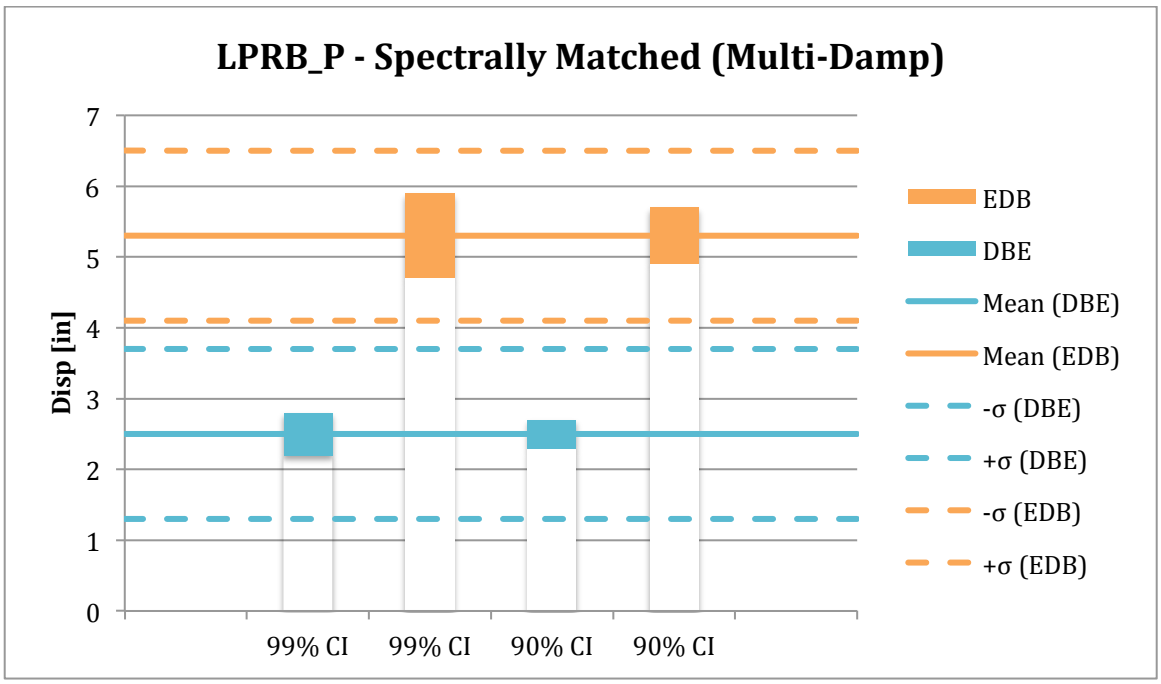

Figure A.124 Graphical Presentation of the Isolator Displacements for the 90- and 99-percent confidence intervals for the DBE and EDB levels with respect to the Standard Deviation and Mean Isolator Displacements – Bilinear Plasticity Spectrally Matched Multi-Damping Disp. (EUR).

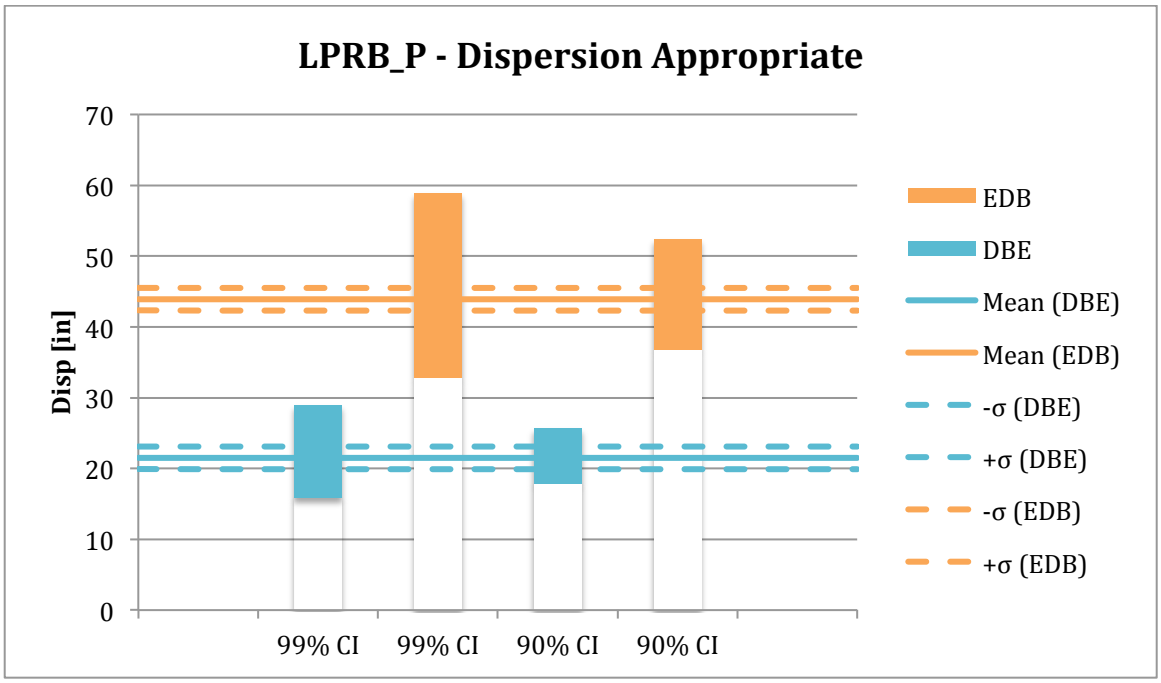

Figure A.125 Graphical Presentation of the Isolator Displacements for the 90- and 99-percent confidence intervals for the DBE and EDB levels with respect to the Standard Deviation and Mean Isolator Displacements – Bilinear Plasticity Dispersion Appropriate Disp. (NRC).

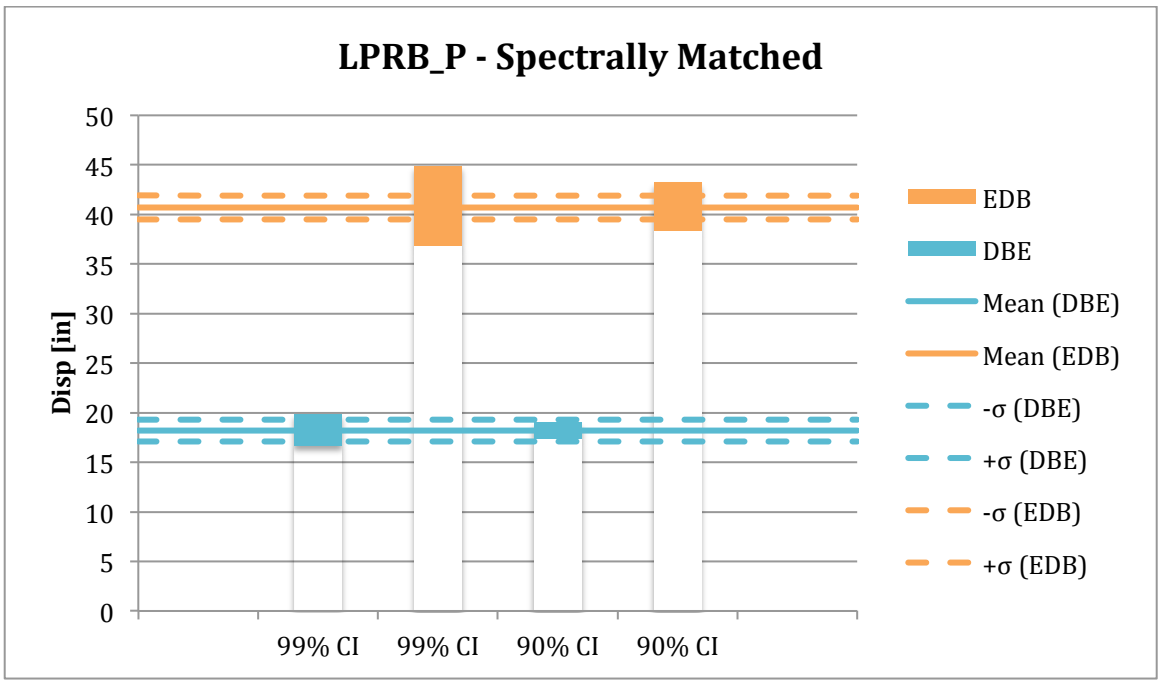

Figure A.126 Graphical Presentation of the Isolator Displacements for the 90- and 99-percent confidence intervals for the DBE and EDB levels with respect to the Standard Deviation and Mean Isolator Displacements – Bilinear Plasticity Spectrally Matched Disp. (NRC).

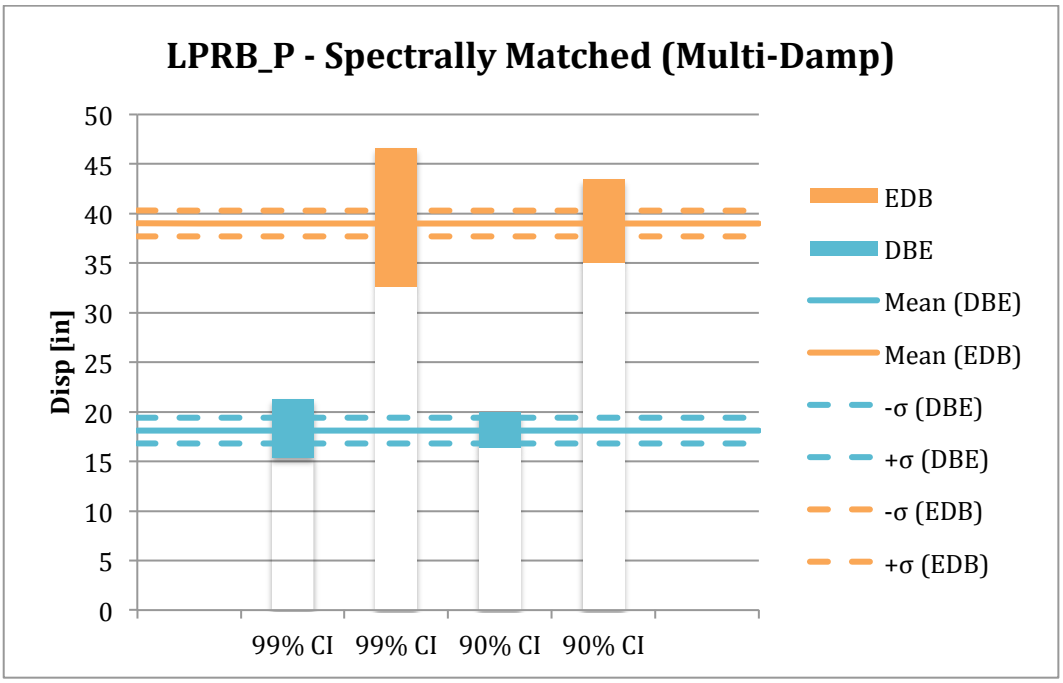

Figure A.127 Graphical Presentation of the Isolator Displacements for the 90- and 99-percent confidence intervals for the DBE and EDB levels with respect to the Standard Deviation and Mean Isolator Displacements – Bilinear Plasticity Spectrally Matched Multi-Damping Disp. (NRC).

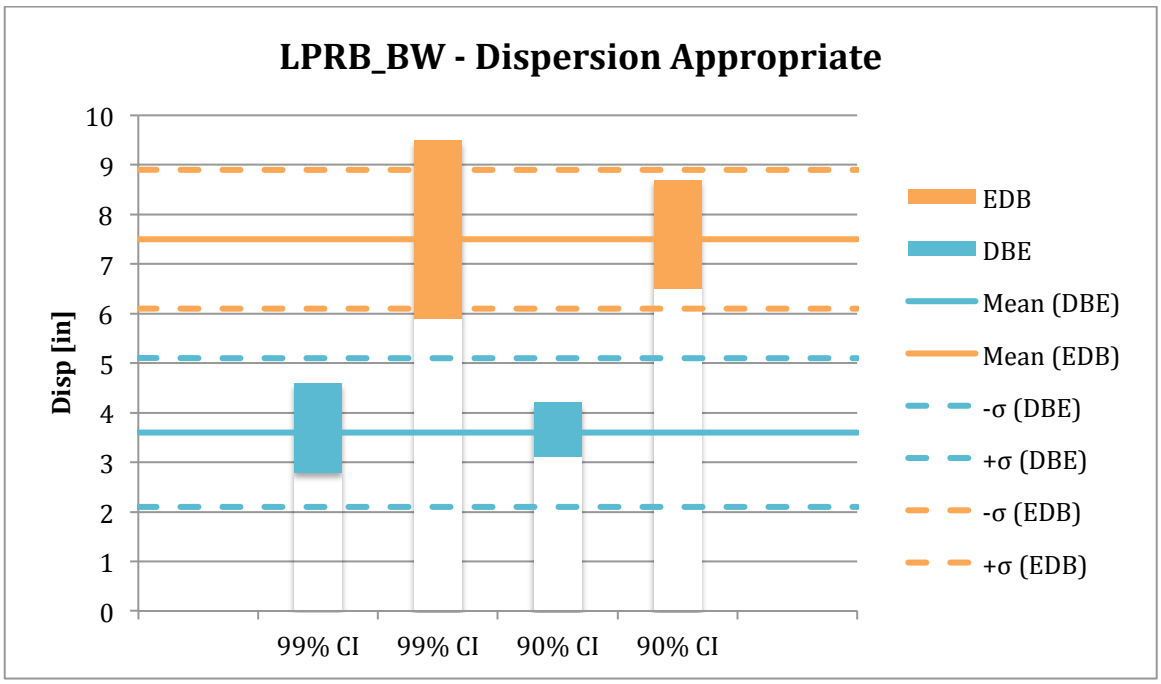

Figure A.128 Graphical Presentation of the Isolator Displacements for the 90- and 99-percent confidence intervals for the DBE and EDB levels with respect to the Standard Deviation and Mean Isolator Displacements – Bilinear Bouc-Wen Dispersion Appropriate Disp. (EUR).

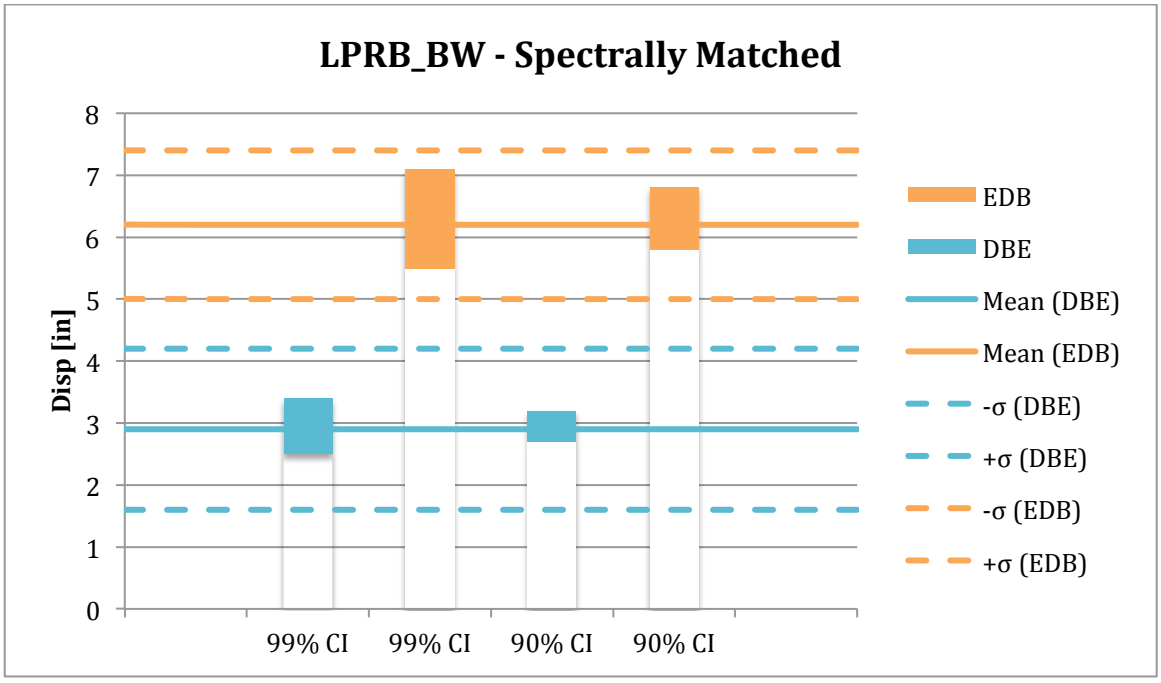

Figure A.129 Graphical Presentation of the Isolator Displacements for the 90- and 99-percent confidence intervals for the DBE and EDB levels with respect to the Standard Deviation and Mean Isolator Displacements – Bilinear Bouc-Wen Spectrally Matched Disp. (EUR).

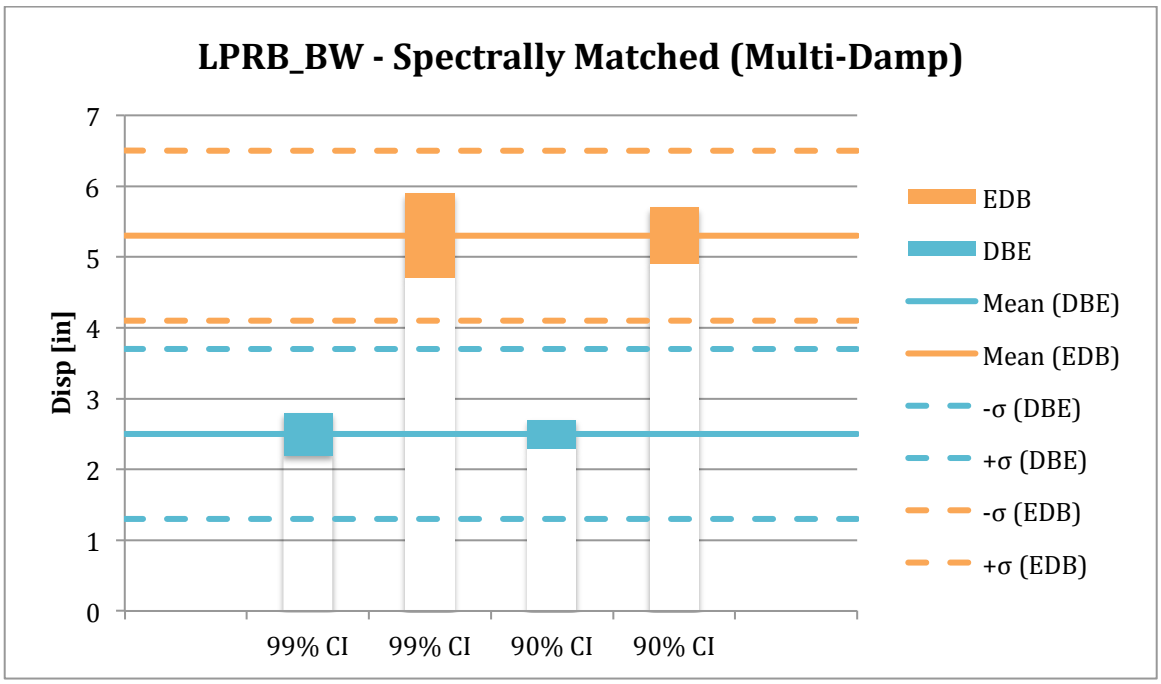

Figure A.130 Graphical Presentation of the Isolator Displacements for the 90- and 99-percent confidence intervals for the DBE and EDB levels with respect to the Standard Deviation and Mean Isolator Displacements – Bilinear Bouc-Wen Spectrally Matched Multi-Damping Disp. (EUR).

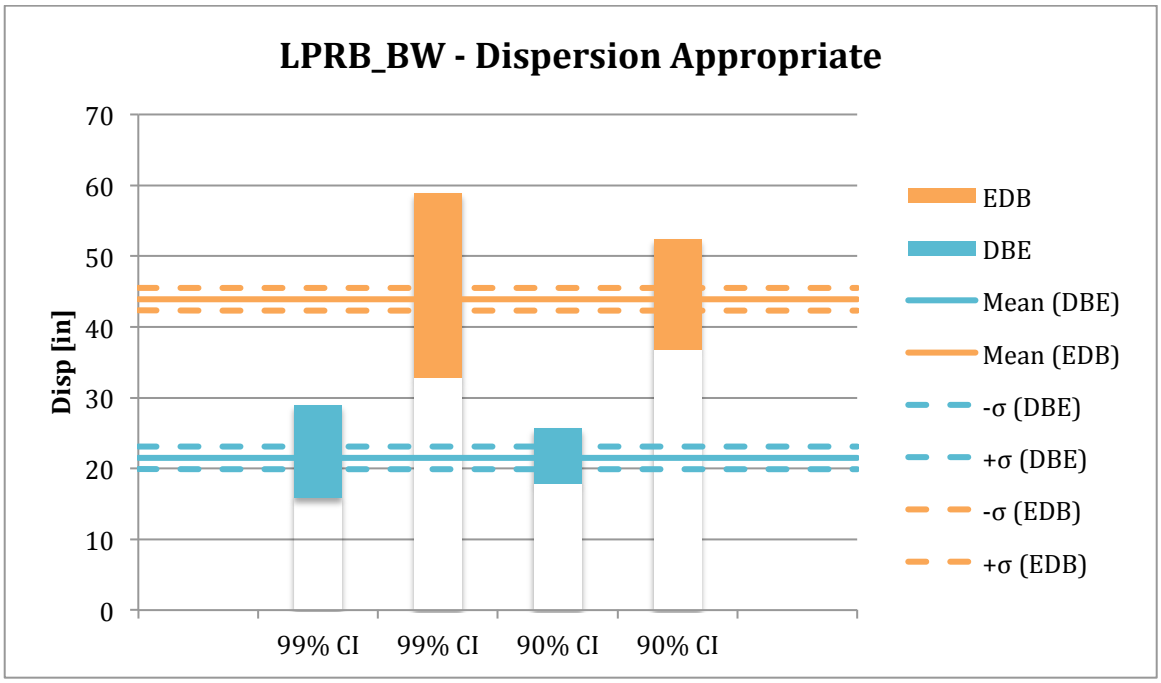

Figure A.131 Graphical Presentation of the Isolator Displacements for the 90- and 99-percent confidence intervals for the DBE and EDB levels with respect to the Standard Deviation and Mean Isolator Displacements – Bilinear Bouc-Wen Dispersion Appropriate Disp. (NRC).

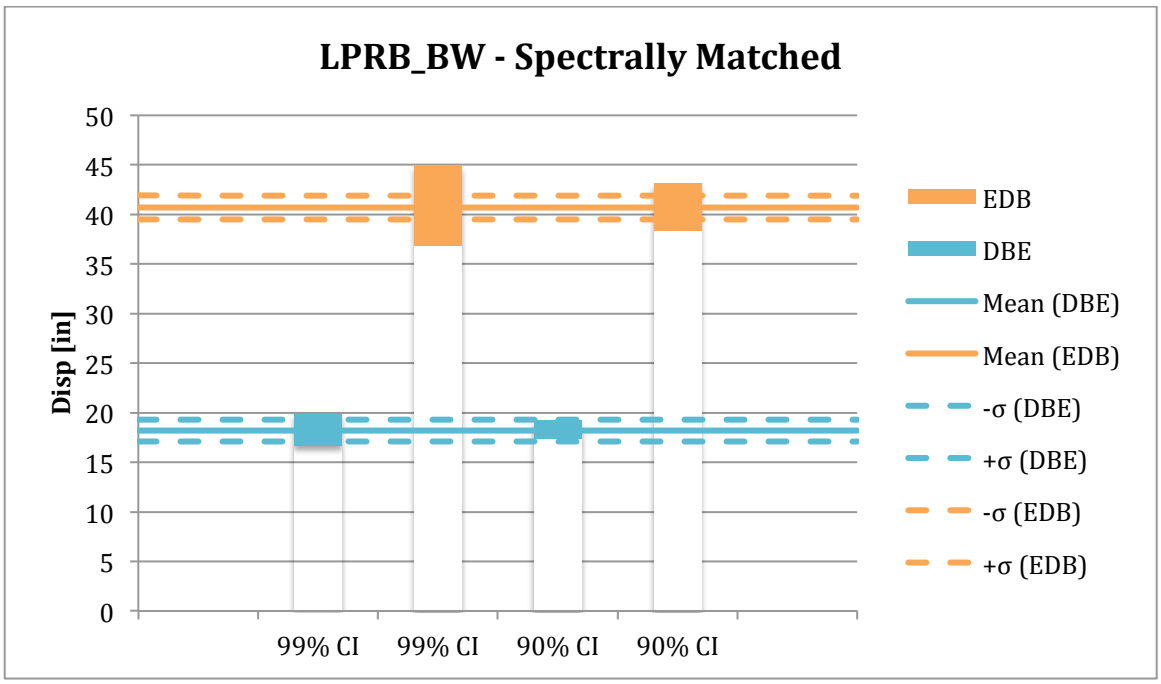

Figure A.132 Graphical Presentation of the Isolator Displacements for the 90- and 99-percent confidence intervals for the DBE and EDB levels with respect to the Standard Deviation and Mean Isolator Displacements – Bilinear Bouc-Wen Spectrally Matched Disp. (NRC).

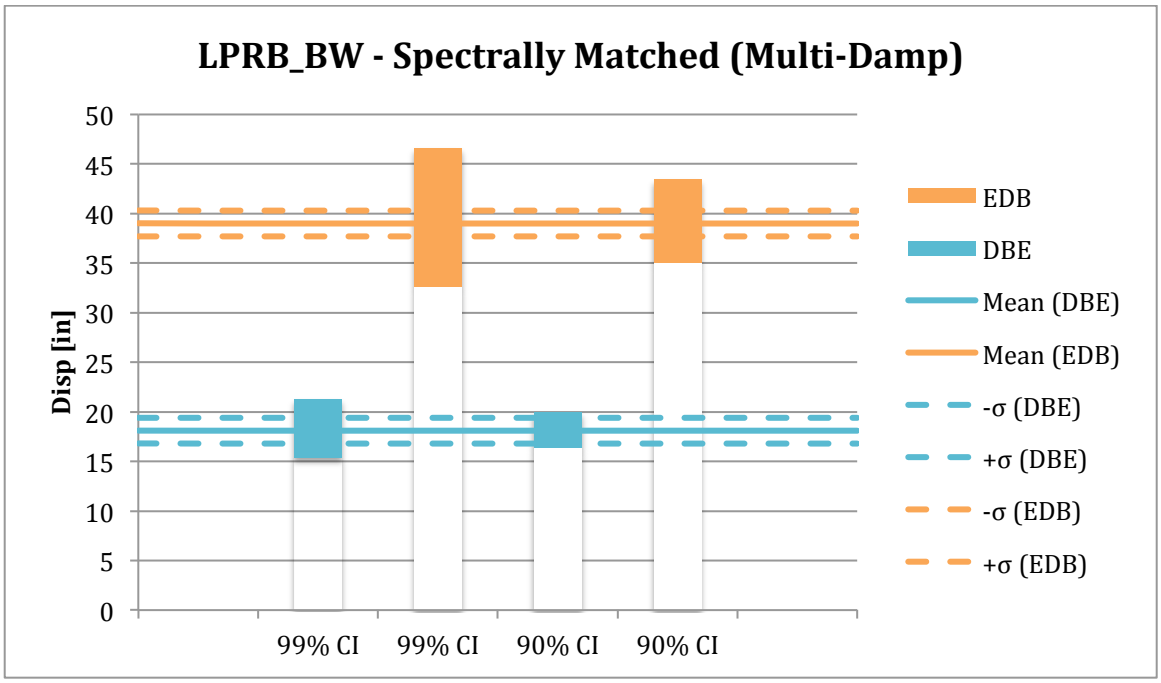

Figure A.133 Graphical Presentation of the Isolator Displacements for the 90- and 99-percent confidence intervals for the DBE and EDB levels with respect to the Standard Deviation and Mean Isolator Displacements – Bilinear Bouc-Wen Spectrally Matched Multi-Damping Disp. (NRC).

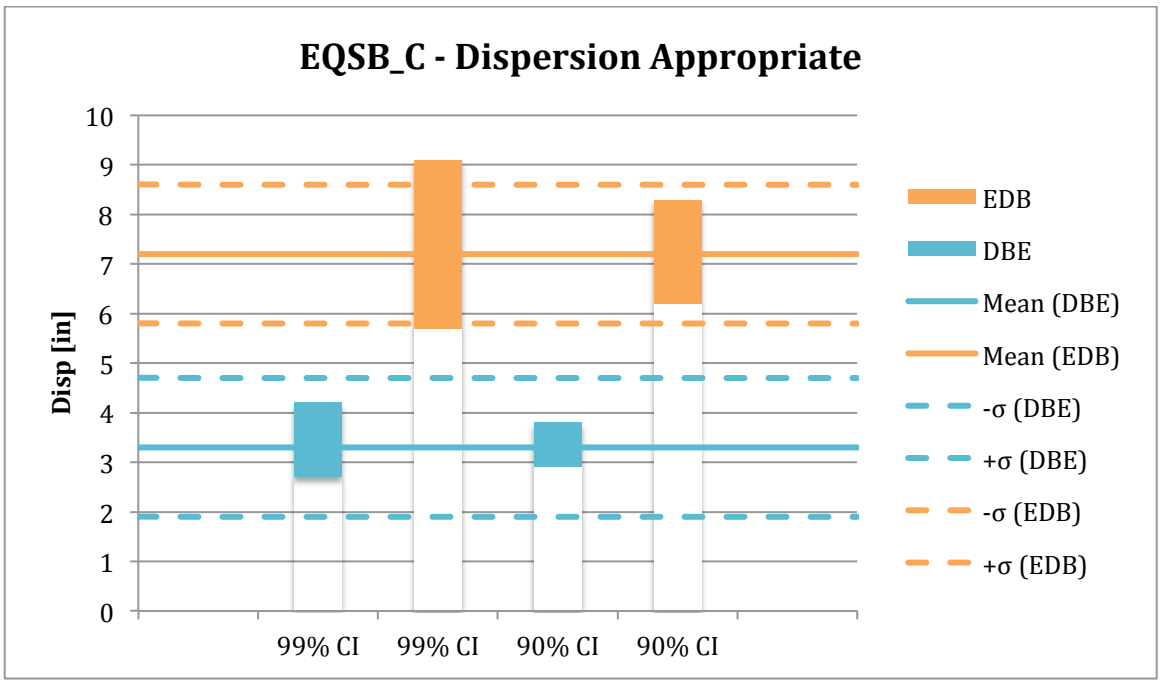

Figure A.134 Graphical Presentation of the Isolator Displacements for the 90- and 99-percent confidence intervals for the DBE and EDB levels with respect to the Standard Deviation and Mean Isolator Displacements – EQS Constant Friction Dispersion Appropriate Disp. (EUR).

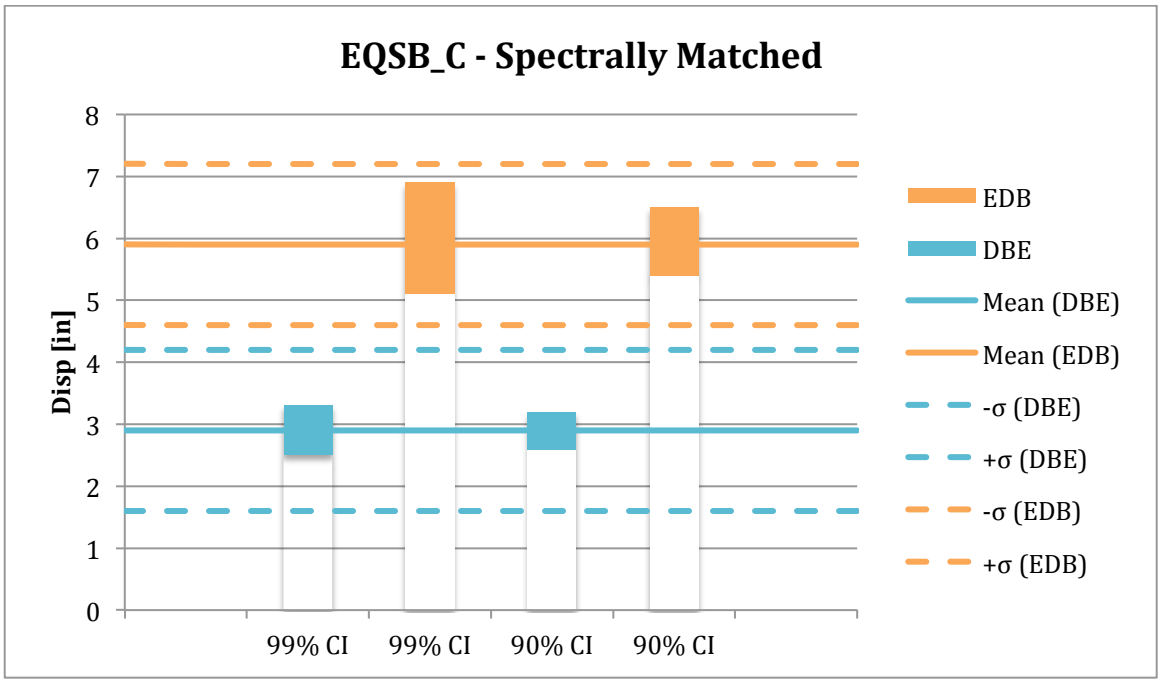

Figure A.135 Graphical Presentation of the Isolator Displacements for the 90- and 99-percent confidence intervals for the DBE and EDB levels with respect to the Standard Deviation and Mean Isolator Displacements – EQS Constant Friction Spectrally Matched Disp. (EUR).

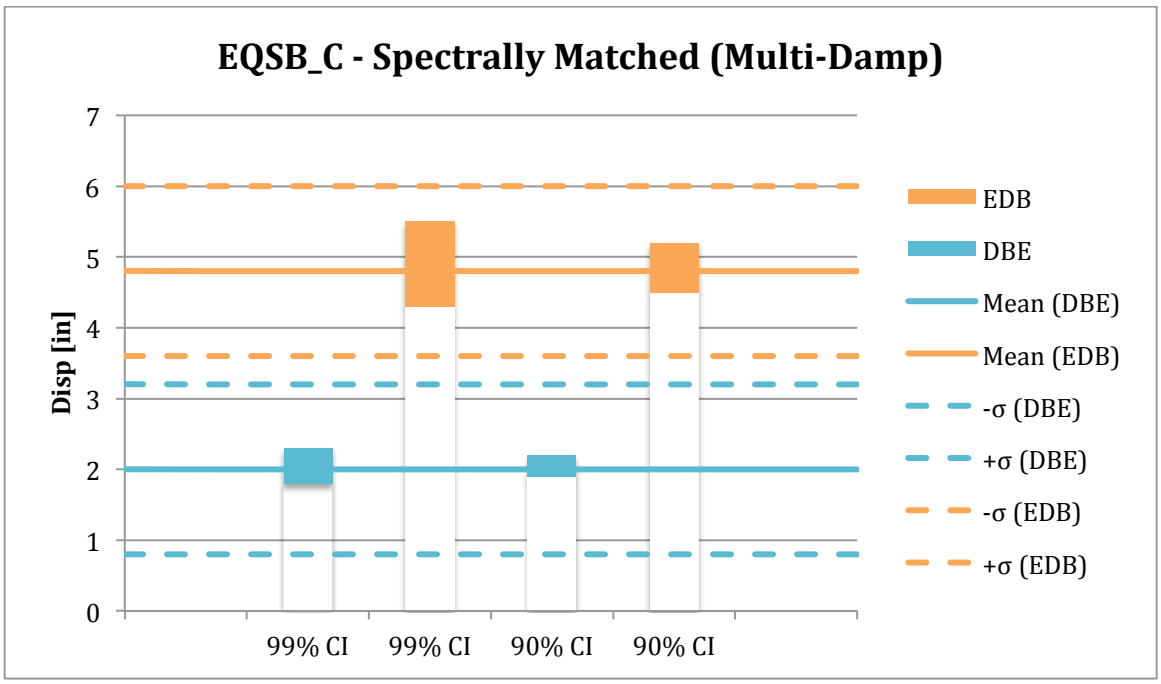

Figure A.136 Graphical Presentation of the Isolator Displacements for the 90- and 99-percent confidence intervals for the DBE and EDB levels with respect to the Standard Deviation and Mean Isolator Displacements – EQS Constant Friction Spectrally Matched Multi-Damping Disp. (EUR).

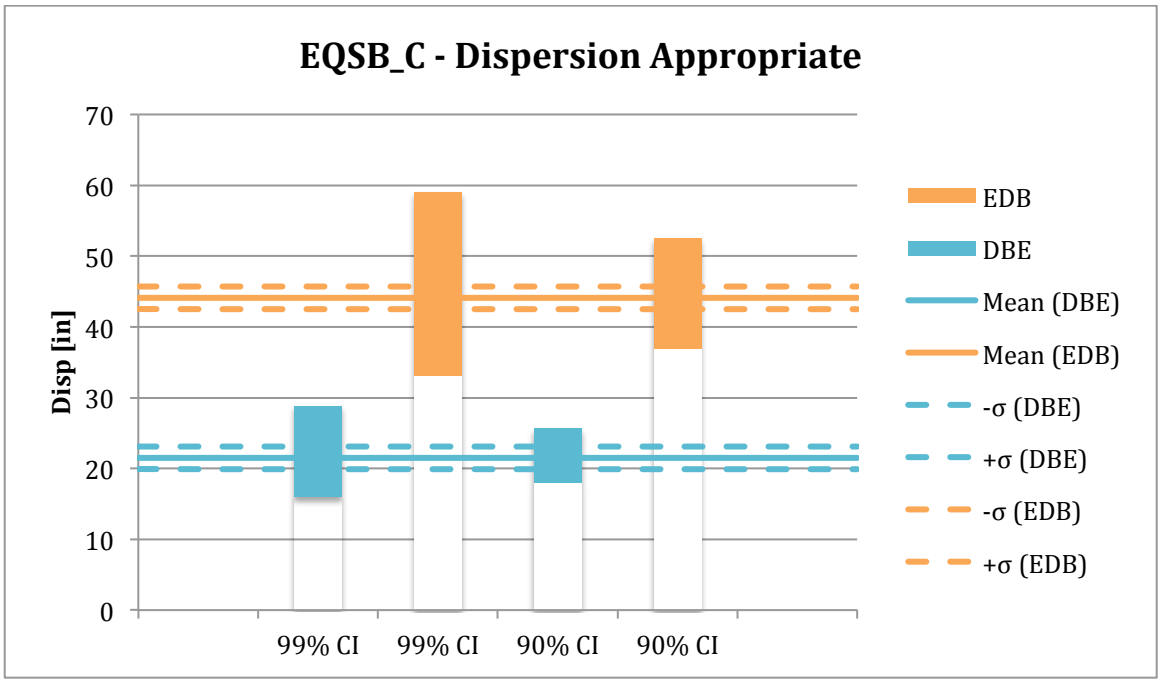

Figure A.137 Graphical Presentation of the Isolator Displacements for the 90- and 99-percent confidence intervals for the DBE and EDB levels with respect to the Standard Deviation and Mean Isolator Displacements – EQS Constant Friction Dispersion Appropriate Disp. (NRC).

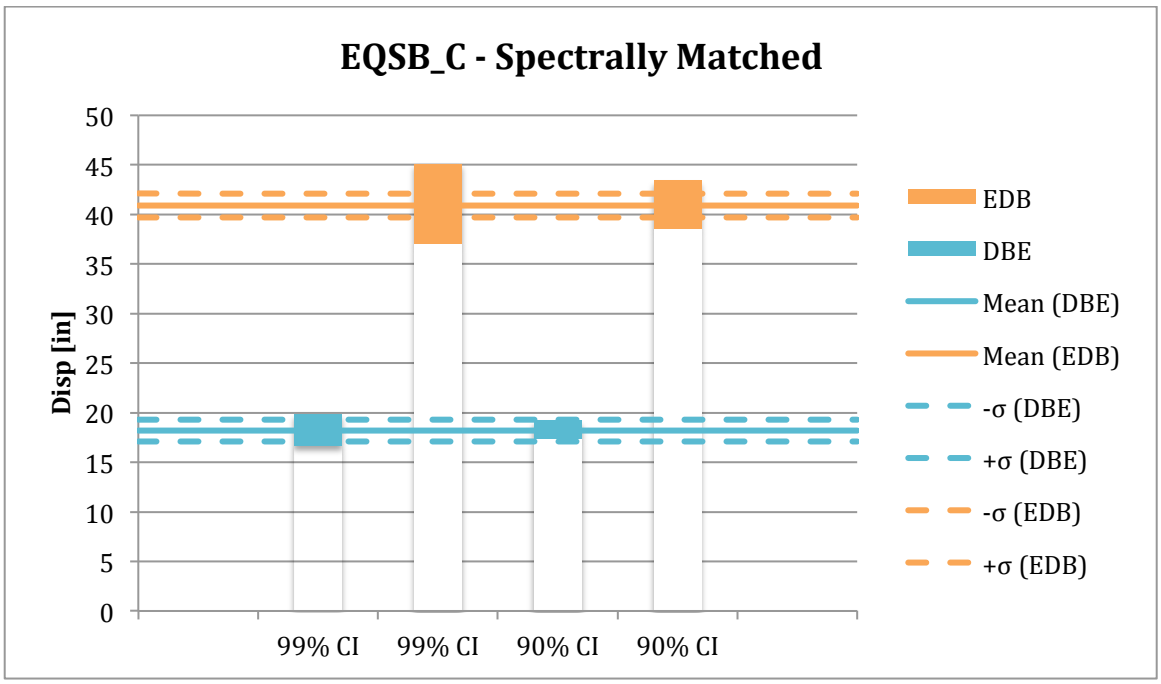

Figure A.138 Graphical Presentation of the Isolator Displacements for the 90- and 99-percent confidence intervals for the DBE and EDB levels with respect to the Standard Deviation and Mean Isolator Displacements – EQS Constant Friction Spectrally Matched Disp. (NRC).

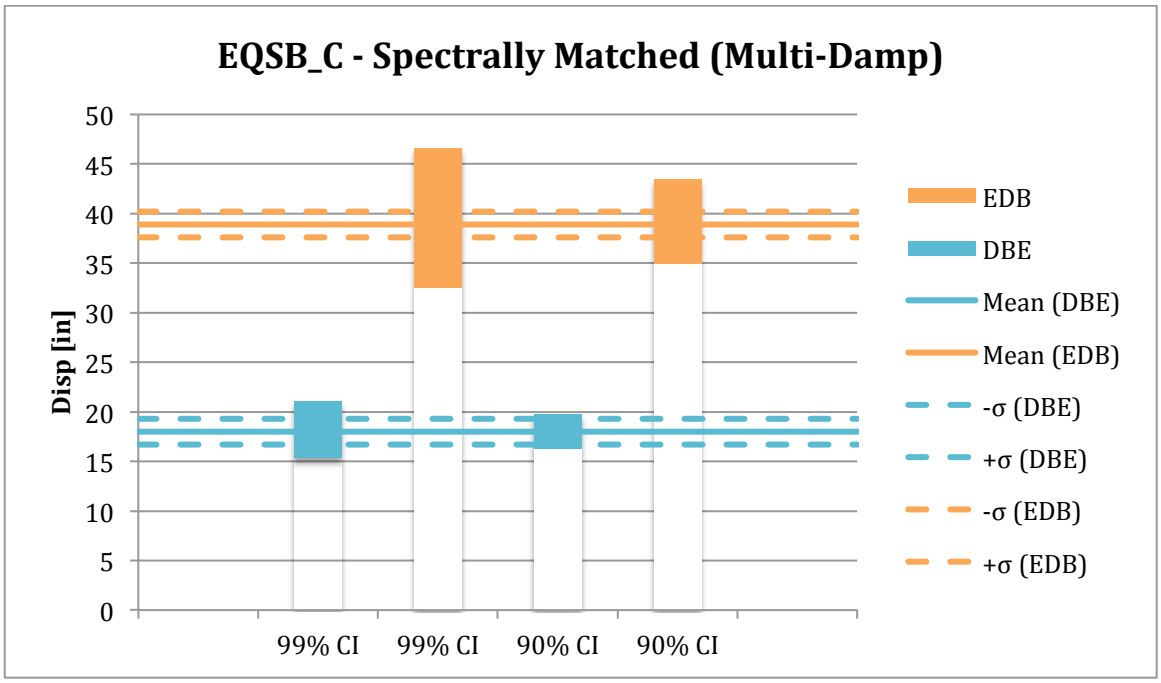

Figure A.139 Graphical Presentation of the Isolator Displacements for the 90- and 99-percent confidence intervals for the DBE and EDB levels with respect to the Standard Deviation and Mean Isolator Displacements – EQS Constant Friction Spectrally Matched Multi-Damping Disp. (NRC).